A Multidisciplinary Approach to the Study of Slope Instability in Derbyshire, with particular reference to Matlock

by

Susan Helen Dakin, B.Sc.

Thesis submitted to the University of Nottingham for the degree of Doctor of Philosophy, May 1989

CONTENTS

LIST OF FIGURES

LIST OF TABLES

LIST OF PLATES

ACKNOWLEDGEMENTS

This work was carried out in the Departments of Geography and Geology, University of Nottingham whilst in receipt of a research grant from the Natural Environment Research Council. I wish to express my gratitude to my supervisors for their help: to Dr. John Doornkamp and Professor Paul Mather for the excellent and inspirational training in geomorphology and remote sensing, and to Dr. Tim Brewer for his encouragement and support without which this work would not have been possible.

In addition, my thanks go to Dr. Martin Cross and Dr. Ron Jones for their advice and to Mr. Leadbeater of the Derbyshire County Council for his time and information on recent slope failures in the Matlock region.

I also owe a great deal to Dr. Bob Dugdale for his support, his word processor and for his help in surveying Oker Hill landslide. Other worthy members of the surveying and field work teams were Cath Keane, Howard Willson, Janet Murray, Martin Way and Ian Westwood - I hope your payment was sufficient. (Excellent place to put a pub, don't you think?!)

I would particularly like to thank the various members of the drilling and salvage teams who battled against all odds to provide me with something to work on; they are, in order of appearance: Ian Conway, John Winn, Graham Morris, George Reeve, Chris Hawkins,

Professor Peter Worsley, Allan James, Gordon Hardy (The Expert) and Paul Andrews. I am indebted to Mr. Ron Greatorex, the farmer of Oker Hill, for his co-operation and patience during the drilling of the boreholes - I hope we didn't leave too much of a mess behind!

I am very grateful to the members of the Department of Geology for their hospitality and help with the mineralogical and geochemical analyses. To Chris Sommerfield, the man who can't survive at temperatures below 200°C - you did a brilliant job teaching me how to make beads and pellets for XRF analysis - ta duck! Mark Townsend was also of great help in the clay identification by XRD.

Thanks also to Dave Jones and Merv Evans for the black and white photography.

Finally, I wish to acknowledge the friendship and support of Janet Murray during the writing-up stages of this work. Her tragic death has touched many people and she is greatly missed.

ABSTRACT

This study of slope instability in the Matlock region of Derbyshire uses, and tests the applicability of, a variety of techniques from reconnaissance through to site investigation. The aims have been to (i) provide a greater understanding of landsliding in this area and (ii) produce a critical assessment of the techniques employed.

A procedure was developed for the application of Landsat-5 TM imagery to slope stability studies, however, such imagery was found to be of very limited use in the study area. Morphological and geomorphological mapping from aerial photographs and in the field proved to be of greatest use for supplying information on landslide location, morphology, type and recent activity, and also in identifying surface water conditions. These techniques are relatively rapid, require the minimum of equipment, and provide a large amount of relevant data in a short time. They are also applicable to both reconnaissance surveys and site investigations.

The geomorphological survey of Oker Hill near Matlock revealed a large multiple rotational landslide. An ochre-precipitating spring is situated within this landslide. A similar spring occurs on Mam Tor landslide in north Derbyshire, and Vear (1981) has shown this to be evidence of pyrite oxidation of the shale, a process which is believed to lead to periodic slope failure. Analysis of core material from two boreholes through the Oker Hill landslide confirmed that pyrite has been lost from the failed material and that the

present base of the weathered zone is in the pyritic shale. Pyrite oxidation is resulting in iron oxide staining, the loss of sulphur (presumably as sulphuric acid which will participate in further reactions) and in an overall deterioration of the rock quality of the shale.

CHAPTER 1 BACKGROUND TO THE STUDY

1.1 Aims of the Study

According to a recent survey for the Department of the Environment, the county of Derbyshire has one of the highest densities of landslips in Great Britain (GSL, 1987): a total of 428 landslips have been identified on the British Geological Survey 1:10,000 and 1:10,560 maps, twenty-one of which cover an area greater than 0.25km^2 (Figure 1.1), and many small landslips remain unmapped. The majority of the landslips occur in the Carboniferous strata of the Millstone Grit Series where competent sandstones overly incompetent mudstones. Locations where massive limestones overly weathered basalts are also common sites for slope failure.

It is agreed among authors that the main period of slope instability in this area occurred during the past 10,000 years with the return to a warmer climate after the periglacial conditions of the last Ice Age (Franks and Johnson, 1964; Johnson and Vaughan, 1983; Tallis and Johnson, 1980). However, instability still exists on all scales (from Mam Tor, covering an area of 0.5km^2, to small failures) creating problems for civil engineering structures and housing. For example, the road across Mam Tor was closed in 1979 as a result of continued landsliding, and a house built in the 1970's on Starkholmes landslide near Matlock had to be demolished before completion and rebuilt with deep pile foundations. The problem of landsliding also

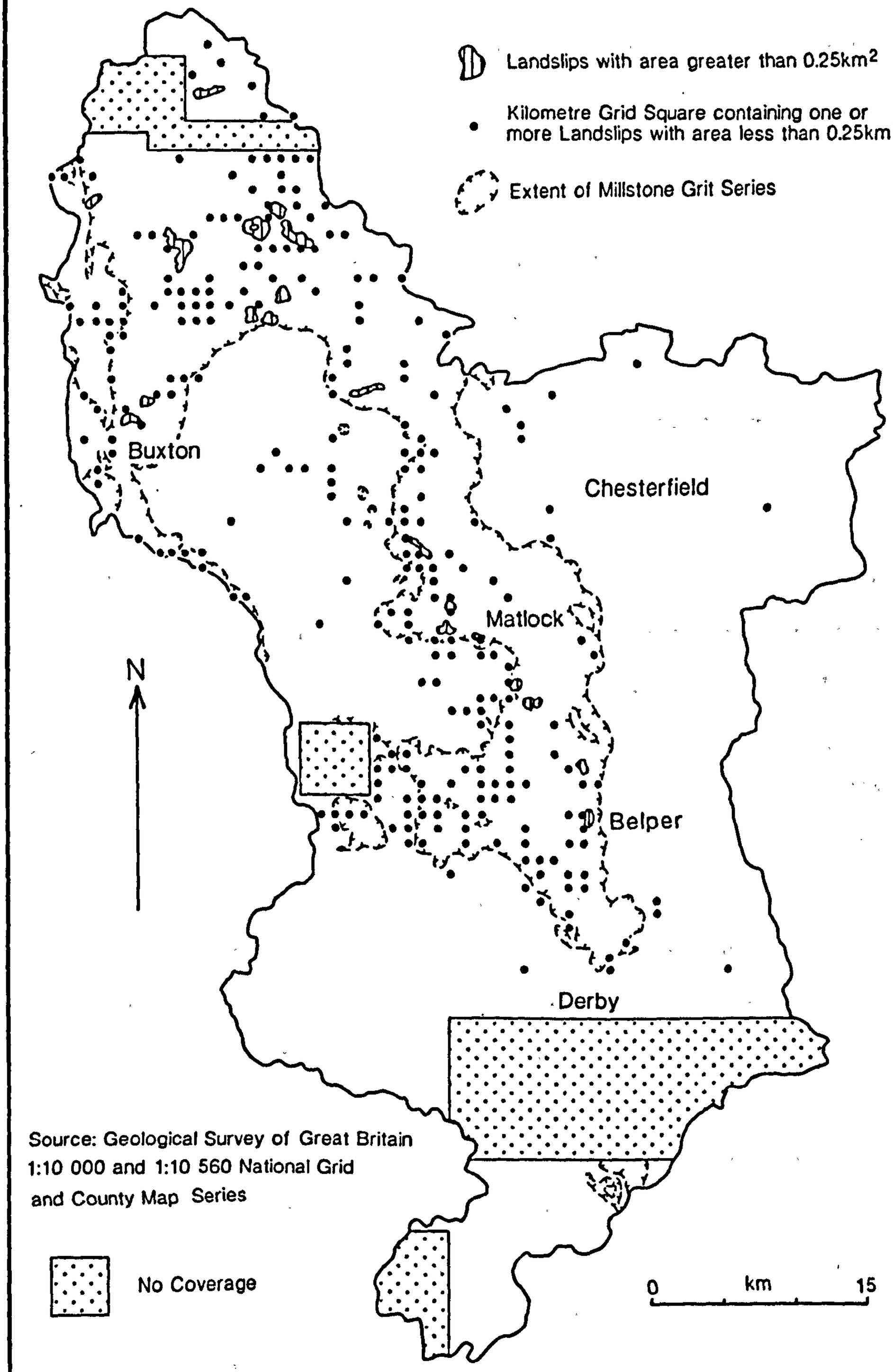

Figure 1.1 The Distribution of Landslides in Derbyshire

had to be considered by the Trent River Authority in an assessment of suitable sites for reservoirs in the county (Trent River Authority, 1971).

The aim of this study is to investigate slope instability in the Matlock region of Derbyshire (Figure 1.2) using a variety of techniques, in order to provide (i) a greater understanding of landslides in this area and (ii) a critical assessment of the techniques employed.

Much of the previous work on landsliding in Derbyshire has been focused on the northern part of the county in the sandstones and shales of the Carboniferous Millstone Grit Series, for example, the landslides of Longdendale, Charlesworth, Alport and Ashop Dales and Edale (Amin, 1979; Franks and Johnson, 1964; Johnson, 1965, 1980, 1981; Johnson and Vaughan, 1983; Johnson and Walthall, 1979; Leadbeater, 1985; Steward, 1984; Vear, 1981). This work focuses on the Matlock area (Figure 1.2) which lies further south where the geology is slightly different but time-equivalent; i.e. deposition of sediments is believed to have occurred within a shallow semi-restricted basin environment into which a delta was encroaching (Amin, 1979), as compared to the area to the north where deep basinal mudstones (Edale Shale) and turbiditic sediment (Mam Tor Beds) were deposited. Within the Matlock area Oker Hill (Figure 1.2) has been singled out for detailed study of the landslides present, with respect to morphology, subsurface conditions and possible causes of failure.

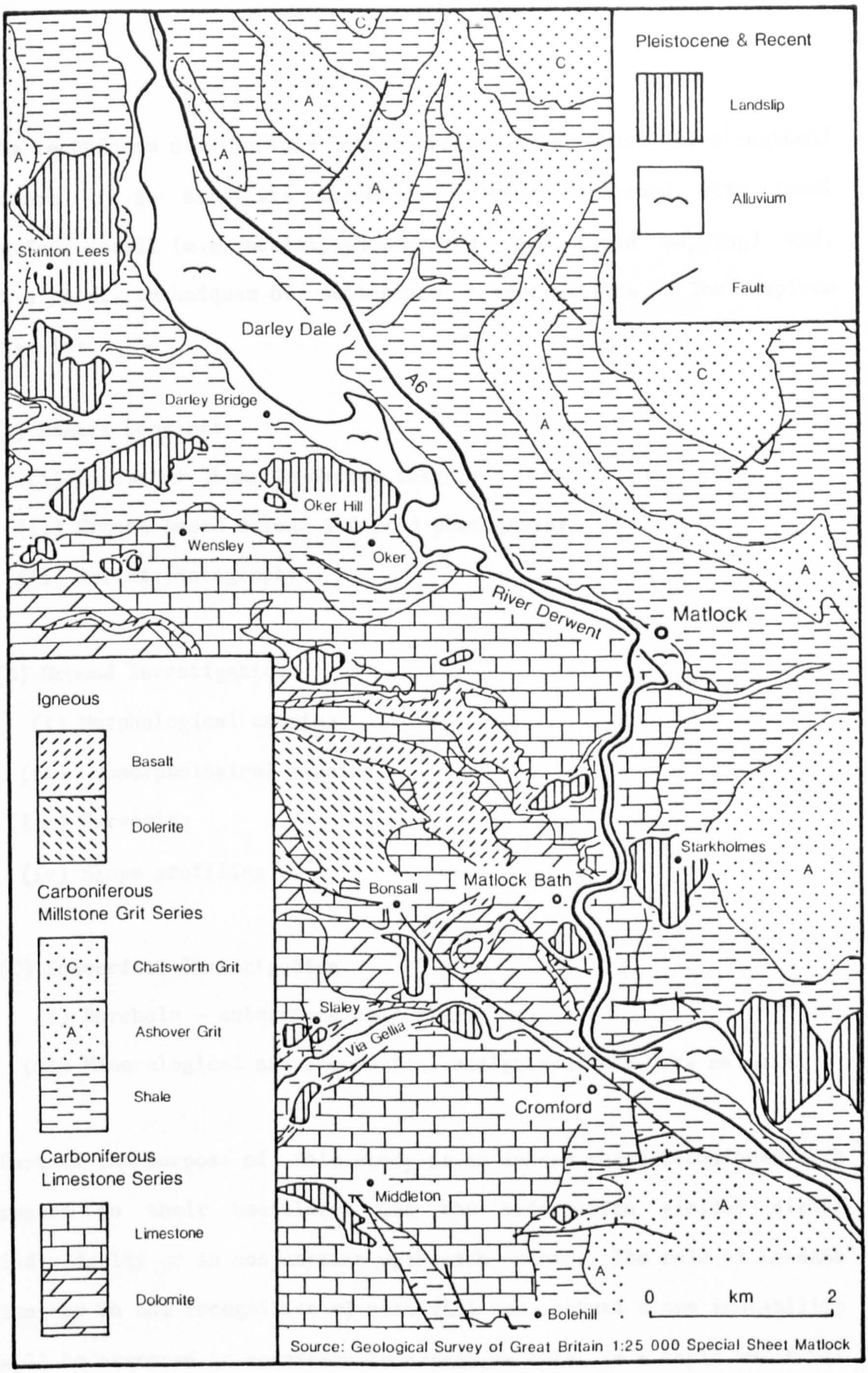

Figure 1.2 Landslides and Geology of the Matlock Region

The techniques used in this study range from those of a regional nature (e.g. satellite imagery), to those concerned with local surface detail (e.g. aerial photography and field mapping) and, at a point, techniques of subsurface investigations. The complete list is:

(A) Remote Sensing:

(i) Landsat-5 Thematic Mapper imagery

(ii) Ground-based colour infrared photography

(iii) Aerial photography

(B) Ground Investigation:

(i) Morphological mapping

(ii) Geomorphological mapping

(iii) Surveying

(iv) Slope profiling

(C) Subsurface Investigation

(i) Borehole - subsurface conditions

(ii) Mineralogical and geochemical analysis of the core material

Part of the purpose of this study is to assess these techniques with regard to their usefulness and the information yielded either individually or in conjunction with each other. The role of Landsat imagery in the recognition of potential and actual slope instability will be assessed in considerable detail as this is a topic which has

been little investigated in the past. For this purpose a Landsat image analysis procedure was developed on images of the Edale area, where landslide data were already available, in order to calibrate this approach.

1.2 Geological History

To understand the locations, causes and mechanisms of slope instability in Derbyshire it is necessary to consider the geological history of the region.

In the late Devonian to early Carboniferous, about 360 Ma ago, this region experienced a major marine transgression together with the formation of blocks and basins produced by faulting (Anderton et al., 1979). At this time semi-arid, low latitude climatic conditions prevailed, hence there existed a shallow sea into which there was very little input of terrigeneous sediment. Under these conditions the Carboniferous Limestone Series was laid down consisting mainly of massive limestones with interbedded basalts resulting from contemporaneous volcanic activity (Smith et al., 1967). These rocks now form the White Peak area of Derbyshire with carbonate reefs exposed and forming such distinctive features as Treak Cliff and Winnats Pass in Castleton and High Tor at Matlock. The interbedded basalt can be seen in Cave Dale at Castleton and Via Gellia near Cromford (Figure 1.2).

Towards the end of the Lower Carboniferous period the area began to subside with a corresponding increase in supply of argillaceous material to the sea resulting in interbedded limestones and shales. Eventually limestone formation ceased and the deposition of mainly marine shales continued into the Millstone Grit Series of the Namurian (Smith et al., 1967). A maximum of over 2,000 metres of sediments derived from a landmass in the north were deposited in the South Pennines during Namurian times (Anderton et al., 1979) in a cyclic sequence of:

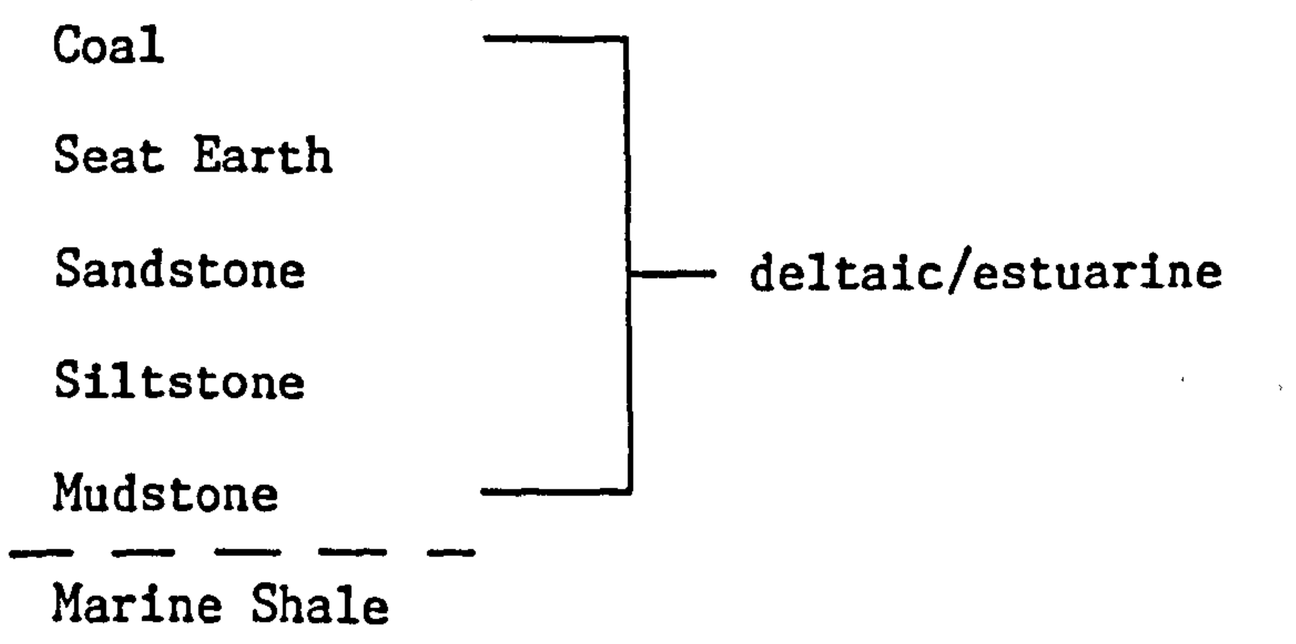

The Kinderscout Grit, Ashover Grit, Chatsworth Grit, Redmire Flags and Rough Rock are the sandstone units of this cycle (Smith et al., 1967). The marine shales were shown by Allen (1960) to have been deposited by turbidity currents issuing from submarine fan channels. This cycle of deposition is also reflected in the faunal phases identified by Ramsbottom et al. (1962), enabling correlation of boreholes through the Namurian strata of the Ashover area.

This pattern of sedimentation continued throughout the Coal Measures Series of the Westphalian, the increase in occurrence of coal in the

later Carboniferous indicating that the climate was becoming increasingly humid and tropical enabling the development of peat swamps (Anderton et al., 1979).

Carboniferous sedimentation was terminated by uplift with the formation of major anticlines and synclines creating the Pennines about 280 Ma ago, and was followed by denudation (Smith et al., 1967). On this eroded surface the sediments of the Permo-Triassic were deposited, sandstones accumulating under continental conditions and mudstones and limestones being deposited under marine conditions. During Tertiary times the Carboniferous and Permo-Triassic rocks together with any subsequent strata were subjected to prolonged erosion creating the present eroded anticline with the Carboniferous limestone plateau surrounded by the Millstone Grit edges (Figure 1.3).

The next geological period of significance to landsliding in Derbyshire was the Pleistocene during which there appears to have been three glacial advances that affected the area (King, 1966): the Anglian, the Wolstonian and the Devensian. In the Anglian and Wolstonian advances ice is believed to have flowed southward on both sides of the Pennines and overflowed onto the Peak District. Hence the area was covered with slow-moving ice which caused little erosion, thus explaining the absence of corries and "U"-shaped valleys. Nearly all the till present in the Peak District was brought by the Wolstonian advance; only small patches now remain (King, 1966; Smith et al., 1967).

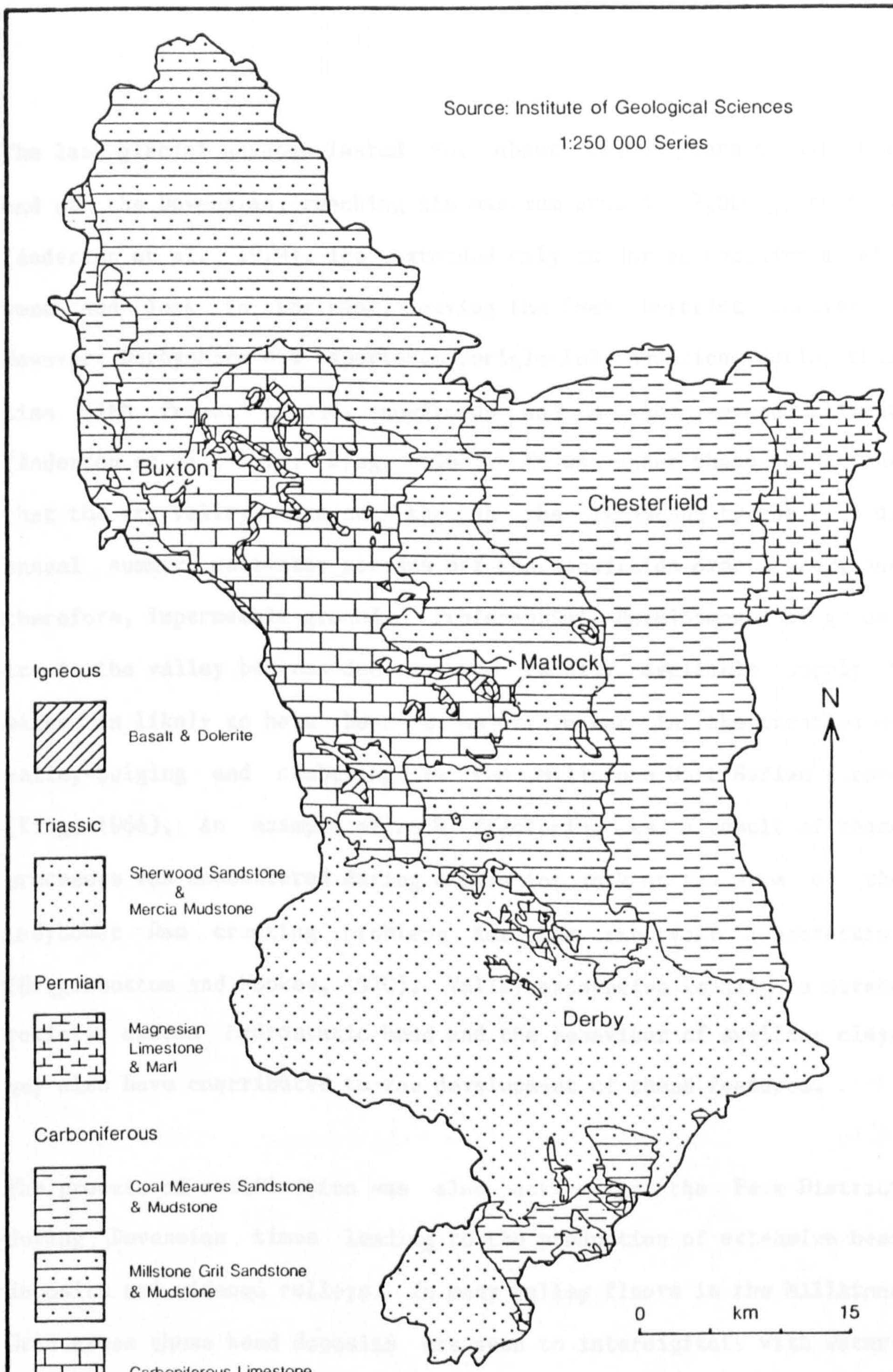

Figure 1.3 The Geology of Derbyshire

The last glacial advance lasted for about 10,000 years towards the end of the Devensian, reaching its maximum around 17,000 years B.P. (Anderton et al., 1979). Ice extended only as far as Cheshire in the west and York in the east, leaving the Peak District uncovered. However, Derbyshire did experience periglacial conditions during this time with frozen ground, snowfields and a very severe climate (Anderton et al., 1979; King, 1966). It was under these conditions that the dry valleys were cut through the limestone by the flow of annual summer meltwater streams off the snowfields over frozen, and therefore, impermeable ground. Preferential development of ground ice in the valley bottoms due to the readily available supply of water is likely to have been a major factor in the creation of valley-bulging and cambering in the Millstone Grit Series strata (King, 1966). An example of rock fracturing as a result of these processes was encountered during excavation work at the site of the Ladybower Dam creating problems for the reservoir construction (Higginbottom and Fookes, 1970). Valley excavation leading to stress relief, excess hydrostatic head and the behaviour of swelling clays may also have contributed to the development of these features.

The process of solifluction was also active in the Peak District during Devensian times leading to the production of extensive head deposits and widened valleys. In many valley floors in the Millstone Grit areas these head deposits are seen to interdigitate with water-lain sands and gravels (Edwards and Trotter, 1954; Said, 1969). Frost activity was also high, resulting in frost-shattering, scree

formation, and disturbance of soil profiles (King, 1966; Said,1969).

The presence of arctic winds during the Devensian are indicated by loess deposits that have been recognised in the White Peak as two to five centimetres of ochreous yellow silty subsoil above the limestone. Further evidence can be seen in the wind-etched rocks on the Millstone Grit plateaus and edges (Edwards and Trotter, 1954).

The Devensian Ice Age ended approximately 10,000 years B.P. Since then the strata of the Millstone Grit Series have been subjected to extensive landslipping in response to the periglacial landscape attaining an equilibrium condition with the present environment (Johnson and Walthall, 1979). The rocks and superficial deposits have weathered to produce soils, and alluvial deposits have been laid down; a series of terraces have been interpreted to indicate several falls in the base level of the rivers (Waters and Johnson, 1958). The wetter climate has also allowed the growth of peat blankets on the high ground of the sandstones of the Millstone Grit Series.

An important feature of landscape evolution in the Post-Glacial period has been the removal of forest vegetation by man. Said (1969) has identified three phases of deforestation in northeast Derbyshire, 495±85 B.C. (Iron Age), 220±90 A.D. (Roman Period) and 1300-1830 A.D., resulting in soil erosion to expose the present rugged, boulder-strewn landscape. The problems of soil and peat erosion by man's activities are also recorded by Shimwell (1981).

From this brief geological history the key elements with respect to the potential for landsliding are:

(i) the presence of shale bands beneath and within more massive arenaceous strata.

(ii) the presence of igneous beds (capable of weathering to a relatively weak state) within the Carboniferous limestone.

(iii) the steep slopes generated by glacial and periglacial activity.

(iv) the legacy of periglacial landforms and deposits (including cambering of some sandstone scarps).

(v) valley deepening and stream erosion since the Pleistocene.

In general, the effect of periglacial conditions for almost 60,000 years in Derbyshire has been to weaken the rocks by cambering, valley-bulging and frost shattering; these processes have also created fractures which enable the penetration of ground water deep into the rock. Also the rapid downcutting of meltwater streams has formed oversteepened valleys, and caused the further exposure of the weaker shale beneath the sandstone. Johnson (1980) notes that the slopes that have failed tend to be those where the sandstone cap rock contributes between twenty and fifty percent of the total slope height.

The role of man (e.g. through vegetation clearance and civil

engineering works) in causing landslides has to be set into this geological context, and will be discussed with reference to the Matlock area in Chapter 6.

1.3 Landsliding in North Derbyshire

The initiation of landsliding is believed to have started at least as late as 8,000 years B.P., 2,000 years after the Devensian on the return to a more temperate climate. From pollen analysis of peat, which infills depressions within a landslide in Longdendale, Tallis and Johnson (1980) concluded that movement, in that particular case, ended approximately 2,000 years ago and that sliding had taken place on this slope intermittently for at least 6,000 years. Peat deposits at a landslide near Glossop date slope failure at c.7,200 years B.P. during the late Boreal climatic period (Franks and Johnson, 1964), and the Alport Castles landslide has been dated at 8,300 to 7,600 years B.P. (Johnson and Vaughan, 1983). At Edale End landslide debris overlies peat deposits. Redda et al. (1985) radiocarbon-dated the upper peat section at 2560±50 years B.P. (SRR-2525).

The above dates imply that there was a time lag between the end of the Devensian and the start of major slope failure. This has been explained by Johnson and Walthall (1979) in their work on the Longdendale landslides. At the end of the Devensian the fall of the ground water level was extremely slow as the lower slopes were heavily mantled by till and head deposits which prevented the free

drainage of the slopes. In addition to this, as the permafrost thawed and the ground water began to circulate more freely the shear stresses increased leading to a progressive weakening of the shale, as explained by Terzaghi (1950). Consequently, the critical state for slope failure was attained whenever pore-water pressures or the variation of pressures within the rock were increased after periods of heavy rainfall.

The Longdendale landslides are generally multiple regressive bedding plane slides with a strong degree of translation and often with slight non-circular rotational movement in addition. The slip planes tend to be located at the base of the Grindslow Shales above the Shale Grit (Johnson and Walthall, 1979). A consequence of this confined sandstone aquifer at the foot of the valley slope would have been the generation of high piezometric levels within the rock leading to an increase in effective shear stress and a lowering of the effective angle of resistance of the shale, hence increasing the potential for slope failure. Also, this would be a zone of active weathering destroying the rock fabric and lowering the rock strength. Therefore, Johnson and Walthall (1979) suggest that failure was caused by general rock decay and by the low effective resistance created by the high pore-water pressures at the base of the shale. After initial failure the strength of the slipped material would be reduced further to its residual shear strength thus allowing later slip movement to be achieved by lower stress forces.

The initiation of landsliding at Mam Tor is likely to be of a similar

age to that in Longdendale, evidence for a post-Devensian glacial date at Mam Tor being provided by the foot of the slide which overlies solifluction deposits (Vear, 1981). Mam Tor still experiences instability and after many years of constant resurfacing the A625 road over the landslide was finally closed in 1979. The current periodic major slope failures within the slide have been attributed to pyrite oxidation causing deterioration of the shale and resulting in failure after heavy rainfall (Steward, 1984; Vear, 1981; Vear and Curtis, 1981).

Another major area of present instability in north Derbyshire is the A57 Snake Pass road. Between 1970 and 1985 there were seven major landslips on this road (Leadbeater, 1985) which can, in part, be attributed to undercutting by the River Ashop. During heavy rainfall and at times of snowmelt this river is capable of rapid erosion at the base of the hillside thus reducing support of the slope. On average, the road settles by fifty to seventy-five millimetres each winter and has to be resurfaced almost every year. This disruption by slope movement is a common occurrence on many Derbyshire roads, including those around Matlock.

1.4 Landsliding around Matlock

There are numerous landslides in the Matlock area; the larger ones are on the steeper, undercut, shale slopes of the Derwent valley (Figure 1.2). Derbyshire County Council is constantly repairing

roads which cross these landslides, for example, at Starkholmes, Stanton Lees and Oker Hill (Leadbeater, pers. comm.).

Rapid snowmelt, excessive rainfall and flooding of the river at Matlock during the winter of 1965/1966 are cited by Taylor (1966) as contributing to slope instability which affected the roads across the landslides at Starkholmes, Bolehill (south of Cromford) and Stanton Lees (Figure 1.2). In addition to these disruptions the failure of a mass of limestone in Matlock Bath demolished a house and the debris blocked the A6 trunk road.

Up until 1982 Starkholmes Road used to subside two to three times a year at a cost of £200,000 for resurfacing (Leadbeater, pers. comm.). A thickness of about one metre of tarmac built up which had the effect of holding up water on the upslope side of the road resulting in a rise of pore-water pressure and further failure. In 1982 the old road was completely removed and replaced by a permeable road with a thin surface. This consisted of a permeable base layer of limestone from 200 millimetres to dust-sized diameter with three membranes (one at the base, one in the middle and one at the top), then five centimetres of road surfacing (the minimum thickness possible) was laid down. The road was then cut into ten metre lengths and down the centre so that when one block subsided it would not affect the rest of the road. Since these measures were taken there have been no repairs necessary. Further west on this road in the village of Starkholmes the verge of the road collapsed several years ago in a two metre trench-like form; the ground downslope did not move. At

first it was thought this was due to the collapse of old mine workings but none were detected in boreholes. It may be that the shale suddenly lost its strength and collapsed (Leadbeater, per. comm.).

At Oker Hill the road on the southern slope has often been repaired due to slipping; at present the slopes have been stabilised by simple shallow drainage. Current problems are occurring on Sitch Road on the eastern side (Leadbeater, pers. comm.).

It is not only the roads which are affected by landslide movement. Recent building work at Starkholmes was severely interrupted when a house had to be rebuilt with deep pile foundations after movement even before its completion, and at Oker End the removal of trees resulted in earth slumping against a house.

Smaller slides are also found where the Carboniferous Limestone overlies lavas which have weathered into soft clays, for example on the upper slopes of Via Gellia. In May 1987 slight movement was observed at Slaley (Figure 1.2); this may have been due to quarrying on the lower slopes undercutting the toe of an old landslide thus removing support and resulting in reactivation.

To summarise, the Matlock area includes many landslides, both in sandstone overlying shale and in limestone overlying weathered basalt, the majority of which were probably initiated after the last glacial period at a time of higher pore water pressures than those

occurring today. However, some of these landslides (it is not known how many) are still on the verge of instability and are reactivated from time to time by either natural causes (i.e. excess rainfall or snowmelt leading to increased pore-water pressures) or man-induced causes (i.e. slope undercutting or artificially increased pore-water pressures).

CHAPTER 2 REMOTE SENSING OF SLOPE INSTABILITY

2.1 Introduction to Remote Sensing of Slope Instability

Little previous work has been carried out on the use of satellite imagery in the study of geomorphology and of landslides in particular. Astaras and Silleos (1984), Howard and Mitchell (1980) and Parry (1978) have used Landsat successfully for land systems mapping on a regional scale, and various other workers (e.g. Kondratyev et al., 1973; Pain, 1985; Ni and He, 1984) have used this type of imagery for recognition of landforms with varying degrees of success.

Rib and Liang (1978) reviewed past work on landslide recognition from remotely-sensed imagery. They came to the conclusion that the most useful Landsat MSS (Multispectral Scanner) images were provided by Band 5, recording reflected electromagnetic radiation of visible red wavelengths, and by infrared false-colour composites. However, the most useful wavelengths for terrain analysis occur between 8 and 14μm. This waveband represents infrared heat emission from the ground providing information on soil-water conditions. Band 6 of Landsat TM (Thematic Mapper) records electromagnetic radiation from infrared heat emission and may, therefore, prove useful in studying slope stability by providing information on water conditions within slopes.

Sauchyn and Trench (1978) assessed the application of Landsat MSS imagery to landslide mapping in the USA. They found that although some slides could be identified by tonal banding and mottling caused by the irregular terrain and by the presence of ponds within the slide area, many smaller landslides were not identified. They concluded that Landsat MSS imagery was only suitable for preliminary landslide mapping in relatively unknown areas.

Alfoldi (1974), Gagnon (1975) and Saroso et al. (1984) used various forms of remotely-sensed imagery in assessing landslide hazards in Canada and West Java. They employed Landsat and radar imagery, and aerial photography; all concluded that although the landslides could be identified on the Landsat images the most appropriate form of imagery was aerial photography. However, they stress that aerial photo-interpretation should be integrated with the regional information provided by Landsat. The integration of several types of imagery is further stressed by Rib (1966) where an approach for engineering soil mapping was developed using multichannel sensor imagery (with a minimum of seven bands from the ultraviolet to the far-infrared) obtained simultaneously with medium-scale colour aerial photography and, where available, colour infrared photography.

Imagery from SLAR (Side-Looking Airborne Radar) is useful in studying geomorphology as relief is defined clearly by shadow effects. Radar, under certain circumstances, exhibits a degree of penetration through either vegetation or soil cover, therefore, features that cannot be detected by the conventional multi-spectral

satellites may be observed. Soil moisture may be recorded and general information about geological conditions of lithology and structure may thus be identified. For further information on radar remote sensing the reader is referred to the accounts by Kritikos and Shuie (1979) and Trevitt (1986).

Remote sensing also includes panchromatic, colour and infrared aerial photography. Much previous work has involved the use of aerial photographs for geomorphological mapping, and their importance in such work has been adequately demonstrated. Norman et al. (1975) provide an assessment of aerial photographs in landslide recognition. This type of imagery provides greater spatial detail than the satellite imagery and has a major advantage of readily available stereoscopic viewing. This stereoscopic photography allows better interpretation of relief which is essential in geomorphological applications. The French satellite SPOT, which operates in the visible and near-infrared wavelengths like Landsat, is able to provide stereoscopic imagery by looking at the same area of ground on successive orbits. However, this sort of imagery is expensive. As with satellite imagery, additional information can be obtained from infrared aerial photography as explained by Penn (1984). He demonstrates that variations in vegetation and soil moisture are enhanced on a false-colour infrared photograph of the Mam Tor landslides.

This project uses Landsat-5 Thematic Mapper imagery, aerial photography and hand-held infrared photography of the Edale and

Matlock areas of Derbyshire to assess their use in the recognition of potential and actual slope instability and in the study of landsliding in general.

2.2 Introduction to Landsat Imagery in Landslide Studies

The characteristics of the Landsat-5 satellite are set out in Table 2.1. Basically, the Thematic Mapper sensor detects and records electromagnetic radiation reflected (or emitted in the case of the thermal infrared band) from the Earth's surface. Interpretation of this imagery is based on the principle that surface cover can be recognised by its "spectral signature" (Figure 2.1). The wavebands of TM were chosen by NASA to give good spectral resolution in those parts of the spectrum useful in the study of vegetation, and of geology in arid and semi-arid lands. The intended capabilities of each individual waveband are described below so that a rationale can be established for selecting the most appropriate wavebands for the study of slope failure:

Band 1: This band was included on the Thematic Mapper as electromagnetic radiation at these wavelengths can penetrate water to a certain depth, therefore, it is useful for studying sediment load of water bodies. It was also selected with the intention of differentiating between soil and vegetation, and between coniferous and broadleaved trees. Unfortunately, this part of the spectrum is affected by interference from the atmosphere in the form of haze.

TABLE 2.1 LANDSAT-5 THEMATIC MAPPER

ORBIT CHARACTERISTICS:

Height	705 kilometres
Period (time/orbit)	98.9 minutes
Inclination	98.2°
Orbits/day	14.6
Repeat cycle	16 days
Timing	Sun synchronous, 0930 local sun time

THEMATIC MAPPER WAVEBANDS:

Waveband	Wavelengths (μm)	Description	Ground Resolution
1	0.45 - 0.52	visible blue	30m x 30m
2	0.52 - 0.60	visible green	30m x 30m
3	0.63 - 0.69	visible red	30m x 30m
4	0.76 - 0.90	near-infrared	30m x 30m
5	1.55 - 1.75	mid-infrared	30m x 30m
7	2.08 - 2.35	mid-infrared	30m x 30m
6	10.40 - 12.50	thermal infrared	120m x 120m

(N.B. Some texts number the thermal infrared waveband as 7 and the second mid-infrared band as 6.)

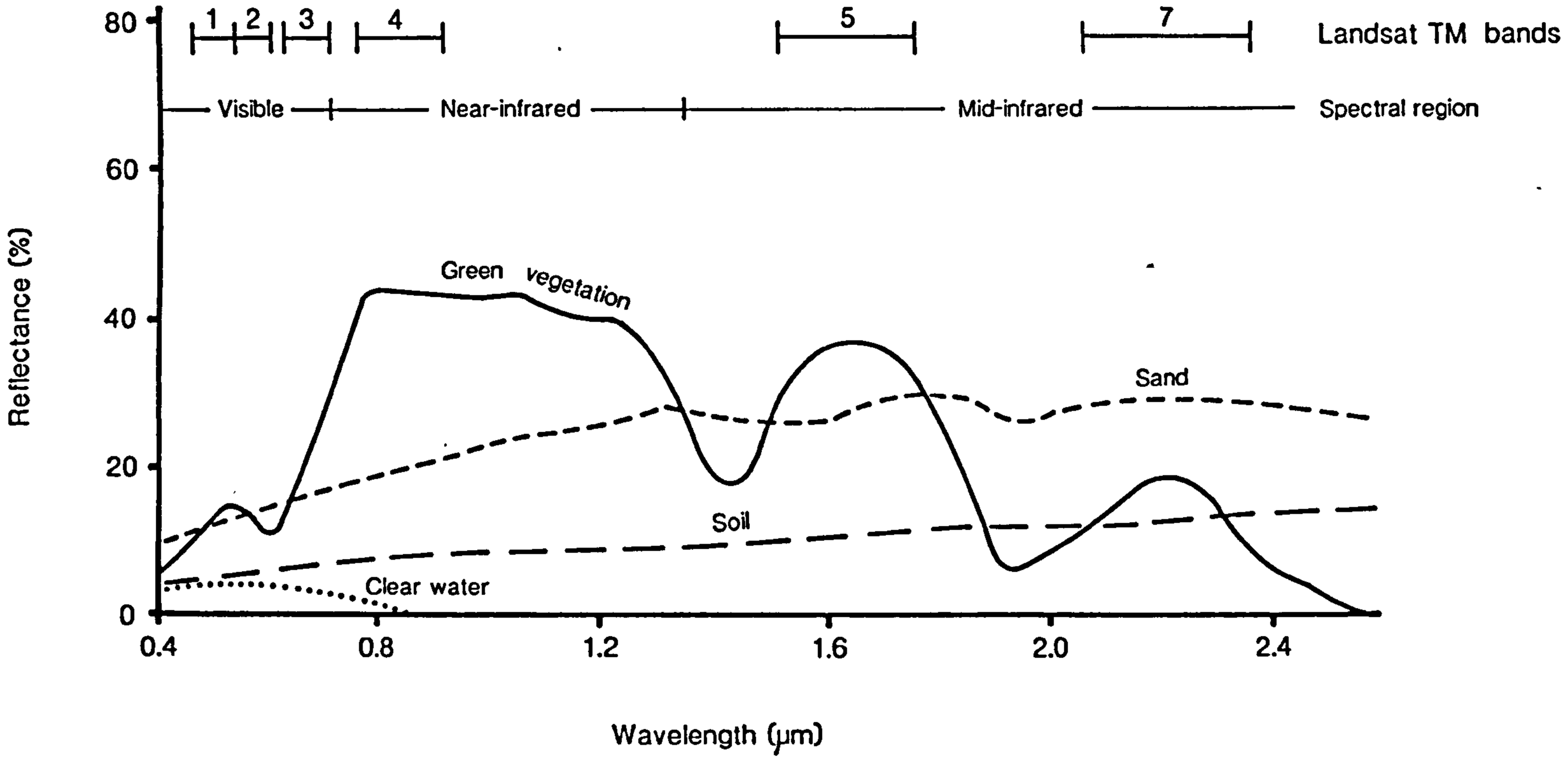

Figure 2.1 Spectral Signatures of Surface Cover Types

Band 2: The visible green reflectance peak of vegetation occurs between 0.52 and 0.60μm and consequently Band 2 aids in vegetation discrimination and in the assessment of vegetation vigour.

Band 3: This is considered to be the most important band for the discrimination of vegetation type due to chlorophyll absorption for photosynthesis; it also emphasises the contrast between vegetated and non-vegetated areas.

Band 4: The near-infrared plateau of reflectance values characteristic of vegetation occurs in Band 4, therefore, this part of the spectrum is useful for the determination of vegetation type. There is also good contrast between soil and vegetation, and between land and water in this waveband.

Band 5: Like Band 4, this band aids in the identification of vegetation type. It also contains information on plant and soil moisture conditions, and was designed with the additional aim of detecting clay-rich areas associated with hydrothermal alteration.

Band 6: This is different from the other bands in that it is not reflected energy being detected but heat emission from the Earth. It has applications in vegetation classification and stress analysis, and in the study of soil moisture variation and other features producing thermal anomalies.

Band 7: Band 7 was included specifically for geological purposes, particularly for the discrimination of rock formations in unvegetated regions. Clay-rich areas associated with hydrothermal alteration zones are also detectable between 2.1 and 2.4μm.

For further information on the principles of remote sensing the interested reader is referred to the textbooks by Curran (1985), Sabins (1987), Siegal and Gillespie (1980) and Townshend (1981).

Although the waveband widths and limits of the Thematic Mapper sensor were chosen mainly for applications in vegetation studies and in geological studies of arid and semi-arid regions, there appears to be much information which can be extracted for geomorphological purposes in temperate climates (e.g. drainage pattern, relief, geology and soil moisture).

The aim of this work is to assess the use of Landsat TM in the direct recognition of landslides and also in the identification of potentially unstable slopes. The latter aim involves the mapping of the distribution of a number of controlling factors on slope stability. Cooke and Doornkamp (1974) have constructed a checklist of such factors which includes conditions of relief (e.g. angle of slope, relative relief), drainage (e.g. seepage flow, pore-water pressure, slope undercutting), bedrock (e.g. strong beds over weak beds, amount of dip, degree of weathering, strength), soils (e.g. depth, shear strength), and the presence of previous landslides and man-made features (e.g. reservoirs, excavations). By mapping the

spatial distribution of these factors they may, in effect, be superimposed to produce a landslide hazard map showing zones of differing degrees of potential instability.

Several such hazard maps have been produced in the past for areas of high landslide risk to aid in land management and planning; the various methods of construction are reviewed by Hansen (1984) and Varnes (1983). The majority of hazard maps use data gathered from field work and aerial photo-interpretation (e.g. Carrara et al., 1978; Hicks and Smith, 1981; Kienholz, 1978; Mahr and Malgot, 1978), whilst the landslide hazard zonation produced by Cross (1987) for Edale in Derbyshire employed data extracted on a grid basis from existing map sources. Although these methods of data collection allow detailed maps to be produced, extensive field work is very time-consuming and is difficult in areas of poor accessibility which tend to have poor map coverage. It is under these conditions that satellite imagery may be of most use, however, the potential of Landsat TM for collecting such data has yet to be assessed. This study aims, therefore, to assess the role of such imagery in landslide hazard assessment.

As little work has been carried out on the use of Landsat imagery in the study of geomorphology, and of landslides in particular, an assessment of the technique must be made and a procedure for its use must be developed before it can be applied to the landslides of the Matlock region. The area around Edale was chosen for this purpose as ground information is readily available and much work has already

been done on slope instability in this part of Derbyshire (e.g. Cross, 1987).

2.3 Landsat-5 TM Imagery of Edale

A scene covering approximately 15km x 15km, centred on the Vale of Edale, was extracted from the Landsat-5 TM image, Path 203 Row 23, taken on 26 April 1984 (Figure 2.2). This area covers part of both the High Peak and the White Peak in which several large landslides and many smaller ones are located.

Descriptions of the individual TM bands of the Edale sub-image are given in Table 2.2. Topographic maps (O.S. 1:50,000 Sheet 110 and 1:10,000 Sheets SK08, 09, 18, 19) and geological maps (Geological Survey Sheet 110) were used as ground information together with field observations and aerial photographs.

The reservoirs, coniferous woodland and moorland are seen to be poor reflectors in all wavebands and thus appear dark; for separate discrimination they need to be studied in a combination of two or more of the infrared bands. The rough grassland tends to be of medium tone, as does the land cover in the valleys and the south, except in Band 4. As stated in Chapter 2.2, Band 4 records the near-infrared reflectance plateau of vegetation (Figure 2.1); the greater the amount of chlorophyll in the leaves the higher the reflectance in the near-infrared. Therefore, the land in the valleys

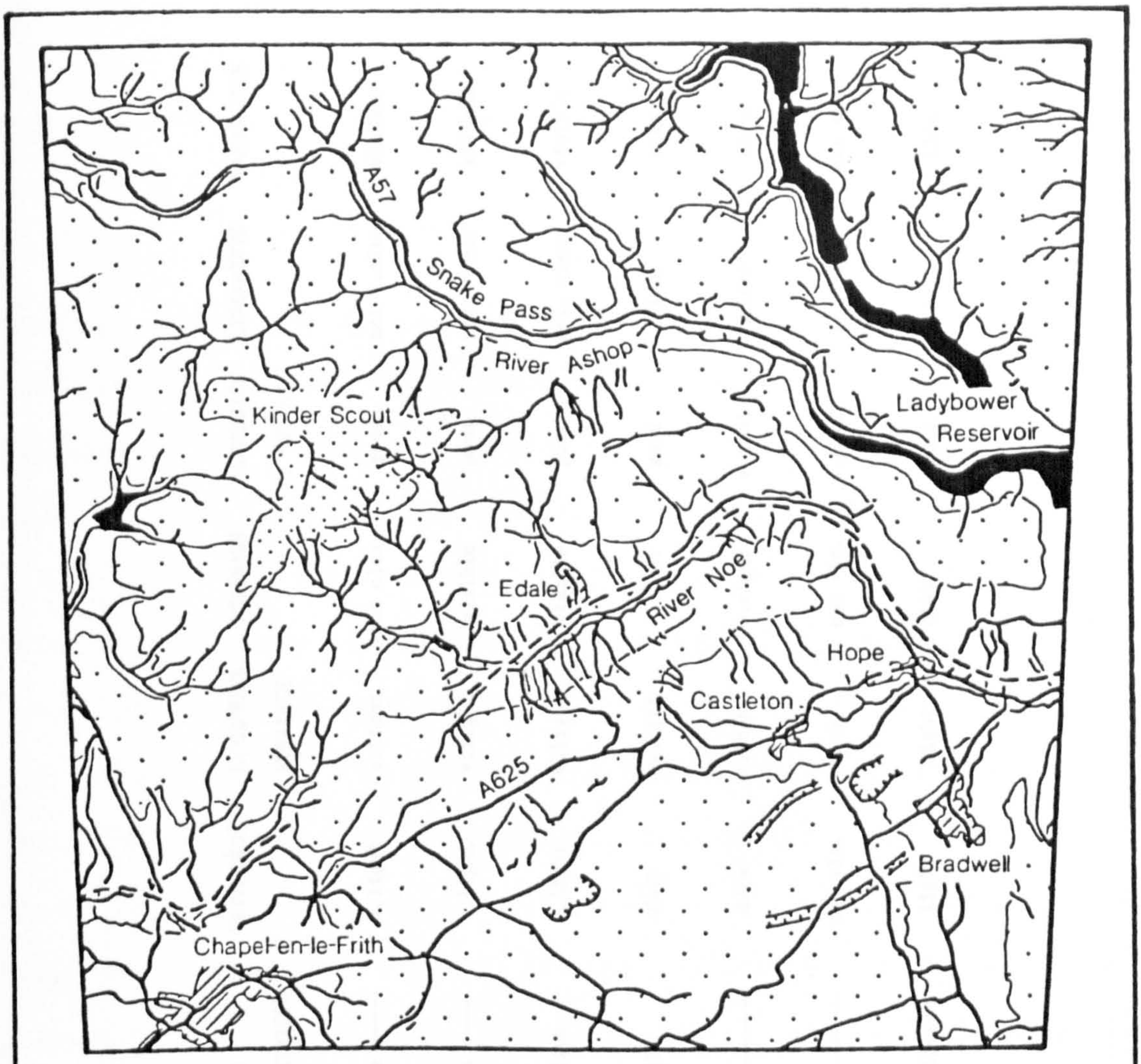

Figure 2.2 The Edale Region

TABLE 2.2 DESCRIPTIONS OF THE MONOCHROME IMAGES OF EDALE

BAND	RESERVOIR	CONIFEROUS WOODLAND	MOORLAND	ROUGH GRASSLAND	LUSH VEGETATION	SETTLEMENT	LIMESTONE WORKINGS	DRAINAGE	IMPRESSION OF RELIEF	LINEAMENTS	LANDSLIDES
1	——v.dark; indistinguishable ——			—— medium tone ——		v.light	v.light	not clear	poor	not v.clear	visible
2	——v.dark; indistinguishable ——			—— medium tone ——		v.light	v.light	visible	poor	rel. clear	visible
3	——v.dark; indistinguishable ——			light	medium	v.light	v.light	visible	poor	rel. clear	visible
4	v.dark	—— dark ——		medium	light	dark	v.light	v.clear	good	clear	clear
5	——v. dark ——		dark	—— medium ——		dark	v.light	v.clear	v.good	clear	clear
6	——v. dark ——		—— medium ——			not vis.	dark	not vis.	v.good	not clear	not vis.
7	——v. dark ——		med/dark	light/med	med/dark	light	light	clear	good	clear	clear

and the south is supporting lusher vegetation than the uplands in the north.

Drainage, lineaments and landslides are most discernible in the near- and mid-infrared; the thermal infrared channel (Band 6) is of little use here as the ground resolution is too coarse at a pixel size of 120m x 120m. The best impressions of relief are obtained in the infrared part of the spectrum, particularly in the thermal infrared. This is due to the fact that the electromagnetic energy recorded in Band 6 is heat emission from the Earth; as the image was taken at approximately 0930 local sun time the sun is shining on the south and east facing slopes and therefore, these slopes are warmer than those facing north and west. This results in a shading of the image according to slope and aspect. If the effect of relief was to be removed the remaining variations would be due to differences in vegetation, soil moisture, water bodies and possibly geology.

Similarly, descriptions of three false-colour composite images are given in Table 2.3. Plate 2.1 is a composite of the three visible Bands 3, 2 and 1 displayed in red, green and blue respectively. This image is much easier to interpret in terms of land cover than any individual band as it is a "true-colour" image; it is not difficult to perceive the green area as grassland and the brown as moorland. However, more information is contained in the infrared and a composite image of Bands 5, 4 and 1 (Plate 2.2) enables better discrimination between vegetation types. More detail is also apparent on the Kinder plateau, possibly as a result of variations in

TABLE 2.3 DESCRIPTIONS OF THE FALSE-COLOUR COMPOSITE IMAGES OF EDALE

FCC	RESERVOIR	CONIFEROUS WOODLAND	MOORLAND	ROUGH GRASSLAND	LUSH VEGETATION	SETTLEMENT	LIMESTONE WORKINGS	DRAINAGE	IMPRESSION OF RELIEF	LINEAMENTS	LANDSLIDES
3,2,1 (Plate 2.1)	v.dark	v.dark green	brown	light brown	green	white	white	rel. clear	rel. good	clear	clear
5,4,1 (Plate 2.2)	dark	dark green	brown/red	pink/brown	bright green	purple	pink	v. clear	v. good	clear	clear
6,5,3 (Plate 2.3)	dark	dark brown	red	blue	green	pink	blue	clear	excellent	clear	clear

PLATE 2.1 LANDSAT TM IMAGE (BANDS 3, 2 AND 1)

OF THE EDALE REGION

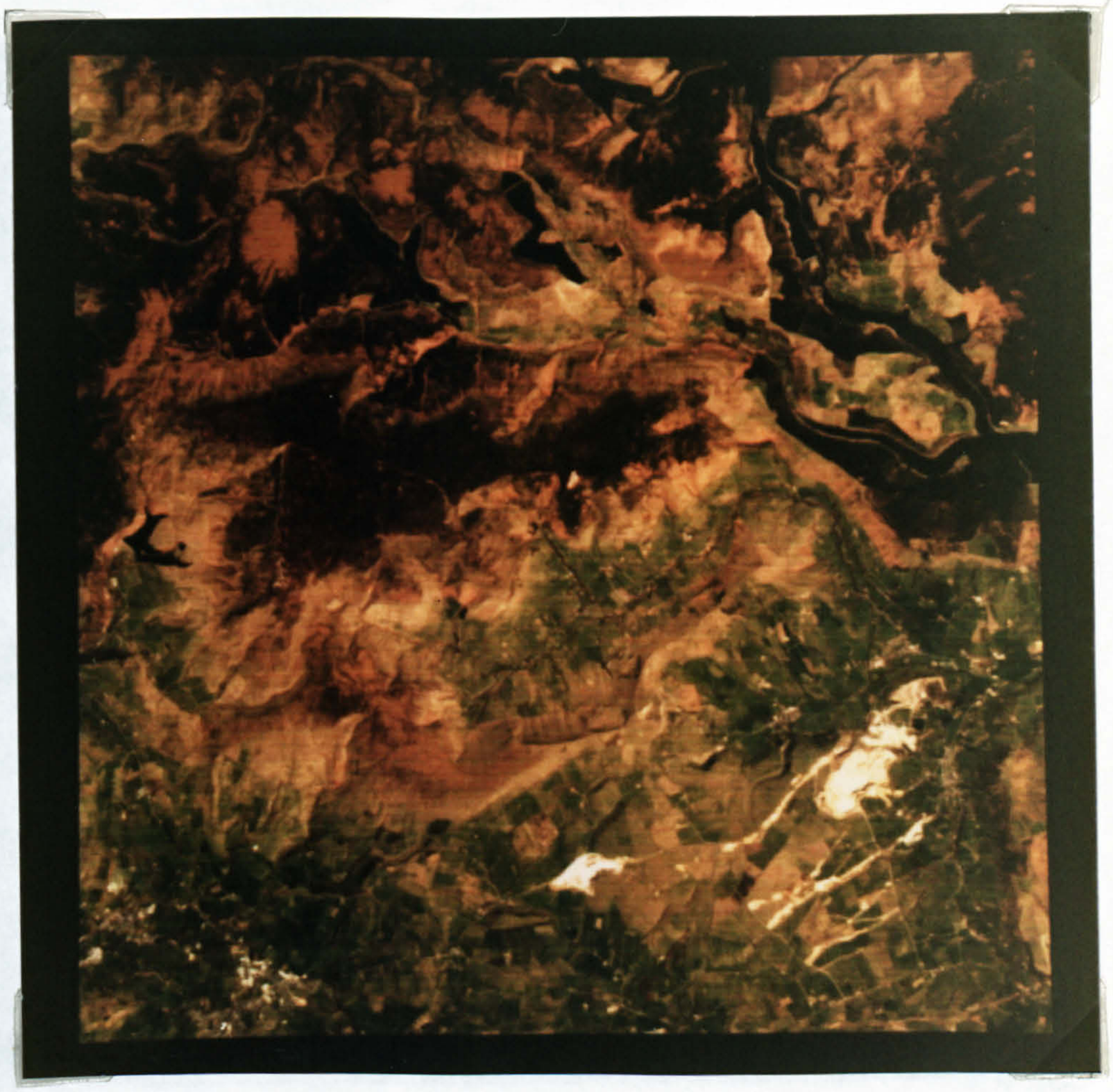

False Colour Composite 3,2,1

Sampling rate: 1,1

Image Processing: Linear Contrast Stretch

Band 3 = red ; limits of 15-150 (forward)

Band 2 = green ; limits of 10-120 (forward)

Band 1 = blue ; limits of 50-130 (forward)

PLATE 2.2 LANDSAT TM IMAGE (BANDS 5, 4 AND 1)

OF THE EDALE REGION

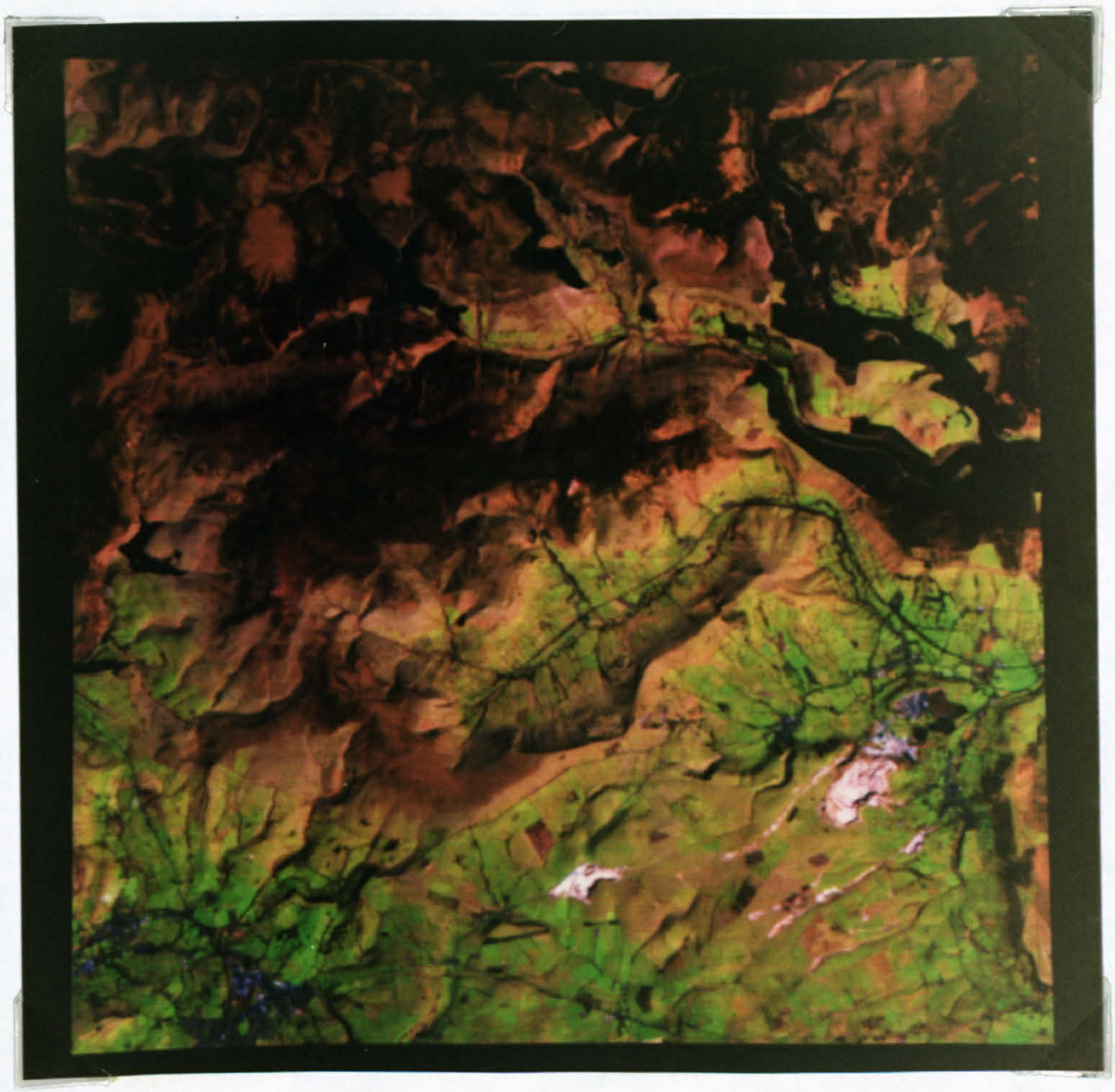

False Colour Composite 5,4,1

Sampling rate: 1,1

Image Processing: Linear Contrast Stretch

Band 5 = red ; limits of 15-150 (forward)

Band 4 = green ; limits of 10-120 (forward)

Band 1 = blue ; limits of 50-130 (forward)

PLATE 2.3 LANDSAT TM IMAGE (BANDS 6, 5 AND 3)

OF THE EDALE REGION

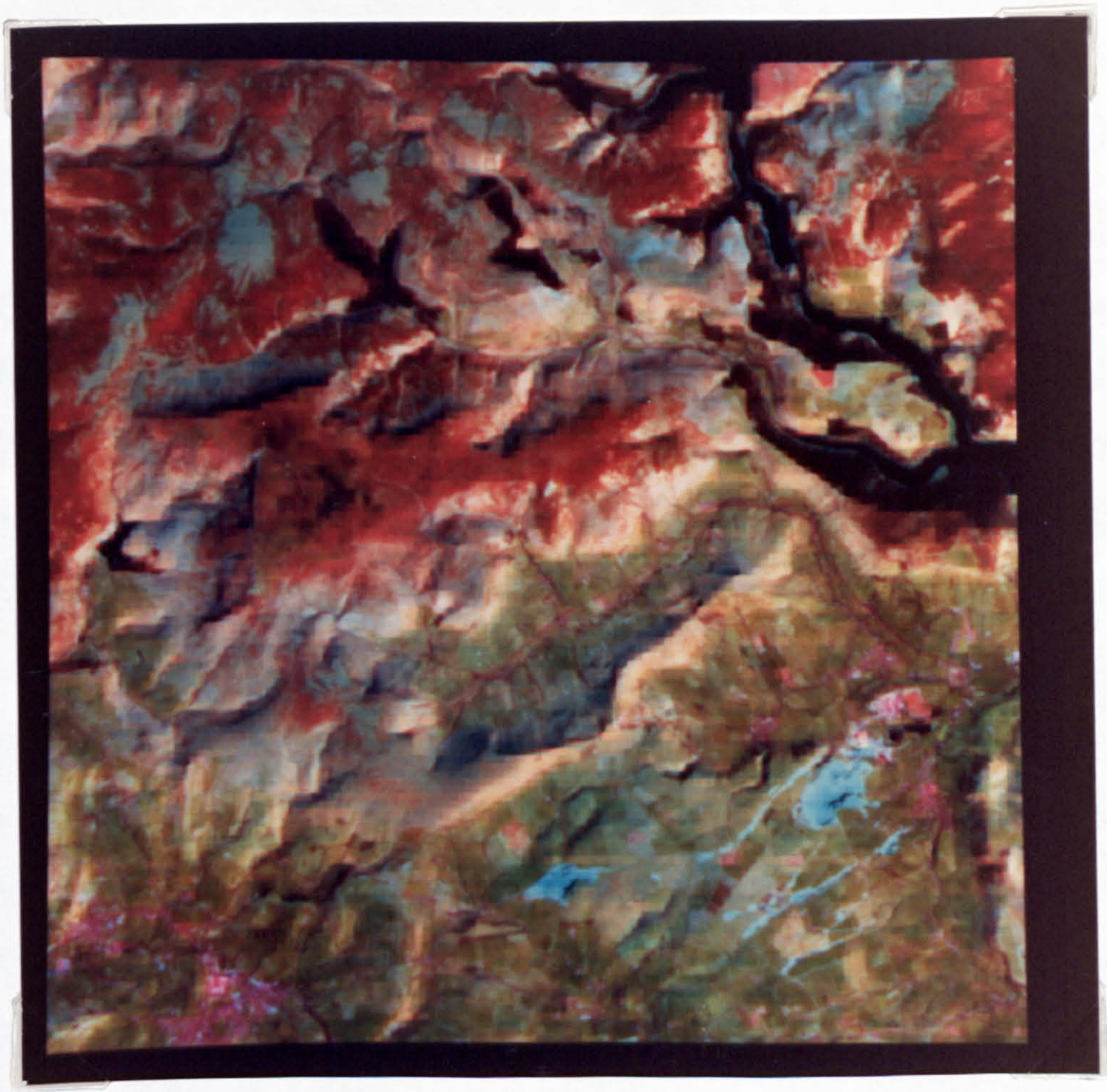

False Colour Composite 6,5,3

Sampling rate: 1,1

Image Processing: Linear Contrast Stretch

Band 6 = red ; limits of 15-150 (forward)

Band 5 = green ; limits of 10-120 (forward)

Band 3 = blue ; limits of 50-130 (forward)

soil moisture content or moorland plant species. The inclusion of the thermal infrared band in Plate 2.3 enhances the impression of relief due to differential solar heating and shadowing as described above.

2.4 Interpretation of the Landsat Images

To assess the use of Landsat imagery in the recognition of potential and actual landslides it is necessary to produce an interpretation of the image with respect to the controlling factors on slope instability. Of the factors listed by Cooke and Doornkamp (1974) Landsat TM imagery may yield information on (i) relief: slope steepness, cliffs, valley-side shape; (ii) drainage: drainage density, slope undercutting, standing water; (iii) bedrock: strong beds over weak beds, jointing; (iv) legacies from the past: fossil solifluction lobes and sheets, previous landslides; and (v) man-made features: excavations, reservoirs, drainage diversions, loading of valley sides. The spatial distribution of these factors may then be combined to produce a landslide hazard map.

The first stage in developing a landslide hazard zonation from TM imagery must start with the visual interpretation of the individual bands and false-colour composite images. The only image processing required for this purpose is contrast enhancement (linear contrast stretch), then the images may be used in the same manner as aerial photographs, although stereoscopic viewing is not possible. The optimal band, or combination of bands, to use is determined by the

characteristic spectral response of the feature being studied. (For example, Tables 2.2 and 2.3 show that to distinguish coniferous woodland from reservoirs Band 4 should be used, and that the mid-infrared channels discriminate between coniferous woodland and moorland; from this it follows that a false-colour composite image such as that of Bands 5, 4 and 1 will separate all three land cover types). Table 2.4 shows the bands that were found to be best suited for studying the factors contributing to slope instability which may be detected on Landsat imagery.

Other methods of image processing were investigated, however, most were found to reduce the impression of relief. This feature aids in the recognition of drainage, slopes, lithology and landslides and consequently, it is desirable that any image enhancement or transformation should increase the appearance of relief. Donker and Meijerink (1977) and Doornkamp (pers. comm.) recommend the use of a principal component analysis transformation to produce a maximum impression of terrain ruggedness; this was not evident when applied to the Edale image which, fortunately, already exhibits good relief detail through Bands 5 and 6 (Table 2.4). The only advantage of a more processed image for this study appears to be in the recognition of drainage. This was achieved by the use of a Laplacian filter, an edge enhancement technique, whereby the image is "sharpened" by emphasising boundaries between different ground features. By this means, the edge between the river and the adjacent land becomes clearer. However, taking into account the success with which the drainage pattern was defined from the unfiltered Edale image (see

TABLE 2.4 OPTIMAL BANDS FOR THE INTERPRETATION OF THE EDALE IMAGES

FEATURE	MONOCHROME	FALSE-COLOUR COMPOSITE
Relief	5 ; 6	5,4,1 ; 6,5,3
Drainage	4 ; 5	5,4,1 ; 6,5,3
Geology:		
Lithology	4 ; 6	5,4,1 ; 6,5,3
Lineaments	4 ; 5 ; 7	5,4,1 ; 6,5,3
Vegetation		5,4,1 ; 6,5,3
Soil Moisture	4 ; 5 ; 6 ; 7	
Landslides	4 ; 5; 7	3,2,1 ; 5,4,1 ; 6,5,3

Chapter 2.4.2) the extra time and effort involved, in this particular case, was considered not worthwhile.

Essentially, most processing techniques create an artificial-looking picture and so, as interpretation of landforms is most simply achieved via visual interpretation, it is this author's opinion that the Landsat imagery should be used in the least processed and, therefore, "natural-looking" form as possible for the study of landforms.

2.4.1 Relief

Relief is an important control on slope instability. Obviously, the greater the angle of slope the greater the potential for instability. Slope form may also need to be considered as, according to Cooke and Doornkamp (1974), coves may be more susceptible to landsliding than straight slopes which in turn may be more susceptible than spurs.

Slope geometry may be assessed to a certain extent from TM imagery. The images of most use are those that give the best visual impression of relief (Table 2.4). Valley slopes can be distinguished from the flatter land of plateaus and valley floors, and coves and spurs can be identified (Figure 2.3) due to shading and highlighting by the sun. It is not possible to measure slope angle from the imagery but it is apparent that the slopes identified are greater than 15° (Cross, pers. comm.).

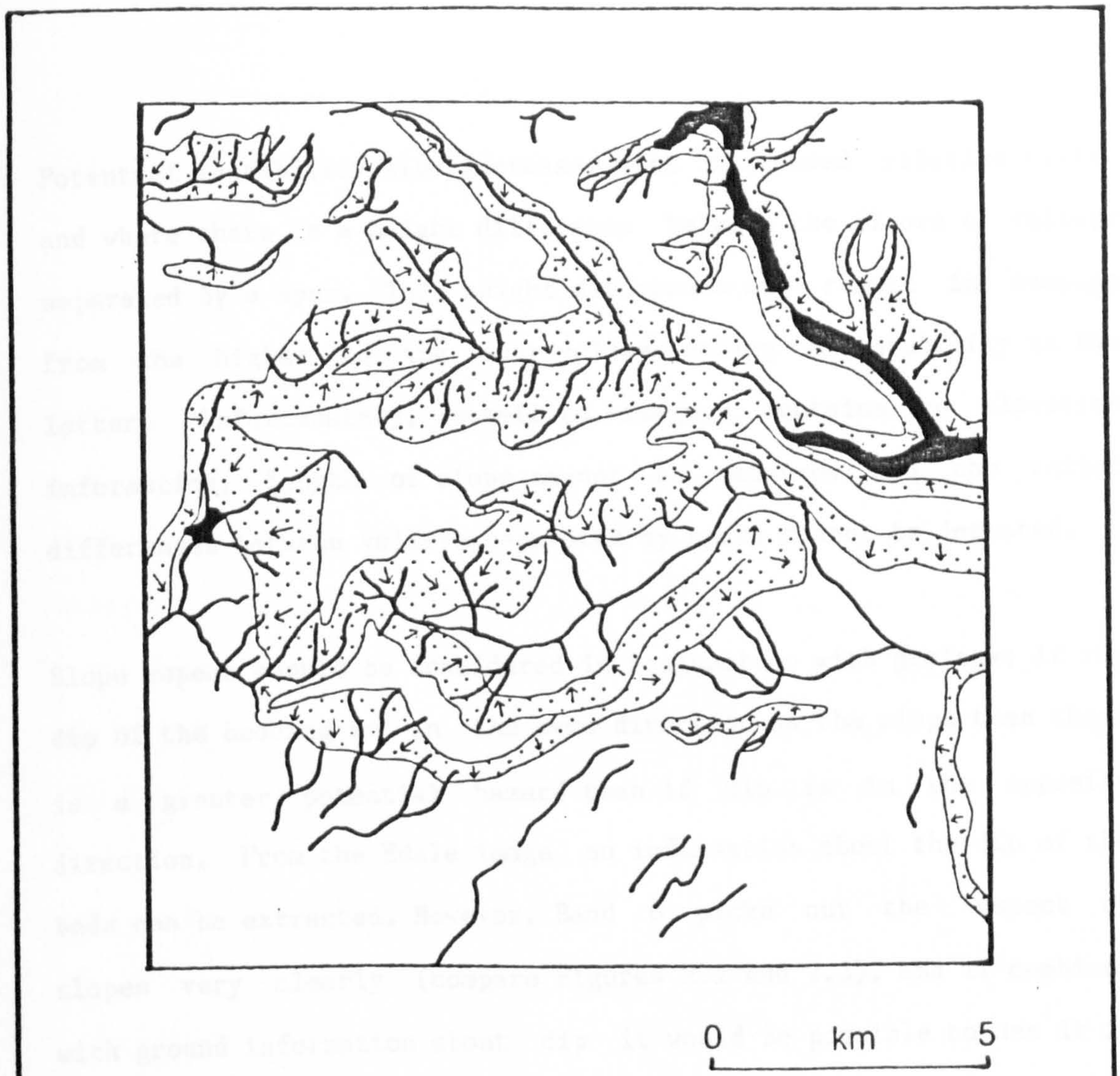

Figure 2.3 Relief and Drainage of the Edale Region
- derived from Landsat TM imagery

Potential instability also increases with increased relative relief and where there is a height difference between the floors of valleys separated by a spur. This height difference may result in seepage from the higher to the lower valley leading to instability in the latter. Unfortunately, satellite imagery contains no elevation information, length of slope cannot be measured and the relief differences between valleys separated by spurs cannot be detected.

Slope aspect should be considered in conjunction with geology; if the dip of the bedding is in the same direction as the slope then there is a greater potential hazard than if dip is in the opposite direction. From the Edale image no information about the dip of the beds can be extracted. However, Band 6 picks out the aspect of slopes very clearly (compare Figures 2.2 and 2.3), and if combined with ground information about dip it would be possible to use it in hazard zoning, although if such information about dip is available then ground information about slope aspect is also likely to be at hand.

2.4.2 Drainage

The presence of a stream will contribute to potential instability as streams may undercut slopes thus removing support and leading to sliding. The near- and mid-infrared channels are the most useful bands as this part of the spectrum contains hydrographic

information, and the impression of relief is also good, therefore, valleys are easily recognised (Table 2.4).

Figure 2.3 shows the drainage pattern derived from the images. There are many features such as roads, railways and ridges which appear similar to rivers, but a comparison with other bands may show that they have a different spectral signature to water and can in this manner be dismissed. For example, although the river of the Edale Valley is visible in Band 2, the railway (the smooth dark line in Bands 4 and 5) does not show up. Rivers may be distinguished from ridges on the false-colour composite image of Bands 6, 5 and 3 as the slopes on the southeast side of rivers are in shadow and those on the northwest side are highlighted, and vice versa for slopes on either side of a ridge (Figure 2.4).

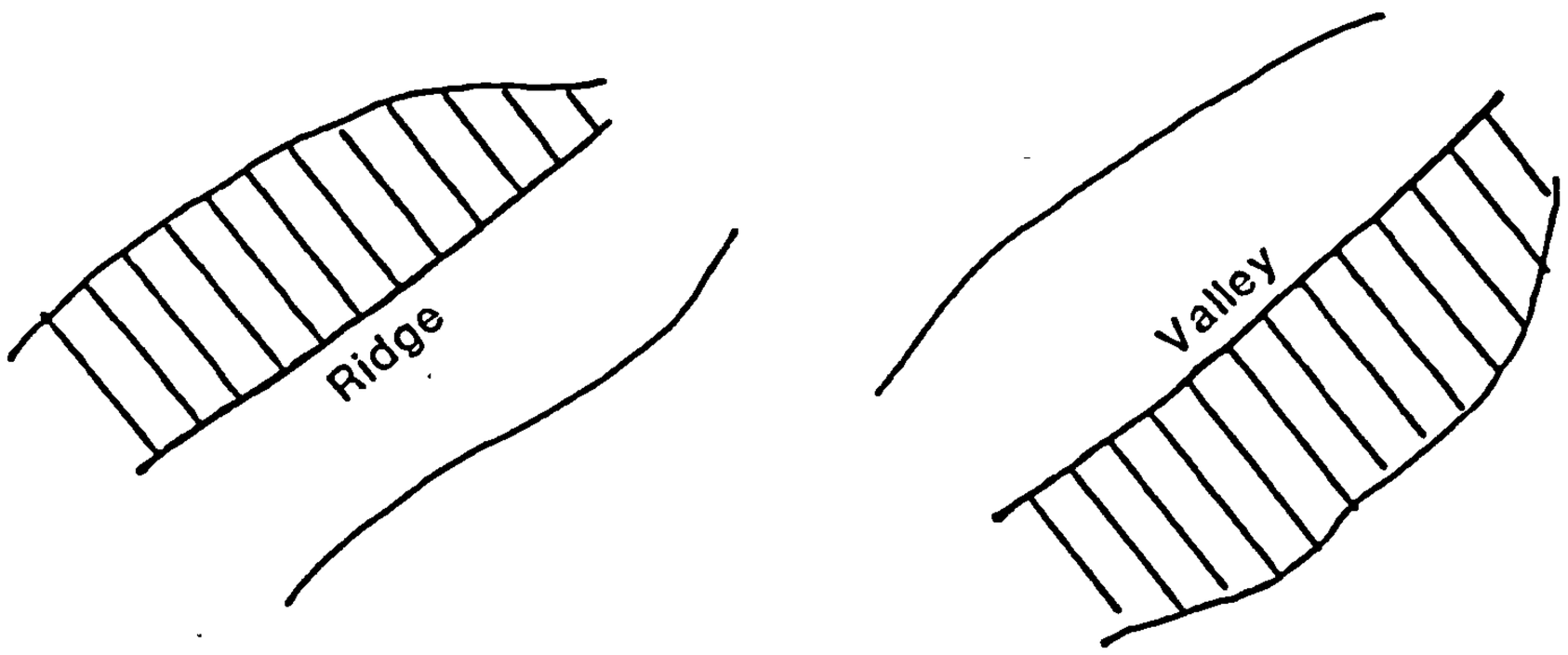

FIGURE 2.4: SLOPE ASPECT

On the Edale image most of the main streams were identified (compare Figures 2.2 and 2.3). Dry valleys were also identified as one of the criteria used in recognising the drainage network is relief. The presence of reservoirs may also contribute to potential

instability by raising the water table. Reservoirs are easily identified on this image.

Drainage pattern and density can also be used to infer lithology and to detect lineaments, this is discussed with the interpretation of geology.

2.4.3 Geology

The main geological points of interest in relation to slope instability are lithology and structure. Landslides are more likely to occur in weak beds, such as shale, clay and highly-weathered rock, than in competent beds, such as granite and sandstone. Densely-jointed and fractured rock will be weaker than massive sparsely-jointed and unfractured beds, and beds dipping "out of the slope" (where the bedding plane daylights on the slope) are also more susceptible to landsliding. Instability is also higher where massive competent beds overly weak incompetent beds.

Rock types may be identified from remotely-sensed multispectral imagery as they have different bidirectional reflectance spectra resulting from their differing compositions (Hunt and Salisbury, 1971, 1976). An overview of the use of Landsat MSS imagery in geological studies is provided by Goetz et al. (1983). However, both MSS and TM imagery predominantly record the reflectance from vegetation, so little information is directly recorded about

lithology in a vegetated area except where isolated outcrops occur. Siegal and Goetz (1977) considered the effects of vegetation on the discrimination of rock and soil type from Landsat MSS imagery and concluded that the most diagnostic images of the spectral response of the ground involve the ratios of Bands 4/5 and 6/7 as these ratios are least affected by vegetation. The equivalent TM ratio, 2/3, did not yield any information on rock type when applied to the Edale images. Drury (1986) suggests that for vegetated regions the best Landsat TM images to use are those of Band 5 taken early in the growing season. Furthermore, he recommends the use of spatial filtering techniques to enhance geological structures. Again, such imagery of Edale was not found to yield more geological information than the contrast enhanced images recommended in Table 2.4.

In the area of the Edale image outcrops of rock are known to occur in the southeast as limestone quarries and rakes, on the backscars of several landslides such as Mam Tor and on many of the upper slopes surrounding the Kinder plateau. A comparison of the false-colour composite images shown in Plates 2.1, 2.2, and 2.3 reveals that the bedrock of Mam Tor has a different spectral signature from that of the limestone (Table 2.5), therefore, it can be assumed that it is of different lithology. The response of the Mam Tor rock in the false-colour composite image of Bands 6, 5 and 3 is similar to that of the shale quarry, and geology maps show that the Mam Tor rock is interbedded sandstone and shale. However, this is the only false-colour composite image presented here that displays this, and therefore, further information from other bands is

required.

	FALSE-COLOUR COMPOSITE		
	3,2,1	5,4,1	6,5,3
Mam Tor	white	purple	pink
Limestone	white	pink	blue

TABLE 2.5 SPECTRAL SIGNATURES OF BEDROCK ON THE EDALE IMAGES

Some lithological inferences can be made from the Edale images by studying surface expression. From field work in the Ashover and Middleton areas of Derbyshire where the rocks are similar, it was noted that vegetational differences reflected underlying lithological differences. In general, heather and moorland vegetation grow on the sandstone, and grass on the shale and limestone. This relationship also holds for the Edale area. Table 2.4 shows that the best images presented in this study for discriminating between vegetation types are the false-colour composites of Bands 5, 4 and 1 and 6, 5 and 3 (Plates 2.2 and 2.3). Table 2.3 contains the descriptions of these images. It should be noted that the change of vegetation on the sandstone and shale slopes at a height of about 1,000 feet is largely a result of farming practice rather than geology. The lower slopes have been improved by the application of lime and fertilizers and by improved drainage and controlled grazing.

Lithology also influences relief through bedding, jointing and resistance to erosion. For example, approximately horizontal beds form

the Kinder plateau. In Ashover and Middleton it was noted that the junction between the sandstones and the shales was marked by a change in slope gradient and by the presence of surface water on the shales, and in temperate climates limestone is generally characterised by gently-rolling relief with solution features.

Drainage pattern may also reflect lithology. Figure 2.2 shows drainage identified from the image. The dendritic pattern is characteristic of the sandstone and shale, whereas the sparse, intermittent pattern in the southeast suggests the presence of limestone with its greater permeability. The drainage lines in the limestone are, in fact, dry valleys although this cannot be determined from the image.

A geology map (Figure 2.5) has been constructed by the visual interpretation of the images which best show relief, drainage and vegetation. It is quite similar to the Geological Survey 1:50,000 geology map of this region (Figure 2.6). The main difference occurs in the west where sandstone forms lower ground which has been interpreted from the imagery as shale. The presence of drift may mask the solid geology; its detection is also important as landslides may occur in this material. However, drift cannot be identified from these images.

Geological structure also plays an important role in the stability of rock slopes; faults, joints and bedding planes can provide planes of weakness along which slope failure may occur. The presence of these

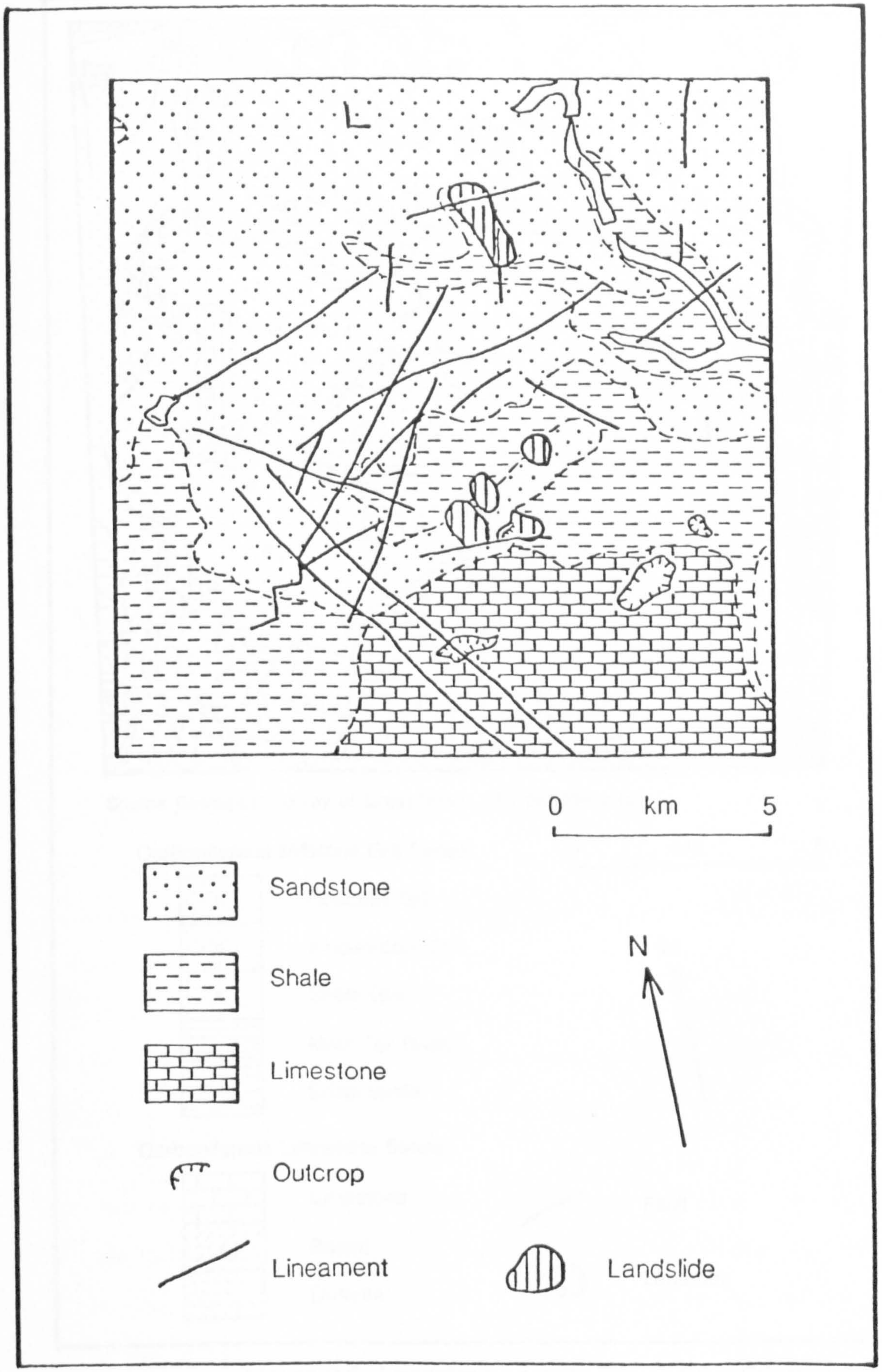

Figure 2.5 Landslides and Geology of the Edale Region - derived from Landsat TM imagery

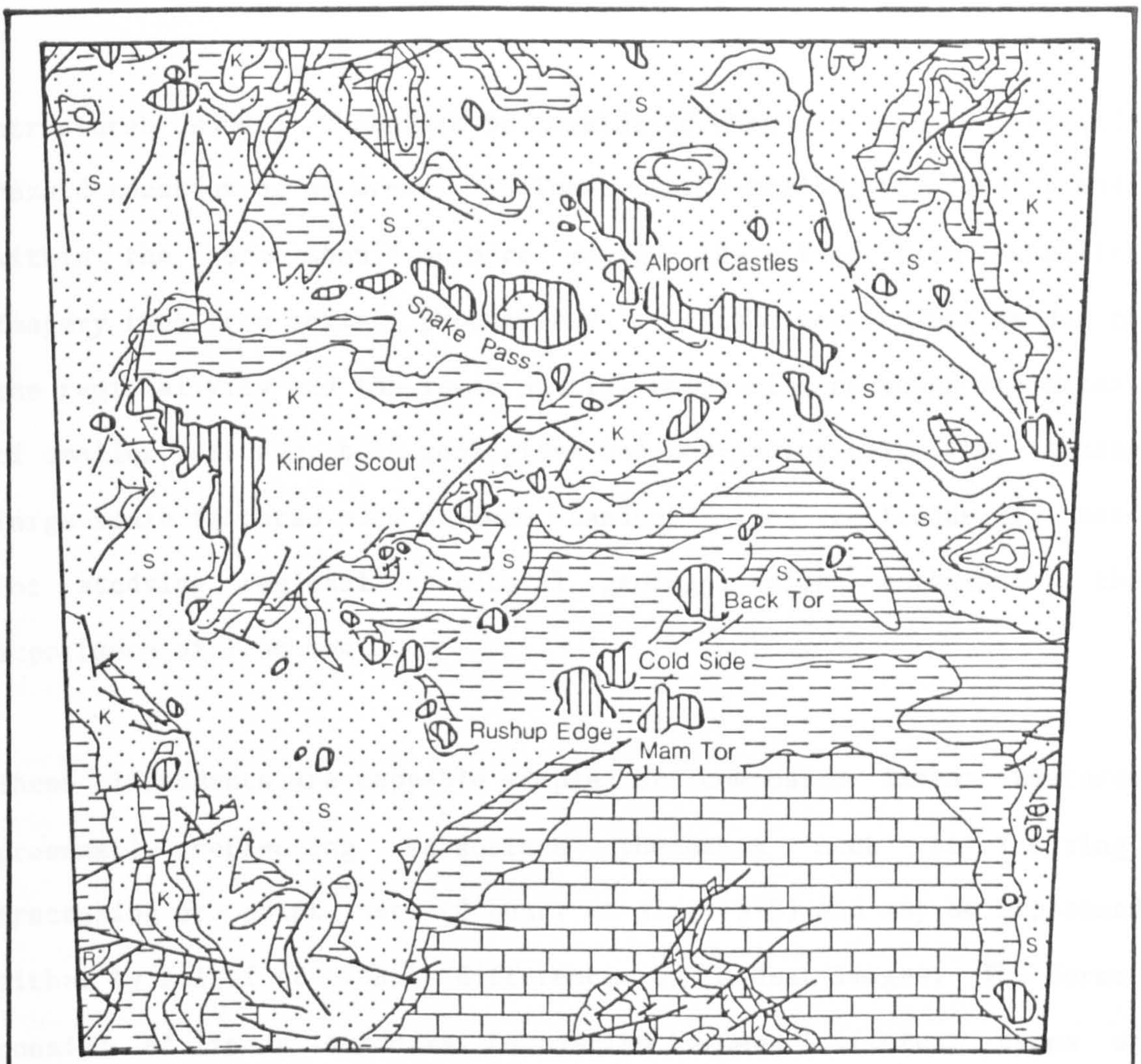

Source: Geological Survey of Great Britain 1:50 000 Sheet 99

Figure 2.6 Landslides and Geology of the Edale Region

structures should therefore be considered when producing a landslide hazard zonation of an area. Dominant (large-scale) structural trends within the rock should be more easily identified from satellite imagery than from aerial photographs or field work. This is due to the regional view and the lower spatial resolution reducing the detail of smaller features, both geological and non-geological, thus making large-scale features more obvious. Landsat images are frequently used for studying regional structural geology, often emphasising the importance of lineaments.

These lineaments are mappable simple or composite linear features presumably reflecting subsurface phenomena such as faulting, fracturing or joint sets (O'Leary et al., 1976) and may be expressed either by relief or tonal differences on Landsat images. The former consist of linear landforms, boundaries between different types of terrain and breaks within a uniform terrain; for example fault scarps, straight valleys and river courses. Tonal lineaments are recognised as either straight boundaries between areas of contrasting tone or as a line of contrasting tone to the background; for example, differences in rock, soil and vegetation type and varying moisture content. Simple lineaments consist of one of the features described above; composite lineaments are made up of several of these features.

Lineaments expressed by features of relief such as valleys may either be enhanced or suppressed on Landsat images according to their orientation with respect to the sun azimuth; as Landsat images are taken at approximately 0930 local sun time the sun is in the

southeast, therefore valleys trending northeast to southwest will be enhanced by shadows and highlights, but those trending northwest to southeast will be harder to detect.

The best bands for detecting lineaments are those in the near- and mid-infrared (Table 2.4). In previous studies Landsat MSS Band 7 (equivalent to TM Band 4) has been used. This is likely to be due to the fact that lineaments may be defined by water, either in the form of rivers or increased soil moisture associated with faults, fractures or joints. Water has low reflectance in the near-infrared and so shows up as dark-toned on images of this part of the spectrum. Linear man-made features such as roads, railways and pipelines also have low spectral responses in the infrared and may, therefore, be mistaken for lineaments. However, roads and railways can be eliminated with reference to maps, if available. Attempts at enhancement of the lineaments on the Edale image by edge enhancement and other methods of image processing where not successful as they appeared to increase the complexity of the images and suppress the impression of relief.

The majority of the lineaments on the Edale image are composite, mainly aligned valley segments and tonal features. They are shown on Figure 2.7 which should be used with Plates 2.1 to 2.3. By overlaying Figures 2.7 and 2.8 it can be seen that some landslides coincide with lineaments. This may be due to a concentration of moisture along these lines and may thus indicate saturated zones, possibly with high pore-water pressures, contributing to instability; these lineaments may also be zones of weakness through fracturing. These hypotheses need

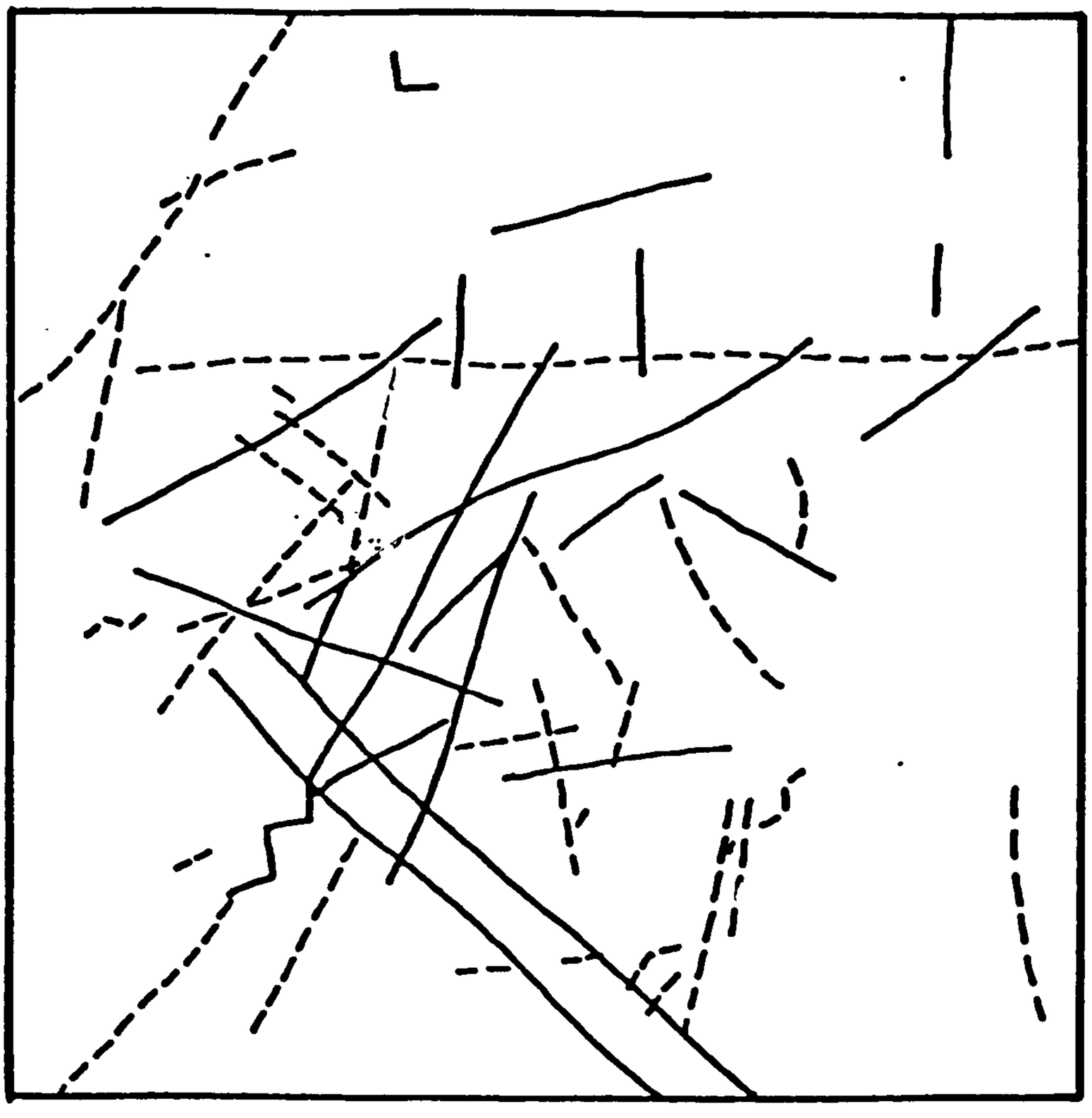

Figure 2.7

to be tested, but if this association is shown to exist, then the presence of lineaments contributing to slope instability would provide a new contributary explanation for the location of some of the landslides in the Peak District of Derbyshire. Therefore, the significance of lineaments on landsliding will be considered in more detail in Chapter 3.

2.4.4 Soil Moisture

High pore-water pressures are a major factor in the initiation of some forms of landsliding. Although this parameter cannot be measured from satellite imagery, it may be possible to use soil moisture as a surrogate. The wavebands of most use in this case are in the infrared; in unvegetated areas damp soil will appear darker than dry soil as it has a lower reflectance. However, vegetation masks this response although vegetation type and vigour may be related to soil moisture content.

It has already been suggested that water is concentrated along the zones of weakness of lineaments thus increasing slope instability and this will be considered in Chapter 3.

Band 6 is likely to contain most information about ground moisture conditions. Damp ground is cooler than dry ground due to the cooling effect as absorbed water evaporates (Sabins, 1987), therefore, on thermal infrared imagery it should show up as a dark tone. However,

the temperature difference between the ground and water vary with season. For example, during the winter seepages and springs issuing from the warmer, deep ground will be represented as warm points against the cold ground, whereas during the summer the ground will be warmer than the issuing ground water (Sowers and Royster, 1978). Night-time (or pre-dawn) imagery is of most use as differential solar heating and shadowing on daytime imagery such as Landsat TM causes the effects of relief to dominate. Other types of remote sensor than Landsat are, therefore, better suited to the measurement of soil moisture. For example, airborne thermal inertia imagery may be used to identify areas of greater moisture concentration, springs, seepages and other water features (Townshend, 1981) which may prove to be sites of potential slope instability.

Pre-dawn airborne thermal infrared imagery was used successfully to identify seepage zones, water saturated soils, standing water and run-off conditions on the catastrophic landslide at St.-Jean-Vianney in Canada which occurred on 4 May 1971 (Tanguay and Chagnon, 1972). Used in conjunction with black and white infrared aerial photographs this thermal infrared imagery also provided information for a drilling programme and proved useful in monitoring the mudflow through repetitive coverage.

Thermal infrared imagery is also being used by Elkington and Hogg (1981) and Gurney (1979) to develop a digital model for estimating soil moisture content and daily evaporation with the aim of using the model on data from the Heat Capacity Mapping Mission for the U.K.

Radar imagery may also be of use in measuring soil moisture due to the limited amount of penetration of microwaves into the ground thus recording information about the ground conditions. However, information on soil moisture from remotely-sensed data is difficult to isolate (Idso et al., 1975) and therefore, information on soil moisture conditions remains limited.

2.4.5 Evidence of Instability

Landslides are generally identifiable as a result of their anomalous character with respect to the surrounding conditions. The features which may thus be detected are morphology, drainage, and vegetation (Crozier, 1984).

Morphology will vary according to the type of landslide. On Landsat TM imagery, with a ground resolution of 30m x 30m and lack of stereoscopic viewing, the landslides which may be detected due to their form are likely to be large and to have strong morphological expression. For example, a deep-seated rotational landslide is more likely to be observed than a mudflow with a narrow track and relatively smooth surface form.

Landslides cause anomalies in the drainage system: undrained depressions and ponds elongated parallel to the slope contours may occur on the slopes, while deposition in stream valleys may result in "pushing" the river course away from that slope and around the toe of

the landslide, or it may result in constriction or even the impounding of lakes. Again, due to the coarse ground resolution of Landsat TM relative to the area of a single landslide, drainage within landslides is unlikely to be detected; however, the infrared channels may pick out both the concentration of soil moisture and the presence of water in depressions.

Vegetation has been used as an indicator of landslide type, degree of activity, and age and in the identification of the component parts of landslides; vegetation may also indicate the presence of certain clay minerals which promote instability (Crozier, 1984). Light-tolerant and fast growing species may occur on unstable ground and in areas with disrupted drainage. Scars are likely to be characterised by shallow-rooting, drought-tolerant plants, and the foot of the slide may support deeper-rooting, moisture-tolerant vegetation. However, after a certain period of time the evidence of vegetation disturbance will be removed by succession. These vegetational differences might be detectable on imagery provided the resolution is high enough and the differences are marked.

The false-colour composite image of Bands 3, 2 and 1 of Edale (Plate 2.1) was initially studied for evidence of landsliding as being "true-colour" it is the easiest to comprehend. There are at least 130 landslides within the area of this image, only five of which can be recognised from the Landsat images. Bands 4, 5 and 7 are the best individual bands for identifying landslides and all three of the false-colour composite images are good with respect to the five

identifiable landslides (Table 2.4). Figure 2.8 can be overlain on the images in Plates 2.1 to 2.3 to show the location of the detected and undetected landslides. The smallest landslide detected is approximately 0.25km^2, there are several undetected landslides larger than this and therefore, it would appear that size is not the only factor influencing the chances of recognition (this will be considered in greater detail in Chapter 4).

Plate 2.4 is a zoomed image of the landslides around Mam Tor; Figure 2.9 should be overlain on this image to locate the landslides. The three landslides on the north-facing slope of the Mam Tor ridge - Rushup Edge, Cold Side and Back Tor landslides - all appear to be discernible as a result of shadow enhancing morphology. The exposed rock of the backscar of the Mam Tor landslide can be identified on Plate 2.4 as a purple band. The road is also purple but the upper part of it is wider and is probably due to the presence of another scar.

Variations in spectral response are also visible within the Mam Tor landslide. In both the false-colour composite images of Bands 5, 4 and 1 and 3, 2 and 1 the toe to the east of the lower part of the road is pink-toned, while the rest is of varying shades of green (not including the scars). This may be due to differences in vegetation and from field work it can be confirmed that the foot of the landslide is vegetated by bracken and deciduous trees and the slump blocks by grass. The lower limit of both the Mam Tor and Rushup Edge landslides are visible due to a change of colour from the pink or brown of the

Figure 2.8

PLATE 2.4 LANDSAT TM IMAGE (BANDS 5, 4 AND 1)

OF THE EDALE VALLEY

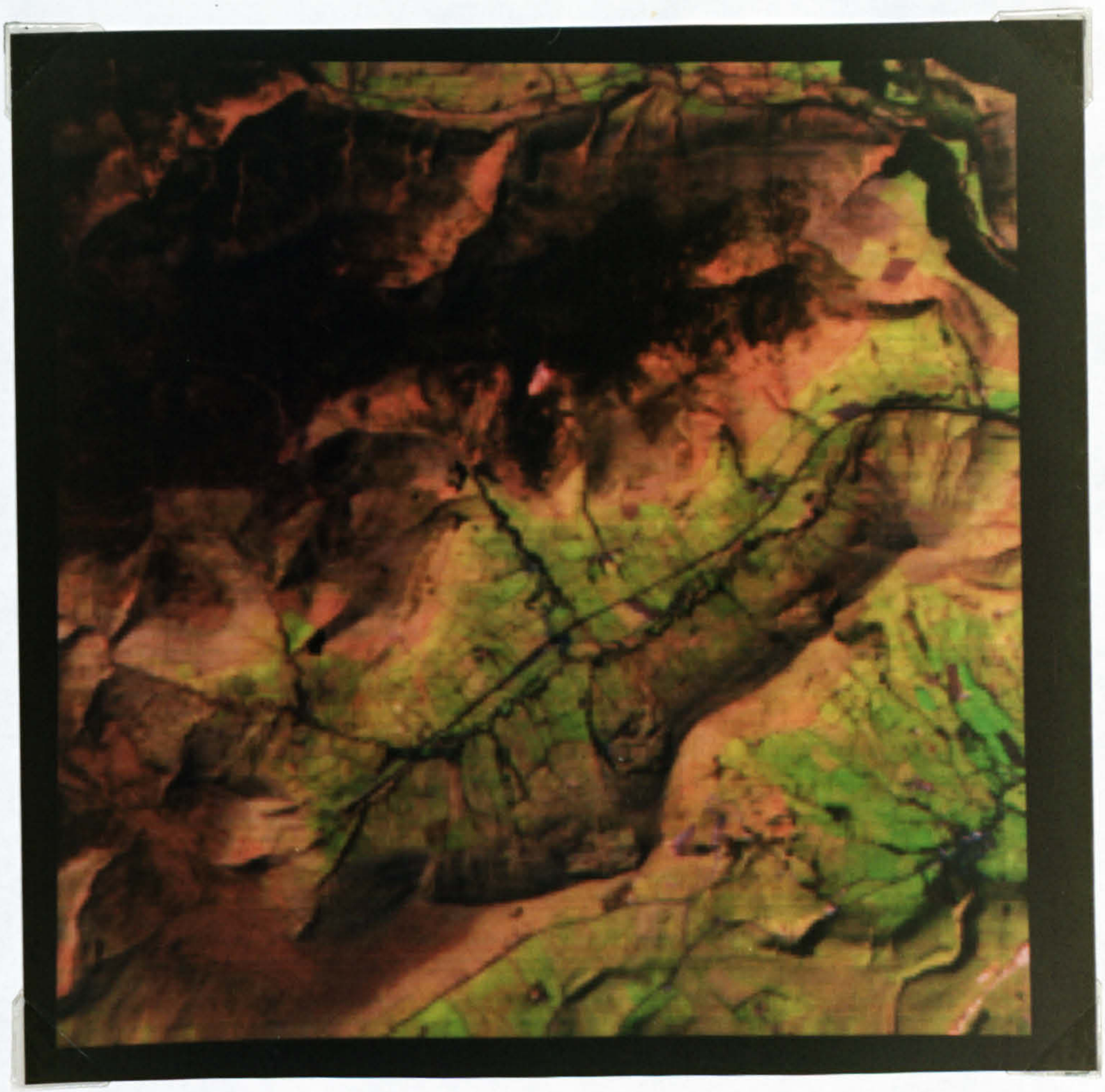

False Colour Composite 5,4,1

Sampling rate: 1,1

Image Processing: Linear Contrast Stretch

Band 5 = red ; limits of 15-150 (forward)

Band 4 = green ; limits of 10-120 (forward)

Band 1 = blue ; limits of 50-130 (forward)

ZOOM FACTOR 2

Figure 2.9

toe to the green of the valley floor on all three of the false-colour composite images presented here (Plates 2.1 to 2.3), this is also due to a change in vegetation to the grass-covered valley floor.

No anomalies in the drainage system were detected, possibly due to the relatively coarse ground resolution of the Landsat-5 TM sensor.

2.4.6 Landslide Hazard Zoning

Of the factors listed by Cooke and Doornkamp (1974) as contributing to slope instability only information on a few of them may be extracted from the Edale TM imagery. These are slope steepness, the occurrence of cliffs, valley-side shape, drainage density, slope undercutting, the presence of strong beds over weak beds, and the location of reservoirs and some landslides.

In Figure 2.10 the above factors have been combined to produce a preliminary landslide hazard map. The land identified as relatively flat has been classed as being the most stable. River banks in the flat areas and slopes well above the sandstone/shale contact without streams or coves are considered to be of low potential hazard. Slopes above this lithological contact but with undercutting streams and coves, together with the broad band on the contact without streams or coves have been grouped as being of moderate instability. The slopes of greatest potential hazard are those on the sandstone/shale contact with coves, streams or reservoirs. If the location of landslides is

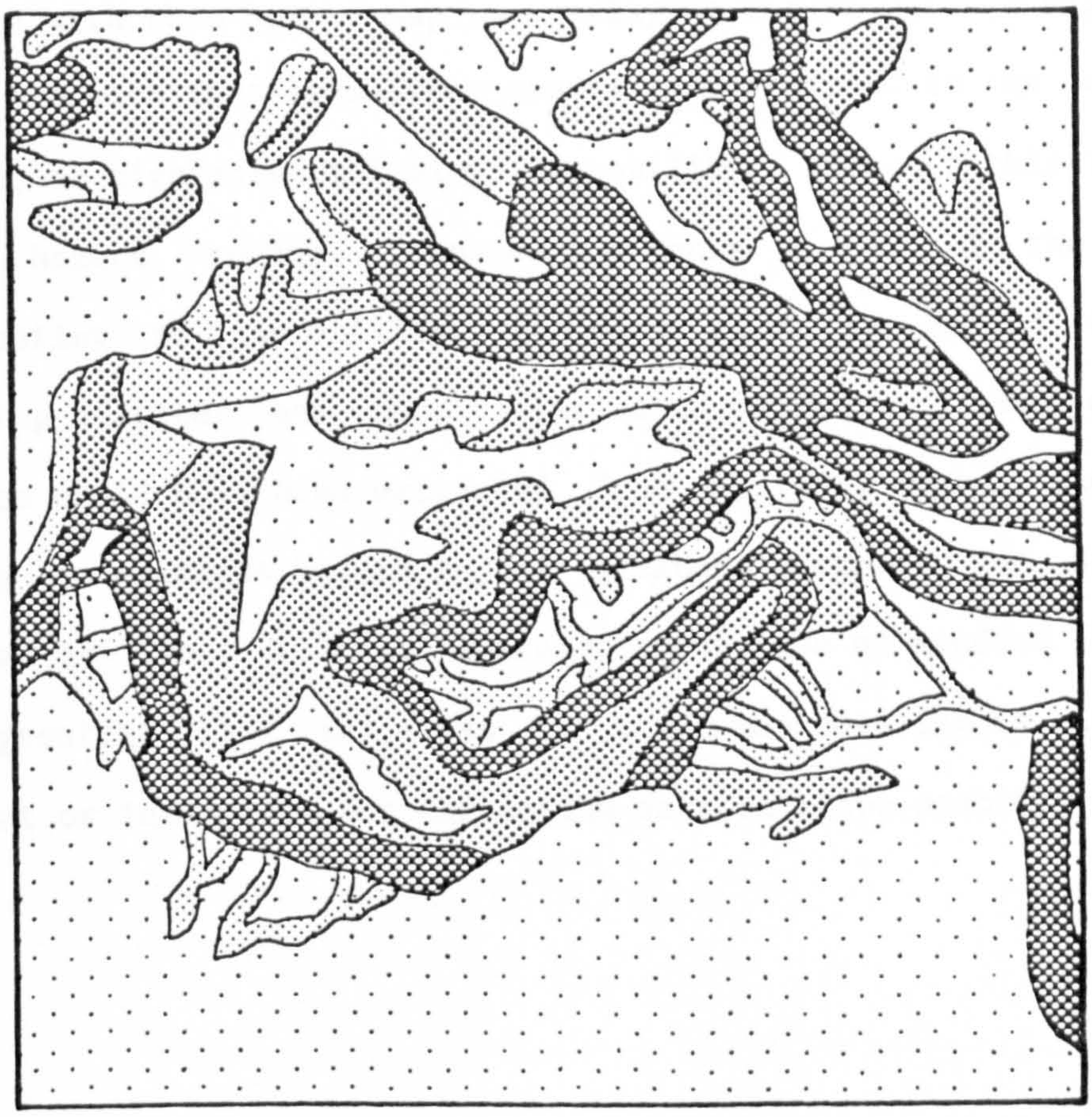

Potential Landslide Hazard

High

Moderate

Low

Extremely Low

(see text for explanation of hazard categories)

Figure 2.10 Landslide Hazard Zonation of Edale - derived from Landsat TM imagery

compared with this hazard map by overlaying Figure 2.8 on Figure 2.10 it will be seen that landslides generally correspond to the zones of moderate to high potential slope instability. Although this is a very basic hazard zoning, considering only a few of the factors contributing to instability, it does serve to define the areas requiring further and more detailed investigation. However, these features could have been extracted from published maps of the area to produce a landslide hazard map of greater accuracy and detail as produced by Cross (1987). Therefore, this use of Landsat TM imagery is of greatest value in areas for which map coverage is either non-existent or inadequate for extracting data on slope stability.

CHAPTER 3 LINEAMENTS FROM LANDSAT

3.1 Lineaments and Slope Instability

In Chapter 2.4.3 it was shown that some landslides lie on lineaments. It was tentatively suggested that this could be due to a concentration of moisture along these lines which may indicate zones of high pore-water pressure contributing to instability. This chapter discusses the significance of lineaments on slope instability and assesses the ability of Landsat TM imagery to detect lines of faulting and fracturing in the Edale region of the Peak District.

The potential for slope instability is known to be greater in areas with extensive faulting or close jointing than in areas without structural discontinuities (Sowers and Royster, 1978). Several reasons may account for this. Firstly, faults and fractures are often zones of weakness which will be preferentially weathered and/or eroded thus further reducing the shear strength of the rock along this potential failure plane (Patton and Deere, 1970). Secondly, fracturing may increase the porosity and permeability of the rock enabling higher moisture content and possibly higher cleft-water pressure than the adjacent rock, thus reducing its effective strength still further. Faults characterised by uncemented fault-breccias often carry immense amounts of water (Richey, 1964).

The nature of the fracture zone (i.e. joint spacing, direction,

inclination, continuity, roughness, weathering products) is also important in determining the stability of a rock slope (Brunsden, 1979; Cooke and Doornkamp, 1974; Piteau, 1970; Whalley, 1984). Increased joint density will result in decreased strength of the rock mass as a whole. It will also create higher secondary permeability and therefore, these zones may contain more water than areas with sparse jointing. However, if the fractures are continuous, then free flow may prevent the build-up of high water pressures.

The orientation of a faulted or fractured zone with respect to the direction of slope is also important. A discontinuity in a downslope direction will act as a channel for water flow rather than result in slope failure. However, in an area with competent beds overlying incompetent beds such as the sandstone and shale of the Edale region of the Peak District, this may result in downcutting to expose the weaker lithology thus providing conditions conducive to landsliding. However, this aspect of lineaments need not be considered in the production of a landslide hazard zonation map as this downcutting takes place on a geological time scale. A fracture cutting across a slope and thus producing a wedge of ground may increase instability, as will intersecting fractures. A line parallel or sub-parallel to the contour of a slope may retard the movement of water downhill resulting in a build-up of water pressure and a decrease in stability.

The angle of inclination of joints with respect to both the angle of friction and the slope is also important (Terzaghi, 1962). In

addition, the roughness of the fracture plane may affect the angle of friction, greater roughness producing more friction and hence a higher critical angle. However, if these planes contain weathering products of lower strength than the rock then the resistance to failure will be lowered along this plane. Grainger and Harris (1986) found that faults in the Carboniferous shale of southwest England typically contain a clay gouge of very low permeability and, consequently, they form barriers to ground water flow. Springs and seepages commonly occur on sloping ground above these impermeable faults as a result of the perched water table.

Not all of these aspects of fractures can be studied by remote sensing; most need detailed field work. The line of fracturing may be visible on satellite images if it has different characteristics from the surrounding area at a spatial scale which can be detected by the sensor. From Landsat, with its coarse spatial resolution, the only information that may be extracted about a zone of fracturing is its location and orientation, although more detailed study may be carried out subsequently. However, it will only have a chance of being detected if it has a topographic expression, differing adjacent lithologies or high water content.

The influence of fracturing on slope instability was demonstrated during the construction of a by-pass near Tyrone, central Pennsylvania, where structurally-disturbed and friable rock was found to coincide with some of the lineaments mapped from Landsat imagery (Gold and Krohn, 1976). At three of these sites the artificial slopes

became unstable especially during spring thaw and run-off and at times of heavy prolonged rain. At one site there was a rise in the piezometric surface of approximately one metre. Elsewhere on the cutting the slopes were stable despite thin rock units and steeply dipping strata. This suggests that lineaments may contribute to slope instability, and should be included in a hazard assessment.

3.2 Limitations of Lineament Analysis

In the previous section the importance of geological structure on slope stability was described, and it was suggested that lines of faulting and fracturing may be detected on remotely-sensed imagery as lineaments. Therefore, lineaments could be incorporated into a landslide hazard assessment - a contributory factor not easily available by means other than remote sensing. However, in practice there are many problems associated with the sensor, the interpreter and the ground conditions which limit the potential use of lineaments. These problems are discussed below with suggestions for avoiding or minimising them.

3.2.1 Human perception

The variation in detection resulting from human perception is probably the greatest limiting factor to the utility and significance of lineaments, it is also the main cause of the widespread scepticism

among geologists (see Wise, 1977, 1982). The observer does not always detect a feature where it is present and may report a feature where none exists. Consequently, two interpretations of the same scene by the same observer will vary, as will interpretations of the same scene by different observers (Burns and Brown, 1978; Burns et al., 1976; Huntington and Raiche, 1978). Although there may be some similarity in the gross pattern there will be very little agreement in detail. Burns et al. (1976) calculated a coefficient of reproducibility: +1 indicating complete agreement between two interpretations, 0 meaning no systematic relationship, and -1 showing complete disagreement. They found that the coefficient for two interpretations of the same image by the same observer or by two observers was between +0.1 and +0.3. As Burns and Brown (1978) pointed out: "the areas between the lines are more significant geologically than the lines", i.e. areas without lineaments can be identified repeatedly with greater accuracy than the lineaments themselves.

There is no real solution to this problem. The closest one can come is to regard only those lineaments identified by several observers as being real features; whether the other lineaments are real or imaginary remaining unknown. A more time-consuming and expensive alternative would be to verify the geological nature of every lineament by field work. Whichever approach is adopted, there will always be lineaments which are not detected either due to the sensor or the interpreter; this must be recognised and taken into consideration.

3.2.2 Angular relationship between the source of illumination and the lineament

Lineaments expressed by relief may be either enhanced or suppressed according to their orientation with respect to the sun azimuth. Landsat imagery is taken at approximately 0930 local sun time so the sun is in the southeast in the northern hemisphere. Therefore, valleys trending northeast to southwest will be enhanced by shadows and highlights, but those trending northwest to southeast will be suppressed. The look-angle of the sensor will also affect lineament detection. Consequently, mapping lineaments from one type of imagery results in a biased data set; this has been recognised by Goetz and Rowan (1981).

This bias can be reduced by combining the Landsat lineaments with a data set obtained from imagery with a different angular relationship with the source of illumination, e.g. radar. Also, mapping from stereoscopic images provides information on relief with less interference from the angle of illumination.

3.2.3 Illumination angle

The detection of lineaments varies with illumination angle, i.e. the position of the sun in the sky. Landsat is sun-synchronous,

therefore, illumination varies with season but only by a relatively limited amount compared to some other satellite remote sensors. This further biases the data set (Goetz and Rowan, 1981; Huntington and Raiche, 1978; Siegal and Gillespie, 1980).

This problem could be reduced by using several types of imagery with differing illumination angles; however, the cost of obtaining several images may far exceed the benefits gained depending on the reason for the lineament analysis. As shadow is greater at lower sun elevation angles, the moderately low illumination angles of Landsat are sufficient for detecting lineaments defined by relief, but this leads back to the problem of angular relationship between illumination source and lineament.

3.2.4 Spatial resolution and scale

In theory, coarse spatial resolutions give a more regional view of a scene than imagery with finer resolutions, and therefore, longer lineaments or those affecting a wider zone of ground, can be expected to be more easily identified. Conversely, at higher resolutions more short and/or narrow lineaments should be visible (Huntington and Raiche, 1978; Lake et al., 1984). This is exemplified by comparing Landsat MSS and TM, with spatial resolutions of eighty metres and thirty metres respectively. Images from sensors with different spatial resolutions should then be used.

A much simpler and cheaper alternative is available in the form of studying an image at different scales. In the case of Landsat TM, after the identification of the area of interest and subsequent mapping of lineaments, the scale could be increased by zooming for more detail of several parts of the scene, and decreased by sampling lines and pixels to include the surrounding region enabling the identification of longer lineaments (e.g. Plates 2.2, 2.4 and 3.1). This is most easily achieved by using a digital image display system. The variation of lineament detection according to scale is one of the few problems which can be solved.

3.2.5 Spectral band

Lineaments with differing characteristics may be best detected by different bands. For example, the detection of tonal lineaments will vary depending on whether they are defined by rock, soil, vegetation or moisture differences as they will have differing spectral signatures. Topographic lineaments will show up best on bands which give good impressions of relief. In constructing a lineament map it is therefore necessary to use information from all available bands, both as monochrome and false-colour composite images.

3.2.6 Image processing

Lineament maps produced from images generated by different processing

methods will vary as certain lineaments will be enhanced by some techniques but suppressed by others. For example, varying degrees of contrast enhancement will affect interpretation, and the orientation of detected lineaments may be influenced by the direction of filtering. In addition, image transformations, such as ratios and principal component analyses, may improve the recognition of tonal boundaries associated with rock or soil type, or improve the impression of relief.

However, it is impractical to map lineaments from images generated by every processing technique with every degree of enhancement, and it is difficult to generalise about which techniques will be of most use as it will depend on the nature of the terrain and on the nature of the lineaments. The process of "trial and error" is therefore recommended to produce several images using a cross-section of techniques.

3.2.7 Monoscopic imagery

According to Siegal and Gillespie (1980), the mapping of linear features from monoscopic imagery is highly subjective, partly because the morphological nature of lineaments cannot be fully or accurately recognised. By stereoscopic analysis the mapping reproducibility of length and position is greatly improved. Furthermore, bias in the data set due to the angular relationship between the source of illumination and the lineament may be reduced as information on

relief is available regardless of orientation.

Unfortunately, aerial photography is the only type of imagery for which stereoscopic capabilities are readily available. Although the SPOT satellite has stereoscopic capabilities the amount of finance available for the project and the necessity to detect lineaments will determine whether the cost of such imagery is warranted. Adjacent passes of Landsat provide limited overlap at high latitudes but the vertical exaggeration is very small. A solution to this may be the production of a stereopair from a single image by the introduction of parallax (Batson et al., 1976; Eliason et al., 1981).

3.2.8 Masking by ground cover

In areas with sparse to moderate vegetation cover the location of faults and joints may be indicated by lusher vegetation resulting from higher moisture content due to structural control on ground water movement. However, in areas where vegetation covers the surface completely such anomalies are not apparent (Siegal and Gillespie, 1980). It is also probable that tonal lineaments in solid geology may be obscured by thick drift cover; lineaments expressed by morphology are more likely to persist.

The problem of masking by ground cover is only avoided in areas with no superficial geology and with sparse to moderate vegetation cover. In other areas it must be acknowledged as another factor resulting in

incomplete lineament data sets.

3.2.9 Ground water conditions

Faults and fractures with higher moisture content will be most easily detected when there is greatest contrast between the moisture content of the lineament and the surrounding land as this will result in greatest contrast in tone on an image. A period of very low rainfall may produce this effect which will either be expressed as a dark tone in the infrared directly recording moisture, or as a line of lusher vegetation passing through vegetation in a stressed condition induced by a lower supply of ground water. However, if the image being studied was not taken during dry conditions then such lineaments have a lower chance of being detected. Therefore, it is important to know the weather conditions directly preceding the time the image was taken.

3.2.10 Snowcover

In comparing Landsat MSS and TM imagery for lineament mapping, Lake et al. (1984) found that more lineaments of less than five kilometres in length were observed from MSS than from TM - the reverse to what one would expect as TM has the greater ground resolution as discussed in Chapter 3.2.4. However, their test was based on MSS imagery taken when the ground had a snowcover. They suggest that snowcover on the

MSS image enhances very small linear features which would be lost against the high spatial frequency ground cover variations of a snow-free image.

As both snowcover and dry climatic conditions may enhance lineaments of differing characteristics multi-temporal imagery may aid in lineament detection.

3.2.11 Misidentification of cultural features

Linear cultural features such as roads, railways, canals and pipelines may be misinterpreted as tonal lineaments, although their courses may reflect a morphological lineament. Stefouli and Osmaston (1984) recommend that initially image analysis should be based on the perception of linear features but not their interpretation. These linear features must then be screened to remove those related to cultural features. Roads, railways and canals can easily be eliminated by reference to maps, if available, but pipelines which have disturbed the soil and possibly affected moisture conditions or temperature of the ground cannot be isolated so easily. Also, lines of trees planted by man, drainage courses determined by man, field boundaries, footpaths and tracks may be difficult to dismiss without very detailed and accurate maps or extensive field work.

3.2.12 Significance of lineaments as faults

Very few of the lineaments identified on the Edale images correspond to faults known from surface mapping, although inaccuracy in locating lineaments on the ground may account for this. However much literature has been produced claiming some such correlation (e.g. Gold and Krohn, 1976; Lake et al., 1984; Stefouli and Osmaston, 1984), and the degree of correlation with faults detected by seismic surveys still remains largely untested.

Some faults will escape detection due to the problems discussed above; other faults may have no surface expression and no contrasting conditions to the surrounding land. Conversely, some lineaments could be faults which have so far remained unmapped. It is, therefore, difficult to assess the significance of any correlation between the locations and orientations of lineaments and known faults as both may be incomplete and biased data sets. However, where there is a coincidence ground-based information (about the style and age of faulting, for example) may be useful in assessing the geological significance of the lineaments identified.

3.2.13 Locating lineaments in the field

In most cases lineaments are mapped from small-scale imagery. This presents a problem when trying to locate them on aerial photographs, maps or in the field, and increases the difficulties in verifying

their geological nature. The best way to deal with this is to locate the lineament on images of gradually increasing scale and resolution before transferring to a large-scale map. In doing this, the nature of the expression of the lineament may be discovered, as well as improving the accuracy of location. With TM imagery it is often possible to identify the position of a lineament relative to field boundaries in the U.K. and to use this as a basis for locational precision.

3.2.14 Recommendations

To summarise, lineaments will be most easily detected where faults and joints have strong surface expressions, especially in areas with sparse to moderate vegetation cover and no superficial deposits. Furthermore, lineament analysis should involve:

(i) several types of imagery

(ii) all available parts of the electromagnetic spectrum

(iii) a range of scales and spatial resolutions

(iv) multi-temporal imagery

(v) stereoscopic imagery

(vi) screening of cultural features

(vii) the use of large scale aerial photographs and maps (approximately 1:10,000)

(viii) extensive field work to verify the geological nature of every lineament

The more of these conditions that can be satisfied, the greater the reliability of the lineament analysis.

However, even if all these are satisfied, some lines of faulting and fracturing will almost certainly escape detection. Taken individually any lineament may be geologically significant, but a lineament map as a whole will represent an incomplete data set. In addition, the greatest problem, that of human perception, remains unsolved, and as such will continue to limit the utility and significance of lineaments, and to maintain the associated scepticism.

3.3 Lineaments of the Edale Image

With the above limitations and problems in mind, the Edale image was interpreted with respect to lineaments. Unfortunately, the only types of imagery available are Landsat TM for one date and aerial photography. All seven bands of the Landsat imagery have been studied. The near- and mid-infrared wavebands were found to be of most use (Table 2.4), this is probably because these bands give good impressions of relief, and lineaments defined by water, either in the form of rivers or increased soil moisture content, are also best defined.

Lineaments were first identified on an image at a scale of approximately 1:61,500 with every line and every pixel displayed

(Plate 2.2). A more regional view was then obtained at a scale of 1:123,000 with every second line and second pixel displayed (Plate 3.1), and finally more detail for part of the scene was provided at 1:31,000 with every line and every pixel (Plate 2.4). Further image processing was found to offer no additional information about the lineaments. With reference to maps it was found that no roads or railways had been misinterpreted. The valley floors are covered by head deposits, therefore, it is debateable as to whether lineaments in the bedrock would be detected in these areas. Figure 2.7 should be used with Plates 2.1 to 2.3 to show the positions of the lineaments; the solid lines represent those lineaments which were detected by several observers and, therefore, more confidence may be placed in these as being real features. It must be remembered, however, that the geological nature of these linear features has not been verified and they do not coincide with known faults, and that they do not represent a complete data set.

The majority of these lineaments have a morphological expression, although there may well be an equal number of tonal lineaments which have not been identified as this particular observer believes these are most likely to be misinterpreted cultural features or "suspect lineaments" created by perception. Most lineaments are also composite: aligned valleys, streams, breaks in slope and possibly lines of higher moisture content. The lineaments were located on aerial photographs at a scale of 1:12,000. The enlarged TM image (Plate 2.4) was useful in locating the lineaments in this area more accurately. The lineaments have been transferred to a base map in

PLATE 3.1 LANDSAT TM IMAGE (BANDS 5, 4 AND 1)

OF THE DARK PEAK

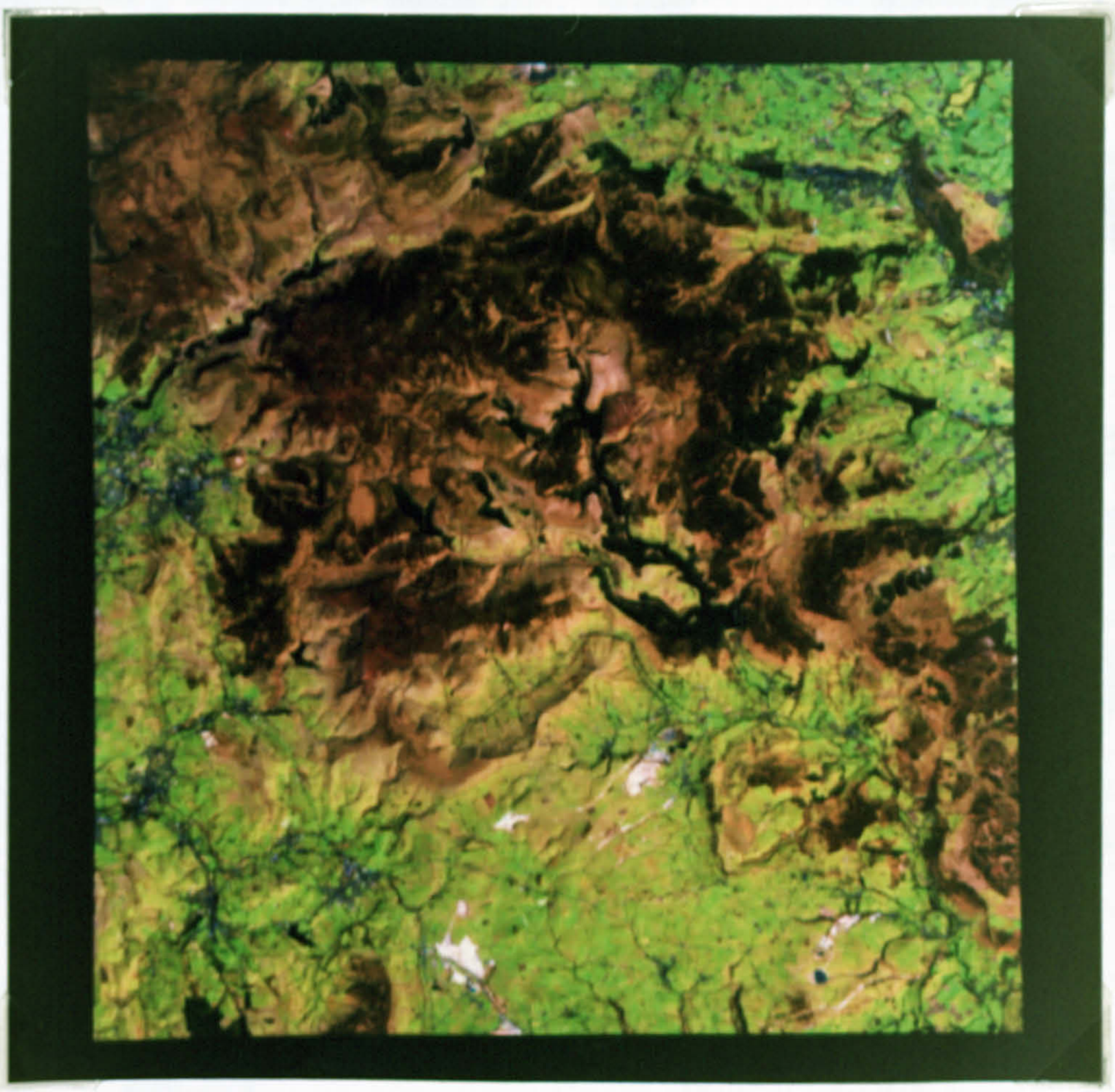

False Colour Composite 5,4,1

Sampling rate: 2,2

Image Processing: Linear Contrast Stretch

Band 5 = red ; limits of 15-150 (forward)

Band 4 = green ; limits of 10-120 (forward)

Band 1 = blue ; limits of 50-130 (forward)

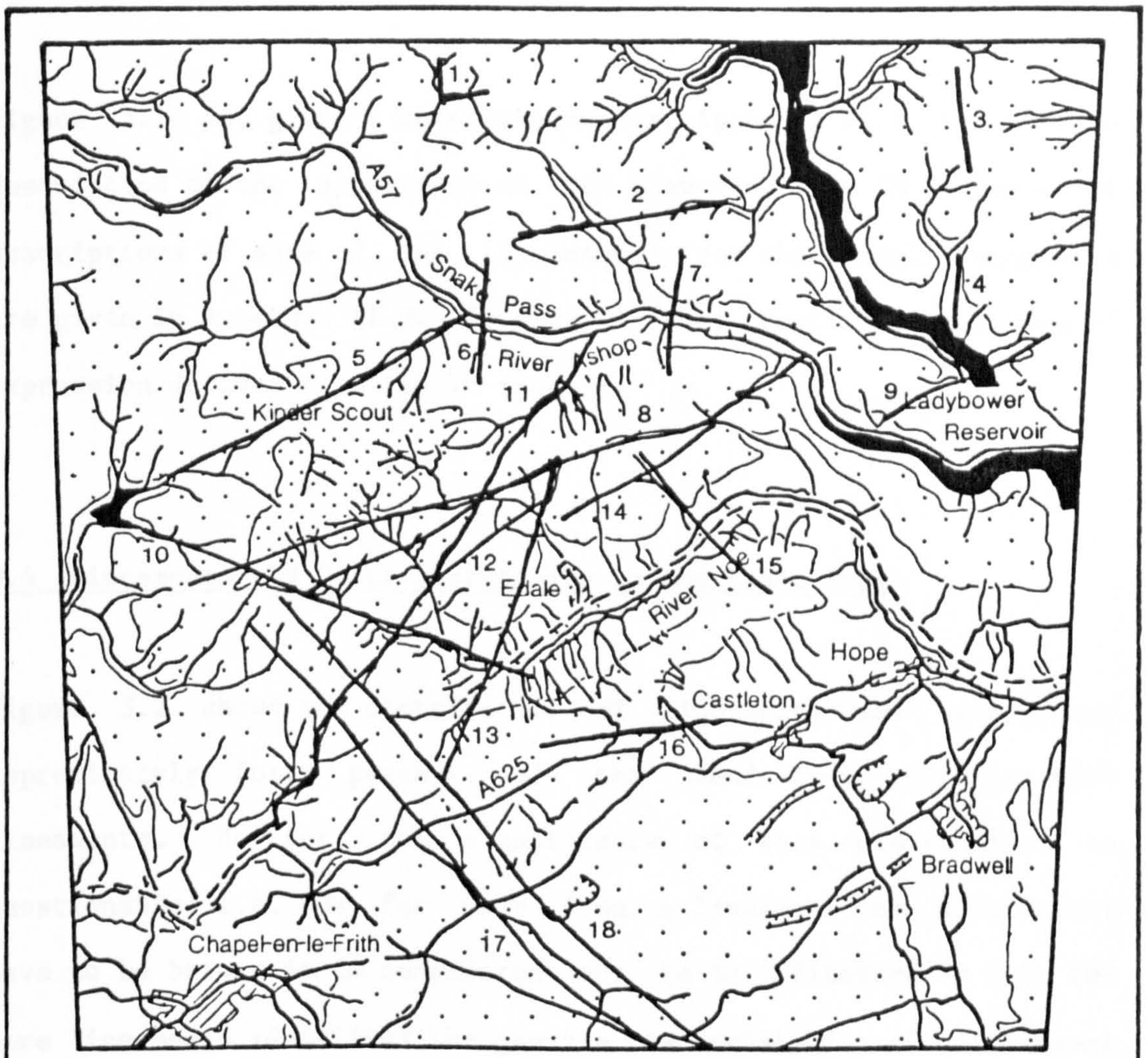

Source: Ordnance Survey Tourist Map 4 Peak District

Figure 3.1 Lineaments of the Edale Region

Figure 3.1 and given a reference number. Appendix A1.1 contains a description of the appearance of each lineament from TM imagery, and descriptions of some of the lineaments from the aerial photographs are given in Appendix A1.2. In general they confirm the nature of expression derived from the TM imagery.

3.4 Lineaments and Slope Instability in the Edale Area

Figure 3.2 shows the distribution of lineaments and landslides; approximately forty percent of the landslides coincide with lineaments. However, the significance of this distribution is questionable: i.e. how far away from a lineament does a landslide have to be before it is considered not to be influenced by it?; the more lineaments identified the greater the probability of coincidence with landslides; the data set is incomplete and the geological nature of the lineaments has not been verified. Also, a random set of lineaments was created with the same total length as those of Figure 3.2. As before, approximately forty percent of the landslides coincided with these random lineaments. Consequently, these shortcomings prevent coincidence alone being sufficient to test the hypothesis that lineaments increase slope instability, therefore, the characteristics of the lineaments themselves must be investigated for evidence.

Firstly, the geological nature of the lineaments must be verified. It may be sufficient evidence that two valleys, one on each side of a

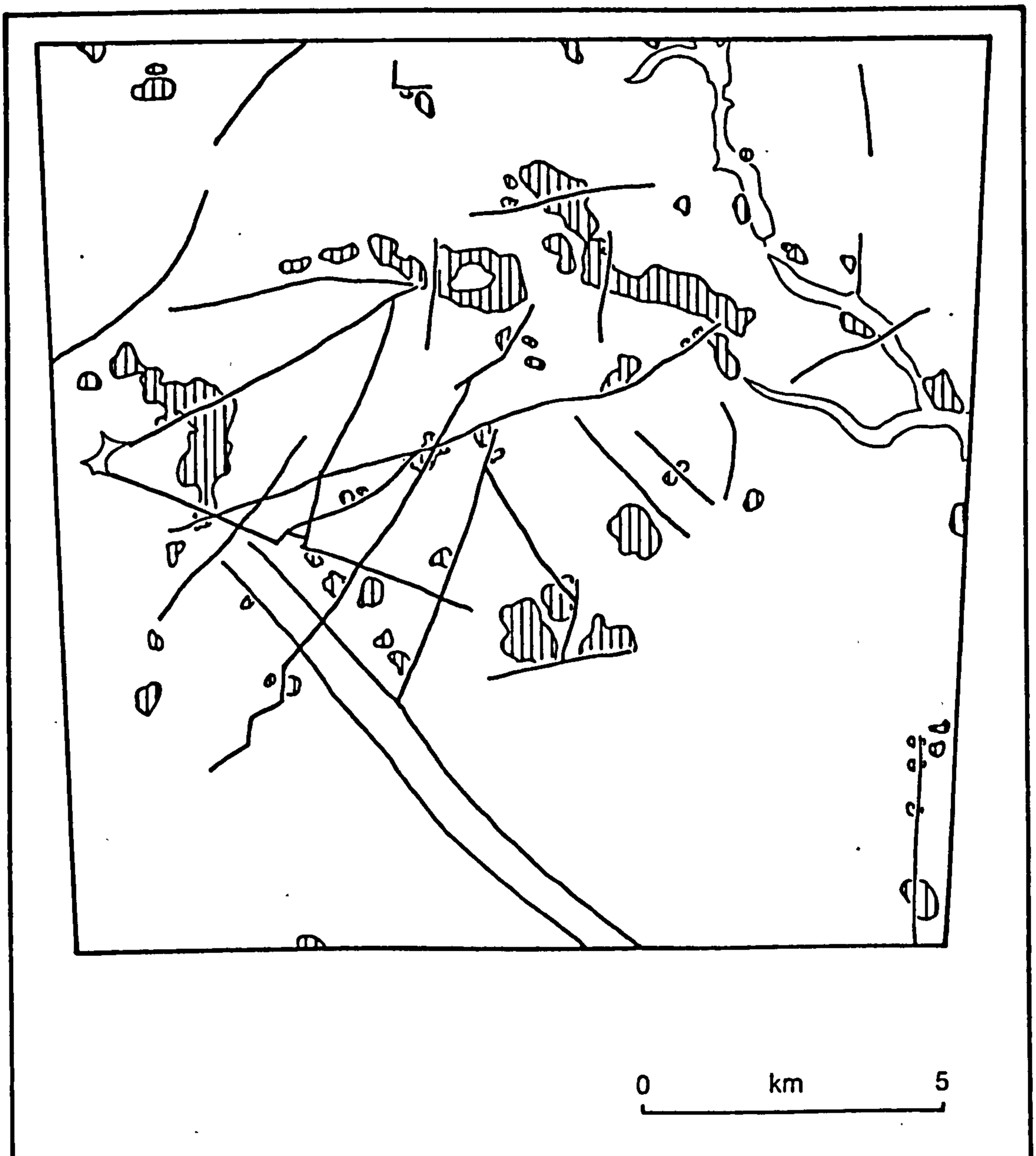

Figure 3.2 Location of Landslides and Lineaments in the Edale Region

ridge or of a plateau, are aligned showing where weathering and erosion have exploited lines of weakness, for example Lineaments 5 and 10 of Figure 3.1. Sharp changes in stream valley directions, such as Lineaments 1 and 11, also suggest an underlying structural control - possibily jointing. Lineament 16 is interesting in that it is defined by the backscars of two large landslides surrounding Mam Tor; structural control on these backscars is clearly demonstrated.

Such morphological evidence should be backed up by direct geological evidence of the nature of any faulting or jointing. Therefore, a joint survey should be carried out at a number of outcrops in the area both on and away from lineaments which includes measurement of joint spacing, orientation, inclination, continuity, roughness, weathering products and cleft-water pressure. Joint surveys are described by Piteau (1970), Robertson (1970) and Terzaghi (1965).

Field work around Mam Tor did not reveal the presence of Lineament 16 which passes along the backscar of Rushup Edge landslide and continues along the side of Mam Tor landslide. This was partly due to the difficulty of access to the backscars. A detailed joint survey of these sandstone/shale outcrops would be necessary to pick up any variation in joint spacing or moisture content related to the lineament as there was no obvious increase or decrease of fracture spacing or moisture content evident. Such work is beyond the scope of this thesis. However, with the aid of such a survey, if a lineament is confirmed to represent a line of fracturing, then it

should be possible to determine whether the lineament represents the zone of most intense joint density, or the fractures with greatest moisture content. At the same time continuity, roughness and width of the joints may be measured and the presence of any weathering products in the fractures may be noted. Hence the contribution to slope instability of lineaments can be assessed at the site investigation stage.

3.5 Lineaments in Landslide Hazard Zoning

After consideration of all the problems involved with lineament analysis, it is recommended that lineaments should be omitted from a hazard zonation of potential slope instability. However, they should not be dismissed completely. After a site of interest has been identified with the aid of the hazard zonation then the contribution to instability of any lineament passing through that site should be assessed.

Further work may involve field work to determine the influence of lineaments on slope instability, and geophysical techniques could also be employed to aid in the verification of the presence and nature of lineaments.

CHAPTER 4 THE ROLE OF LANDSAT TM IMAGERY IN LANDSLIDE STUDIES AND ITS APPLICATION TO THE MATLOCK AREA OF DERBYSHIRE

4.1 Detection of Landslides by Landsat TM

Information from several spectral bands may be of use in the detection of landslides on Landsat images. Sauchyn and Trench (1978) found the near-infrared band of Landsat MSS was most effective for showing ponds and shadows, whilst the combination of the near-infrared and the visible red gave most information in general. From the study of the Edale imagery it was found that landslides could most easily be detected from TM Bands 4, 5 and 7 displayed in monochrome and from most false-colour composite combinations especially those including bands from the infrared (Table 2.4). However, only five out of 130 landslides were identified. The smallest landslide detected is approximately 0.25km^2 and, as there are several undetected landslides larger than this, it would appear that size is not the only factor influencing the chances of recognition in this region.

Landslides cannot be expected to have a characteristic spectral signature as they are inhomogeneous features with variations in material, vegetation, moisture content and slope angle. Consequently, their detection from remotely-sensed imagery must be concerned with pattern recognition involving the identification of areas of anomalous character with respect to the surrounding

conditions. The features which may thus be detected are morphology, drainage and vegetation (Crozier,1984).

Areas of slope failure may exhibit internal variations on imagery. Sauchyn and Trench (1978) found that tonal mottling and banding were characteristic of rotational landslides in Colorado on Landsat MSS imagery. The mottling is thought to be caused by the hummocky terrain, and is, therefore, a function of variation in radiance due to differences in aspect; variations in vegetation type and cover and ponds may also produce mottling. However, other features may produce such speckling, for example glacial drift. Tonal banding is believed to be caused by parallel ridges which also affect radiance as a function of aspect. Where such banding is present the probable direction of slip movement is perpendicular to the bands. Sauchyn and Trench (1978), however, concluded that it was difficult to detect landslides on Landsat MSS imagery. Slope failure may also be defined by the presence of an upper and lower boundary corresponding to the backscar and the toe, respectively; although with only one boundary visible the landslide may be misinterpreted as just a break of slope or a band of vegetation.

The characteristics of landslides influence their chances of being detected on satellite imagery, these include size, type and morphology, relative relief, aspect, surface water, vegetation cover and age. Firstly, the landslide must be large enough to be detected. The minimum size will depend on the spatial resolution of the sensor. For Landsat TM with a spatial resolution of thirty metres, a

landslide must cover an area of at least four by four pixels - 120m x 120m - (depending on contrast with the background) to be identified as a feature.

Morphology is the main factor in the recognition of a failed slope both in the field and from aerial photographs. Similarly, on Landsat imagery those landslides with strong morphological expression may be defined by shadows and highlights. In this respect, the type of failure is significant: deep-seated landslides may produce steep high backscars, slump blocks and longitudinal ridges, whilst shallow failures such as flows in superficial deposits are more likely to have a smoother form. Sufficient relative relief of deep-seated failures is also required to produce shadow or highlight, therefore, perhaps those slides with greatest depth to the failure plane will have the best chance of detection. Another consideration that must be made concerns the age of the landslide - has the morphology been degraded? So, the landslides that can be expected to be enhanced by shadow and highlight are the relatively undegraded, deep-seated failures.

The detection of these landslides will depend to a great extent on their aspect as relief is are either enhanced or suppressed on images according to slope orientation with respect to the sun azimuth. Landsat TM takes images at 0930 local sun time, therefore, the sun is in the southeast in the northern hemisphere and valleys trending northeast to southwest will be enhanced by shadows and highlights, but those trending northwest to southeast will be suppressed.

Landslides with an aspect south to east will have brighter backscars and ridges for example, but shadow is better for identifying steep backscars and so landslides with strong morphological expression facing north to west will be the easiest to detect.

Landslides cause anomalies in the drainage system: undrained depressions and ponds elongated parallel to the slope contours may occur on the slopes, while deposition in stream valleys may result in constrictions or impounded lakes. Drainage within landslides is unlikely to be detected on TM imagery due to the coarse ground resolution, however, the infrared channels may pick out concentrations of soil moisture and water in depressions. Water accumulation in depressions at the back of rotated blocks may be detected by remote sensing; either marsh vegetation or ponds may be recorded if they cover a large enough area and are not obscured by shadow.

Vegetation has been used as an indicator of landslide age, degree of activity, and type, and in the identification of the component parts of a landslide; it may also indicate the presence of certain clay minerals which promote instability (Crozier, 1984). The vegetation cover of disturbed ground may differ from that of adjacent stable slopes being composed of light-tolerant, colonising and fast growing species. Differences may also be noted within a landslide: scars are likely to be characterised by shallow-rooting, drought-tolerant plants, and the foot of the slide may support deeper-rooting moisture tolerant species. Absence of vegetation may indicate fresh backscars

representing shallow as well as deep-seated failure. The age of the landslide is again important as after a certain period of time the evidence for vegetation disturbance will be removed by succession. These vegetational differences might be detectable on imagery provided that differences are marked and the ground resolution is sufficiently high. However, vegetation may also mask any evidence of slope failure. An area of woodland will reduce or eliminate the effect of morphology of a landslide, and woodland may easily be confused with shadow. Masking by vegetation is demonstrated at the Ladybower Reservoir where woodland covers a landslide (Figure 2.8).

The landslides of the Edale image are mainly deep-seated rotational failures with some translation and flow. Many of them are greater than 120m x 120m in area and, therefore, large enough to be detected by the Landsat TM sensor. The majority of the landslides have been considerably degraded, and some are only identifiable on aerial photography due to minor hummocks and apparently differ very little from the adjacent ground.

The five landslides that can be confidently recognised on the Edale image are discernible on the basis of morphology, as backscars and ridges produce shadow, and, in the case of Mam Tor, the vegetation cover of bracken and marsh plants on the poorly drained foot which contrasts with the grass cover of the stable valley floor. The reasons for the rest of the 125 or so landslides failing to be detected are suggested as:

(i) the area of failed ground is too small to occupy a sufficient number of pixels on the image for recognition.

(ii) the landslide has weak morphological expression due to either degrading or shallow nature of failure.

(iii) for those landslides with strong morphological expression aspect will influence their detection: those landslides in valleys trending northwest to southeast will be suppressed.

(iv) tree cover, whether partial or complete, will obscure the landslide.

Figure 4.1 classifies the landslides of the Edale image according to the factors affecting their detection. In general, the order of the factors in the key is the order in which they eliminate landslides from the probability of being detected. It shows that this area is not ideal for the identification of landslides from Landsat-5 TM imagery.

It is concluded that the classification of an area of ground as a landslide can be done with greatest confidence if the outline of the landslide is expressed as a result of the difference in nature of the failed ground to the stable ground, whether the difference is due to morphology and therefore shadow and highlight, or vegetation, or drainage. Within this area, tonal mottling or spectral reflectances contrasting with the surrounding land increase the confidence of classification as a landslide. However, some causes of mottling on an image, as already described, may have nothing to do with slope

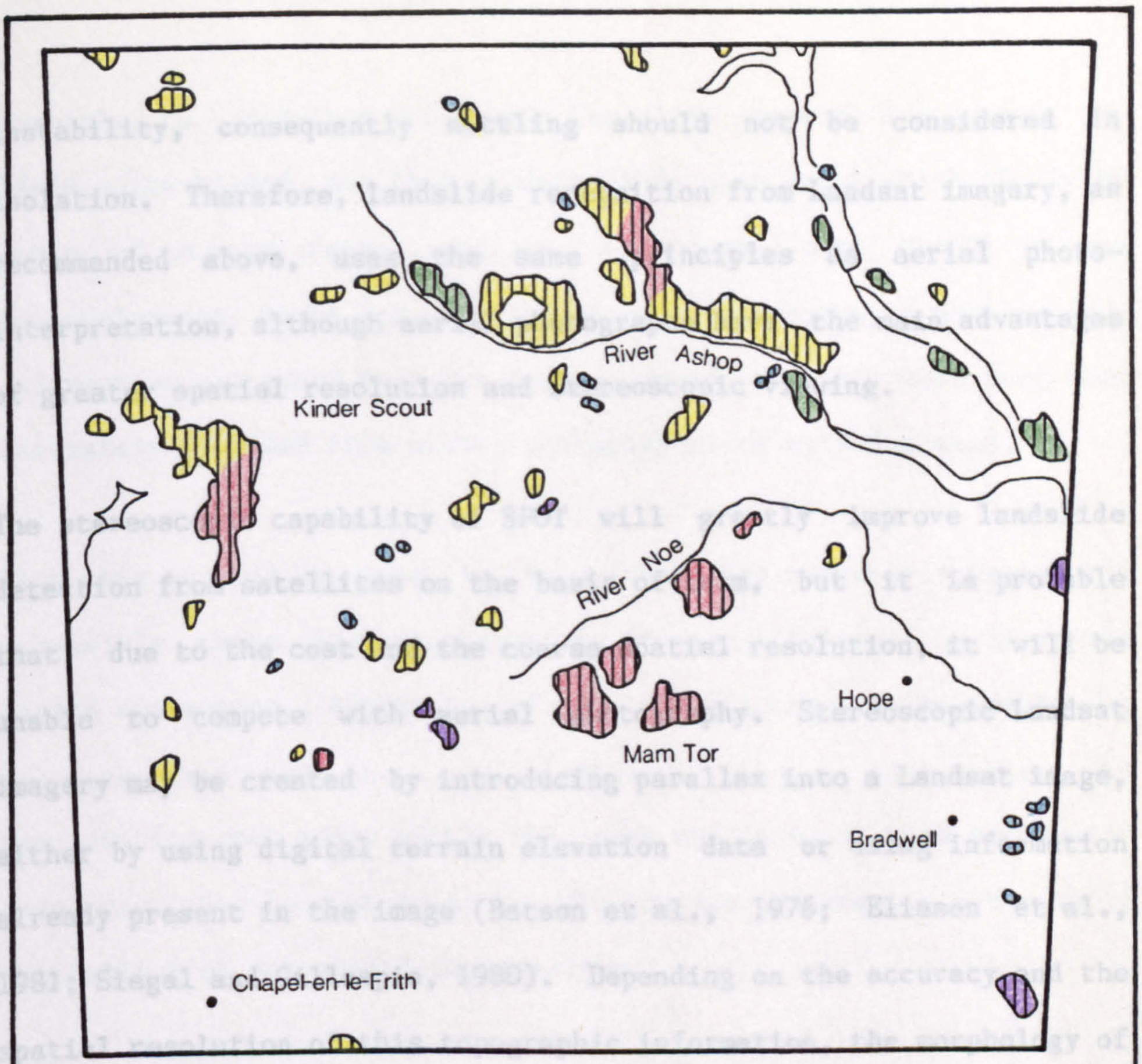

Figure 4.1 Factors Affecting the Detection of Landslides by Landsat in the Edale Region

instability, consequently mottling should not be considered in isolation. Therefore, landslide recognition from Landsat imagery, as recommended above, uses the same principles as aerial photo-interpretation, although aerial photographs have the main advantages of greater spatial resolution and stereoscopic viewing.

The stereoscopic capability of SPOT will greatly improve landslide detection from satellites on the basis of form, but it is probable that, due to the cost and the coarse spatial resolution, it will be unable to compete with aerial photography. Stereoscopic Landsat imagery may be created by introducing parallax into a Landsat image, either by using digital terrain elevation data or using information already present in the image (Batson et al., 1976; Eliason et al., 1981; Siegal and Gillespie, 1980). Depending on the accuracy and the spatial resolution of this topographic information, the morphology of landslides may be enhanced. Conversely, the elimination of the effect of relief may enhance vegetation and surface water associated with the detection of landslides as any confusion with shadow or highlights will be avoided. However, in its monoscopic form Landsat imagery appears to be of little use in detecting landslides in the Edale region.

4.2 Landslide Hazard Zoning by Landsat TM

With respect to the recognition of factors contributing to instability, as discussed in Chapter 2, it was concluded that it is

possible to produce a very basic landslide hazard assessment for Edale. The hazard map thus produced indicates areas which should be looked at in more detail and is, therefore, most useful at the reconnaissance level of a slope instability survey. However, the information extracted from the images would probably have been more accurately obtained from aerial photographs and existing maps.

With this in mind it must be said that for adequately mapped and accessible areas Landsat imagery is of very little use in landslide hazard assessment. Although, if the significance of lineaments can be determined and shown to influence slope instability by representing weak zones within the rock and lines of high pore-water pressures, then Landsat imagery would provide information not readily available from any ground-based source.

Other types of remotely-sensed imagery may be of potential use in lineament recognition and for the regional measurement of soil moisture. Radar is likely to be of most use as its side-looking character results in the recording of the impression of relief due to shadow and enables the structure of the bedrock to be enhanced, therefore landslides and lineaments may be detected. It is also possible to derive relief from single radar images by a mathematical model produced by Wildey (1984) which, like the pseudo-stereoscopic Landsat imagery developed by Batson et al. (1976), may be of use in landslide recognition. Also, as microwaves can penetrate the ground to a certain extent, radar may be able to provide information about soil moisture. Loffler (1977) assessed Landsat imagery and SLAR

(Side-Looking Aperture Radar) imagery for use in landform interpretation for a poorly mapped area in Papua New Guinea. He concluded that Landsat was a tool for regional mapping and was more suited to a less complex terrain than Papua New Guinea, whilst the radar imagery provided greater detail and was equivalent to aerial photography. The recognition of water conditions (e.g. seepage, water saturated ground, and springs) by thermal infrared imagery is also important in studying landslides as outlined in Chapter 2.4.4. It is therefore recommended that any further work on the use of remote sensing in landslide studies should focus on radar and thermal infrared imagery.

To summarise, from assessing the use of Landsat imagery for studying landsliding it has been found that, although a basic hazard map can be produced and certain landslides can be recognised, this type of imagery is of greatest value in areas for which map and aerial photograph coverage is either non-existent or inadequate and for areas of poor accessibility.

Where Landsat is going to be employed in studying slope instability it is recommended that the imagery should be used in a similar manner to aerial photography for visual interpretation. The only image processing required in the case of Edale was contrast enhancement. It is possible that for an area with different vegetational or geological characteristics further processing may be necessary or may yield further information. For example, Donker and Meijerink (1977) found that a principal component analysis transformation on images of

the mountainous regions of Basilicata in southern Italy enhanced the impression of terrain ruggedness, which was not the case when applied to the Edale image. Consequently, it is not possible to give a generalised procedure for the interpretation of Landsat imagery for landslide studies, but the individual wavebands and false-colour composite images should be analysed first in all cases to provide a regional framework from which the interpreter can progress to more processed and, therefore, more "false-looking" images if wished.

4.3 Landsat Imagery of the Matlock Area

The main conclusions drawn from assessing the use of Landsat imagery in studying landslides in the Edale region were that only landslides with certain characteristics of morphology, vegetation cover and aspect are likely to be detected and that any hazard assessment of slope instability can only be very basic. Consequently, Landsat imagery will be of greatest use at the reconnaissance stage of landslide investigations in areas with poor map coverage and/or poor accessibility.

Matlock does not fulfil either of the above conditions, therefore, little is likely to be learnt from looking at the area from Landsat. However, this part of central Derbyshire is of a slightly different character to northern Derbyshire as the Matlock area is more densely populated than Edale, with urban and industrialised areas stretching from Cromford in the south through to Darley Dale in the north

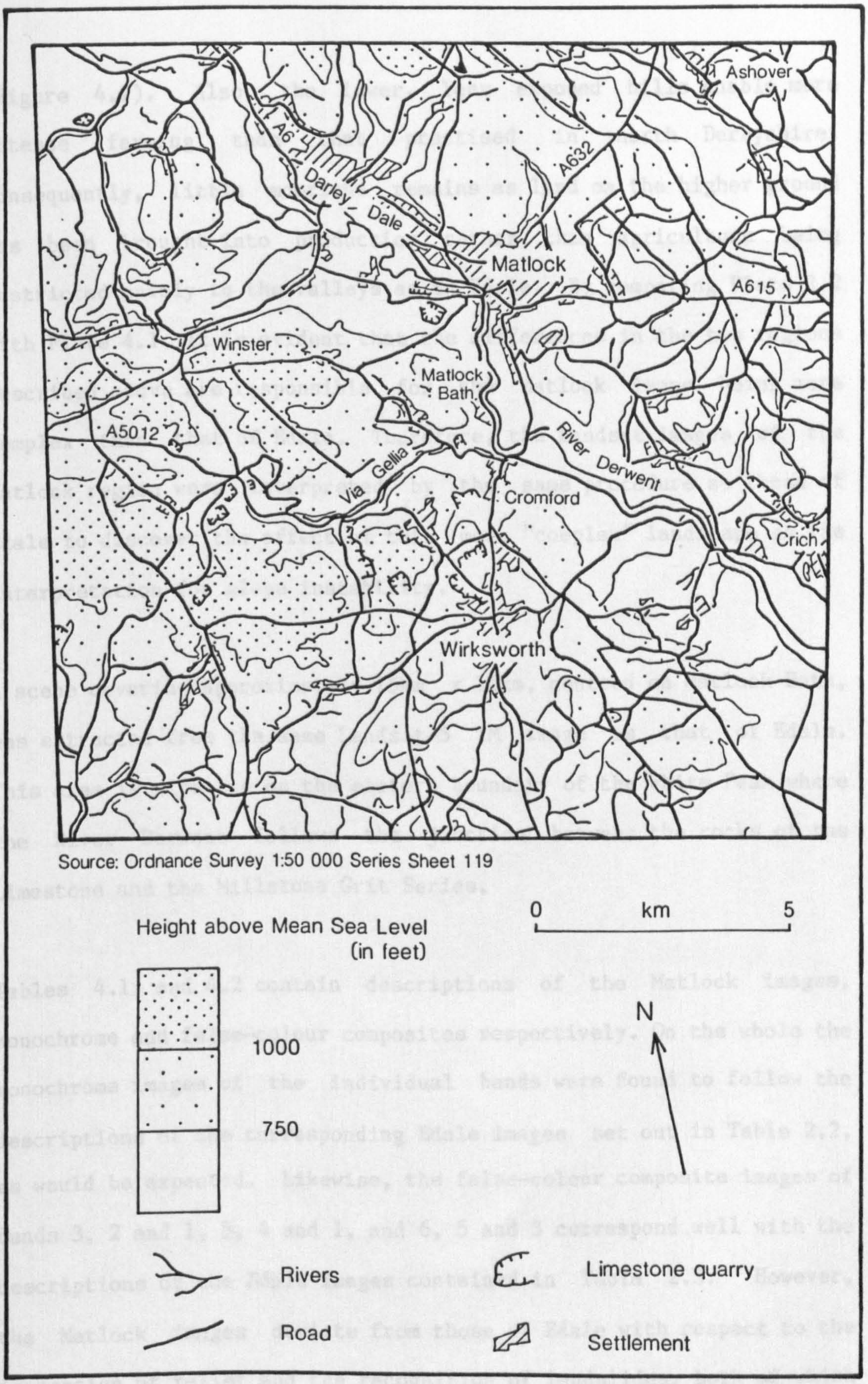

Figure 4.2 The Matlock Region

(Figure 4.2). Also, the lower, less exposed hills enable more intense farming than that practised in north Derbyshire. Consequently, little moorland remains as land on the higher ground has been brought into production rather than agriculture being restricted mainly to the valleys as in Edale. By comparing Plate 2.2 with Plate 4.1 it is evident that the differences in the two regions described above are responsible for the Matlock image being more complex than that of Edale. Therefore, the Landsat images of the Matlock region were interpreted by the same procedure as those of Edale to discover the effect of this more "complex" landscape on the interpretation for slope instability.

A scene covering approximately 15km x 15km, centred on Matlock Bath, was extracted from the same Landsat-5 TM image as that of Edale. This area is situated on the eastern boundary of the White Peak where the River Derwent follows the junction between the rocks of the Limestone and the Millstone Grit Series.

Tables 4.1 and 4.2 contain descriptions of the Matlock images, monochrome and false-colour composites respectively. On the whole the monochrome images of the individual bands were found to follow the descriptions of the corresponding Edale images set out in Table 2.2, as would be expected. Likewise, the false-colour composite images of Bands 3, 2 and 1, 5, 4 and 1, and 6, 5 and 3 correspond well with the descriptions of the Edale images contained in Table 2.3. However, the Matlock images deviate from those of Edale with respect to the impression of relief and the recognition of landslides, both of which

PLATE 4.1 LANDSAT TM IMAGE (BANDS 5, 4 AND 1)

OF THE MATLOCK REGION

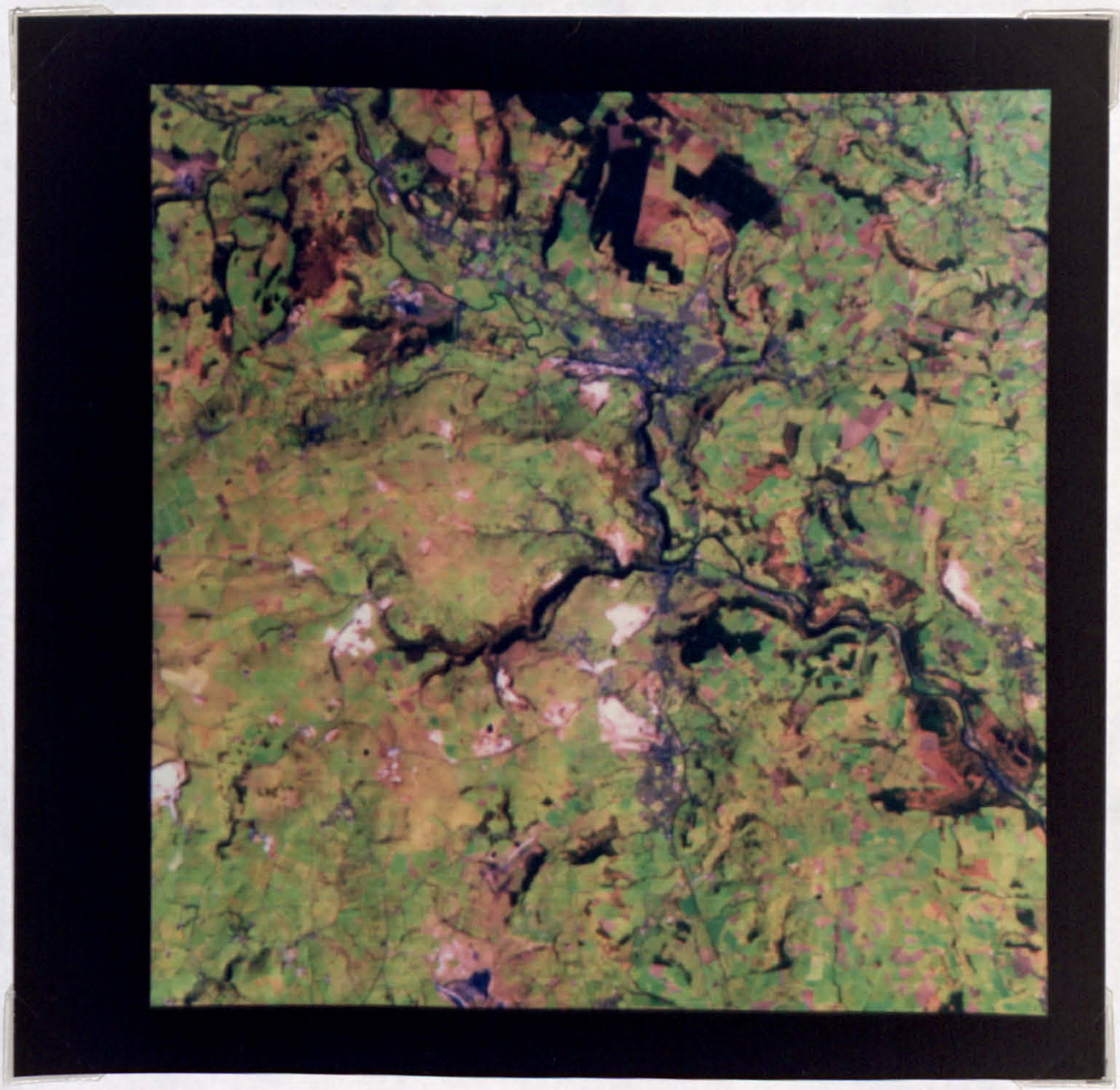

False Colour Composite 5,4,1

Sampling rate: 1,1

Image Processing: Linear Contrast Stretch

Band 5 = red ; limits of 15-150 (forward)

Band 4 = green ; limits of 10-120 (forward)

Band 1 = blue ; limits of 50-130 (forward)

TABLE 4.1 DESCRIPTIONS OF THE MONOCHROME IMAGES OF MATLOCK

BAND	CONIFEROUS WOODLAND	MOORLAND	ROUGH GRASSLAND	LUSH VEGETATION	SETTLEMENT	LIMESTONE WORKINGS	DRAINAGE	IMPRESSION OF RELIEF	LINEAMENTS	LANDSLIDES
1	—— v.dark ——		—— medium tone ——		v.light	v.light	not clear	poor	not vis.	not vis.
2	—— v.dark ——		—— medium tone ——		v.light	v.light	visible	poor	not vis.	not vis.
3	—— v.dark ——		light	medium	v.light	v.light	visible	poor	not vis.	not vis.
4	—— dark ——		medium	light	dark	v.light	v.clear	moderate	not vis.	not vis.
5	v. dark	dark	—— medium ——		dark	v.light	v.clear	moderate	not vis.	not vis.
6	v. dark	—— medium ——			not vis.	dark	not vis.	moderate	not vis.	not vis.
7	v. dark	med/dark	light/med	med/dark	light	light	clear	rel. poor	not vis.	not vis.

TABLE 4.2 DESCRIPTIONS OF THE FALSE-COLOUR COMPOSITE IMAGES OF MATLOCK

FCC	CONIFEROUS WOODLAND	MOORLAND	ROUGH GRASSLAND	LUSH VEGETATION	SETTLEMENT	LIMESTONE WORKINGS	DRAINAGE	IMPRESSION OF RELIEF	LINEAMENTS	LANDSLIDES
3,2,1	v.dark green	brown	light brown	green	white	white	rel. clear	poor	not vis.	not vis.
5,4,1 (Plate 4.1)	dark green	brown/red	pink/brown	bright green	purple	pink	v. clear	rel. good	not vis.	not vis.
6,5,3	brown/red	red	blue	green	pink	blue	clear	moderate	not vis.	not vis.

are vital in studying slope instability. Possible reasons for the virtual loss of these factors from the Matlock images will be discussed in the following section.

4.4 Interpretation of the Matlock Images

4.4.1 Relief

The infrared bands appear to contain most information about relief, the false-colour composite images of Bands 5, 4 and 1 and 6, 5 and 3 providing the basis for the derivative map of slope (Figure 4.3). By comparison with Figure 4.2 it can be seen that the impression of relief of Matlock from Landsat imagery is poor. Relief on the Edale image was picked out by shading and highlighting due to the sun being in the southeast thus suppressing the impression of relief of valleys orientated northwest to southeast. This is likely to account for slopes bordering the River Derwent and several smaller valleys going undetected. The complexity of the image, which was explained in Chapter 4.3, may also detract from the recognition of slopes as the dense patchwork of fields of variable tone in the east and the urban areas may mask the shading and highlighting caused by slope aspect.

4.4.2 Drainage

As morphological expression is poor the recognition of valleys is of

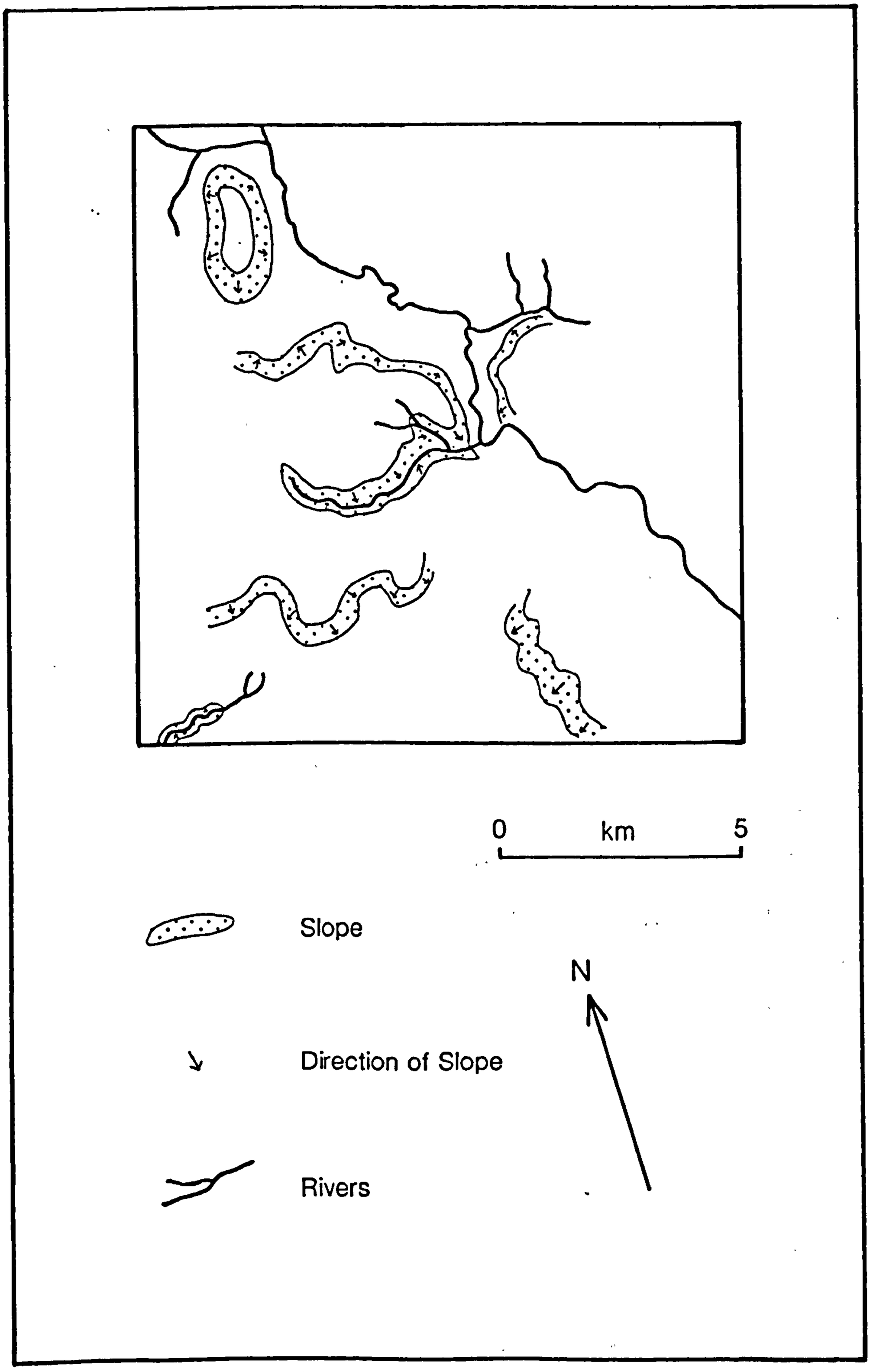

Figure 4.3 Relief and Drainage of the Matlock Region - derived from Landsat TM imagery

limited use in locating the route of rivers, therefore more emphasis has to be placed on the identification of rivers by tonal differences with the background land cover and by recognition of the meandering form. The pattern of drainage defined on the Landsat images is shown in Figure 4.3. With reference to Figure 4.2 it is again apparent that the interpretation of these images is not complete, however, the major rivers have been positively identified with little difficulty. Drainage lines on the limestone in the west are represented in Figure 4.3 although whether these are dry valleys or contain rivers cannot be judged from Landsat imagery.

4.4.3 Geology

With the prior knowledge that the rocks found within the Matlock region are of the Carboniferous Limestone and Millstone Grit Series Figure 4.4 was drawn by visual interpretation as described in Chapter 2.4.3. The limit of the limestone was quite accurately defined (compare with Figure 4.5) due to its "smoother" appearance best seen on the false-colour composite image of Bands 5, 4 and 1 (Plate 4.1). The boundary between the shale and the sandstone was less accurately identified as it was drawn purely an the prediction of shale forming the valley floors and sandstone forming the higher ground.

No lineaments were recognised on the Matlock image This may be a true representation of the structure of the region, however it is more likely to be caused by the masking of lineaments by the

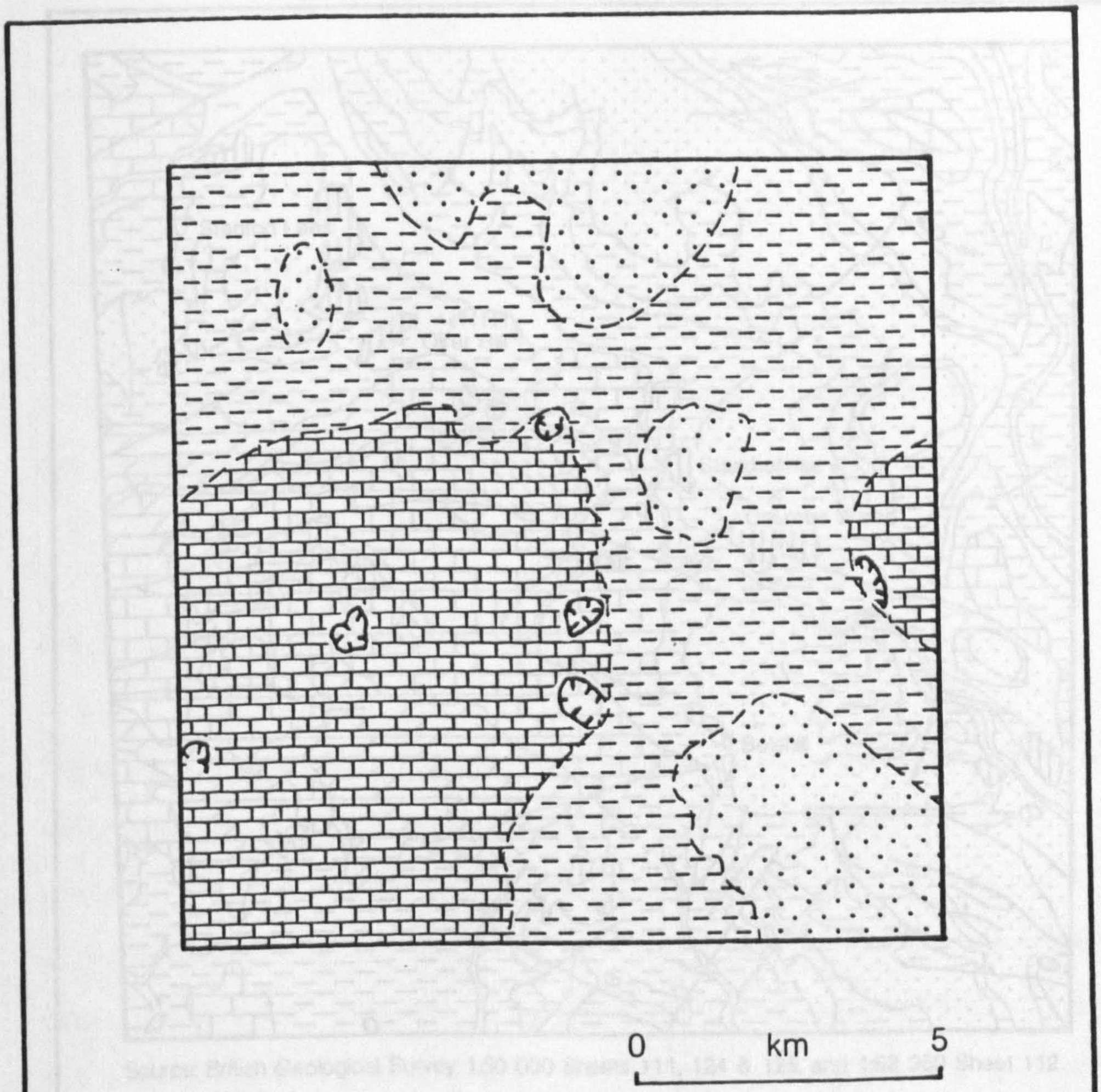

Figure 4.4 Geology of the Matlock Region
- derived from Landsat TM imagery

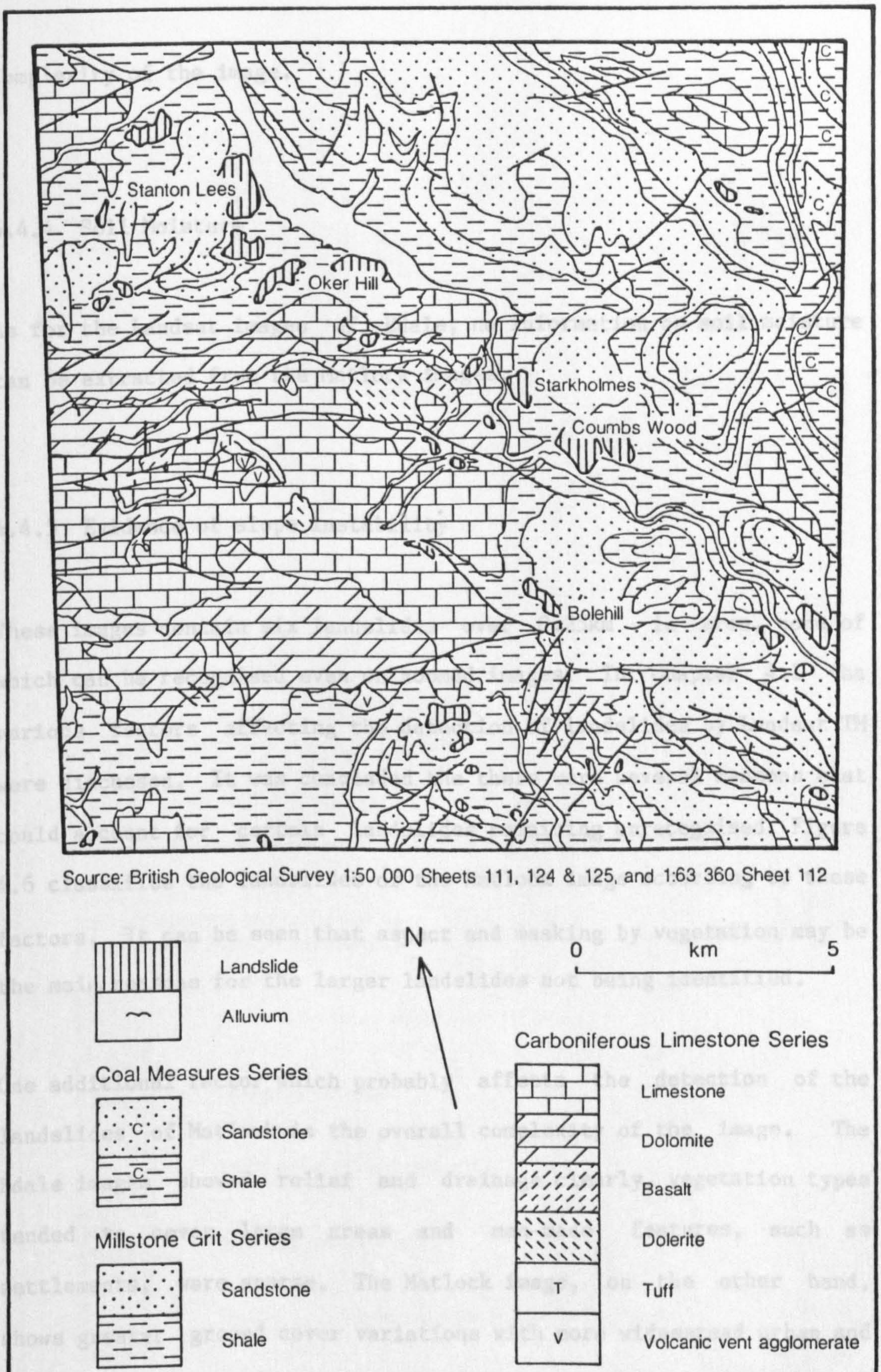

Figure 4.5 Landslides and Geology of the Matlock Region

complexity of the image.

4.4.4 Soil Moisture

As for the Landsat images of Edale, no information on soil moisture can be extracted from the Matlock images.

4.4.5 Evidence of slope instability

These images contain six landslides over 0.25km^2 in area, none of which can be recognised even on zoomed images. In Chapter 4.1 the various factors affecting the detection of landslides by Landsat TM were discussed. It was concluded the there were several reasons that could account for certain landslides remaining unrecognised. Figure 4.6 classifies the landslides of the Matlock image according to these factors. It can be seen that aspect and masking by vegetation may be the main reasons for the larger landslides not being identified.

One additional factor which probably affects the detection of the landslides of Matlock is the overall complexity of the image. The Edale images showed relief and drainage clearly, vegetation types tended to cover large areas and man-made features, such as settlements, were sparse. The Matlock image, on the other hand, shows greater ground cover variations with more widespread urban and industrial areas, more intense farming and vegetation types in small

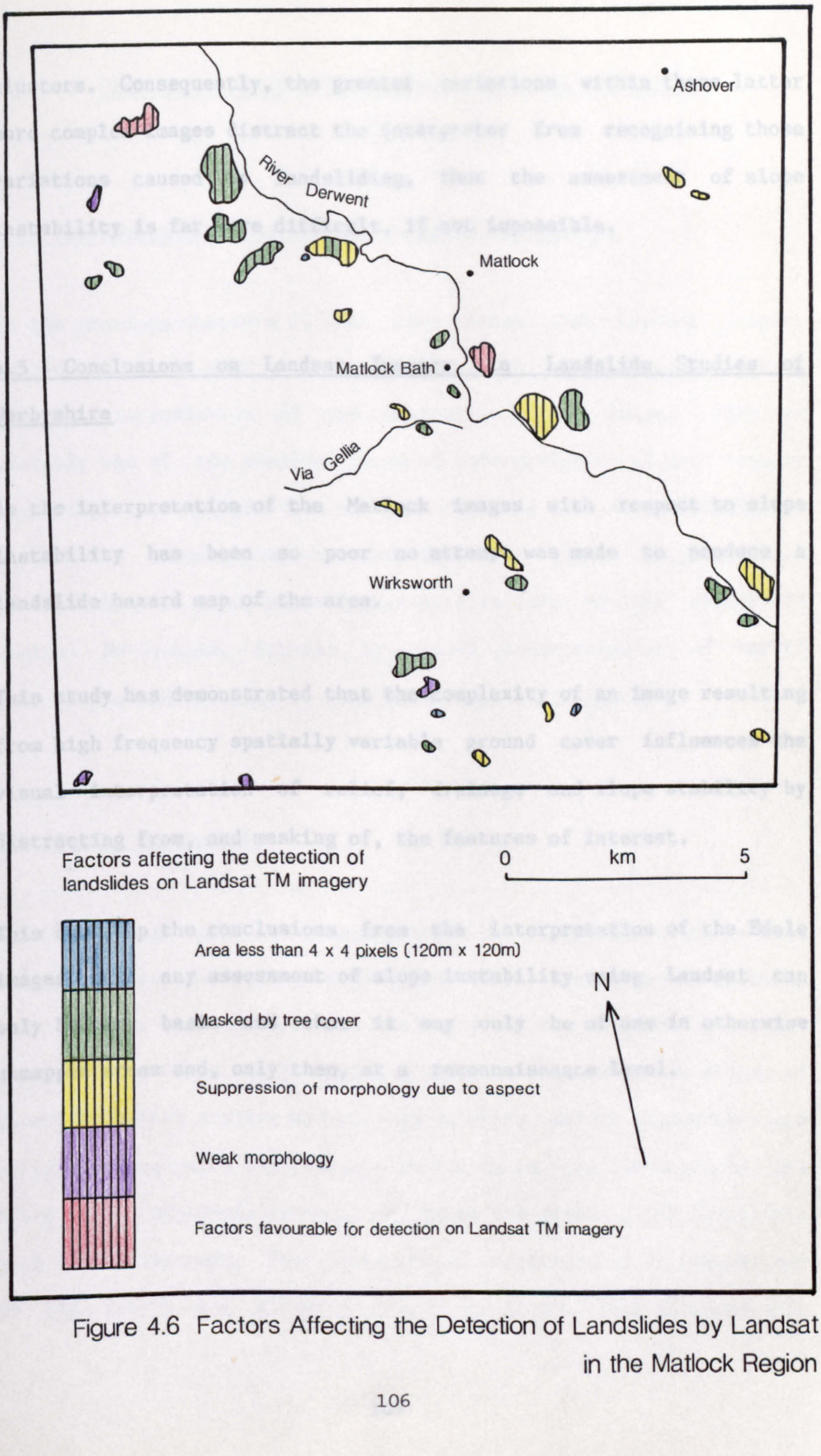

Figure 4.6 Factors Affecting the Detection of Landslides by Landsat in the Matlock Region

clusters. Consequently, the greater variations within these latter more complex images distract the interpreter from recognising those variations caused by landsliding, thus the assessment of slope instability is far more difficult, if not impossible.

4.5 Conclusions on Landsat Imagery in Landslide Studies of Derbyshire

As the interpretation of the Matlock images with respect to slope instability has been so poor no attempt was made to produce a landslide hazard map of the area.

This study has demonstrated that the complexity of an image resulting from high frequency spatially variable ground cover influences the visual interpretation of relief, drainage and slope stability by distracting from, and masking of, the features of interest.

This backs up the conclusions from the interpretation of the Edale images that any assessment of slope instability using Landsat can only be very basic and that it may only be of use in otherwise unmapped areas and, only then, at a reconnaissance level.

CHAPTER 5 PHOTO-INTERPRETATION OF SLOPE INSTABILITY

5.1 Introduction to Photography in Landslide Studies

In the previous chapters it has been shown that Landsat imagery should first be used in a similar manner to aerial photographs by a visual interpretation of the contrast-enhanced image. This is probably one of the simplest forms of interpretation of such imagery requiring least manipulation of the data and also it is a technique with which geomorphologists are familiar. This chapter uses photography to study slope instability in the Matlock region of central Derbyshire, firstly by visual interpretation of aerial photographs and secondly by hand-held infrared photography.

5.2 Aerial Photography

Much previous work in geomorphology has involved using aerial photographs to provide an overall view of the area of study enabling the features of interest to be studied in relation to their environment. Cooke et al. (1982) provide an account of the stages of geomorphological mapping and surveys at which aerial photographs are of use. Stereo-pairs are commonly available as the photographs are taken with a sixty-six percent overlap of the ground along the flight path of the aircraft. This stereoscopic capability is of immense use to the interpreter allowing the recognition of form of geomorphic

features. A detailed account of the use of aerial photographs in interpretation and mapping of geology and landforms is provided by Ray (1960).

In this study of slope instability in the Matlock region stereoscopic aerial photography at a scale of 1:12,000 was used to produce morphological and geomorphological maps, the former involving the mapping of surface form and the latter providing the interpretation of the morphology. Figure 5.1 provides a geomorphological interpretation of the Matlock region constructed from several photographs. More detailed morphological and geomorphological maps were produced of Oker Hill (Figures 5.2 and 5.3) from photographs enlarged to a scale of approximately 1:7,270 (Plate 5.1).

5.2.1 Relief

Impression of relief can be gained from a single photograph if the slopes are shaded and highlighted by the sun. With overlapping photographs stereoscopic viewing is possible which clearly depicts morphology. Such photographs can also be used to contour the ground and to provide height data (Lillesand and Kiefer, 1979; Ray, 1960). Manually, this is very time-consuming but it can also be done automatically. The work shown in Figure 5.2 does not involve such photogrammetric techniques, but a morphological map was derived from stereo-pairs of aerial photographs of the Matlock area and Oker Hill in particular. This is a quick and effective method for defining the

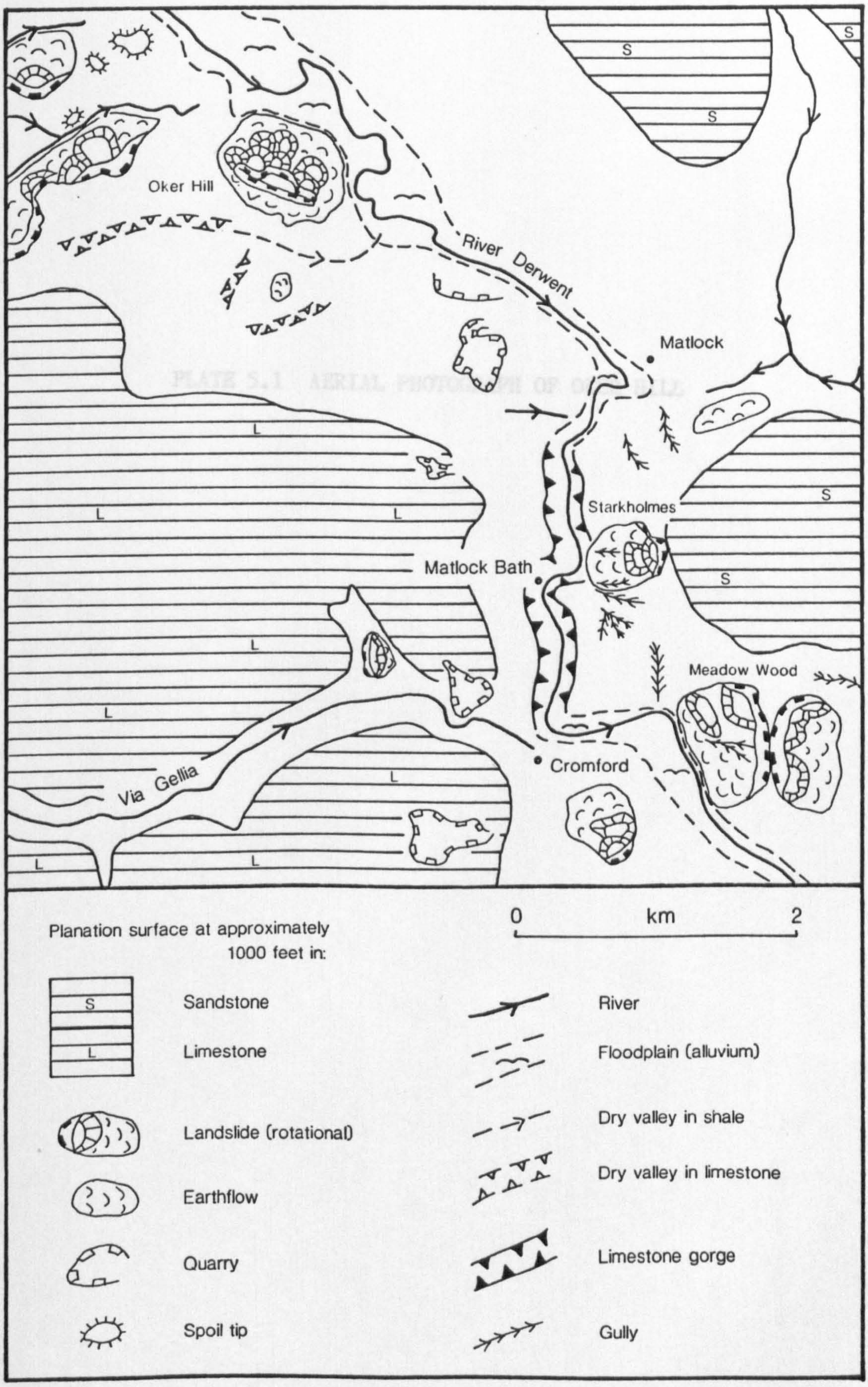

Figure 5.1 Geomorphological Sketch Map of the Matlock Region - derived from aerial photographs

PLATE 5.1 AERIAL PHOTOGRAPH OF OKER HILL

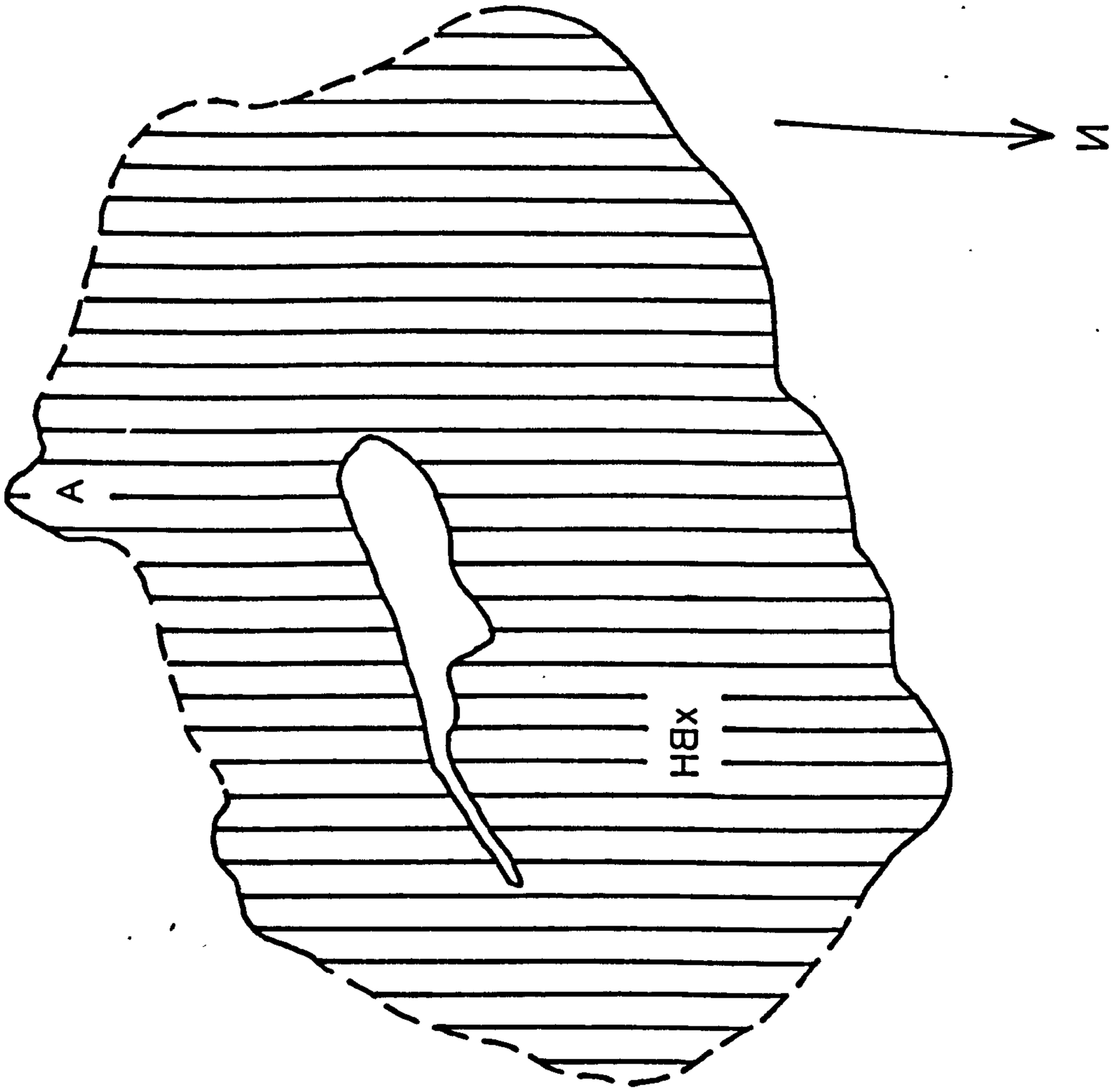

Landslide

Recent Slump

Site of Boreholes

0 metres 300

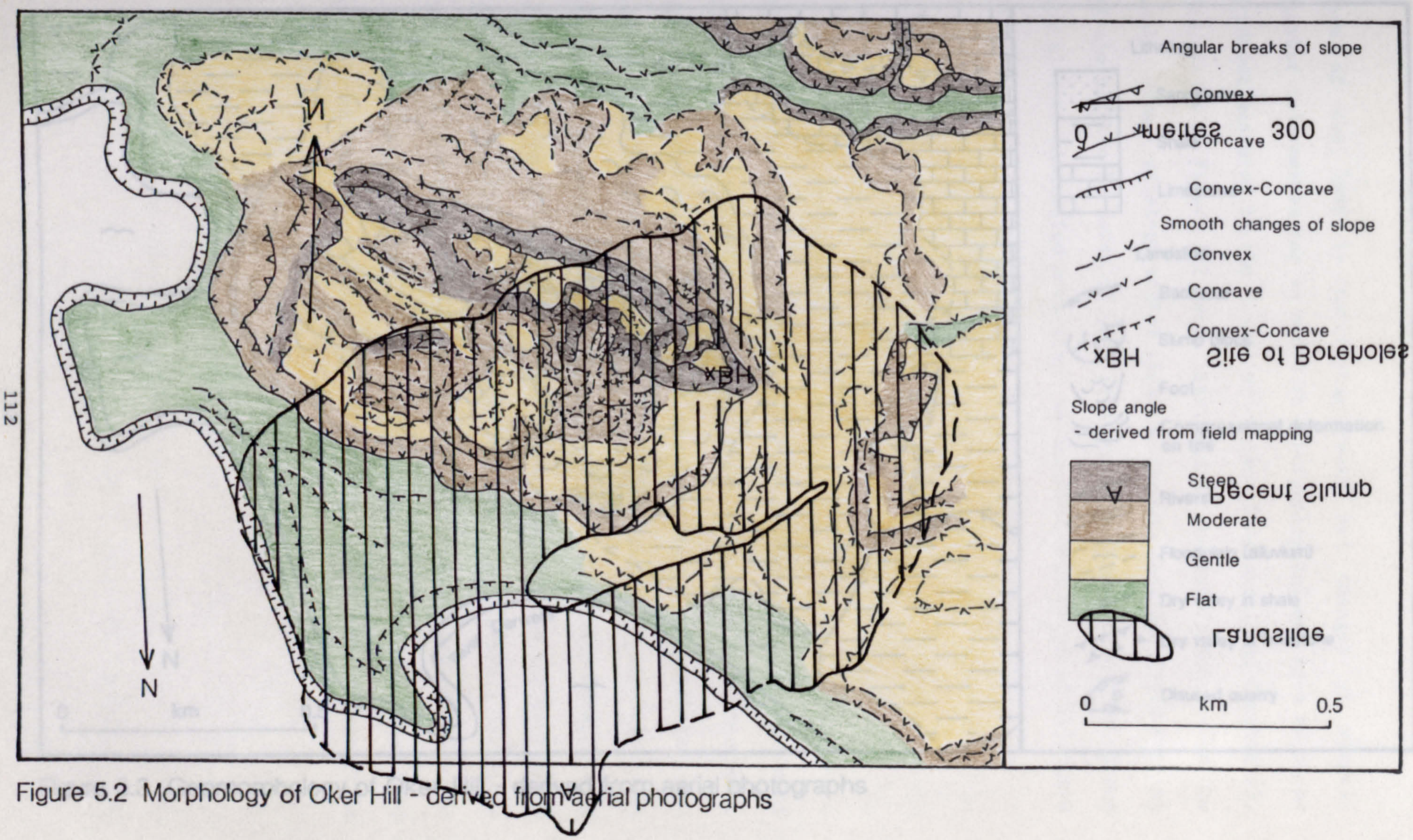

Figure 5.2 Morphology of Oker Hill - derived from aerial photographs

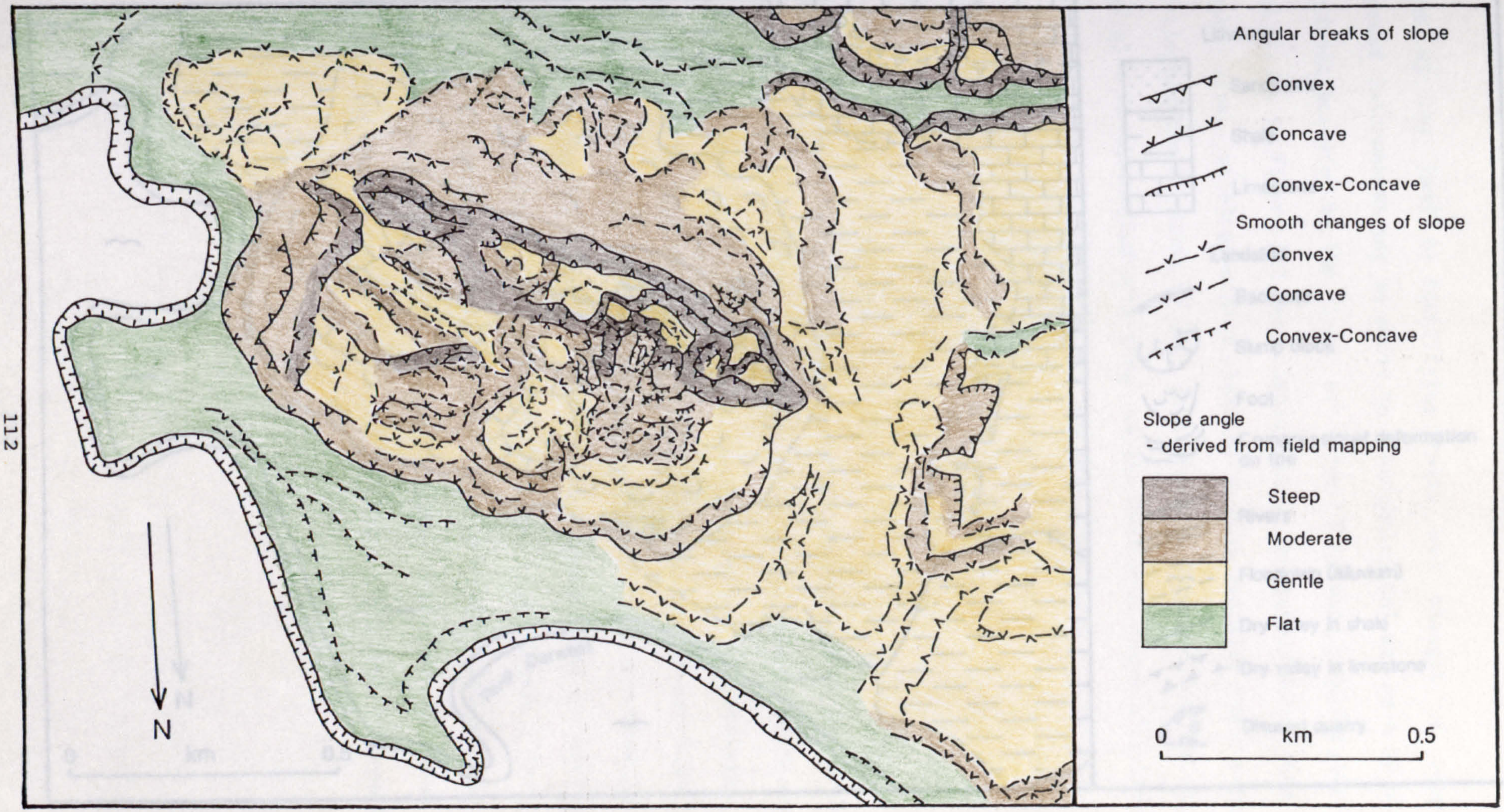

Figure 5.2 Morphology of Oker Hill - derived from aerial photographs

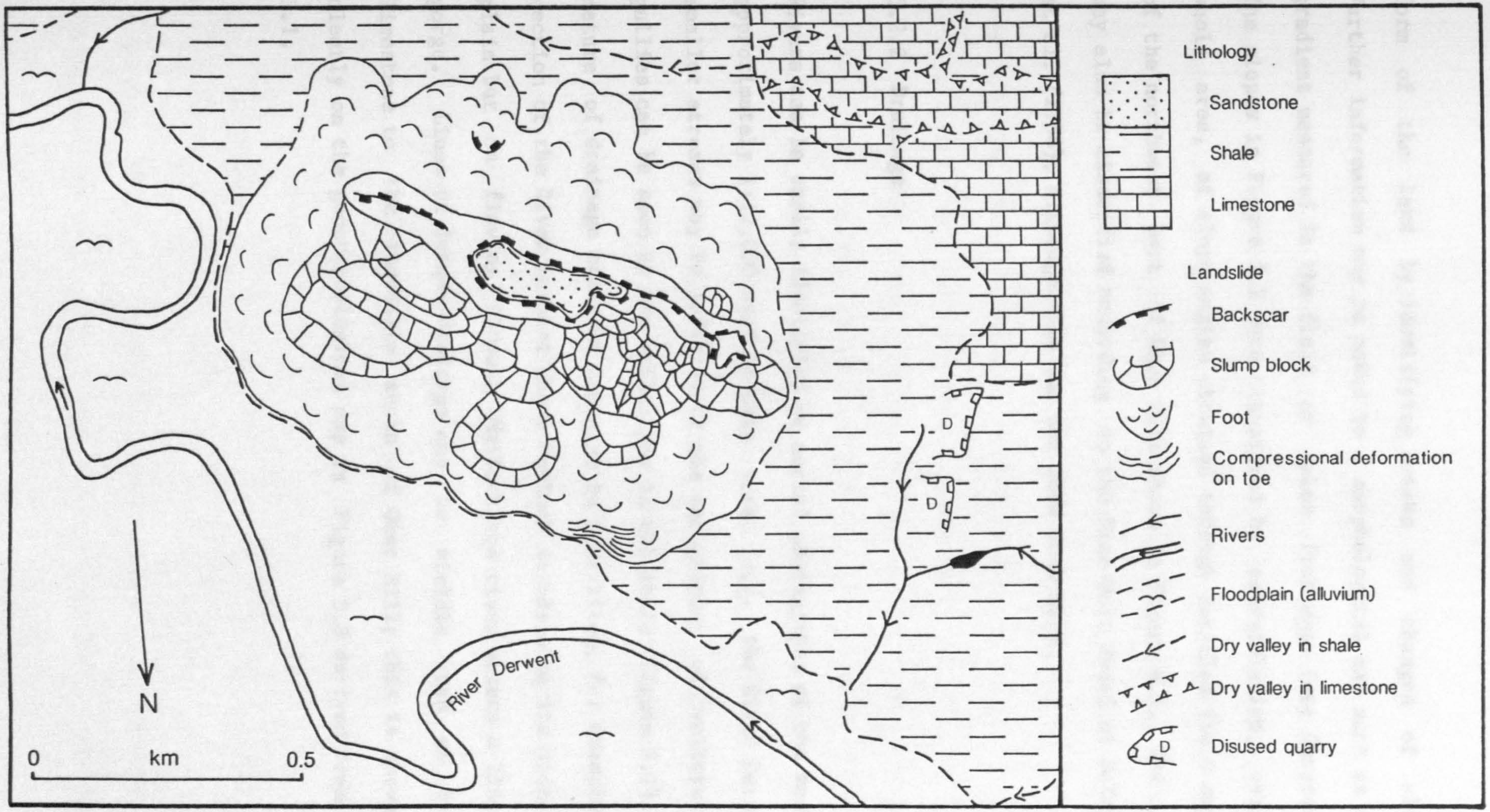

Figure 5.3 Geomorphology of Oker Hill - derived from aerial photographs

form of the land by identifying breaks and changes of slopes. Further information may be added to a morphological map such as slope gradient measured in the field or taken from maps (see Chapter 6). The slopes in Figure 5.2 were classified by extrapolation, over the whole area, of slope angles obtained through detailed field mapping of the northwest part of Oker Hill shown in Figure 6.5. The slopes may also be classified according to the Nine-Unit Model of Dalrymple et al. (1968), although this has not been done here.

5.2.2 Drainage

Rivers can be easily identified on aerial photographs of the scale of approximately 1:12,000 used in this work (e.g. the River Derwent), smaller streams may be inferred by the recognition of valleys, and gullies can be seen on the hillslopes in the shale (Figure 5.1). The nature of drainage channels can also be identified, for example, the section of the River Derwent above Matlock meanders on its wide flood plain but on flowing through Matlock the river enters a limestone gorge. Lines of former drainage may be visible such as on the limestone to the immediate south of Oker Hill; this is shown more clearly on the geomorphological map in Figure 5.3 derived from Plate 5.1.

5.2.3 Geology

Aerial photography is an important tool in geological mapping as the underlying geology influences surface form, drainage and vegetation through resistance to weathering and erosion, permeability, jointing and structure (Lillesand and Kiefer, 1979; Ray, 1960). From the aerial photographs of Matlock and the corresponding geomorphological sketch map it can be seen that the limestone forms a plateau in the west on which there is little surface drainage. Where the River Derwent cuts through the limestone it is bordered by high cliffs and steep slopes, this is also the case where a river flows through Via Gellia. The surface of the limestone area is generally smooth and grass covered, and quarries and mineral workings are common man-made features in this part of Derbyshire. In contrast to the limestone, shale, being prone to weathering and erosion and being impermeable, tends to form the low-lying ground and carries much surface drainage. Also, Figure 5.1 indicates that where the River Derwent undercuts steep shale slopes, landslides tend to be present (e.g. Starkholmes and Meadow Wood). The shale is overlain by resistant sandstone forming a plateau in the east and north. These areas are well-drained and may support moorland vegetation.

5.2.4 Vegetation

Basic types of vegetation may be discernible on panchromatic aerial photographs of this scale, for example grassland, moorland and

woodland. Plate 5.1, at a scale of approximately 1:7,270, also enables the tentative identification of marsh vegetation within the slump blocks of the upper part of the landslide on the basis of texture and tone, although the darker tone may be due to moisture.

5.2.5 Soil Moisture

Little information concerning soil moisture can be extracted from these panchromatic aerial photographs. However, as mentioned above, the recognition of marsh indicates a concentration of water.

5.2.6 Existing Landslides

On stereoscopic aerial photographs landslides can generally be recognised by their morphology: steep backscar, slump blocks and hummocky foot. This is the case for the landslides identified in the Matlock area where form was defined by morphological mapping and subsequently interpreted to produce the geomorphological sketch map (Figure 5.1). Also, the boundaries of previously failed ground and stable slopes can be clearly seen where they are not obscured by woodland. Unfortunately, in this area many slopes are wooded and this tends to mask landslides, for example, although the landslides in the northwest part of the region (Figure 5.1) can be detected the detail has been lost through the trees. Oker Hill landslide (Figure 5.3 and Plate 5.1) is part-wooded and detail in these places is also

lost to a great extent.

5.2.7 Geomorphological Interpretation

One of the main benefits of aerial photo-interpretation is that landforms can be studied easily in the context of situation, i.e. in relation to the surrounding environment.

Firstly, in the Matlock region, the presence of former drainage channels indicates the importance of past conditions and processes on the present form of the land. Consequently, in a geomorphological interpretation the geological history of Derbyshire must be borne in mind, particularly the period during and after the Ice Ages of the Quaternary. The rivers of this area are believed to represent superimposed drainage (Clayton, 1968; Doornkamp, 1971; King, 1966; Linton, 1956), strong evidence for this being the limestone gorge at Matlock Bath. At an earlier time in the river's history the Millstone Grit would have extended further west covering the limestone and the Derwent would have flowed wholly within the shale and sandstone at a higher level corresponding to the planation surfaces (the limestone and sandstone plateaus in the west and east of Figure 5.1). The river would have tended to migrate eastward down the dip of the Millstone Grit Beds and the shale and sandstone would thus have retreated eastward by erosion exposing the limestone. However, during the Pleistocene, at a time when the volume of water was greatly increased by meltwater, the river became incised in response

to falling sea levels resulting in local superimposition on the limestone, as seen at Matlock Bath (Doornkamp, 1971; King, 1966; Linton, 1956).

The incision of the main valleys resulted in a lowering of the water table below the floors of many smaller valleys within the limestone plateau thus creating dry valleys (Linton, 1956). Such dry valleys can be seen to the south of Oker Hill in Figures 5.1 and 5.3. The water table in this region of Derbyshire has been lowered further by soughs driven in the eighteenth and nineteenth centuries to drain the lead mines.

At one point in the limestone gorge at Starkholmes the river has once again eroded into the shale (Figures 1.2 and 5.1); combined with other factors contributing to slope instability, this undercutting has resulted in landsliding. The River Derwent also undercuts a shale slope downstream from the gorge and this is also the location of a large landslide at Meadow Wood (Figure 5.1). To the north of Matlock, in the broader valley cut in shale, the river is at present in a position where it can undercut the eastern extremity of an existing landslide at Oker Hill. From the geomorphological map of Figure 5.3 it can be seen that the foot of the landslide touches the flood plain, implying that in the past the Derwent undercut this hillside, possibly at times of higher water levels due to meltwater or heavy rainfall or during normal meander migration. The site of Oker Hill in relation to the limestone gorge should also be noted; it is possible that at times of high river discharge (i.e. meltwater

during the Pleistocene) the gorge would act as a bottleneck and water would be held up on the Oker Hill side of Matlock causing flooding thus increasing the potential for slope instability through undercutting and raised pore-water pressures at the foot of the slopes.

To conclude, with a knowledge of the conditions responsible for creating the landforms in an area, aerial photographs can be used to study geomorphology and to gain the regional view required to put each landform in context with its surrounding environment.

5.3 Infrared Photography

Aerial photographic surveys can also use colour or infrared films; Curtis (1973) describes the use of the various types of film for soil mapping, listing the advantages and disadvantages of each. Colour infrared film has the advantage of enhancing contrast between certain features such as types of vegetation, this was also found to be the case for the infrared bands of Landsat TM in Chapter 2 (Tables 2.2, 2.3, and 2.4). Infrared wavelengths may penetrate haze to a certain extent, and information on soil moisture may be extracted.

Penn (1984) compares the ability of panchromatic, colour and false-colour infrared film to record various features associated with landsliding. The infrared film has the potential to provide more information on moisture conditions through the effect on plant health

and development. As the reflected electromagnetic radiation in the near-infrared is dominated by vegetation, differences in vegetation density and health are recorded by varying intensity of colour, therefore, bright red areas on the photographs correspond to healthy, well-developed plant cover which may reflect high soil moisture levels or springs and seepage zones. Areas without vegetation appear blue-grey. Colour infrared photography may be helpful in mapping hidden cracks and fissures through their influence on vegetation growth. For example, freely-drained fissures above the water table may inhibit plant growth thereby appearing dull red coloured (Sowers and Royster, 1978).

Curran (1981) describes a technique for estimating the surface moisture content of a vegetated soil using aerial infrared photography. This involves measuring and plotting the relative proportion of leaves and soil against the near-infrared bidirectional reflectance value of a point on the ground, the y-axis intercept provides an estimate of the surface soil moisture content.

Penn (1984) describes an oblique aerial false-colour infrared photograph of the Mam Tor, Cold Side and Rushup Edge landslides. Variations in vegetation can be recognised and an area of wetter ground within Cold Side landslide can be identified, however, it is possible that these features would also have been visible with panchromatic or colour film. In addition, the shadows created by backscars and hummocky ground create tonal variations which distract from those caused by vegetation and soil moisture.

Unfortunately, no aerial colour infrared photographs exist for the Matlock region of Derbyshire. However, it was possible to take hand-held, ground-based infrared photographs in order to gain some idea of the additional information available at the longer wavelengths and for comparison with the Landsat imagery and the panchromatic aerial photographs. Technical details of these photographs are set out below:

Camera: Minolta

Film: Kodak Ektachrome Infrared Film

Filters: Kodak Wratten No. 12 and UV

Meter Setting: ASA 100, 21 DIN

Exposure: Best results obtained by underexposure by one stop

Colour infrared film differs from ordinary colour film in that the three sensitive layers are sensitive to green, red and infrared radiation, instead of the visible blue, green and red wavelengths. The green, red and infrared sensitive layers are developed to yellow, magenta and cyan positive images respectively (see Figure 5.4), therefore, the photographs are false-colour. This colour-shift causes water and wet soil to be represented in blue and blue-grey tones and healthy vegetation to appear in shades of red to magenta and yellow.

Three landslides were studied via infrared photography: Mam Tor in Edale and Starkholmes and Oker Hill landslides near Matlock. The

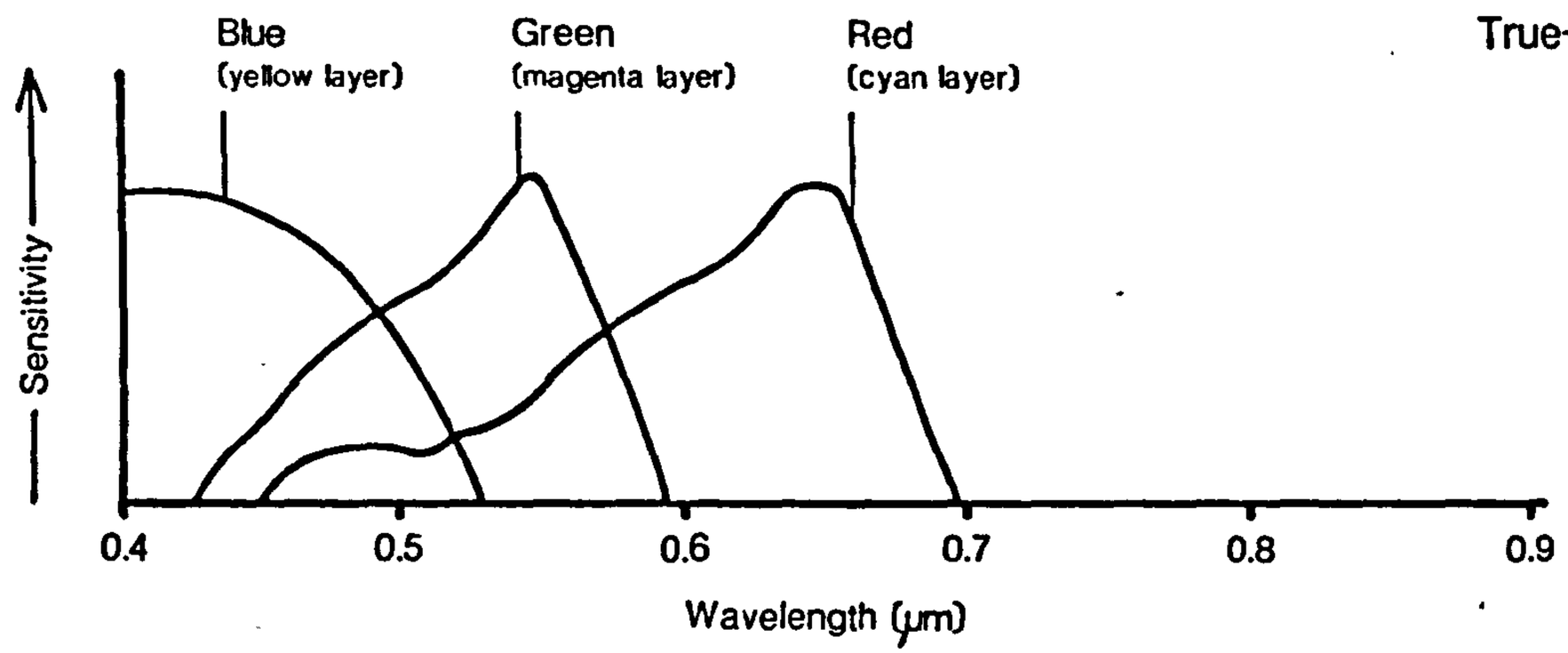

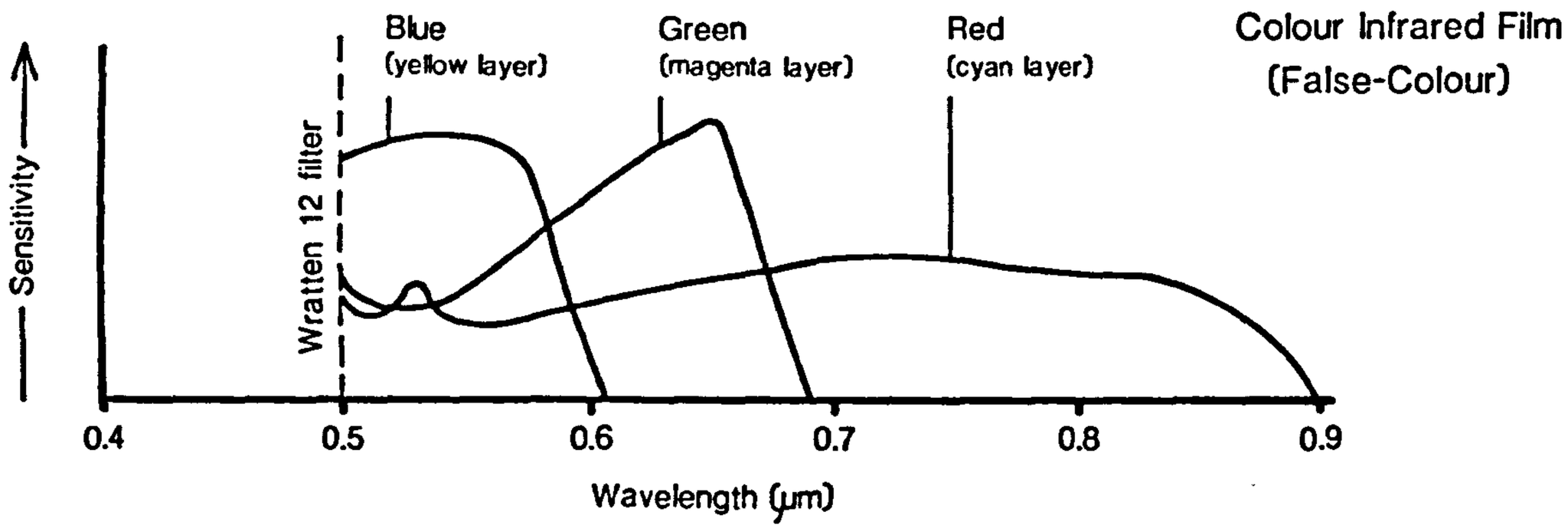

Figure 5.4 Wavelengths of Colour and Colour Infrared Films

effects of shadow were kept to a minimum by taking the photographs at Mam Tor when there was a complete cloud cover and at Matlock when there was hazy sunlight. This was necessary in order to avoid confusion between tonal variations caused by ground conditions and by shadow.

Plates 5.2a and 5.2b are typical examples of normal colour and colour infrared photographs of these landslides. It can be seen that on the infrared photograph lush grass is pink, and dry or dead vegetation is blue to blue-grey toned. The small scars of soil and shale can be seen more clearly in Plate 5.2b due to the greater contrast of this film. Pools and marsh appeared blue toned but they were just as clearly visible on the normal colour photographs. Limestone and shale exposures were also blue-grey toned. In general, the infrared photographs penetrated haze better than the corresponding normal colour photographs, this is because haze is recorded in the visible blue part of the electromagnetic spectrum which the Kodak Wratten No. 12 filter cuts out. However, although the infrared film has the potential to record additional information to normal colour film, from this brief study it was not found to have much advantage over normal photography. Soil moisture conditions expressed either directly or through the effect on vegetation were not noticeably recorded to any greater extent than already apparent by the visible wavelengths.

These photographs were taken at the same time of year as the Landsat imagery (mid-April to early May) in order to allow comparison between

PLATE 5.2a HAND-HELD COLOUR PHOTOGRAPH

OF OKER HILL LANDSLIDE

PLATE 5.2b HAND-HELD COLOUR INFRARED PHOTOGRAPH

OF OKER HILL LANDSLIDE

PLATE 5.3 LANDSAT TM IMAGE (BANDS 4, 3 AND 2)

OF DARLEY DALE, MATLOCK

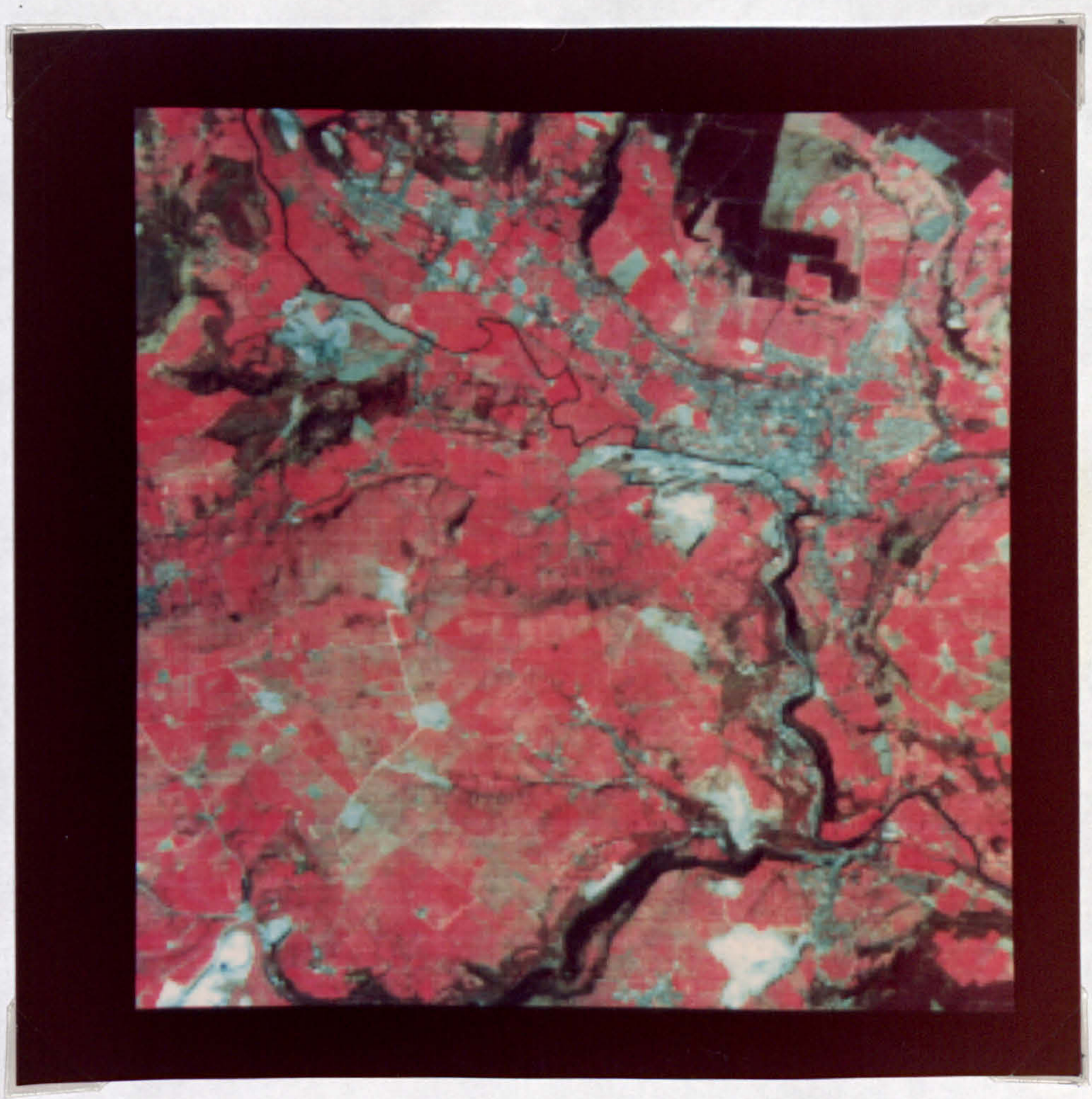

False Colour Composite 4,3,2

Sampling rate: 1,1

Image Processing: Linear Contrast Stretch

Band 4 = red ; limits of 15-150 (forward)

Band 3 = green ; limits of 10-120 (forward)

Band 2 = blue ; limits of 50-130 (forward)

the two types of imagery as the vegetation would be at the same growth stage. Also, it is intended to assess whether more information could be extracted when used in conjunction with each other. The equivalent Landsat TM image to colour infrared photography is the false-colour composite of Bands 4, 3 and 2. Plate 5.3 is such an image of Matlock and it includes the Oker Hill and Starkholmes landslides. The similarity between Plates 5.2b and 5.3 is clear, however, it would appear that the only advantage of using both types of imagery together is that the infrared photography can provide ground information on vegetation type for use with the satellite imagery. It should be borne in mind that aerial colour infrared photography, due to the wider area of coverage, will undoubtedly be of more use in conjunction with Landsat imagery than hand-held photographs.

5.4 Conclusions on Photographic Surveys in Slope Stability Investigations

Although the types of photography used in this chapter are very limited it is still possible to draw some conclusions.

Firstly, aerial photo-interpretation is an invaluable technique in both specific slope instability studies and general geomorphological surveys. It provides a regional view of an area, as does Landsat, but the much greater spatial resolution and stereoscopic capability allow a more detailed and accurate analysis. Repeated aerial surveys

also enable monitoring of unstable slopes (e.g. Bonnard, 1983).

A variety of films may be employed in aerial surveys: panchromatic, colour, black and white infrared and colour infrared. Interpretation of land form is unlikely to be influenced by film type although colour and colour infrared photography will provide more information on vegetation type and land cover in general. Although the ground-based colour infrared photography described in the previous section proved to be of little advantage over normal colour photography at such a close range, it was evident that it provided greater contrast between vegetation types. Therefore, it is understandable that this type of film is so useful in aerial surveys involving vegetation. It should also be noted that the time of the year will affect infrared photography as vegetation growth is dependent on season. For example, in spring last year's bracken growth, although dead, still covers the ground; it is in the late spring to early summer that new growth begins. This variation in vegetation throughout the year will influence the use of infrared imagery in detecting such factors as soil moisture conditions. The effect of season on the study of slope instability by photography is therefore of great importance.

Finally, the various forms of photography are useful in the interpretation of Landsat imagery by providing ground information. The photographic coverage of the ground is likely to be more limited than that of a Landsat image and, therefore, the confirmation of a certain ground cover type or feature in an area with ground information allows extrapolation to other similar areas for which no

such information exists. In the interpretation of the Edale and Matlock Landsat images both panchromatic aerial photographs and field work were used as ground information.

To conclude, aerial photography is of great use in studying landsliding as it provides much information about the geomorphology of the area of interest and enables an understanding of the interaction of the various processes in operation which may affect slope stability.

CHAPTER 6 GROUND INVESTIGATION OF OKER HILL

6.1 Introduction to Oker Hill

The remainder of this work deals exclusively with one landslide, and involves field mapping and subsurface investigations to further the understanding of slope failure in the Carboniferous sandstone and shale of Derbyshire.

The landslide of interest is situated two kilometres to the northwest of Matlock on Oker Hill at the point where the River Derwent flowing from the north is deflected to the east into the limestone gorge section (Figures 6.1, 6.2 and 6.3). This hill is formed from Namurian shale capped by Ashover Grit and rises from ninety-four metres above ordnance datum at the valley floor to 193 metres at the summit. The valley floor is covered by alluvium and a remnant of a terrace occurs on the north side of the river (Waters and Johnson, 1958).

During and after the periglacial conditions of the Devensian Ice Age the River Derwent to the north of Matlock would have eroded and cut into the sandstone and shale while slope processes such as solifluction widened the valley. Between Matlock and Cromford this downcutting resulted in the formation of the limestone gorge (Clayton, 1968; Doornkamp, 1971; King, 1966; Linton, 1956). From the geomorphological sketch map constructed from the aerial

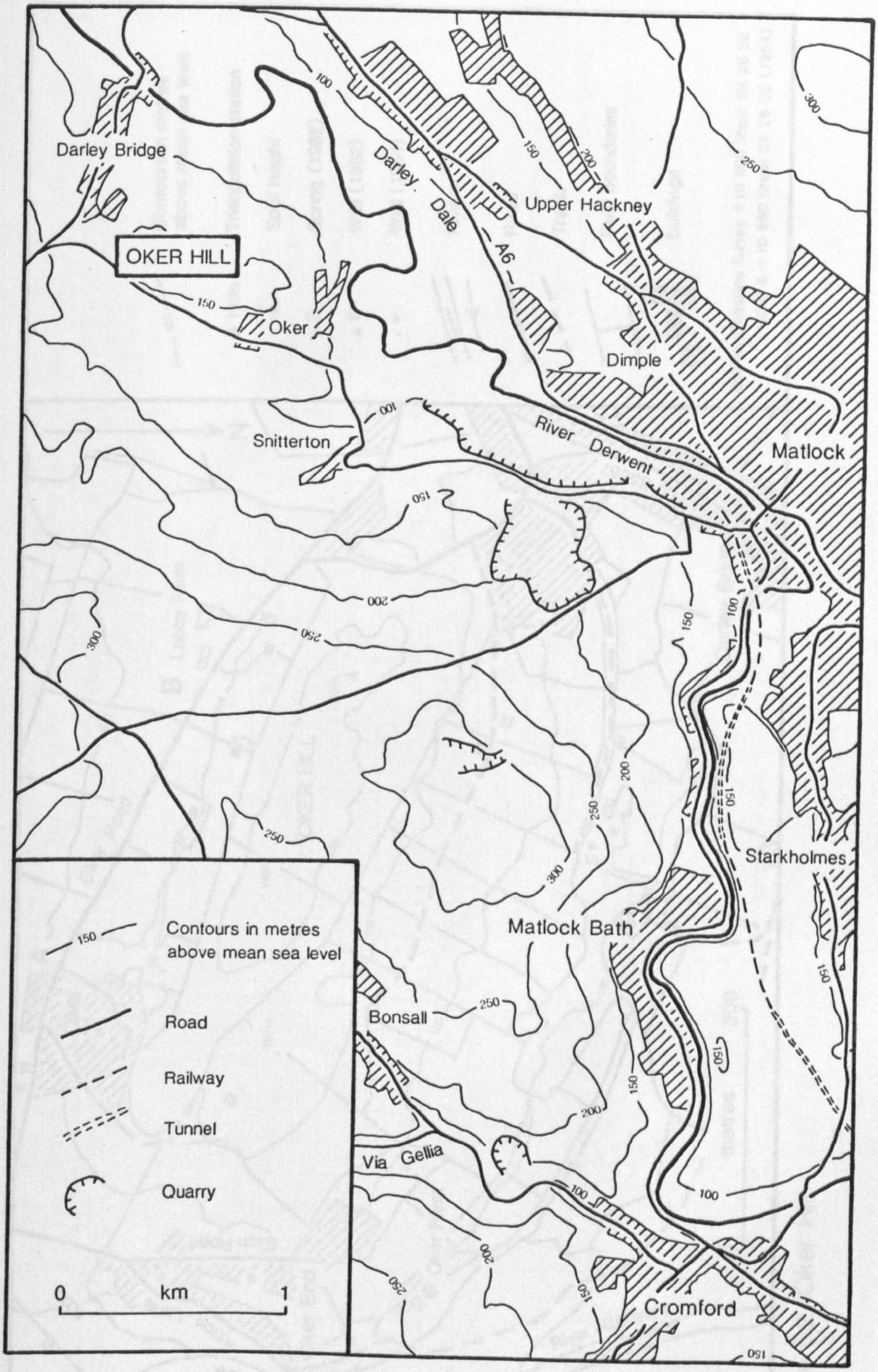

Figure 6.1 Location of Oker Hill

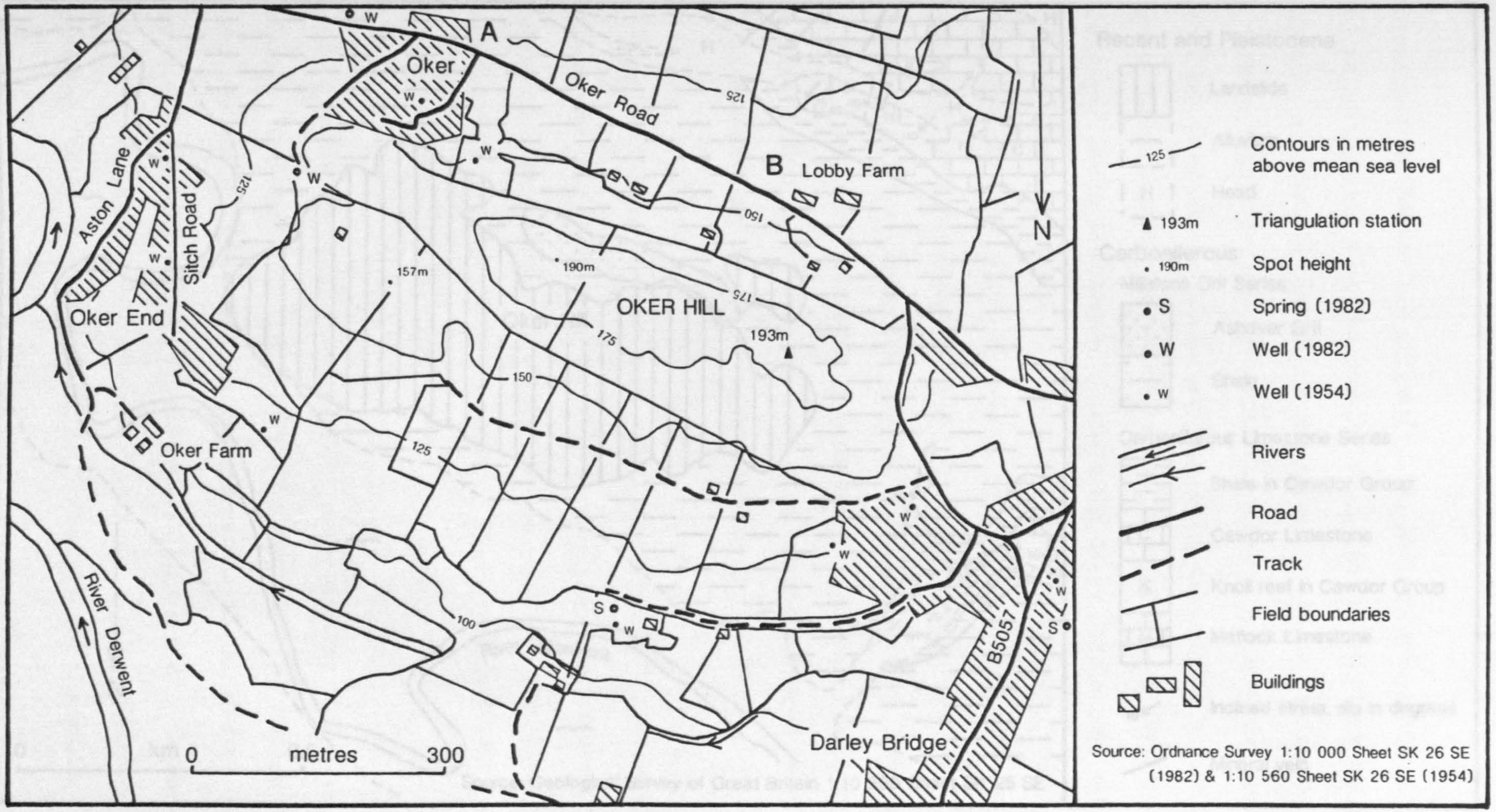

Figure 6.2 Oker Hill

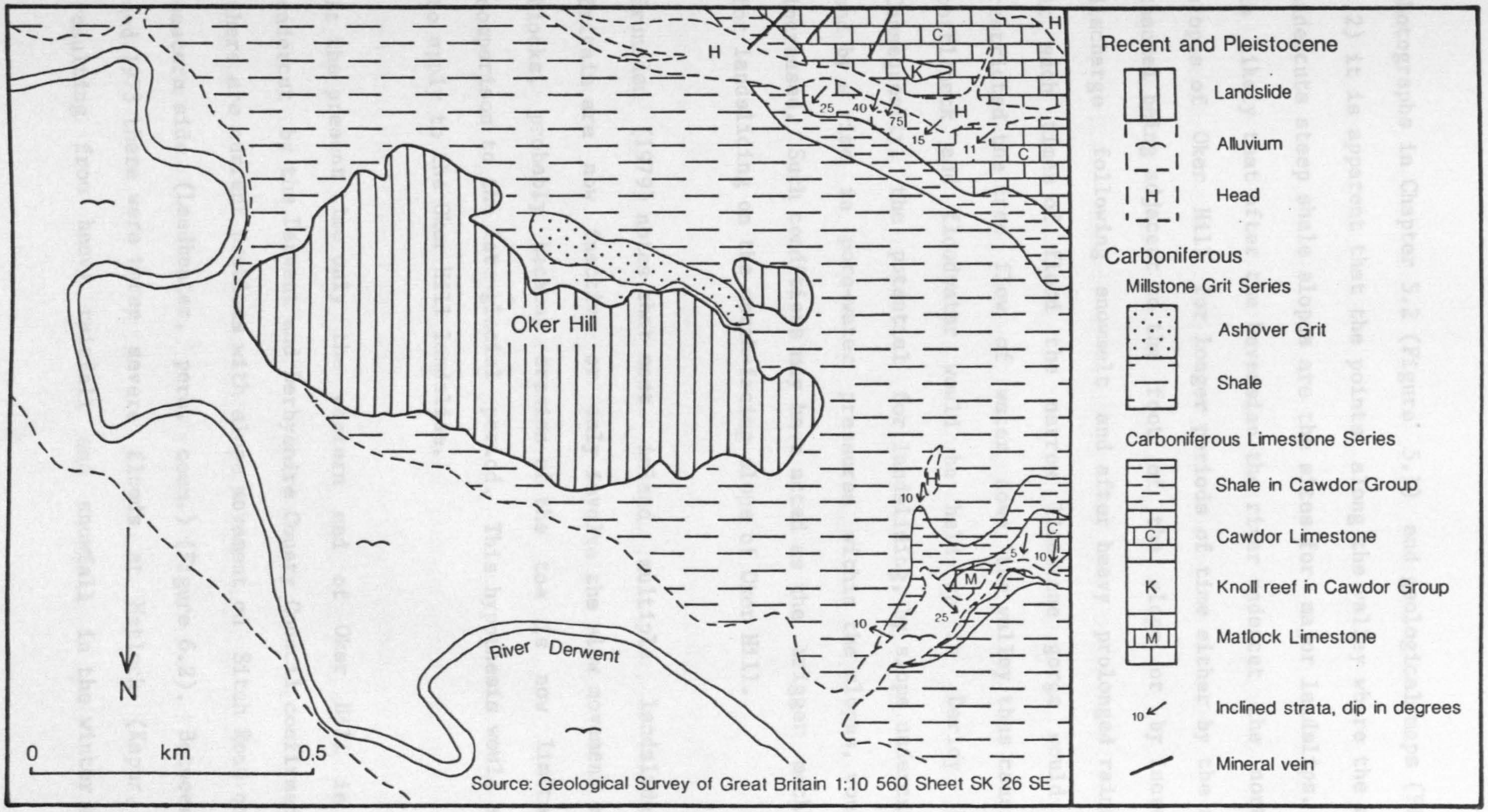

Figure 6.3 Geology of Oker Hill

photographs in Chapter 5.2 (Figure 5.1) and geological maps (Figure 1.2) it is apparent that the points along the valley where the river undercuts steep shale slopes are the sites for major landslips. It is likely that after the Devensian the river undercut the northern slopes of Oker Hill for longer periods of time either by the river channel being adjacent to the foot of the slope or by increased discharge following snowmelt and after heavy prolonged rainfall. At such times of flood the narrow limestone gorge would have restricted the free flow of water down the valley thus causing a bottleneck and floodwater would be held up in Darley Dale. Consequently, the potential for landsliding, by slope undercutting and by a rise in pore-water pressures within the slopes, would be increased. Such conditions may have acted as the trigger mechanism for landsliding on the north-facing slope of Oker Hill.

Brunsden (1979) notes that most inland multiple landslides in Britain are now inactive or only involve the slow movement of old blocks, probably because erosion of the toe is now limited in comparison to the late-glacial period. This hypothesis would appear to apply to the Oker Hill landslide.

At the present time only the eastern end of Oker Hill is being undercut by the Derwent and Derbyshire County Council confirmed that there are current problems with slope movement on Sitch Road on this eastern side (Leadbeater, pers. comm.) (Figure 6.2). Between 1930 and 1973 there were three severe floods at Matlock (Kapur, 1974) resulting from heavy rainfall and snowfall in the winter months

followed by rapid thawing preventing infiltration and thus swelling the reservoirs and rivers. Before the completion of the Matlock flood prevention scheme in the late 1970's, the river was known to flood the area covered by alluvium to the north of Matlock (Greatorex, pers. comm.), floodwater would, therefore, have reached the toe of the main area of slipping on the northern side. Flooding of the River Derwent at Matlock, rapid snowmelt and excessive rainfall during the winter of 1965/1966 are cited by Taylor (1966) as contributing to slope instability which affected the roads across the landslides at Starkholmes, Bolehill (near Cromford) and Stanton Lees (Figure 1.2). In addition to these disruptions, the failure of a mass of limestone in Matlock Bath demolished a house and debris blocked the A6 trunk road.

There is evidence of instability on both sides of Oker Hill, although movement on the northern side has been deep-seated whilst the southern side is characterised by shallower failures. However, at the present time, it is the southern and eastern sides of Oker Hill that cause most problems as these are the sites of the villages and are crossed by roads. One of the main problem areas is just west of Oker village (Point A on Figure 6.2). The farmer at Lobby Farm remembers that this slump feature appeared fifty to sixty years ago preventing ploughing because of the steep ridges on the foot. The land at the base of the backscar of this landslip is badly drained and is known locally as Reilly's Bog. The section of road which crosses the slump is prone to subsidence and has been regularly repaired, at present it has been stabilised by simple shallow

drainage (Leadbeater, pers. comm.). A similar feature can be recognised on the aerial photographs near Lobby Farm (Point B on Figure 6.2). This slump has weaker morphology and the farmer does not recall it forming while he has farmed the land, therefore it is likely that Slump B is more than sixty years old. However, a 1920's water drain used to pass under the road close to the surface at this point, and being old and weak it frequently burst resulting in subsidence of the road. Recently, a deep drain was installed by the Derbyshire County Council to prevent further slipping.

It is not only the roads that are disturbed by landslide movement, housing has also been affected. Several years ago construction began on a large house at Oker End near Oker Farm (Figure 6.2), unfortunately due to slope movement the house had to be dismantled and two bungalows were built in its place. A similar situation occurred at Starkholmes (Figure 6.1) where a large new house had to be dismantled as its foundations were inadequate and it was rebuilt with deep pile foundations. Local residents have also noted that small slips have occurred where slopes in gardens have been modified (e.g. at Oker End where earth slumped against a bungalow after the felling of trees situated immediately behind the building). As stated above, it is this eastern side of Oker Hill that is experiencing problems due to landslipping at present; this may be partly due to undercutting by the River Derwent removing material and, consequently, support from the base of the steep hillside.

Old records show that Oker Hill has been the site of quarrying and

excavations at various times in its past. The sandstone summit of the hill carries hollows at both the western and eastern ends. These hollows are probably man-made being a source for sandstone boulders for stone walls and buildings. There is a reference to ancient mineral workings in Bateman's (1868) account of Roman and British antiquities found on Oker Hill; these hollows may have had such an origin. It is also known from the 1840 edition of the O.S. One Inch map of Chesterfield (Sheet No. LXXXII S.W.) that there was a Grit Shale quarry on the eastern end of the hill. This quarry is now disused and its exact location could not be determined due to the dense vegetation in this area and the inaccessibility as a result of housing development. Even the inhabitants of Oker village were unaware of the existence of this disused quarry. Recognition of the quarry is desirable however, as the quarry face may be confused with a backscar of a landslide, although quarrying itself may have initiated slope instability in this area due to oversteepening and loss of support for the hillside. Therefore, in interpreting the morphology of Oker Hill it is important to bear in mind man's influence on the land.

6.2 Field Mapping of Oker Hill

From the discussion so far it is apparent that Oker Hill is a complex area of slope instability with various styles of failure. For detailed site investigation it was decided to focus attention on just one discrete landslip within the whole mass. As the intention was to

obtain a core through the landslide, a site was chosen which would cause least inconvenience to the inhabitants of Oker Hill. Unfortunately, this meant that the points of interest on the southern and eastern sides of the hill had to be avoided due to gardens, drains and the lack of a suitable flat and accessible site.

The area that was selected for detailed study that met the requirements for boreholing was the large landslip on the western end of the north-facing slope (Figure 6.4). Morphological field mapping was carried out on this landslide providing greater detail and information on slope angle than was possible from the aerial photographs. The breaks and changes of slope were recorded on the enlarged aerial photograph of Oker Hill at a scale of 1:7,270 (Plate 5.1) to enable the location of these lines to be drawn more accurately than would have been possible on a 1:10,000 O.S. base map. The slope angles were measured using a clinometer held parallel to the slope. The morphological map thus produced was enlarged further to a scale of approximately 1:3,570 for clarity and is shown in Figure 6.5. The slope units on this map may be grouped according to angle of inclination to produce a slope category map (Brunsden and Jones, 1972; Kertesz, 1979). The categories may be chosen on the statistical basis of natural breaks in a frequency histogram of slope unit angles, the resulting morphometric map (shown in Figure 6.6) enables easier interpretation of the land's form at a glance.

A more detailed geomorphological map was also produced (Figure 6.7). The symbols used in this map are modified from those suggested by

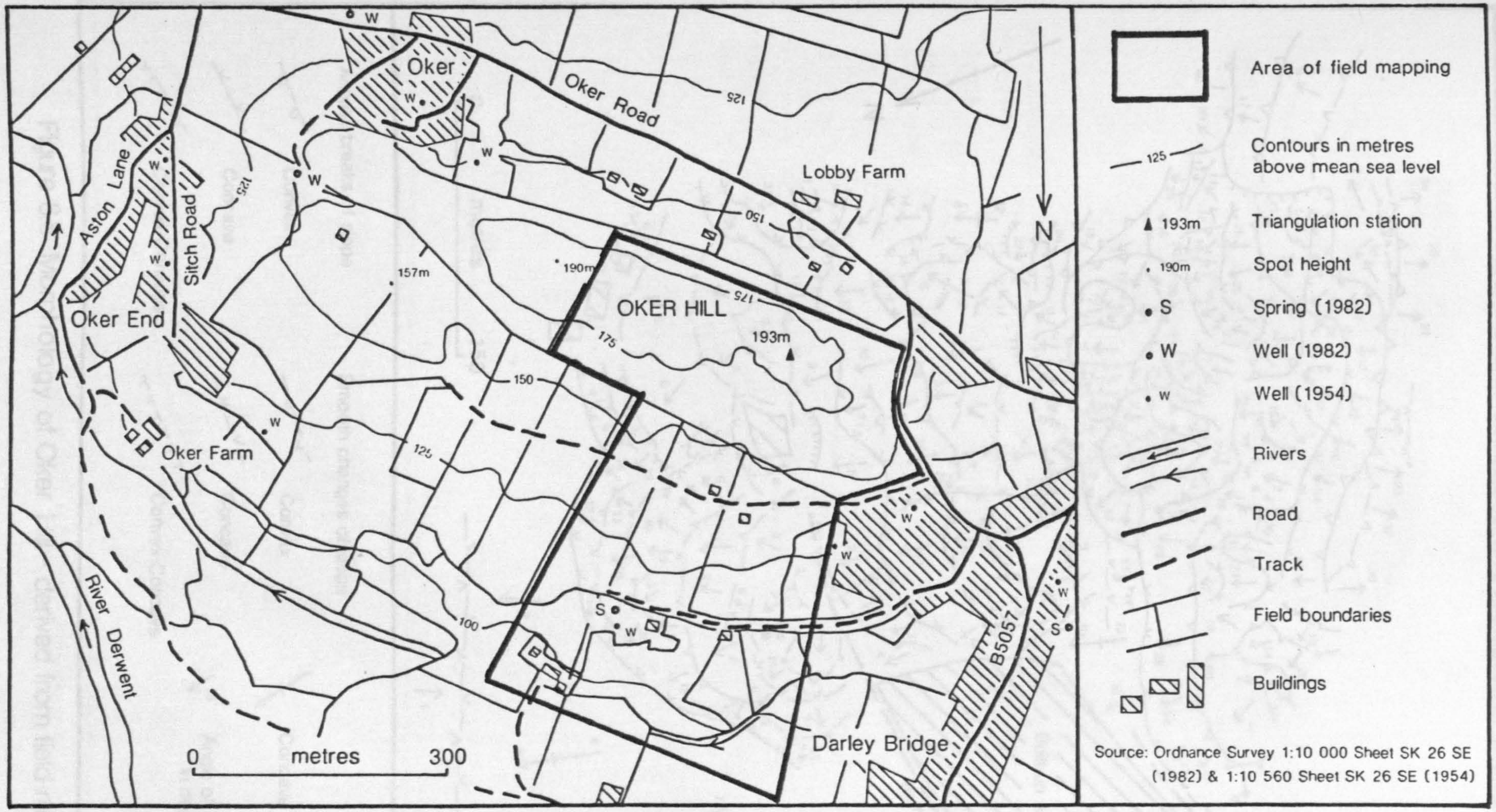

Figure 6.4 Area of Field Mapping on Oker Hill

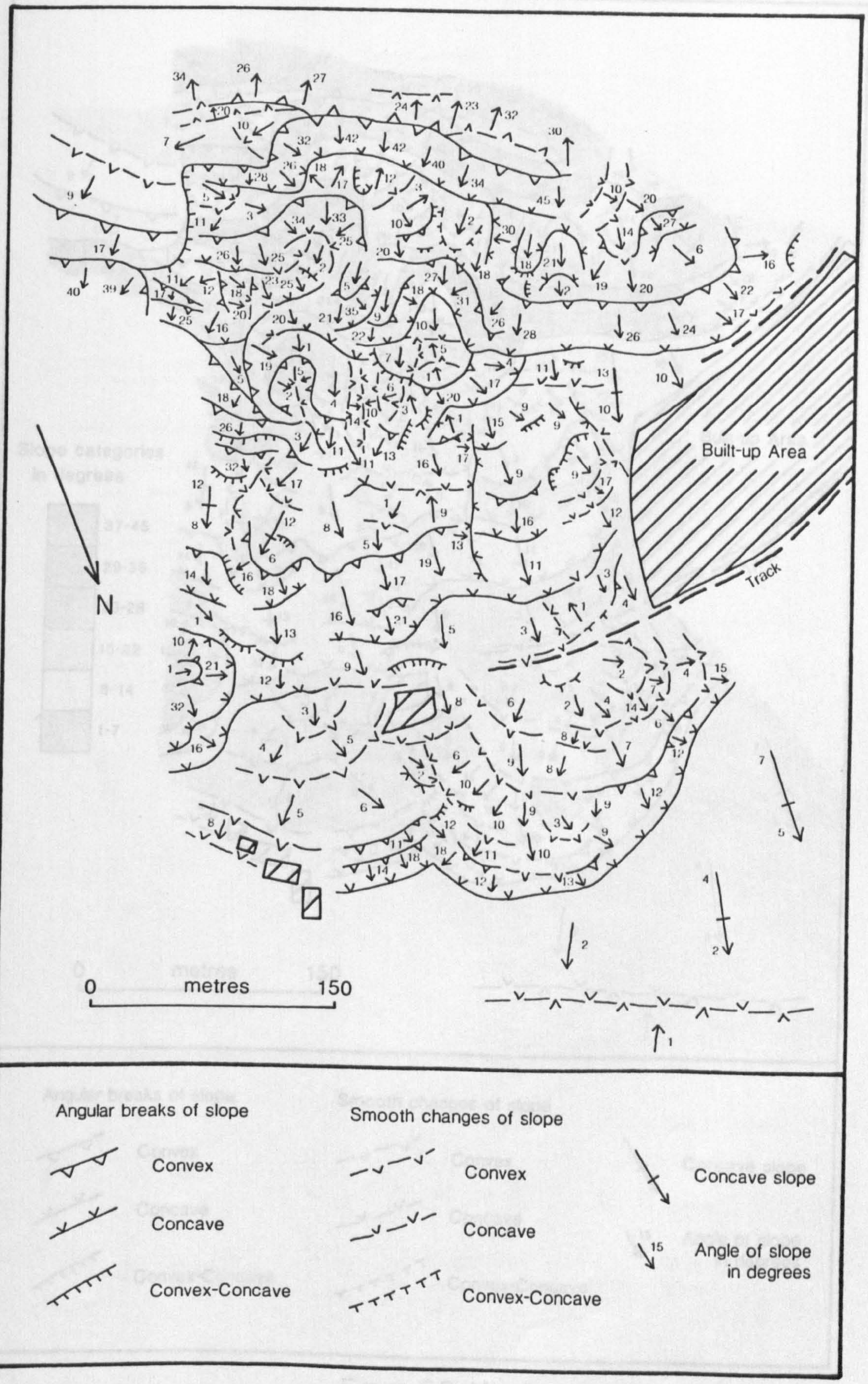

Figure 6.5 Morphology of Oker Hill - derived from field mapping

Slope categories in degrees

37-45

29-36

23-28

15-22

8-14

1-7

Built-up Area

Track

0 metres 150

Angular breaks of slope

Convex

Concave

Convex-Concave

Smooth changes of slope

Convex

Concave

Convex-Concave

Concave slope

15 Angle of slope in degrees

Figure 6.6 Morphometric Map of Oker Hill

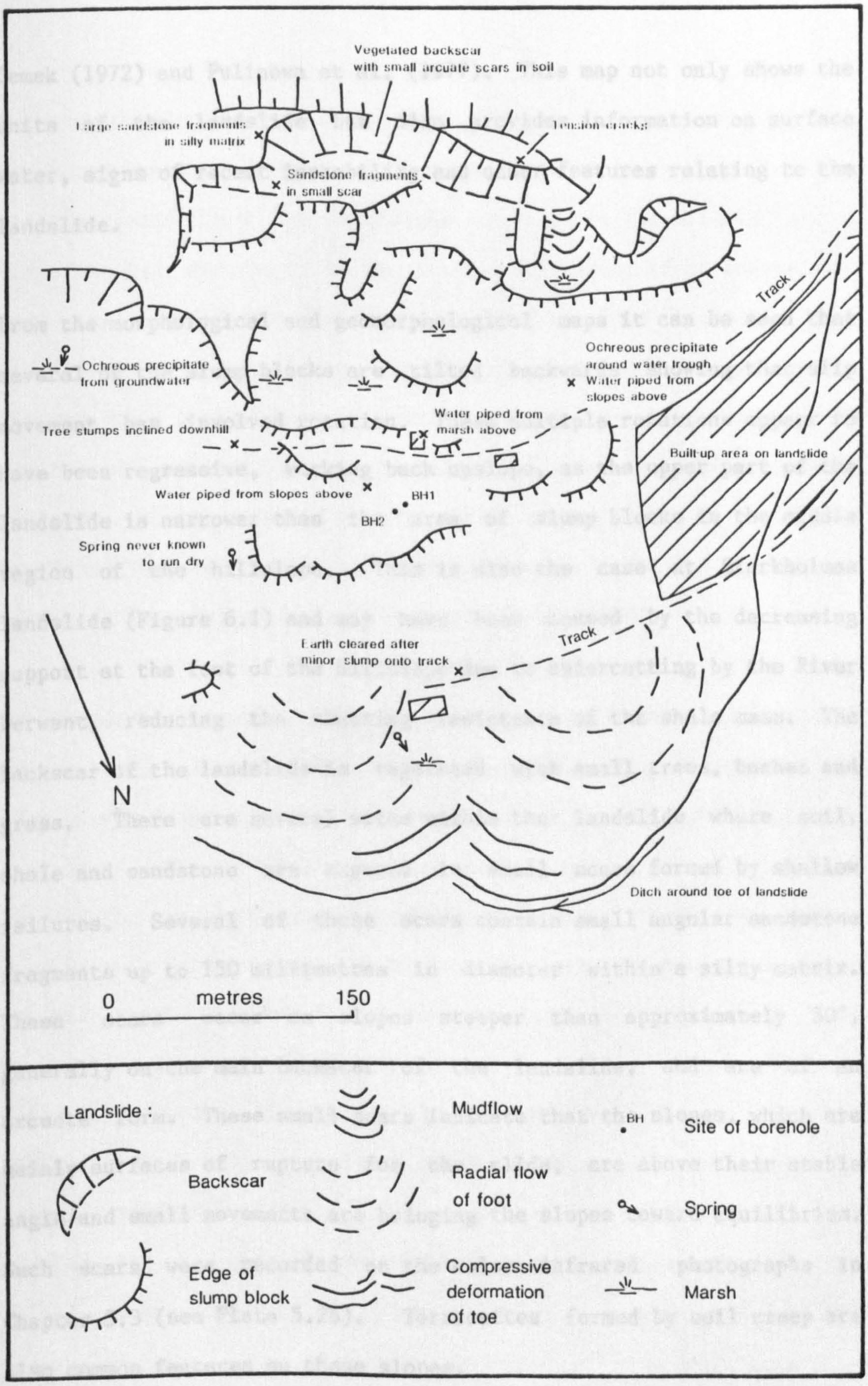

Figure 6.7 Geomorphology of Oker Hill - derived from field mapping

Demek (1972) and Pulinowa et al. (1977). This map not only shows the units of the landslide but also provides information on surface water, signs of recent instability and other features relating to the landslide.

From the morphological and geomorphological maps it can be seen that several of the slump blocks are tilted backwards showing that slip movement has involved rotation. These multiple rotations appear to have been regressive, working back upslope, as the upper part of the landslide is narrower than the area of slump blocks in the middle region of the hillslope. This is also the case at Starkholmes landslide (Figure 6.1) and may have been caused by the decreasing support at the foot of the hillslope due to undercutting by the River Derwent, reducing the shearing resistance of the shale mass. The backscar of the landslide is vegetated with small trees, bushes and grass. There are several sites within the landslide where soil, shale and sandstone are exposed in small scars formed by shallow failures. Several of these scars contain small angular sandstone fragments up to 150 millimetres in diameter within a silty matrix. These scars occur on slopes steeper than approximately 30°, generally on the main backscar of the landslide, and are of an arcuate form. These small scars indicate that the slopes, which are mainly surfaces of rupture for the slide, are above their stable angle and small movements are bringing the slopes toward equilibrium. Such scars were recorded on the colour infrared photographs in Chapter 5.3 (see Plate 5.2b). Terracettes formed by soil creep are also common features on these slopes.

The rock outcrop above the backscar (Figure 6.7) reveals in situ fractured sandstone with two to five centimetres of peaty soil above, this suggests that the sandstone capping to the hill is not a competent bed, and, as it is of limited thickness, it is unlikely to have been a major contribution to instability. This landslide may, therefore, be considered as if it occurred wholly within shale. However, this thin capping of sandstone would have been responsible for the hill not having been considerably lowered by erosion and mass movement, thereby enabling the shale slopes to maintain higher gradients than would otherwise have been possible and adding to the potential for slope failure upslope (Brunsden, 1979).

As already mentioned in the previous section, the summit of Oker Hill is marked by hollows which are probably man-made. However, at the edge of the backscar there is a step in the ground which may be associated with tension cracking and a slight drop of the rock between the crack and the edge of the backscar. Tension cracks are also present further along the hill to the east; these cracks appear to have been widened by the burrowing activity of animals. These burrows may even increase the potential for further slippage as they allow easier access of water into the hillside. The toe of the landslide shows arcuate pressure ridges which are also visible on the aerial photograph (Plate 5.1). These ridges are associated with mudflows and show that the deep-seated rotational movement gives way to flow in the lower slopes indicating high moisture content at the time of failure.

Other flow features were noted elsewhere on Oker Hill. For example, the geomorphological map (Figure 6.7) shows a narrow track of a mudflow originating in a steep slope which was probably the backscar of a previous slump. The track of the mudflow is picked out by moisture-tolerant plants and water-logged ground at the base of the flow on approximately flat ground. In the previous section attention was drawn to flow type movement on the southern side of Oker Hill at Points A and B on Figure 6.2. The main slip movement cannot be dated, although it is assumed to have taken place several thousand years ago (at least since the Devensian), but the mudflow at Reilly's Bog (Point A on Figure 6.2) has been dated at fifty to sixty years old, i.e. at a time when the climatic conditions and geomorphic processes were the same as those of today. This suggests that high moisture content and pore-water pressures within the slopes are still important considerations in slope instability in this area, as they were after the end of the Devensian. Considering the fact that the rainfall catchment area for the hill is so small, the amount of water occurring on the surface of Oker Hill is remarkable and, consequently, the water-holding capacity of the hill would appear to be high.

The geomorphological map (Figure 6.7) indicates the sites where water appears on the surface in springs, marshes and streams. The intersection of an aquifer with the ground surface produces either concentrated outflow (springs) or diffused outflow (seeps), both of these outlets act as a release for ground water pressures (Sowers and

Royster, 1978). Springs and seepage points should be mapped during or immediately after periods of high precipitation as their locations may change under such conditions. Also, as their locations may change after ground movement they should be mapped by repeated surveys. One spring on the landslide has never been known to run dry by the farmer of this land, and other springs (as indicated on Figure 6.7) are of particular interest as the waters precipitate ochre (an iron-oxide crust) on emergence (Plate 6.1). A similar ochreous spring has been noted within the Mam Tor landslide where the path of the stream across the upper section of the road is clearly depicted by the orange staining (Plate 6.2). Research into this by Vear (1981) has demonstrated that the ochre is a product of pyrite weathering of the shale. This chemical breakdown of the pyrite leads to a net volume loss of the shale resulting in an overall deterioration of the rock. It is believed that this process may be responsible for the periodic major movements experienced on the Mam Tor landslide. It is postulated that the presence of similar ochreous springs on Oker Hill is also indicative of pyrite weathering of the shale and may thus be evidence of continued weakening of the rock mass. This aspect will be considered in more detail in the following chapters in relation to the mineralogical and geochemical analysis of core material through the landslide.

Wells are also a common feature on Oker Hill as there was no mains water until the 1920's. The majority of the wells are quite shallow; a recently renovated example of which, Grace's Well, can be found on the east side of the hill. This is a stone-lined, "stepped" well

PLATE 6.1 OCHREOUS SPRING ON OKER HILL LANDSLIDE

PLATE 6.2 OCHREOUS PRECIPITATE AT MAM TOR LANDSLIDE

which collects water issuing to the surface. The deeper wells in the area collect ground water from the shale from depths of three to five metres (Greatorex, pers. comm.). Piezometric levels may be lowered significantly by extraction of water from wells which may increase the stability of a slope. However, lowering of the ground water table may also trigger sliding due to the increase in weight from the buoyed to total weight of the soil or rock (Sowers and Royster, 1978). Information on water extraction from the wells on Oker Hill is not available, however, it is known that many of the wells are now disused.

Several indications of recent slope instability were noted whilst mapping. Figure 6.7 indicates a site where the front face of a hummock contains tree stumps that are leaning at an angle. It is probable that these trees had to be cut down after slope movement as they were blocking the track. Small scars in the soil are also present at this site. Another case of a track being blocked occurred near the houses in the middle of the landslide, this time the track was blocked by earth. On another part of Oker Hill (further to the east) gateposts were found to be leaning at oblique angles due to slipping, although the condition is worsened by the adjacent wet ground.

In order to provide a surveyed control on boundary locations of slump blocks during the morphological and geomorphological field mapping an Autoset level was employed. Only part of the landslide was surveyed (Figure 6.8) as the intention was to assess morphological

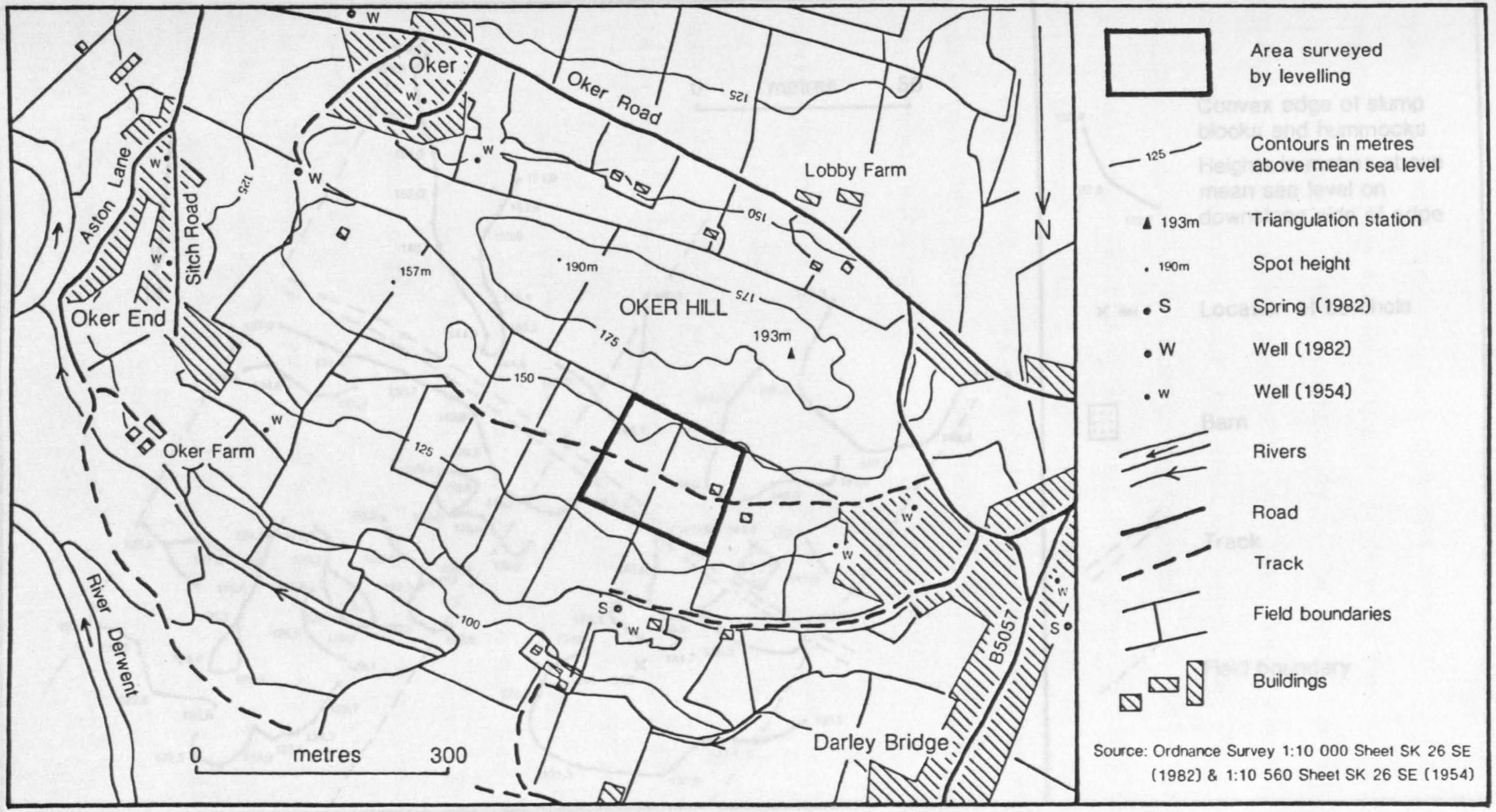

Figure 6.8 Area Surveyed by Levelling on Oker Hill

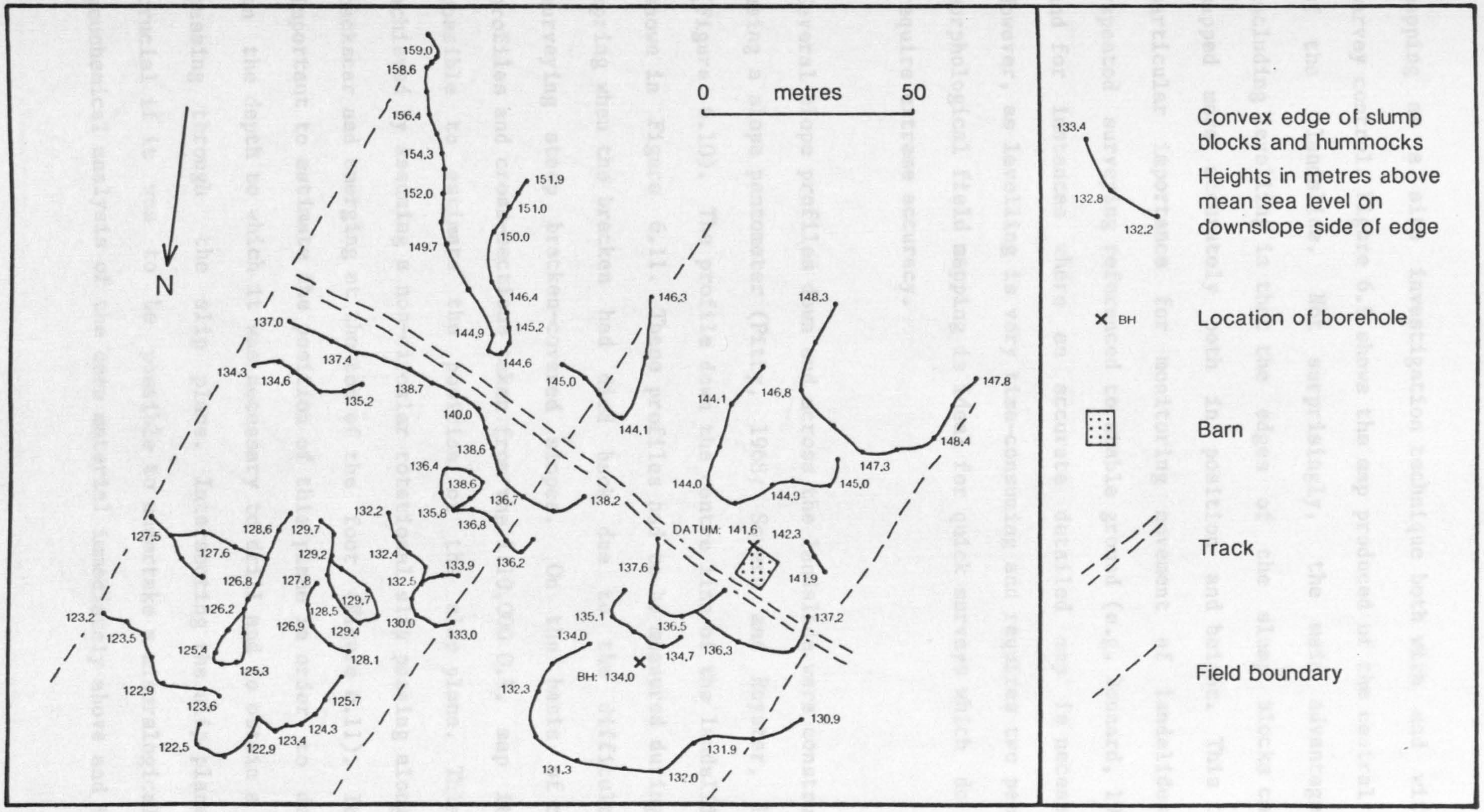

Figure 6.9 Slump Blocks Defined by Surveying on Oker Hill

mapping as a site investigation technique both with and without survey control. Figure 6.9 shows the map produced of the central part of the landslide. Not surprisingly, the main advantage of including levelling is that the edges of the slump blocks can be mapped more accurately both in position and height. This is of particular importance for monitoring movement of landslides by repeated surveying referenced to stable ground (e.g. Bonnard, 1983), and for instances where an accurate detailed map is necessary. However, as levelling is very time-consuming and requires two people, morphological field mapping is ideal for quick surveys which do not require extreme accuracy.

Several slope profiles down and across the landslide were constructed using a slope pantometer (Pitty, 1968; Sowers and Royster, 1978) (Figure 6.10). The profile down the centre line of the landslide is shown in Figure 6.11. These profiles had to be measured during the spring when the bracken had died back due to the difficulty of surveying steep bracken-covered slopes. On the basis of these profiles and cross-sections taken from the 1:10,000 O.S. map it was possible to estimate the position of the slip plane. This was achieved by assuming a non-circular rotational slip passing along the backscar and emerging at the top of the foot (Figure 6.11). It was important to estimate the position of this plane in order to decide on the depth to which it was necessary to drill and to obtain a core passing through the slip plane. Intersecting the slip plane was crucial if it was to be possible to undertake a mineralogical and geochemical analysis of the core material immediately above and below

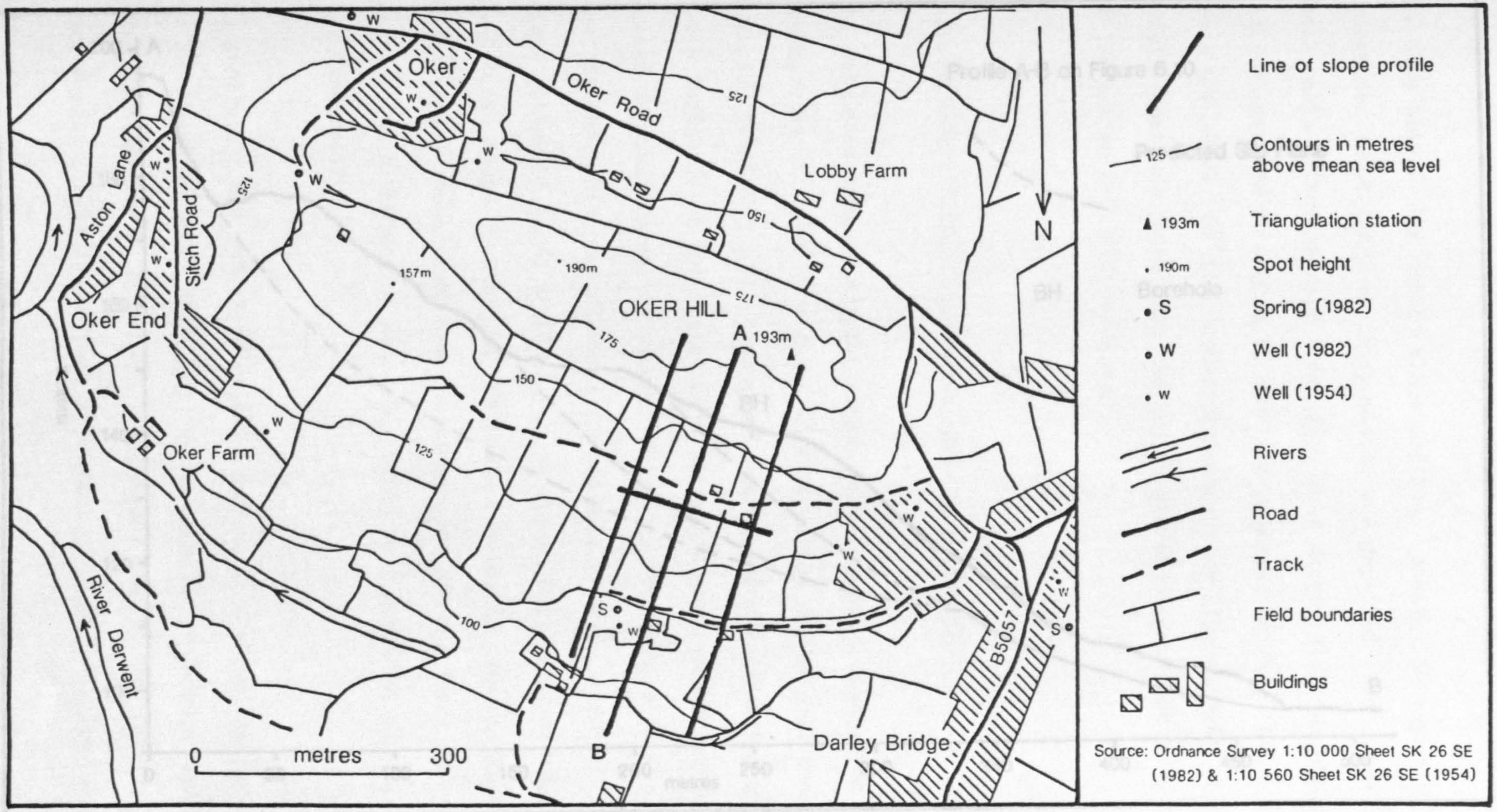

Figure 6.10 Location of Slope Profiles on Oker Hill

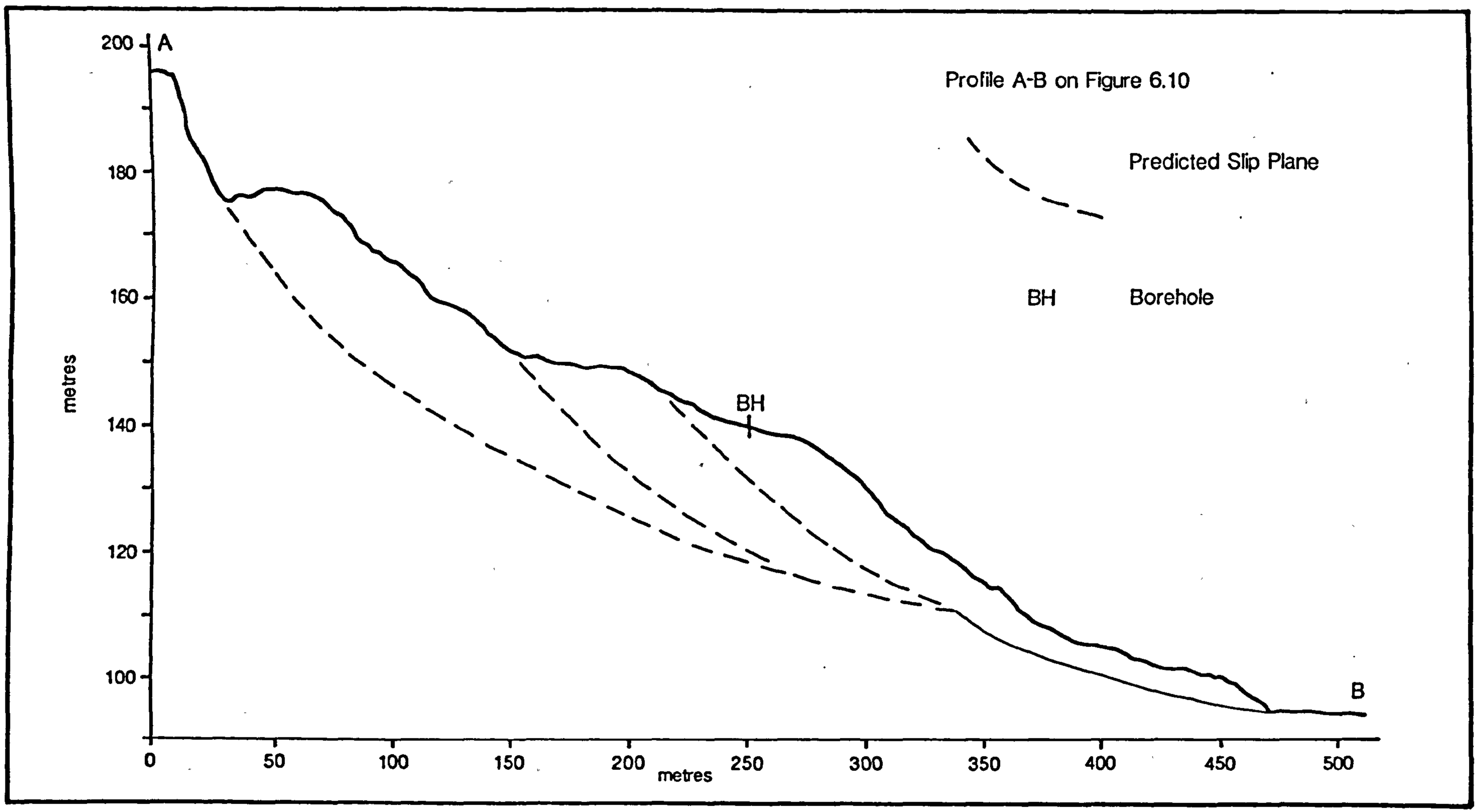

Figure 6.11 Central Slope Profile of Oker Hill Landslide

the slip plane. The centre slope profile passes through the sites chosen for boreholing, at these points the depth of the conjectured basal slip plane is approximately twenty metres with two additional failure surfaces at depths of nine and eighteen metres. The borehole sites are shown on the geomorphological map (Figure 6.7), and from levelling it was found that the top of the boreholes were at a height of 134 metres O.D. (Figure 6.9).

6.3 Conclusions on Ground Investigation of Oker Hill

The main advantage of mapping from field work as opposed to aerial photographs is that more detailed information can be obtained. For example, tension cracks and small scars, surface water features and their influence on the vegetation are more obvious, and evidence of recent instability may be present which is not visible on the aerial photographs. Slope gradients are much more easily measured in the field either by slope profiling as in Figure 6.11 or by measuring the angle of slope units, as in the morphological map of Figure 6.5. Where aerial photography has the advantage of providing a regional setting for a feature of interest, field work provides the detailed site information.

Morphological and geomorphological field work enables the production of quick and detailed maps, but where greater accuracy and height data are required surveying techniques, such as levelling, are necessary. Finally, slope profiling, as well as providing

information on slope form and helping in the recognition of the component parts of the landslide, enables an estimation of the position of the slip plane to be drawn.

All these field techniques aid in the recognition and assessment of slope instability and provide information which is of use in further studies such as subsurface investigations.

CHAPTER 7 THE WEATHERING OF SHALE AND SLOPE INSTABILITY

7.1 Introduction

From field mapping and information from the farmer of Oker Hill two ochreous springs were identified within the landslide area. A similar spring occurs on Mam Tor where it is thought to be indicative of pyrite oxidation, which Vear and Curtis (1981) suggest is responsible for the periodic major instability of this landslide.

Shales pose several problems to civil engineering works through slope instability and heave. These result largely from mineralogy, degree of compaction, susceptibility to volume change, high frequency of discontinuities and their anisotropic character (Taylor and Spears, 1981). Slope stability may be affected by a number of factors which can be divided into external and internal changes (Terzaghi, 1950). External changes are those which produce an increase in shear stress, and include geometric changes of slope form, loading, unloading, and changes in the water regime. Internal changes, such as weathering and progressive failure, result in a decrease in shear strength. Vear and Curtis (1981) have suggested that the relatively occasional major movements at Mam Tor may be caused by weathering reactions taking place at depth within the existing slide. Heave is caused by the oxidation of pyrite to secondary hydrous sulphates of greater volume, and is most common in the darker coloured mudrocks containing pyrite in a disseminated state (Taylor and Spears, 1981).

The present work concentrates on the weathering of shale and, in particular, the oxidation of pyrite, in relation to slope instability, with the aim of assessing the importance of this process identified at Mam Tor in the landslides of the Matlock region using Oker Hill as a case study.

7.2 Weathering of Shale

For engineering purposes Grainger (1984) defines a mudrock as a clastic sedimentary rock with more than thirty-five percent by weight of its grains being of silt and clay size (i.e. less than 0.062 millimetres in diameter). A shale is a fissile indurated mudrock. Fissility parallel to bedding is caused by the alignment of platy clay particles by deposition or compression, and by the presence of laminae produced by changes in composition (Grainger, 1983). Quartz predominates in the 2 to 60μm fraction and clay minerals in the fraction less than 2μm. Other minerals include feldspars and diagenetic carbonates and sulphides.

Mudrocks have characteristics intermediate between those of soil and rock. Their properties are determined by lithology, geological history of loading and unloading, and degree of weathering.

On re-exposure shales are particularly prone to both physical and chemical weathering. The removal of overburden allows the clay to

expand to an extent dependent on its degree of induration, thus the expansion of shale is restricted by the presence of strong diagenetic bonds resulting from cementing minerals. With continued unloading and exposure to further strain from freezing, temperature changes and wetting and drying cycles, these bonds eventually fail causing the development of fissures and ultimately assisting in the disintegration of the rock (Bjerrum, 1967). Polygonal cracking normal to bedding and parting along bedding planes also occur (Sherrell, 1971; Taylor and Spears, 1970). However, Kennard et al. (1967) found that such disintegration in the Carboniferous shale of the Yoredale sequence can be prevented by immersion in water, indicating that stress relief cannot be significant in the development of fracturing in such shales. They propose that desiccation of shale following exposure leads to the creation of negative pore pressures and the consequent tensile failure of weak intercrystalline bonds. The fissures thus created allow the ingress of water resulting in swelling controlled by the fabric of the shale and by the presence of any expandable clay minerals, encouraging general softening of the rock as a whole. The waters also carry dissolved ions and oxygen which induce chemical weathering.

These processes of physical breakdown reduce shale to gravel-sized aggregates; disintegration decreasing with depth.

Chemical weathering is of minor importance with respect to quartz and clay minerals as these are mostly of detrital origin and have been through at least one cycle of weathering and erosion before

deposition. Consequently, they are of greater stability and only minor changes take place upon re-exposure, i.e. ion-exchange reactions whereby clay minerals, in particular, adjust quickly to changes in water composition.

The accessory minerals of diagenetic origin (e.g. pyrite and siderite) were formed in environments different to that encountered upon exposure. Pyrite forms below the sediment-water interface of marine sediments and in the bottom waters of euxinic basins by the reaction of detrital iron minerals (iron-rich clays and ferric hydroxides) with hydrogen sulphide under anoxic conditions (Berner, 1984; Pearson, 1979). Hydrogen sulphide is produced by the reduction of interstitial dissolved sulphate by bacteria using organic matter as the reducing agent and the energy source. In brackish water and non-marine conditions siderite forms below the sediment-water interface where the concentration of dissolved sulphate is very low and, therefore, any bacterial generation of CO_2 leads to the formation of the iron carbonate siderite (Curtis, 1967).

In the Coal Measures rocks of Britain both pyrite and siderite are believed to have been formed within the range of pH 7 to 8 and Eh -0.2 to -0.3 V (Curtis, 1967). Consequently, the mineral assemblage is one that approached chemical equilibrium at depth in contact with aqueous solutions of high ionic strength and in the presence of decreasingly low oxygen partial pressure. On re-exposure meteoric waters of low ionic strength saturated with molecular oxygen enter the weathering zone and cause chemical weathering; rainwater carries

carbonic acid and has a pH of approximately 5.7 when it is in equilibrium with the CO_2 from the atmosphere (Levinson, 1974). The diagenetic minerals often form intergranular bonds or cements and their removal or breakdown can weaken the rock considerably by the loss of cohesion and can increase porosity and permeability. Those minerals which participate in redox reactions are especially reactive; in fine-grained sediments this concerns the minerals of iron, sulphur and manganese, and organic matter.

Sedimentary pyrite is particularly reactive as it is composed of iron and sulphur (FeS_2), oxidising to produce ferrous or ferric ions and sulphate and hydrogen ions through the two end-member reactions depending on the degree of oxidation (Vear, 1981):

$$2FeS_2 + 14(O) + 2H_2O \longrightarrow 2Fe^{2+} + 4SO_4^{2-} + 4H^+ \quad \text{(Eq. 1)}$$

or

$$2FeS_2 + 15(O) + H_2O \longrightarrow 2Fe^{3+} + 4SO_4^{2-} + 2H^+ \quad \text{(Eq. 2)}$$

The rate of oxidation is chiefly a function of the oxidising potential of the solution and proceeds more rapidly where there is a greater percentage of oxygen available even in the absence of moisture (Dougherty and Barsotti, 1972; Garrells and Thompson, 1960). In fact, the oxidation of potentially expansive sulphide minerals is believed to begin in an atmosphere relatively free of water, a situation arising by the lowering of the water table. Indeed, Taylor (1988) notes that pyrite oxidation tends to occur in the partly saturated near-surface zone above the water table. The fine-grained

and amorphous forms of pyrite oxidise most rapidly (Kuznetsov et al., 1963). The presence of ferric ions also encourages reaction; Bastiansen et al. (1957) reported that the presence of very rapidly oxidising pyrrhotite acts as a catalyst for the oxidation of pyrite in the black bituminous shales of Oslo, Norway. Several authors have also noted that oxidation of the iron sulphides pyrite, marcosite and pyrrhotite proceeds more rapidly in the presence of autotrophic bacteria of the Ferrobacillus and Thiobacillus ferrooxidan types (e.g. Quigley and Vogan, 1970; Penner et al., 1972). Furthermore, numerous studies have suggested that these micro-organisms may be more important than oxygen in this process. However, oxygen is essential for the bacteria to be active with the temperature between 30° to 35°C and pH in the range 2 to 4.5.

The products of iron sulphide oxidation include secondary hydrous sulphates (e.g. melanterite, jarosite and gypsum) and iron hydroxides (e.g. limonite, goethite and lepidocrocite). During chemical weathering the composition of the ground water will be changed markedly even if there is little apparent affect on the mineralogy of the solid material (Steward, 1984; Steward and Cripps, 1983). The ground water may become saturated with respect to new minerals which may then be precipitated. Melanterite is easily dissolved in water and may be precipitated at great distances from its source. Dehydration of limonite to haematite accounts for the reddish stain commonly found on fissures within the shales (Quigley and Vogan, 1970; Spears and Taylor, 1972).

The soluble products of the reactions outlined above will take part in subsequent reactions. Clay interlayer cations may be affected and other shale constituents may be destabilised, particularly carbonates (including siderite and calcite) and phosphates (e.g. apatite).

The weathering of pyrite and calcite in mudrocks to form gypsum has been noted by many authors (e.g. Morgenstern, 1970; Parry, 1972; Russell and Parker, 1979). Sulphuric acid derived by the initial oxidation of pyrite takes part in carbonate dissolution producing calcium sulphate (anhydrite) which is hydrated to form gypsum (Equation 3).

$$H_2SO_4 + CaCO_3 + 2H_2O \text{ ---- } CaSO_4.2H_2O + H_2O + CO_2 \quad \text{(Eq.3)}$$

Gypsum is generally found at or near its source bed as it is relatively insoluble. It is precipitated along discontinuities which allow the passage of solutions, particularly where dry air can penetrate to aid evaporation. Quigley and Vogan (1970) found that gypsum only occurred above the water table in the zone probably saturated by capillary rise.

Acidic ground water also attacks clay minerals causing dissolution and rapid leaching of the interlayer cations of illite and smectite, followed by decomposition into iron oxides, aluminium hydroxides (e.g. gibbsite) and kaolinite (Norrish, 1972). Russell and Parker (1979) observed a marked decrease in K_2O content in weathered samples of Oxford Clay attributable to leaching of illite. They also noted

a decrease in the crystallinity of illite in the clay fraction towards the surface, which they believe may reflect the degradation of the crystal structure at the margins where bonding occurs.

Cosgrove and Hodson (1963) observed the production of jarosite from the combination of potassium ions released from illite with ferric and sulphate ions from pyrite oxidation. Jarosite is generally found at greater depths than gypsum. The formation of gypsum and jarosite result in a volume increase (Penner et al., 1973):

		volume increase
pyrite	→ jarosite	115%
calcite	→ gypsum	103%

However, Nixon (1978) considers the formation of gypsum to be a more serious factor than jarosite in the problem of heave.

Chlorites may also degrade to secondary minerals, although Vear (1981) noted increases in chlorite content on weathering in samples from boreholes.

Cancelli (1977) analysed the joint surface material of a highly consolidated Pliocene clay by X-ray diffraction techniques. The proportion of quartz, calcite and dolomite was found to be reduced by half of that present in the ambient clay, illite had reduced crystallinity, vermiculite was replaced by chlorite, and gypsum had been deposited together with an amorphous material.

The reactions described above are restricted to the zone of pyrite oxidation near the base of the weathering profile. The rate of weathering decreases above this zone as the percolating waters are not charged with the aggressive acidic solutions derived from pyrite decomposition (Russell and Parker, 1979).

Siderite is also unstable on exposure to atmospheric conditions but its rate of reaction is slower than that of pyrite due, in part, to the more massive form in which it occurs (Taylor and Spears, 1981).

The main visible evidence for weathering in shales is discolouration; for example the oxidation of iron sulphides and carbon results in a change from dark grey to pale grey-brown with the precipitation of iron oxides along fissures resulting in a reddish stain. Disintegration occurs at a more advanced stage where solution of cementing minerals and corrosion of interparticle bonds produce stiff clay with a relict shale fabric (Grainger, 1983). In the Carboniferous shale of the Coal Measures Series some of the above indications of weathering have been observed (Spears and Taylor, 1972): visible weathering decreases with depth to approximately eight metres, with fissure development and oxidation of iron adjacent to these fissures.

7.3 The Effect of Weathering on the Engineering Properties of Shale

The engineering properties of mudrocks are influenced by lithology, the geological history of loading and unloading and the degree of weathering (Cripps and Taylor, 1981). Peak undrained shear strength is controlled by the history of consolidation and by diagenesis; residual shear strength is controlled by mineralogy.

Weathering causes great variations in engineering properties, ultimately returning a mudrock to a normally-consolidated, remoulded condition by the destruction of interparticle bonds (Cripps and Taylor, 1981). The removal of overburden is probably the most important influence on engineering behaviour through dominantly vertical expansion, resulting from the destruction of diagenetic bonds, producing joints and fissures, and causing softening of the shale. As expansion in the horizontal direction is limited, a difference in horizontal and vertical shear stresses develops. Therefore, when a shale slope is undercut these lateral stresses may trigger slope failure. This time-dependent process is termed progressive failure (Bjerrum, 1967).

The removal of overburden results in a decrease in strength and increases in deformability, water content and plasticity (Cripps and Taylor, 1981). In older, more indurated mudrocks, i.e. shales, fissuring reduces shear strength from rock- to soil-like characteristics.

This progressive softening and degrading is accompanied by a large decrease in effective cohesion (c') to a value close to zero and a smaller decrease in effective angle of internal friction (Ø'). The latter may be reduced to its "fully-softened" value through the development of progressive small-scale failures in the weathered rock mass. The decreases in values of these parameters result in a reduction of strength. This is particularly apparent for the more indurated mudrocks such as those of the Carboniferous Period: a reduction of ninety-three percent in effective cohesion and a reduction in the effective angle of internal friction to twenty-six degrees (when c'= 0) was found by Spears and Taylor (1972). The reduction in the strength parameters through dominantly physical weathering has also been noted for the Keuper Marl (Mercia Mudstone) (Chandler, 1969) and the London Clay (Chandler and Apted, 1988).

The main causes for the reduction from peak to residual shear strength are the orientation of platy clay particles and the formation of slickensides. Skempton and Petley (1967) found that in fissured over-consolidated clays small shearing movements of only a few millimetres after joint formation are probably sufficient to reduce effective shear strength to its residual value and to polish the surface by the alignment of the clay particles. This is important in the context of progressive failure. The strength along joints and fissures thus determines the strength of the whole rock mass. Residual shear stress decreases with increased percentage of platy clay particles, and is sensitive to changes in pore-water composition decreasing with increasing ion concentration (Steward,

1984).

Weathering may also create a change in stress-strain behaviour from brittle to plastic deformation.

Several authors have found that weathering affects the index properties of mudrocks through decreases in strength and increases in water content. Chandler (1969) noted that in the weathering profile of Keuper Marl both liquid limit and natural water content increased towards the surface whilst bulk density decreased. The decrease in strength and associated increase in plasticity have been attributed to the amount and species of clay minerals and to the presence of cementing minerals by many authors (e.g. Burnett and Fookes, 1974; Dumbleton and West, 1966; Russell and Parker, 1979; Skempton, 1964). In particular, Russell and Parker (1979) found a negative correlation between strength and the proportion of mixed-layer clay plus montmorillonite in the less than 2 μm fraction, and a positive correlation between strength and the cementing (diagenetic) minerals pyrite and calcite in Oxford Clay. With respect to plasticity, Voight (1973) suggests that the plasticity index can be used as a guide to the residual shear strength of soils. However, Spears and Taylor (1972) found no relationship in the consistency limits between weathered and unweathered samples of Coal Measures shale, but they did find that as quartz content increases in the range fifteen to forty-four percent liquid limit decreases, and at quartz contents greater than forty-four percent liquid limit increases again. Apted (1977) also noted no change of index properties with weathering of

London Clay which he interpreted as indicating no major mineralogical changes or loss of material. According to Morgenstern and Eigenbrod (1974) liquid limit provides a good indication of the slaking tendency of shale (the tendency to revert back to mud by repeated wetting and drying). For the Carboniferous shales of southwest England Fookes et al. (1971) found a general qualitative correlation between slake durability and the rate of weathering and the stable slope angles of quarries. The composition of pore-water solutions also affects plasticity. Steward (1984) observed that the liquid and plastic limits of Edale Shale at Mam Tor landslide decrease with increasing salt concentrations and increase according to ion type in the order of Na^+ K^+ Ca^{2+} Mg^{2+}, liquid limit being the more sensitive. Furthermore, plastic limit was shown to be highest in the presence of distilled water, and liquid limit highest in the presence of acid.

The products of weathering also increase the shear strength of shales if they are deposited along discontinuities (Piteau, 1970).

In the previous section it was stated that aggressive ground water solutions are most active within the zone of pyrite oxidation which is located at the base of the weathering zone. Marsland (1971) and Chandler (1972) noted breaks in the strength-depth curve at points where abrupt changes in weathering intensity occur, suggesting that the base of the weathering zone is a major point of weakening. However, this was not found by Russell and Parker (1979) in samples of Oxford Clay. According to Bjerrum (1967), Henkel and Skempton

(1954) and Morgenstern (1968) slip planes tend to be located in the lower part of the active weathering zone or at the junction between weathered and unweathered material. This appears to be the case at Mam Tor from the examination of core material through the landslide (Steward, 1984; Vear, 1981). Bjerrum (1967) explains this location of the slip surface by the increase with depth of shear stresses due to the force of gravity and the internal lateral stresses building up by progressive failure. Leussink and Muller-Kirchenbauer (1967) emphasise the importance of discontinuities on rock mass strength and conclude that, as weak zones, discontinuities frequently provide pre-determined slip planes for large movements.

It is, therefore, apparent that the problems presented to engineering in shales are varied and are related in part to their geochemistry.

7.4 Pyrite Oxidation in the Namurian Shales of Mam Tor, Derbyshire

The rocks involved in the Mam Tor landslide are the Mam Tor Beds and the Edale Shales. Amin (1979) identified the former as distal turbidites on the basis of textural and geochemical characteristics, supporting Allen's (1960) interpretation. These beds of alternating sandstone and shale overly the deep basinal mudstones of the Edale Shales.

Core material from the main unit of the landslide has been studied by Vear (1981) and Steward (1984). At this site, highly weathered Mam

Tor Beds extend to a depth of five metres and the underlying Edale Shale becomes progressively less weathered with depth. Fractures are numerous and are coated with orange iron oxides; in places they appear to be widened and filled with euhedral crystals of gypsum. These beds dip at between 30° and 45° degrees in a westward direction, probably indicating back-tilting of the slump block. At a depth of twenty-six metres there is an abrupt change to fresh dark grey shale. This rock is very fine-grained with relatively few bedding planes present dipping at an angle of 5° degrees in a northeastward direction in accordance with the regional dip. Steward (1984) believes that these changes correspond to the location of the slip plane.

Whole rock X-ray diffraction analysis of this core material by Steward (1984) shows that quartz is the major constituent followed by kaolinite and illite. Chlorite, pyrite, goethite and feldspars were also detected. Pyrite was found to increase with depth, particularly in the fresh shale beneath the slip zone, although it was not identified in samples from the Mam Tor Beds. Goethite occurs as a joint-fill material and is present along other surfaces of discontinuity. It was also noted that haematite is present in the region of the slip plane and at the surface. (Mineralogical analysis is not reported for the shale between the surface and twenty-three metres so the presence of haematite within this zone cannot be ruled out.) Jarosite and gypsum were also found in weathered surface exposures. The occurrence of jarosite below the surface is very limited presumably because it precipitates only above the zone of

ground water saturation and is only stable under highly acidic and oxidising conditions (Brown, 1971). No definite trends in the distribution of clay minerals could be identified, but it appears that there is a reduction in expandable clays and an increase in chlorite towards the surface.

The toe region of the Mam Tor landslide is characterised by the emergence of acid-sulphate springs which precipitate ochre (a deposit of iron hydroxides) and gypsum; one stream, in particular, is of almost constant temperature, low pH and has a high concentration of dissolved ions. A striking illustration of the quantity of iron oxides carried in the water can be seen after periods of heavy rainfall when the route taken by the water across the road can be identified by an orange precipitate (Plate 6.2). An excellent study by Vear (1981) demonstrates that these phenomena can be taken to indicate that chemical weathering processes are operating at depth within the slide; Figure 7.1 shows the proposed sequence of reactions to account for the observed concentrations of chemical constituents in the emergent waters.

Essentially, the process which is operating is pyrite oxidation which can be summarised by the two end-member reactions depending on the degree of oxidation (Vear, 1981):-

$$2FeS_2 + 14(O) + 2H_2O \longrightarrow 2Fe^{2+} + 4SO_4^{2-} + 4H^+ \qquad \text{(Eq.1)}$$

or

$$2FeS_2 + 15(O) + H_2O \longrightarrow 2Fe^{3+} + 4SO_4^{2-} + 2H^+ \qquad \text{(Eq.2)}$$

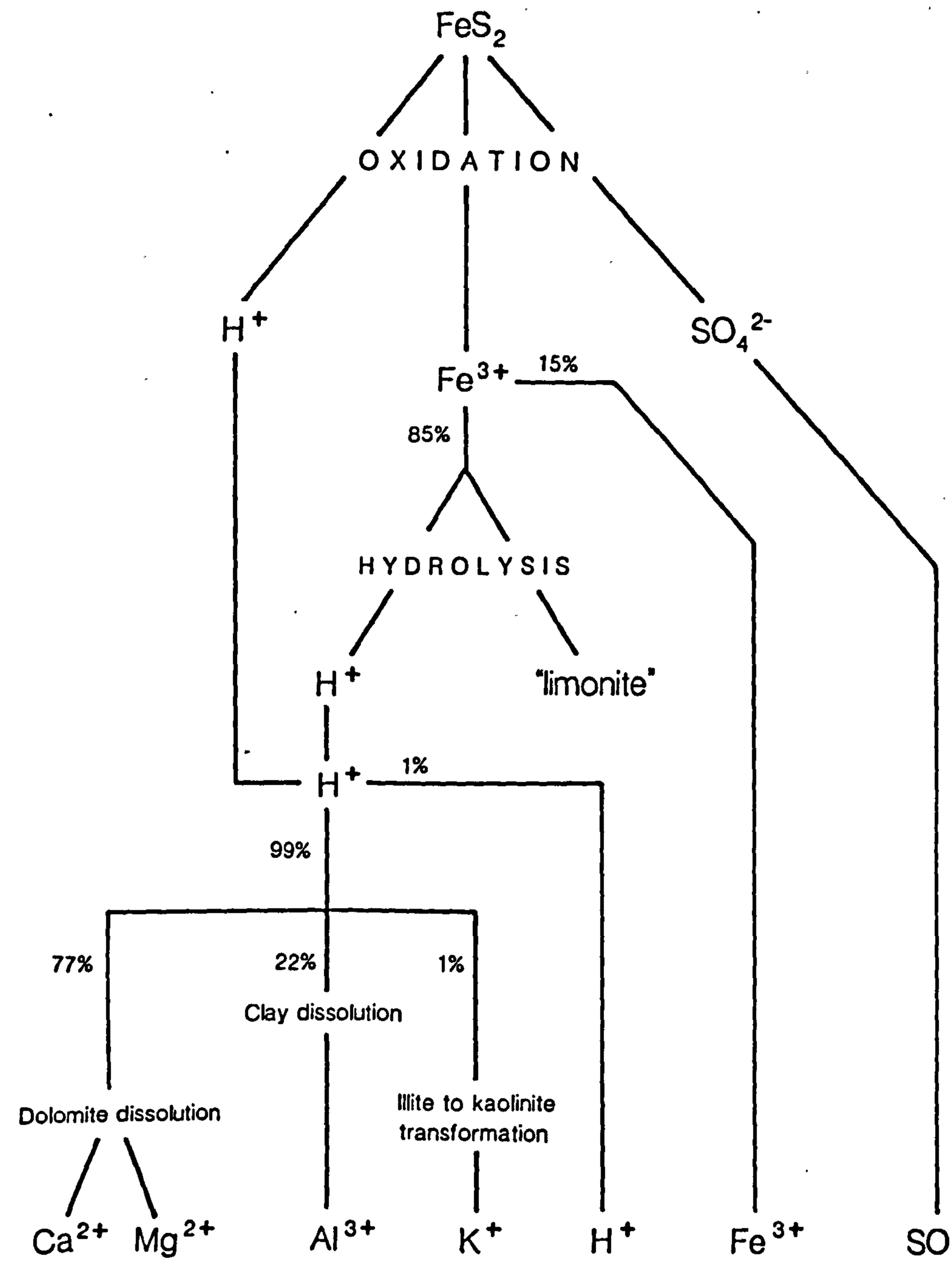

Figure 7.1 The Reaction Path of Pyrite Oxidation
(Vear, 1981)

The reaction path proposed by Vear (1981) is based on Equation 2 as most of the iron in the ground water of Mam Tor is in the ferric form (Fe^{3+}).

On the assumption that all the SO_4^{2-} remains in solution, Vear (1981) calculated that 1.56 grams of pyrite must be destroyed per litre of water. He goes on to suggest further reactions in which the excess H^+ and Fe^{3+} ions take part, i.e. the precipitation of 0.617 grams of Fe^{3+} as "limonite" or goethite, and the consumption of approximately ninety-nine percent of the H^+ ions by dolomite dissolution, clay dissolution and illite to kaolinite transformation. However, the presence of jarosite at depth on joint surfaces suggests that not all of the SO_4^{2-} remains in solution; as Vear (1981) points out, all that this means is that the quantities of minerals and ions involved are higher than those calculated, which would account for his slight under-estimation of the calculated concentrations compared to the observed values. Equation 2 can, therefore, be rewritten as:-

$$14FeS_2 + 105(O) + 7H_2O \longrightarrow 14H^+ + 14Fe^{3+} + 28SO_4^{2-} \qquad \text{(Eq. 4)}$$

8	6	4	24
$8FeOOH$	$2KFe_3(SO_4)_2(OH)_6$		$24SO_4^{2-}$
(goethite)	(jarosite)		(in solution)

Vear (1981) also studied the thermodynamics of the reactions involved

and found that they balanced and agreed well with the raised temperature of the waters which flowed from depth within the rock.

In Chapter 7.2 the importance of autotrophic bacteria in the oxidation of pyrite was outlined. It should also be said that fractured pyritic rocks provide favourable conditions for the development of these iron-oxidising bacteria by enabling access of water via the discontinuities and by creating a larger surface area of rock for the micro-organisms to act on (Kuznetsov et al., 1963). This is usually reported in association with mine workings accounting for the production of acid sulphate waters or "acid mine drainage" (e.g. Singer and Stumm, 1970). Vear (1981) suggests that the Mam Tor water is a natural example of acid mine drainage and postulates that the initial slope failure created the favourable conditions which encouraged the subsequent involvement of these autotrophic bacteria as a catalyst to pyrite oxidation.

Table 7.1: Volume Changes in the Weathering of Shale (Vear, 1981)

Mineral (grams/litre of water)		Volume Change (ml)
1.5596g pyrite	- destroyed	-0.31
1.6880g dolomite	- destroyed	-0.58
0.9816g goethite	- precipitated	+0.23
	Total Volume Change :	-0.66

One of the consequences of the reactions described above is volume change; Vear (1981) considers that three minerals are of particular importance: pyrite, dolomite and goethite. Table 7.1 shows that there is a net volume loss of 0.66 millilitre per litre of water, thus increasing porosity.

It is likely that water flow will be concentrated along bedding planes, joints and fractures (including the slip plane), and therefore, it is in these zones that weathering will be most active. Due to flow of the ground water it is probable that the destruction of minerals is not taking place at the same site as the precipitation of the weathering products, consequently, voids are created in some areas and minerals are deposited in others. This must create internal stresses along these inherent planes of weakness which may influence the stability of the rock. In addition, the stability of the mass as a whole may be dependent on the shear strength of the precipitated weathering products infilling these discontinuities (Piteau, 1970).

Steward (1984) takes the effects of pyrite oxidation on the engineering properties of the shale further by assessing the influence of the composition of the pore-waters. As shown in Figure 7.1, chemical weathering of shale releases ions into the ground waters, particularly Al^{3+}, Fe^{3+}, Ca^{2+}, Mg^{2+}, K^{+}, H^{+} and SO_4^{2-}. Steward (1984) measured the effect of these ions on residual shear strength of shale in a Bromhead ring shear apparatus which had been

adapted to allow the flow of solutions through the sample during testing. Residual shear stress was expressed in terms of the apparent residual angle of friction ($\emptyset_{ra}'$). Compared with values obtained with distilled water, $\emptyset_{ra}'$ was shown to be increased in the presence of K^+ and decreased by Na^+ ions. (Na^+ ions are believed to be introduced into the ground waters mainly through salting of the road.) Sulphuric acid increased $\emptyset_{ra}'$ and the plasticity index, probably through the formation of interparticle bonds involving H^+ ions. Steward (1984) proposes that pore-water composition changes $\emptyset_{ra}'$ in the short-term, while long-term changes are dependent on mineral alteration.

Residual shear strength and plasticity are independent of the state of physical breakdown but are influenced strongly by mineralogy. Al-Dabbagh (1985) found that residual shear strength and cohesion increase with increased quartz content and with decreased clay fraction and mixed-layer clay content. Weathered shale from the surface at Mam Tor has a higher $\emptyset_{ra}'$ than less weathered shale from the quarry at Hope Cement Works, and material from a depth of twenty-eight metres in the Mam Tor borehole has lower strength and higher plasticity in relation to the surface shale. These observations are believed to be explained by the higher quartz content in the weathered material, and by the fact that the weathering products of shale are dominated by quartz, kaolinite, and aluminium or iron oxides and hydroxides, all of which tend to have greater strengths than the original constituents. Therefore, weathering does not necessarily reduce residual shear strength, but

the rock quality does deteriorate.

7.5 Weathering and Slope Stability

As weathering can produce a decrease in strength it follows that there will be a drop in the Factor of Safety of the slope. At Mam Tor in Derbyshire instability is periodic, with relatively frequent small movements occurring especially during wet periods, separated by major failure events every several years. It can be assumed that the Factor of Safety is permanently close to unity so that an increase in ground water level may be sufficient to trigger minor movements. Vear (1981) and Steward (1984) suggest that pyrite oxidation at depth within the slide is responsible for the relatively occasional major movements by weakening the rock through the removal of material and by the consequent change in pore-water composition which affects shear strength. Johnson and Vaughan (1983) propose that this pyritic shale may also have contributed to instability at Alport Castles landslide (Figure 2.6) where it outcrops at the base of the landslide.

Early and Skempton (1972) identified some geochemical differences between material in the slip zone and the ambient clay in a landslide at Walton's Wood in Staffordshire. Clay adjacent to the slip surface had a light grey colour in contrast to the general yellow-brown clay with orange mottling; chemical analysis showed a marked reduction in Fe_2O_3 content along the shear zone. This was thought to be due to

secondary chemical development by reducing waters percolating along the slip zone. A decrease in K_2O/Al_2O_3 ratio from 0.092 in the ambient clay to 0.068 in the shear zone may indicate potassium ion leaching from illite and mixed-layer clays to produce kaolinite (Taylor, 1974). However, no changes in clay mineralogy across the slip surface were observed in the landslide at Walton's Wood, but even a ten percent increase in kaolinite would be unlikely to be detected by the X-ray diffraction techniques employed. A higher percentage of clay-size material was recorded at the slip plane, possibly indicating breakdown of clay aggregates during displacement.

The above discussions indicate how slope stability in shale may be influenced by weathering. A weathering profile through a landslide in shale may be expected to be one showing physical disruption of the slipped material with chemical weathering of detrital minerals, especially pyrite, forming iron oxide coatings along fissures. The material in a landslide is likely to have greater porosity and permeability than surrounding slopes which have never failed. Therefore, the zone of weathering can be expected to be deeper on slopes which have failed regardless of their present degree of stability. The slip plane may form a major discontinuity enabling greater access and flow of water. Consequently, the mineralogy and geochemistry of the slip zone may differ from that of the ambient shale due to alteration of minerals by the percolating waters. There may also be a greater amount of clay-sized material caused by breakdown of aggregates during movement. Finally, the slip plane may form the base of the weathering zone, and thus the shale beneath may

be unweathered; this is believed to be the case at Mam Tor in the Edale Shales of Derbyshire (Steward, 1984; Vear, 1981). The following chapters will assess the weathering of shale at Oker Hill through detailed logging and mineralogical and geochemical analysis of core material through the landslide.

CHAPTER 8 SUBSURFACE INVESTIGATION OF OKER HILL LANDSLIDE

8.1 Mineralogy and Geochemistry of Tansley Borehole near Matlock

The rocks of both the Edale and Matlock regions are of the Carboniferous Millstone Grit Series and were formed contemporaneously. However, the sediments were deposited in slightly differing environments. Amin (1979) compares the mineralogy and geochemistry of the Mam Tor rocks with the time-equivalent shales from the Tansley borehole three kilometres east of Matlock (Figure 8.1). He interprets the data from the Tansley borehole sediments as being indicative of a shallow, semi-restricted basin environment into which a delta was encroaching, thus producing shales overlain by Ashover Grit, whilst the rocks of the Edale region are deep basinal mudstones (Edale Shale) and turbiditic sediments (Mam Tor Beds). Amin (1979) suggests that this lateral variation in facies reveals the influence of the Derbyshire Block acting as a submarine ridge.

The borehole at Tansley (Figure 8.2), drilled by the British Geological Survey, passes through a sequence of shale and sandstone of the Millstone Grit Series strata and into the rocks of the Carboniferous Limestone Series. This succession represents a transition from a wholly marine environment in the Lower Carboniferous, with the formation of limestone, to the mainly non-marine deltaic conditions of the later Carboniferous. The sequence contains several transgressive and regressive cycles which have been

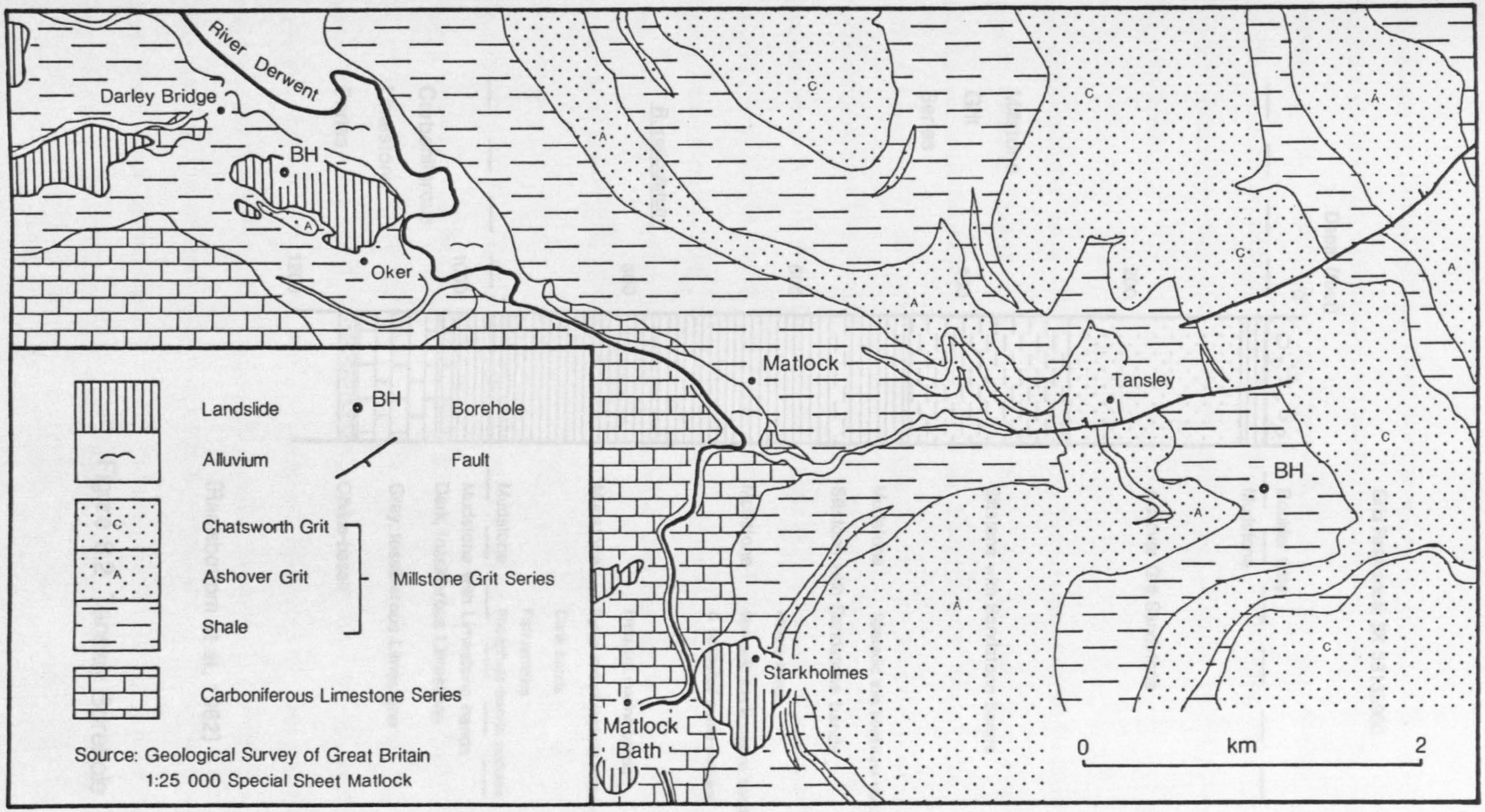

Figure 8.1 Location of Tansley and Oker Hill Boreholes

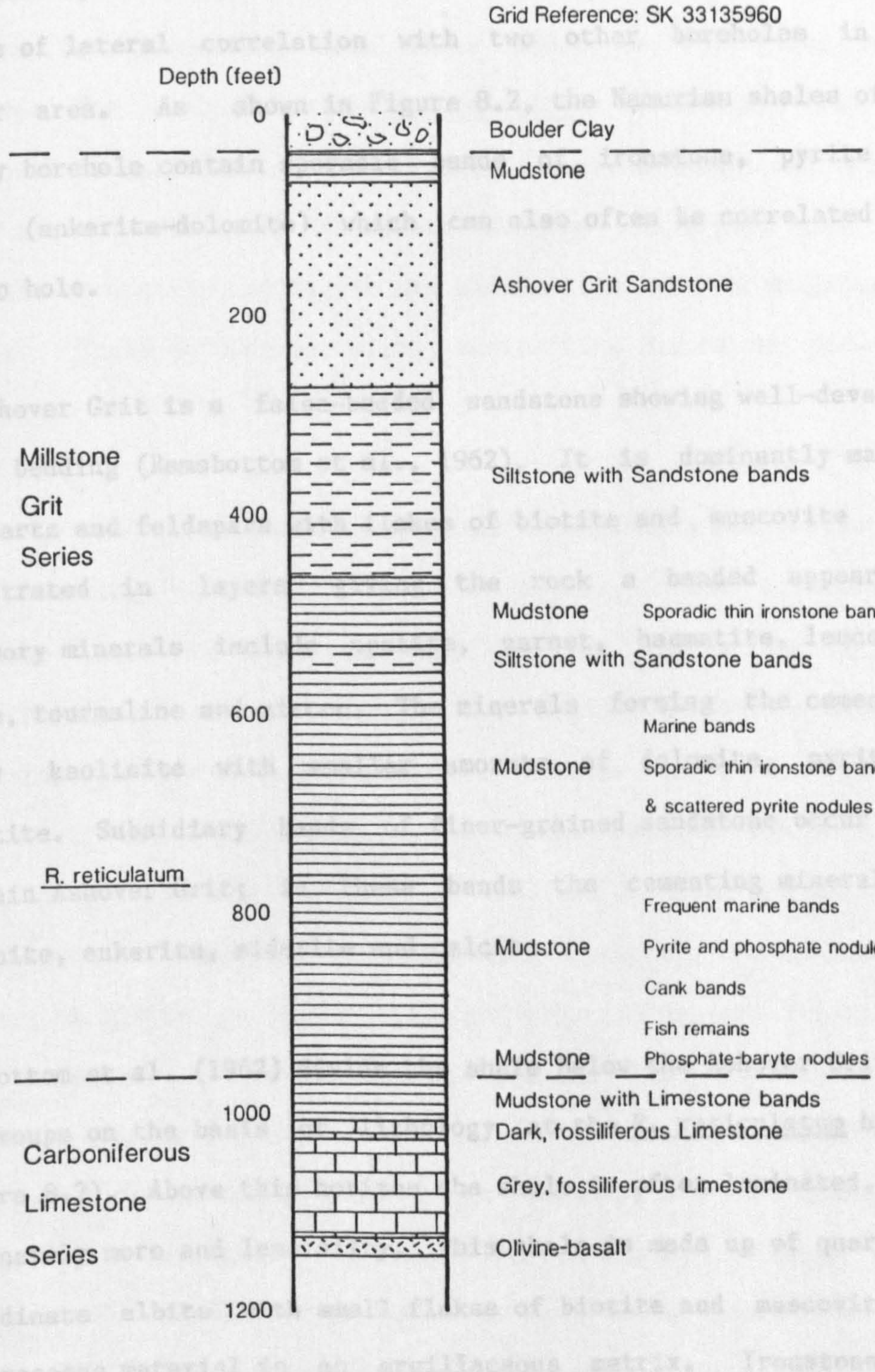

(Ramsbottom et al., 1962)

Figure 8.2 Tansley Borehole

recognised by faunal phases (Ramsbottom et al., 1962). Each cycle is capable of lateral correlation with two other boreholes in the Ashover area. As shown in Figure 8.2, the Namurian shales of the Tansley borehole contain sporadic bands of ironstone, pyrite and "cank" (ankerite-dolomite) which can also often be correlated from hole to hole.

The Ashover Grit is a false-bedded sandstone showing well-developed graded bedding (Ramsbottom et al., 1962). It is dominantly made up of quartz and feldspars with flakes of biotite and muscovite often concentrated in layers giving the rock a banded appearance. Accessory minerals include apatite, garnet, haematite, leucoxene, rutile, tourmaline and zircon. The minerals forming the cement are mainly kaolinite with smaller amounts of dolomite, pyrite and haematite. Subsidiary bands of finer-grained sandstone occur below the main Ashover Grit; in these bands the cementing minerals are kaolinite, ankerite, siderite and calcite.

Ramsbottom et al. (1962) divide the shale below the Ashover Grit into two groups on the basis of lithology at the R. reticulatum horizon (Figure 8.2). Above this horizon the shale is often laminated, being alternately more and less silty. This shale is made up of quartz and subordinate albite with small flakes of biotite and muscovite and carbonaceous material in an argillaceous matrix. Ironstone bands occur sporadically and pyrite occurs as granules, crystals, nodules and rods usually confined to well defined bands which rarely contain marine fossils. Pyrite is also found throughout the shale in a

disseminated form. Bands of "cank" (ankerite-dolomite) are also found and are associated with those mudstones containing marine fossils. The shale below the R. reticulatum horizon are less silty and ironstone bands are rare. Pyrite is more abundant and bands of "cank" are more frequent. Phosphate nodules of either apatite and kaolinite or apatite and baryte are abundant in beds containing fish remains. These nodules are highly radioactive due to the adsorption of uranium.

Changes in the depositional environment of sediments are reflected in their mineralogy and geochemistry. In general, in the Carboniferous sediments there is a decrease in detrital quartz and feldspar contents and an increase in clay and organic carbon contents with increasing distance from the shoreline; this is, in part, related to grain size. Amin (1979) observed that in the Namurian shales beneath the Ashover Grit the transition from marine to non-marine is accompanied by increases in kaolinite content, and decreases in contents of illite, pyrite, calcite and organic matter; siderite was only detected in the non-marine shales. The distribution of diagenetic minerals is attributed to changing physico-chemical conditions, for example the change from pyrite to siderite is considered to reflect a decrease in pH and an increase in Eh consequent on the change from marine to non-marine conditions. The relationship between mineralogy and geochemistry of the shale in the Tansley borehole (Amin, 1979; Spears and Amin, 1981a) can be summarised as follows:-

8.1.1 Major Element Geochemistry

(i) In the marine group, increases in concentrations of Fe_2O_3, SO_3 and CaO are associated with pyrite and calcite. Fe_2O_3 is related to iron hydroxides, illite and pyrite, (although the iron in pyrite is FeO it is determined as Fe_2O_3).

(ii) The K_2O/Al_2O_3 ratio is higher in marine shales as a result of the higher content of illite in this group.

(iii) Siderite is only found in the non-marine shales in which phosphate and TiO_2 are relatively concentrated.

(iv) In the non-marine group, an increase in FeO concentration is related to siderite.

(v) FeO is also related to chlorite.

8.1.2 Trace Element Geochemistry

(i) The elements having the greatest percentage increase from non-marine to marine shales are, in descending order: Pb, Cu, V, Ni, Sr and Zn. The concentrations of Cu, Sr and Pb were found to be the most effective discriminators between the two groups of shale.

(ii) Pb and Cu show a strong positive correlation with Fe_2O_3 (pyrite). Ni, Cu and Pb are believed to be concentrated in pyrite and organic matter.

(iii) V is concentrated in organic matter and in illite.

(iv) Sr is concentrated in calcite.

(v) The increase in Zn appears to be related to the increase in illite and therefore, it is thought that Zn is dominantly of detrital origin. It is also concentrated in the carbonates, pyrite and organic matter together with Co and Mn.

(vi) The non-marine shales were richer in Mn due to the association of Mn with siderite. Also, Zr levels were higher in the non-marine shales; this element is mainly present as elemental zirconium.

(vii) Cr, Rb and Ba are mainly related to illite and feldspars.

(viii) Y could not be assigned to either a particular element group or mineral.

Thus the general trend found by Amin (1979) is from marine shale at the base, rich in pyrite and calcite, to siderite-rich non-marine shales at the top of the sequence, a relationship which has also been recorded by other authors (Curtis, 1969; Hirst and Kaye, 1971;

Spears, 1964). The trace element enrichment is attributed mainly to organic matter and pyrite, explaining the higher concentrations of Co, Cu, Ni, Pb and Zn found in the marine shales than in the brackish water and non-marine sediments. Several samples of the marine shale contained small amounts of gypsum, this is believed to be a result of pyrite oxidation under atmospheric conditions in the presence of calcite or dolomite.

8.2 Aims of Borehole Analysis of Oker Hill Landslide

From the above information it can be predicted that there is potential for pyrite oxidation within the shale of Matlock; this is further indicated by the presence of ochreous springs on Oker Hill. The remainder of this work aims to assess the importance of this process on slope instability in the Matlock region by analysing cores of shale through Oker Hill landslide. This landslide occurs in the same strata as that encountered in the Tansley borehole (Figure 8.1).

To guide the investigation several working hypotheses were constructed:

(i) There is a change of mineralogy and/or geochemistry at the slip plane.

(ii) Any difference in mineralogy and/or geochemistry at the slip plane is pre-slope failure.

(iii) Any difference in mineralogy and/or geochemistry at the

slip plane is post-slope failure.

(iv) The slip plane is located in the pyritic shale due to weakness caused by pyrite oxidation.

(v) There is active pyrite oxidation going on within the landslide at present, and therefore, there is potential for further slip movement.

(vi) The slip plane is located in the zone with most potential, when unweathered, for weathering.

These hypotheses will be tested in the following chapters.

8.3 The Drilling of the Boreholes through Oker Hill Landslide

Two boreholes were drilled through Oker Hill landslide at the sites shown in Figures 6.7 and 6.9 between 22 April and 3 July 1987. They were closely positioned so that any laterally persistent horizon could be easily correlated in both holes, thereby allowing greater confidence to be placed in the data.

A Pilcon Wayfarer shell and auger percussion rig was used to drill the boreholes providing core samples of the shale in U100 aluminium tubes (the metric equivalent of U4 tubes). Details of this method of coring are given by Petley (1984) and Smith (1982). Unfortunately, this technique is not ideal for locating the slip plane and other surfaces of discontinuity within a landslide as the U100 tube samples 450 millimetre lengths with breaks in between (at the cutting shoe).

Also, the material collected in the U100 tube tends to be disturbed at the edges due to friction between the shale and the tube during sampling and extraction, however, the centre of the core is relatively undisturbed. The material in the cutting shoe was collected as a totally disturbed mass sample and stored in a plastic bag. As no method of drilling was available to produce undisturbed core with no breaks this limitation of the shell and auger percussion rig had to be accepted, but by careful drilling and depth measuring the breaks in sampling were kept to a minimum and accurately recorded.

8.4 On Site Borehole Logs

The on site borehole logs in Appendices 2a and 2b provide details of the conditions encountered in Boreholes 1 and 2 respectively during drilling. From field work and the construction of a longitudinal slope profile through the borehole sites it was estimated that the basal slip plane would be encountered at a depth of approximately twenty metres in both boreholes (Figure 6.11) with two additional failure surfaces at nine and eighteen metres.

Unfortunately, the first borehole had to be abandoned at a depth of 9.5 metres due to clutch failure on the rig. As a result of this delay the cutting tool became firmly embedded in the shale and could only be freed by raising the casing. This procedure caused too much disturbance of the borehole to allow further useful exploration, and

therefore, the rig was moved to Site 2. The second borehole was taken to a depth of 12.9 metres. Although Borehole 2 did not reach the depth of the predicted slip plane at twenty metres, the character of the core material at 12.9 metres (unweathered and well-laminated) suggested that the in situ shale had been reached. In addition to this, the strength of the shale was becoming too great for sampling and coring by a shell and auger rig and therefore further drilling was considered impractical.

In both boreholes shattered sandstone boulders in a silty matrix were encountered to a depth of approximately 3.2 metres, and sandstone and siltstone fragments continued to be mixed with clay to approximately 4.5 metres. Below this depth only clay and shale was present. The shale above 9.5 metres was iron-stained and generally more weathered than the shale below this depth; this may correspond to the location of a predicted slip plane which was estimated to occur at approximately nine metres.

During the drilling of the second borehole ground water was encountered at a depth of 3.3 metres; the water-bearing strata was sealed when the casing was driven to 4.3 metres. This perched water table appears to be located in the weathered shale immediately below the sand and silt and would therefore appear to be charged from the overlying permeable strata. The ground water level was reached in Borehole 1 at a depth of 5.5 metres. Water was again encountered in Borehole 2 when the casing was at a depth of 10.5 metres and the hole at 11.2 metres, this was probably due to the interruption in drilling

for twenty-one days which enabled ground water to seep into the hole.

From approximately ten metres downward the shale was noticeably harder as it took a greater number of drops of the sliding hammer to advance the U100 tubes a set distance, in fact, towards the bottom of the hole the shale was becoming too strong for sampling by this method. To aid drilling progress water had to be added to the hole at numerous stages and, as artificial changes in water content affect the accurate estimation of strength properties of shale (Petley, 1984), no samples were collected for the determination of the engineering properties.

The cores were sealed in the U100 tubes and in plastic bags for transport to the laboratory. After extraction from the tubes the core was sealed and stored in plastic bags and aluminium foil (Arman and McManis, 1976) during the short time preceding logging and sampling for mineralogical and geochemical analyses.

8.5 Detailed Logs of the Oker Hill Core

The core material from Borehole 2 was logged and sampled for mineralogical and geochemical analyses (Appendix 3). This log identifies lithology and structure, and describes the weathered state of the shale.

Large fragments of sandstone are present within the shale to a depth

of 5.65 metres with small fragments upto twenty millimetres occurring as deep as 7.4 metres. These fragments are found in disturbed, relatively structureless shale which suggests mixing due to slope movement at failure. Below this level the shale becomes well-laminated with the spacing of these laminations becoming greater with depth and apparently correlating with increasing strength and decreasing disturbance of the rock. Unfortunately, it was not possible to measure strength, however, it was noted that progress in drilling became slower, and sampling of the core material for subsequent analysis also became more difficult with depth which, together with observations of the friability and structure, provided an indication of the strength of the shale.

Below 9.6 metres tiny cubic crystals (possibly pyrite) were noted within the shales. Small oxidised iron nodules were also identified in places, as indicated on the log, above 9.65 metres in both cores. At several depths in the material from Borehole 2 (7.33, 8.84, 9.03 and 9.60 metres) a green to yellow mineral was observed forming a coating on the faces of fractures. This powdery mineral may be jarosite, a weathering product of pyrite and illite. From a depth of 10.10 to 10.90 metres white flecks were visible on the surfaces of the laminae, these may be gypsum.

At 10.70 metres there is a band of angular fragments or crystals which makes an oblique contact with the shale below. (The oblique contact is likely to be due in part to off-vertical coring.) These "fragments" are approximately cubic in shape and upto twenty

millimetres in diameter. Their surfaces are covered by orange iron oxide. Due to their cubic rather than plate-like shape they are unlikely to be fragments of shale and are most likely to be crystals. In the Hepworth Carboniferous sequence in Yorkshire Pearson (1979) found similar bands within the shale which were identified as concretionary siderite. He suggests that these concretions develop as stratiform bodies along coarser sediment horizons which form pathways for the expulsion of fluids during compaction by burial, the drop in partial pressure of CO_2 enabling precipitation of this iron carbonate.

The weathering grade of the shale from Borehole 2 is also recorded on the log in Appendix 3. The classification used is based on the schemes proposed by Fookes and Horswill (1969), Chandler (1969) and the Geological Society Engineering Group Working Party (1970, 1972). However, the schemes had to be modified as disturbance of structures and fracturing in the shale was considered to reflect slope failure and drilling disturbance in addition to weathering. Therefore, the weathering classification used in Appendix 3 is based more on chemical weathering of minerals than on physical breakdown of the rock. An explanation of the modified weathering classification used for the Oker Hill shale is given in Table 8.1.

There appears to be a distinct change at approximately 9.65 metres of the weathering state of the shale. Above 9.65 metres the shale shows orange iron oxide staining on fracture surfaces, whereas below this level such staining is rare. This would appear to be the base of the

TABLE 8.1 WEATHERING CLASSIFICATION OF SHALE

adapted from schemes proposed by Fookes and Horswill (1969), Chandler (1968) and the Geological Society Engineering Group Working Party (1970, 1972).

GRADE	DESCRIPTION OF SHALE
V	Completely weathered - discoloured clay matrix, lithorelicts rare.
IV	Highly weathered - discoloured; lithorelicts separated by altered material (matrix), matrix dominates over lithorelicts.
III	Moderately weathered - discoloured; lithorelicts separated by altered material (matrix), lithorelicts dominate over matrix.
II	Slightly weathered - slight discolouration on surfaces of discontinuities, but otherwise fresh.
I	Fresh - no discolouration; no visible evidence of weathering.

N.B. This scheme does not consider the structure of the shale as it has been affected by landsliding as well as weathering. However, in general, there is a loss of structure with increased weathering grade.

weathered zone. Iron oxide was observed in samples taken from below 9.65 metres during logging which was not present at the time of sampling, therefore, it is probable that this limited amount of iron oxide formed during storage. The present day depth of chemical weathering is rarely greater than three to five metres in Britain (Gallois and Horton, 1981), but in the areas of Britain that were not eroded in the last glacial period the depth of weathering from the Pleistocene is commonly much deeper and may be as great as thirty metres. Although the depth of weathering on stable slopes in the Matlock area is not known, Spears and Taylor (1972) have recorded pyrite decomposition to depths of six feet from the surface in the Coal Measures shales of central England. This would suggest that the depth of weathering in the Oker Hill landslide may be a relic of Pleistocene processes, however, as a slipped mass is more permeable it may be expected to be weathered to a greater depth than an unfailed slope.

During detailed logging of the core from Borehole 2 several planes of discontinuity were noted which may be slip planes. The first of these at 6.80 metres is suggested by the apparent displacement of shale along a diagonal line marking the junction between structureless clay and faintly laminated shale. However, this may be a result of disturbance caused by either sampling, extraction of the core from the U100 tubes or longitudinal splitting of the core for logging, and therefore, caution must be expressed in interpretation. The contact at 6.70 metres between soft grey clay above and slightly stiffer brown/grey clay below may also be associated with this

possible shear zone.

The disturbed sample of shale at 7.45 to 7.50 metres marks the junction between faintly-laminated and well-laminated shale: the junction between weathering grades IV and III, respectively. Unfortunately, the nature of the contact is not known, however, the possibility of this being a slip plane cannot be ruled out.

Between 8.55 and 8.85 metres depth there are several features that may be related to a shear zone. At 8.55 to 8.75 metres there is an increase in weathering grade of the shale with depth from Grade III to IV; the nature of this change is not known as the sample has been disturbed. The shale between 8.75 to 8.85 metres is intensely iron-stained with laminations only just visible. Below 8.85 metres the shale is again well-laminated and of weathering grade III. This increase in weathering grade between 8.55 and 8.85 metres may represent a zone of increased permeability as may be expected of a slip zone.

The deepest discontinuity that may be a slip plane is at 9.65 metres indicated by the diagonal contact between iron-stained and fresh shale dipping at between 40° to 50° (Plate 8.1). This contact between the weathered and unweathered shale at 9.65 metres is along the plane of laminations in the underlying shale, whilst the overlying shale appears to be inclined at a shallower angle, approximately 20°. Also, there is a zone approximately five centimetres deep in which the shale laminae are in smaller fragments than in the ambient rock.

PLATE 8.1 CORE MATERIAL FROM BOREHOLE 2

CONTAINING THE PROPOSED SLIP PLANE AT 9.65 METRES

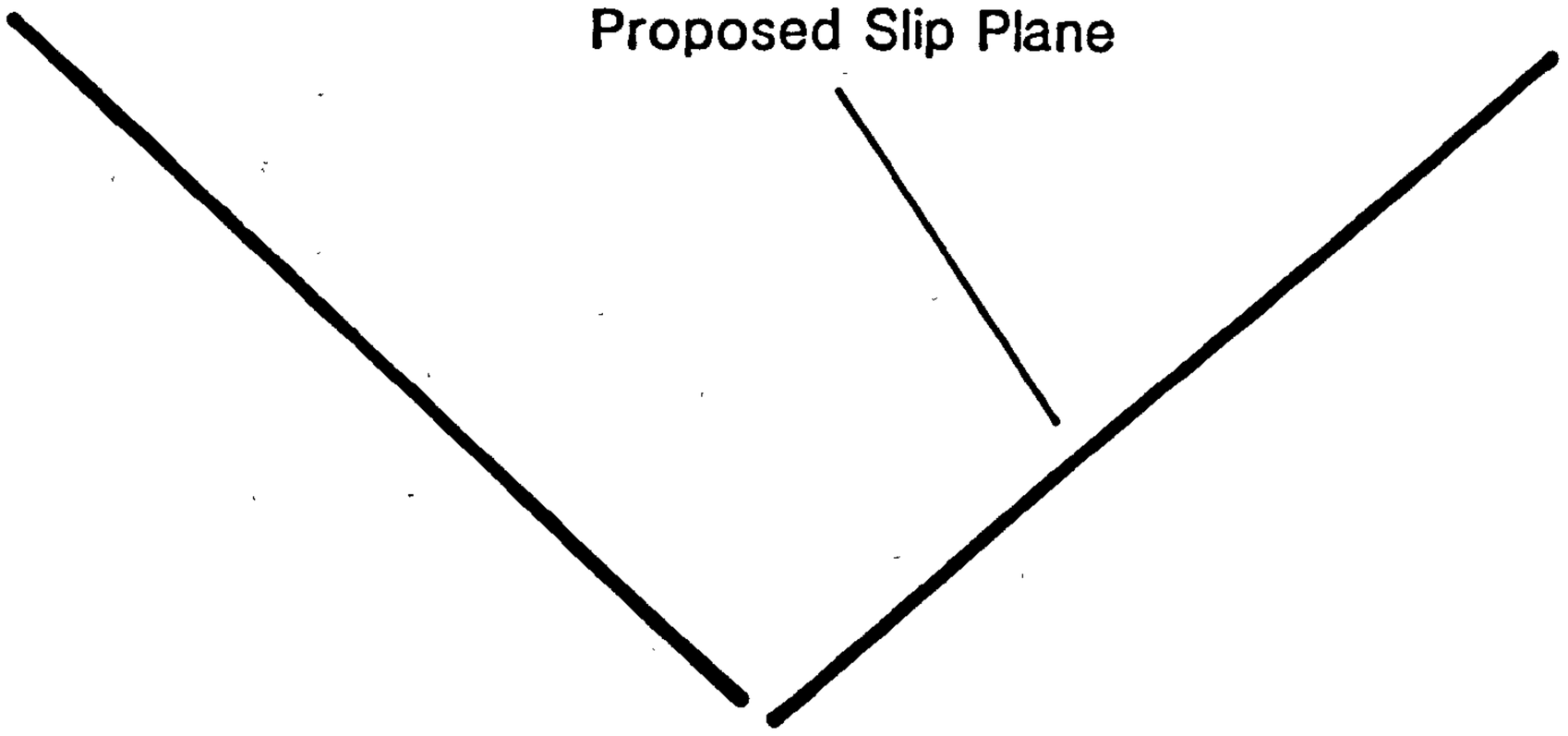
9.65 metres
Base of Weathering
Proposed Slip Plane


15


15

These features suggest that this may be the basal slip plane of the landslide, and this is further supported by the estimated depth to the slip plane of nine metres taken from the cross-section in Figure 6.11. Information from Borehole 2 is combined with the slope profile in Figure 8.3.

It must be borne in mind that it is possible that the slip plane was not sampled or recognised due to the method of drilling, and it is also likely that there will be several slip planes due to the multiple nature of this landslide. In addition, the basal slip plane may be as deep as predicted in Figure 6.11 and was, therefore, not reached.

The identification of the slip plane in the core through Oker Hill landslide is essential for the testing of the hypotheses stated in Chapter 8.2. Hutchinson (1982) advises that several techniques should be used to identify a slip plane and describes the methods available. In this work the geometry of the landslide has been used to predict the position of the basal slip plane and this has been combined with observations of discontinuities within a core.

Other observations of slip planes are described by many authors, for example Henkel and Skempton (1954) noted that the failure zone consisted of a soft clay layer five centimetres thick which had a higher water content than the adjacent shale. Prior and Graham (1974) identified a highly polished and slickensided slide surface in the Carboniferous shale of Northern Ireland which was confined to a

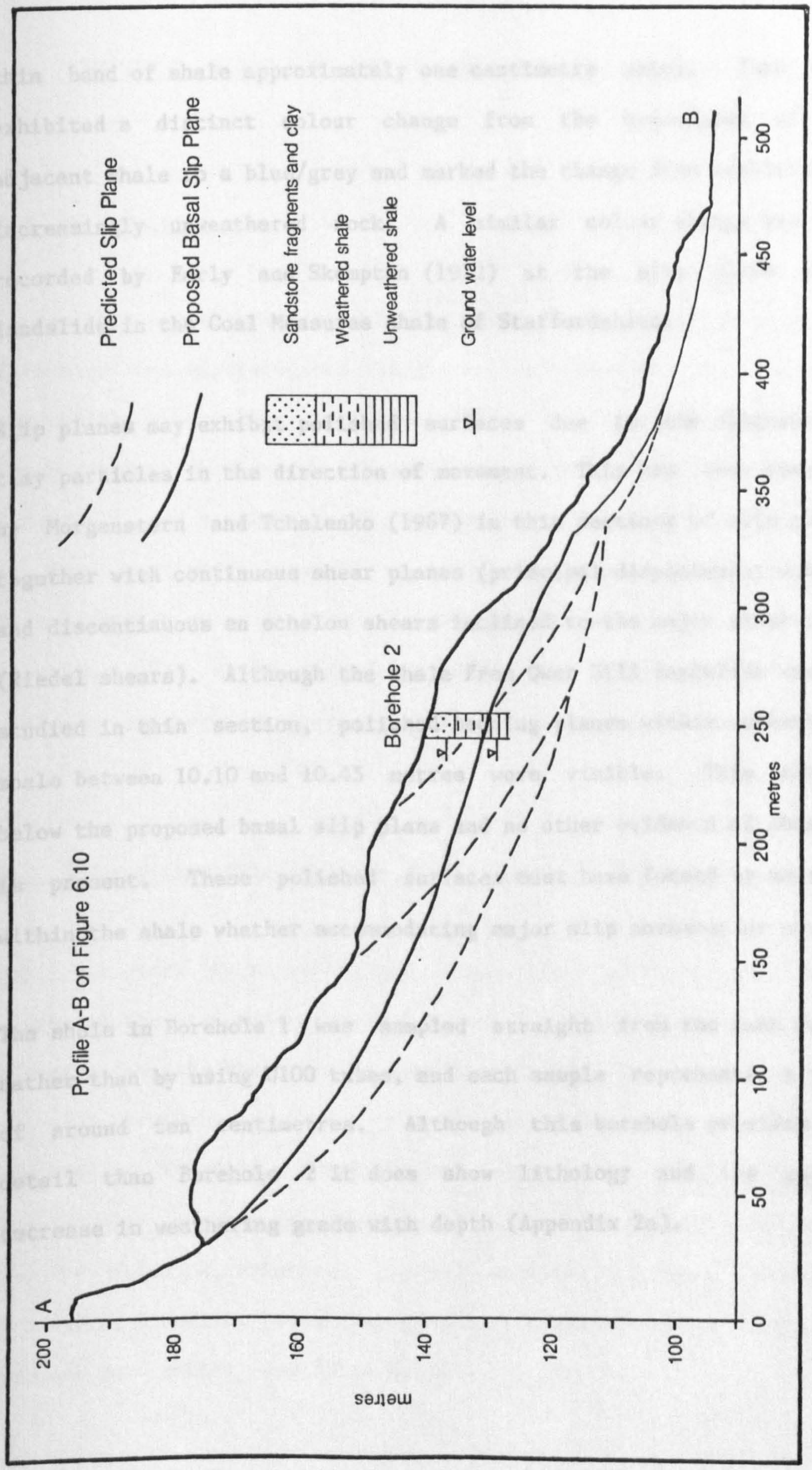

Figure 8.3 Subsurface Conditions Down the Central Slope Profile of Oker Hill Landslide

thin band of shale approximately one centimetre thick. This band exhibited a distinct colour change from the brown/grey of the adjacent shale to a blue/grey and marked the change from weathered to increasingly unweathered rock. A similar colour change was also recorded by Early and Skempton (1972) at the slip plane of a landslide in the Coal Measures shale of Staffordshire.

Slip planes may exhibit polished surfaces due to the alignment of clay particles in the direction of movement. This has been observed by Morgenstern and Tchalenko (1967) in thin sections of slip planes together with continuous shear planes (principal displacement shears) and discontinuous en echelon shears inclined to the major shear plane (Riedel shears). Although the shale from Oker Hill landslide was not studied in thin section, polished bedding planes within unweathered shale between 10.10 and 10.45 metres were visible. This zone is below the proposed basal slip plane and no other evidence of shearing is present. These polished surfaces must have formed by movement within the shale whether accommodating major slip movement or not.

The shale in Borehole 1 was sampled straight from the main cutter rather than by using U100 tubes, and each sample represents a depth of around ten centimetres. Although this borehole provides less detail than Borehole 2 it does show lithology and the general decrease in weathering grade with depth (Appendix 2a).

CHAPTER 9 MINERALOGY AND GEOCHEMISTRY OF OKER HILL SHALE

9.1 Introduction

To test the hypotheses set out in Chapter 8.2 it was necessary to determine the mineralogical and geochemical composition of the shale through the Oker Hill landslide. For this purpose sub-samples (approximately 50cm^3) were taken of each of the thirteen samples from Borehole 1, and a total of 122 sub-samples were taken from Borehole 2 at five centimetre intervals as indicated on the log in Appendix 3. These samples were prepared following the methods described in Appendix 4 for whole rock X-ray diffraction and X-ray fluorescence analyses to determine mineralogy and geochemistry respectively.

9.2 X-Ray Diffraction Analysis of the Oker Hill Shale

Table 9.1 gives the mineralogical composition of the average shale. Quartz is the predominant mineral in the 2 to 60 μm fraction and clay minerals dominate the fraction less than 2 μm. The most common clay minerals present in shales are kaolinite and illite plus smaller amounts of chlorite, smectites and mixed-layer illite-smectites. Shales also contain accessory and diagenetic minerals including calcite, dolomite, ankerite, gypsum, apatite, pyrite, pyrrhotite, marcasite, siderite, haematite, goethite, anatase, rutile, zircon and carbonaceous matter (see Table 9.1).

Table 9.1 Mineralogical Composition of Shale

	Pettijohn (1) (1975)	Shaw and Weaver (1965)	Yaalon (2) (1962)
Clay Minerals	58	60	59
Quartz	28	30	20
Feldspar	6	5	8
Carbonates	5	4	7
Iron oxides	2	<1	3
Organic matter	-	1	-
Others			3

(1) World-wide mudrock average.

(2) Calculated from chemical data.

Other = pyrite, apatite, gypsum, rutile and organic matter.

The mineralogy of shales is best studied by X-ray techniques due to their fine grain size. Identification of minerals by X-ray diffraction is based on the measurement of the d-spacings between planes of atoms in the crystal lattice at various angles of incidence - each mineral producing a characteristic pattern of peaks of reflected X-rays. Further details of the technique are explained by Whalley (1981).

9.2.1 Whole Rock Mineralogy

For X-ray diffraction analysis of the whole rock every sample from Borehole 1 was analysed but only selected samples were taken from Borehole 2 due to the large number of samples and the length of time to complete a scan. From Borehole 2 a sample was taken at intervals of approximately one metre plus those samples that contained interesting mineralogical features noticed in the hand specimen. In addition to these, every sample within one metre of the 9.65 metre slip plane was analysed to record any changes that may occur across this zone. After X-ray fluorescence analysis those samples of shale exhibiting an interesting geochemical composition were also analysed by XRD.

The data was interpreted using tables provided by Chao (1969). Quartz, kaolinite, illite, pyrite, siderite, jarosite, haematite and chlorite were identified in the samples, although only quartz, kaolinite and illite were common to all samples. Smaller amounts of feldspar, probably albite, were also present. The distribution of the minerals down Borehole 2 is shown in Figure 9.1.

From data from the Pierre Shale, Schultz (1964) found that a mineral must be uniformly distributed in a sample in amounts of greater than two percent before it is consistently detected, and that a mineral will not be detected at all if it is present in amounts of less than 0.5 percent. These detection limits, however, depend on the inherent

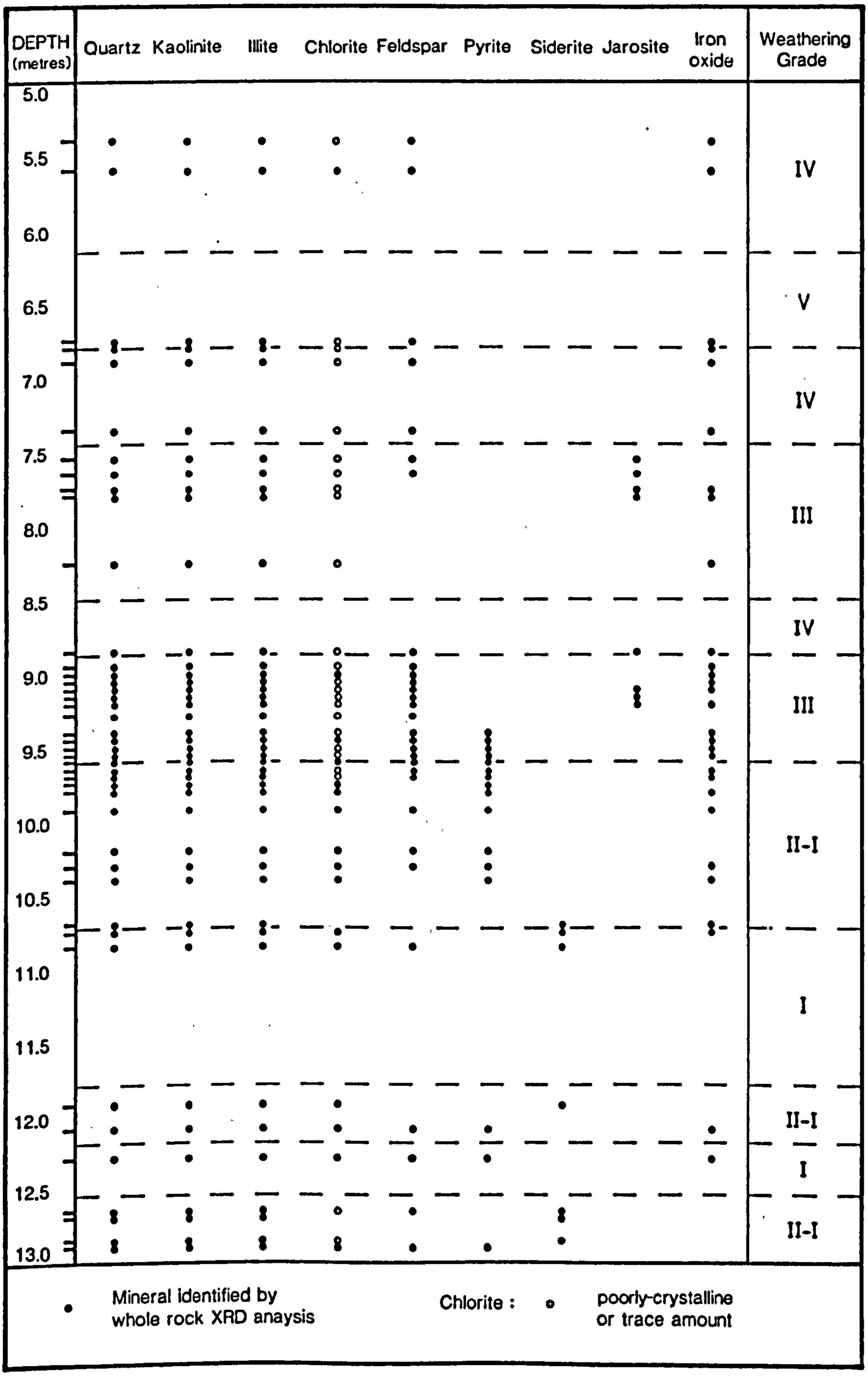

Figure 9.1 Distribution of Minerals Identified by X-Ray Diffraction Through Oker Hill Landslide: Borehole 2

diffracting ability of different minerals, for example the lower limit of detection of quartz is one percent, whereas that of pyrite is two percent. Consequently, the presence of other minerals not detected in the Oker Hill shales cannot be excluded. No attempt has been made to quantify the mineralogical data in this study as several of the peaks exceed the vertical scale and so cannot be accurately measured. Details of quantifying XRD data are provided by Collins (1976), Cubbitt (1975) and Schultz (1964).

The distribution of many minerals is influenced by the environment of deposition. For example, in the Carboniferous sediment sequence at Hepworth in Yorkshire Pearson (1979) found that quartz and zircon distributions were affected by the energy of the depositional environment and that they were the inverse of the distributions shown by the clays. The environment of deposition is also of importance with respect to diagenetic minerals. Marine shales are particularly rich in calcite, pyrite and organic matter (Amin, 1979; Pearson, 1979), whilst non-marine shales may contain siderite (Amin, 1979).

Pyrite is present from a depth of 9.4 to 10.4 metres and from 12.10 metres downward in Borehole 2 of the Oker Hill landslide, but in samples taken from 10.70, 10.75, 10.85 and 11.925 metres the iron-rich mineral is siderite. On the basis of previous work by authors such as Amin (1979), Berner and Raiswell (1984) and Spears and Amin (1981a) this implies a change from a marine environment at the base of the core, providing the conditions favourable for the formation of iron sulphide, to freshwater or brackish conditions under which iron

sulphide is not stable and, therefore, the iron carbonate of siderite is precipitated. The presence of pyrite at 10.4 metres marks the return to marine shale. The XRD trace of the sample taken from 10.70 metres showed it to be mainly composed of siderite with traces of quartz, kaolinite and illite, this supports the interpretation of this horizon as a concretionary band of siderite.

Above 9.4 metres any pyrite or siderite originally present appears to have been oxidised to either jarosite or haematite. This is consistent with the transition from unweathered to weathered shale shown in Appendix 3. The presence of pyrite between 9.4 and 9.65 metres may be explained by the fact that, although there is an iron oxide coating on the fracture surfaces of the shale in this zone, there are intact pieces of shale with unweathered cores. Consequently, this would appear to be a zone of potentially active weathering. Taylor (1988) points out that oxidation of pyrite can occur at weight percentages less than 0.5 percent which are lower than the X-ray detection limits. Therefore, this process cannot be excluded from the samples above 9.4 metres. The only weathering products of pyrite oxidation identified are iron oxides or hydroxides and possibly jarosite (the peak of jarosite is partly obscured by an illite peak); no gypsum has been identified. However, Nixon (1978) suggests that gypsum will not form if the calcium content of the shale is less than 0.5 percent by weight. The values of CaO measured by XRF (Chapter 9.3.1) tend to be around 0.25 percent (Table 9.5), therefore it would appear that calcite is present within the shale at insufficient levels to enable reaction with pyrite to form gypsum.

Many of the samples analysed contain small amounts of feldspar identified by peaks in the range 27° to 29° 2θ. In the Coal Measures mudrocks Fellows and Spears (1978) identified low albite and maximum microcline and they suggest that the feldspar assemblage of a mudrock will not be complex as it is only the low-temperature feldspars that will generally survive in a sedimentary cycle. The Oker Hill shale contains dominantly plagioclase (28.0° 2θ) with smaller amounts of K-feldspar (27.5° 2θ).

9.2.2 Clay Mineralogy

The distribution of clays is related to environmental factors. In recent sediments there is a general increase in smectite content away from the shoreline with a corresponding decrease in kaolinite and illite (Shaw, 1981). This results from differential settling rates caused by grain size, differential flocculation and salinity. Shaw (1981) observes that the clay assemblages of Carboniferous mudrocks are dominated by illite and kaolinite, and that there is a marked reduction in the proportion of expandable clays in the Lower Carboniferous compared to the Upper Carboniferous. Amin (1979) identified the expandable clay in the Tansley borehole shale to be a mixed-layer illite-smectite. Although kaolinite and illite were recognised in large quantities on the XRD traces of the whole rock samples, chlorite was isolated from the other peaks with greater difficulty and the expandable clays were also hidden. Expandable

clays are smectite, vermiculite and mixed-layer phases containing smectite and/or vermiculite and, due to their swelling characteristics, they are of particular importance in slope stability. Therefore, it is necessary to study the clay minerals in greater detail.

The clay fraction from every sample of shale from the two boreholes was analysed by XRD. To distinguish between the different types of clay minerals the samples were run four times under different treatments (Brown, 1961): (i) air-dried, (ii) glycolated, (iii) heated to 375°C for thirty minutes, and (iv) heated to 550°C for thirty minutes (Appendix 4). This enables separation of the clays on the basis of swelling expandable clays by glycolation, and collapsing and destroying the structure of the expandable clays by heating. A few samples were also treated with hot 2NHCl for twenty-four hours to distinguish the peak of kaolinite at 7Å from the 7Å peak of chlorite, chlorite being dissolved by the acid. The proportions of kaolinite, illite, expandable clays and chlorite present were measured by the method used by Weir et al. (1975) as explained in Appendix 4.

The results were plotted against depth (Figure 9.2) and show no distinct trend. However, there are several features worthy of note. Firstly, the dominant clay minerals in all samples are kaolinite and illite, and in the concretionary band of siderite these are the only clays present. The absence of chlorite from samples at 11.95, 12.65 and 12.725 metres is also of interest as XRD analysis of the whole

Figure 9.2

Distribution of Clay Minerals Through

Oker Hill Landslide: Boreholes 1 and 2

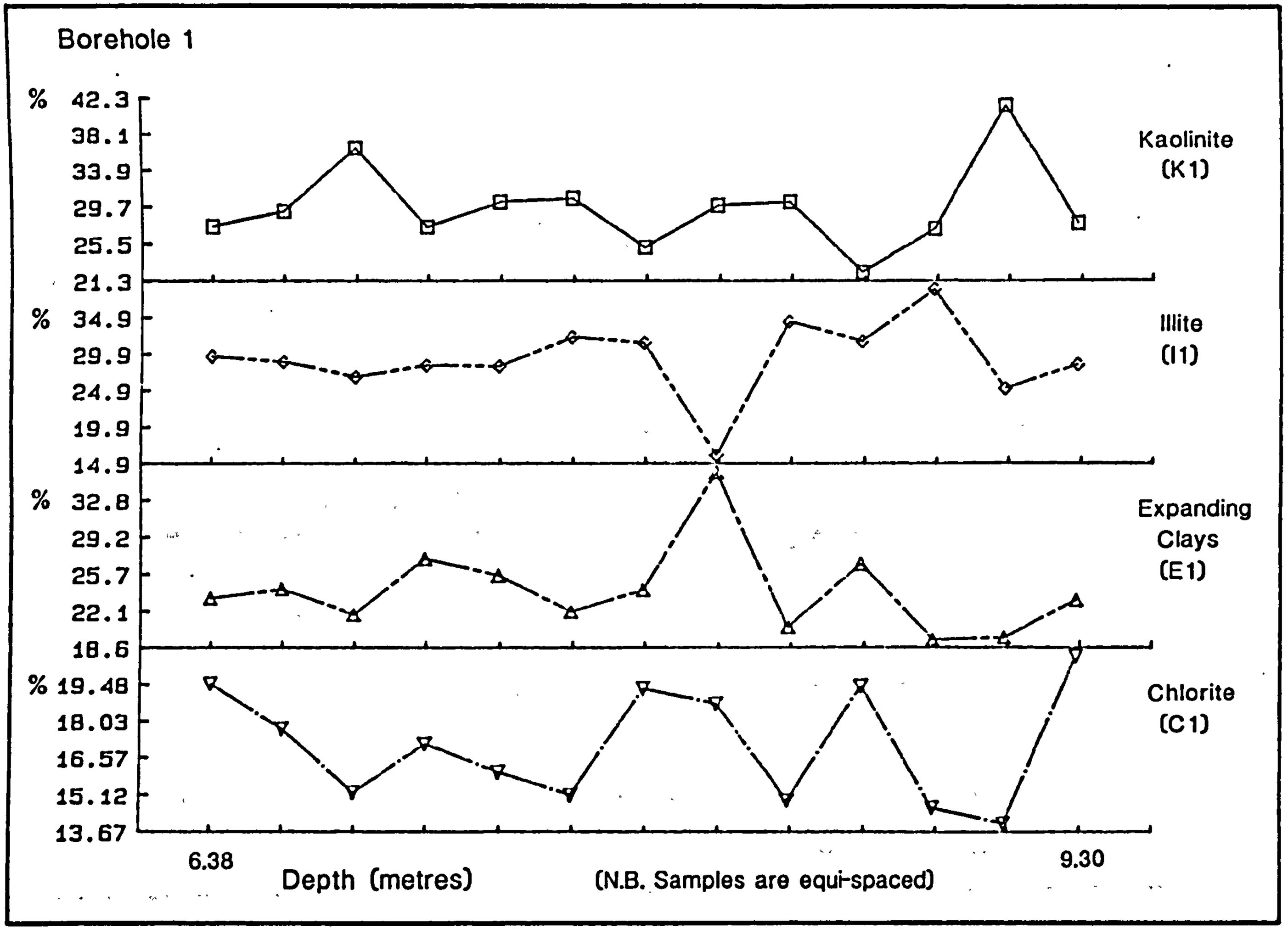
Borehole 1
% 42.3
38.1
33.9
29.7
25.5
21.3
Kaolinite
(K1)
% 34.9
29.9
24.9
19.9
14.9
Illite
(I1)
% 32.8
29.2
25.7
22.1
18.6
Expanding
Clays
(E1)
% 19.48
18.03
16.57
15.12
13.67
Chlorite
(C1)
6.38
9.30
Depth (metres)
(N.B. Samples are equi-spaced)

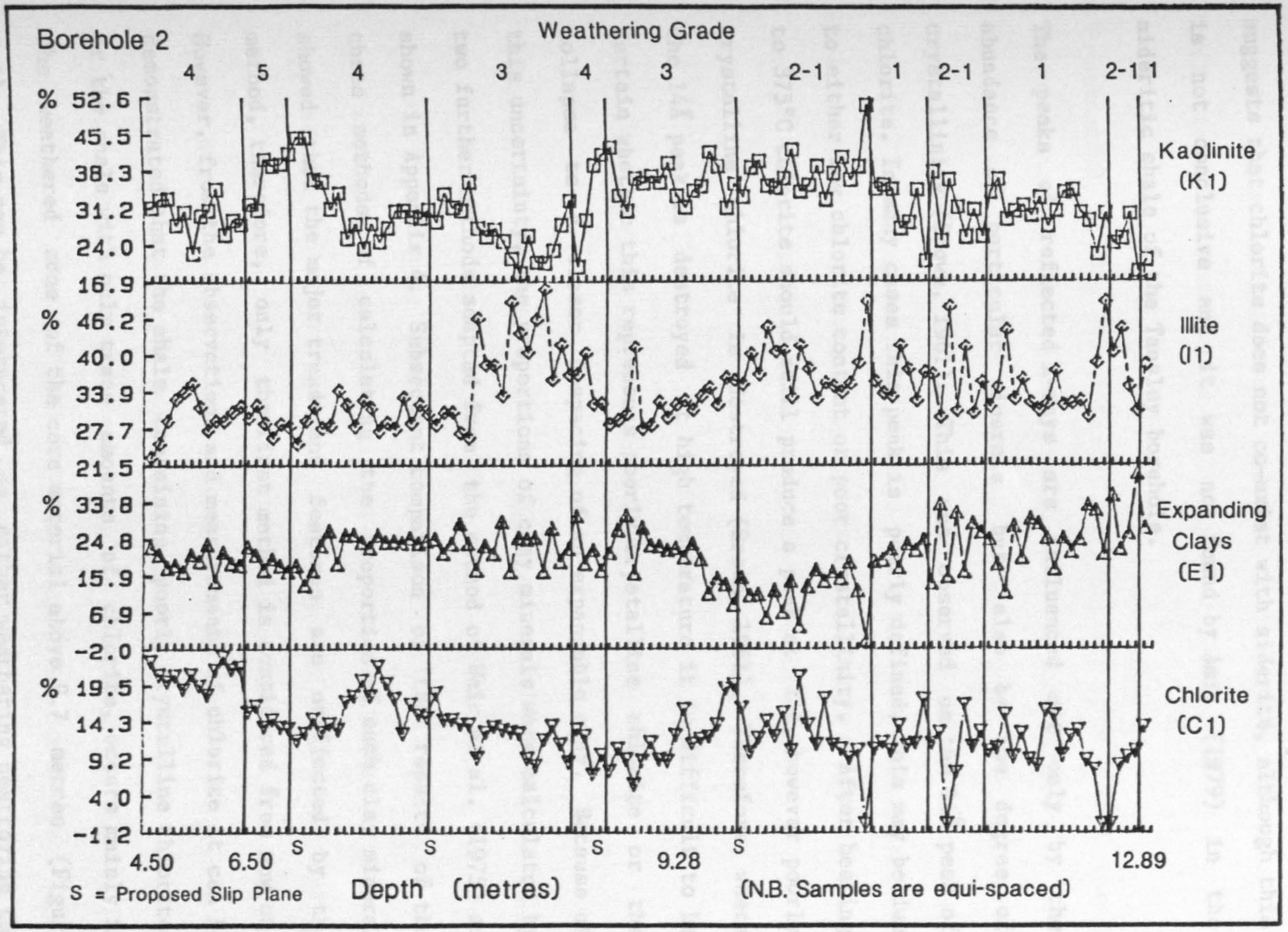
Borehole 2
Weathering Grade
4 5 4 3 4 3 2-1 1 2-1 1 2-1 1
% 52.6
45.5
38.3
31.2
24.0
16.9
Kaolinite (K1)
% 46.2
40.0
33.9
27.7
21.5
Illite (I1)
% 33.8
24.8
15.9
6.9
-2.0
Expanding Clays (E1)
% 19.5
14.3
9.2
4.0
-1.2
Chlorite (C1)
S S S S
4.50 6.50 9.28 12.89
S = Proposed Slip Plane
Depth (metres)
(N.B. Samples are equi-spaced)

rock samples shows that siderite is present at 11.95 metres. This suggests that chlorite does not co-exist with siderite, although this is not conclusive and it was not found by Amin (1979) in the sideritic shale of the Tansley borehole.

The peaks of reflected X-rays are influenced not only by the abundance of particular minerals but also by the degree of crystallinity (Brown, 1961). This was observed on the 14Å peak of chlorite. In many cases this peak is poorly defined, this may be due to either low chlorite content or poor crystallinity. After heating to 375°C chlorite should still produce a peak at 14Å, however poorly crystalline chlorite is destroyed (Brown, 1961). Therefore, where the 14Å peak is destroyed at high temperature it is difficult to be certain whether this represents poorly crystalline chlorite or the collapse to a closer d-spacing of an expandable clay. Because of this uncertainty, the proportions of clay minerals were calculated by two further methods adapted from the method of Weir et al. (1975) as shown in Appendix 4. Subsequent comparison of the results of the three methods of calculating the proportion of each clay mineral showed that the major trends and features are unaffected by the method, therefore, only the first method is considered from now on. However, from the observations and measurements of chlorite it can be demonstrated that the shale containing poorly crystalline chlorite, or the shale with only trace amounts of chlorite, occurs mainly in the weathered zone of the core material above 9.7 metres (Figure 9.1). This may be interpreted as either weathering destroying the crystal structure of chlorite or destroying the mineral altogether.

Attention should also be drawn to the broad peak in illite content around eight metres depth and the corresponding decrease in kaolinite. This feature will be discussed in Chapter 10.

To summarise, the borehole through the landslide at Oker Hill passes through marine and non-marine shale, characterised by pyrite and siderite respectively. The dominant minerals are quartz, kaolinite and illite with smaller amounts of pyrite, siderite, haematite, jarosite, chlorite, expandable clays (mixed-layer illite-smectites) and feldspars, with the presence or absence of the iron-rich minerals strongly reflecting the weathering grade of the shale.

9.3 X-Ray Fluorescence Analysis of Oker Hill Shale

To understand the distribution of the elements through the landslide it is first necessary to consider their association with other elements and minerals. Tables 9.2a and 9.2b contain major and trace element compositions for shales. It can be seen that shale is composed of over fifty percent SiO_2 which is contained mainly in quartz, clay minerals and feldspars. The clay minerals also account for the high proportion of Al_2O_3 as the silica and alumina cations form the framework of the clay structure. The accessory and diagenetic minerals contribute a variety of elements to the overall geochemistry of shales both in their pure forms and by their ionic substitutions (Table 9.3). An additional component of shales is carbonaceous matter.

Table 9.2a Major Element Composition of Shales

	Nicholls & Loring (1) (1960)	Moore (2) (1978)	Ramsbottom et al. (3) (1981)	Spears & Amin (4) (1981b)
SiO_2*	61.35	60.65	54.88	-
Free silica	-	-	-	18.80
Combined silica	-	-	-	32.80
Al_2O_3	21.52	17.53	25.54	23.90
TiO_2	0.92	1.03	1.68	1.00
Fe_2O_3*	-	7.23	3.38	-
Fe_2O_3	1.15	-	1.94	3.67
FeO	1.92	-	2.92	1.92
MnO	0.02	0.10	0.05	0.08
CaO	0.39	0.59	0.51	0.23
MgO	0.90	1.93	0.75	1.83
Na_2O	0.51	1.47	0.21	0.52
K_2O	3.17	3.28	1.65	2.70
P_2O_5	0.14	0.19	0.11	0.15
H_2O^+	5.03	-	-	-
H_2O^-	1.21	-	-	-
H_2O 105°C	-	-	8.29	-
C	1.17	-	0.83	-
CO_2	0.54	-	0.49	0.39

Table 9.2a (continued)

S	0.51	-	0.08	-
SO_3	-	-	0.10	0.06
Cl	-	-	0.04	-
FeS_2	-	-	0.55	-
Organic Matter	-	-	0.57	2.18
LOI	-	-	10.54	-

Concentrations in percent

SiO_2* = total silica

Fe_2O_3* = totatl iron

(1) Average of 5 samples in Carboniferous shale of North Wales

(2) Purington Shale for geochemical standard

(3) Average of Carboniferous argillaceous rocks

(4) Shale of Mam Tor Beds of Millstone Grit Series, Derbyshire

Table 9.2b Trace Element Composition of Shales

	Curtis (1969) (1)			Krauskopf (1979)	Ramsbottom et
	Marine	Non-Marine	Average	(2)	al. (1981) (3)
Ga	31	32	31	25	26
B	85	63	80	100	85
Cr	118	94	110	100	105
V	275	225	258	130	150
Co	23	20	22	20	10
Ni	71	52	65	80	77
Cu	77	53	69	50	31
Pb	47	33	42	20	-
Mn	927	933	929	850	-
Sr	140	88	123	400	150
Ba	988	406	794	600	190
F	-	-	-	600	480
Hg	-	-	-	0.3	0.2
Li	-	-	-	60	125
Zr	-	-	-	180	85

Concentrations in parts per million

(1) Averages of marine and non-marine + total average of British Carboniferous shales

(2) Average world-wide shale

(3) Averages of Carboniferous argillaceous rocks

Table 9.3 Chemistry of Minerals Commonly Occurring in Shales

(Sources: Deer et al., 1966; Krauskopf, 1979)

Mineral		Associated Elements
Quartz	SiO_2	Si: Al, Li, Na, K, Fe, Mn, Ti
Kaolinite	$Al_4[Si_4O_{10}](OH)_8$	(OH): PO_4 Al: Ga
Illite	$K_{1-1.5}Al_4[Si_{7-6.5}Al_{1-1.5}O_2O](OH)_4$	K: Na, Ba $[Al^{3+}]_6$: $[Mg^+,Fe^{2+}]_6$, Ga
"Smectites"	$(\frac{1}{2}Ca,Na)_{0.7}(Al,Mg,Fe)_4[(Si,Al)_8O_{20}](OH)_4.nH_2O$	K, Cs, Sr, Mg, H, Mn, Ni, Li, Zn, Zr, Ti Al: Ga
Chlorite	$(Mg,Al,Fe)_{12}[(Si,Al)_8O_{20}](OH)_{16}$	Mn, Cr, Ni, Ti Al:Ga

Table 9.3 (continued)

Albite	$NaAlSi_3O_8$	Ca, K, Ti, Fe, Mn, Mg, Ba, Sr
Pyrite	FeS_2	Fe: Ni, Co, Mn, Cu, Pb, As, Zn
Pyrrhotite	Fe_7S_8-FeS	Fe: Ni, Co, Mn, Cu
Siderite	$FeCO_3$	Fe: Mn, Mg, Ca
Haematite	Fe_2O_3	Mn, Si, Al, Ti
Goethite	FeO.OH	Si, Mn
Jarosite	$KFe_3(SO_4)_2(OH)_6$	
Rutile	TiO_2	Ti: Nb, Ta, Fe

Table 9.3 (continued)

Anatase	TiO_2	Ti: Fe, Sn
Zircon	$ZrSiO_4$	Fe, Sn, Nb, Ta
Calcite	$CaCO_3$	Ca: Mg, Mn, Fe, Sr, Ba, Co, Zn
Dolomite	$CaMg(CO_3)_2$	Mg: Fe, Mn, Zn, Pb
Ankerite	$Ca(Mg,Fe^{2+},Mn)(CO_3)_2$	-
Apatite	$Ca_5(PO_4)_3(OH,F,Cl)$	Ca: Mn, Sr, rare earths (predominantly Ce)
Gypsum	$CaSO_4.2H_2O$	-

Trace elements tend to be enriched in fine-grained sediments by ionic substitutions and adsorption in clays, and by association with organic matter which is more abundant in fine-grained sediments. The clays have high ionic potentials and are capable of adsorption of ions which is believed to be the chief process of enrichment (Krauskopf, 1979) and, therefore, many elements may be associated with these minerals (Table 9.3). The chemical composition of kaolinite is subject to very little variation as it has a low cation exchange capacity compared to the other clays, but it has a higher anion exchange capacity attributable to the presence of replaceable hydroxide ions thus allowing the fixation of phosphate ions (Deer et al., 1966). In addition to the substitutions given in Table 9.3, other elements associated with clay minerals include As, Ba, Cu, Mo, Nb, Rb, Th, U, and V.

Several of the trace elements are collected and enriched by organic matter (organophiles) (Table 9.4). These elements may form specific minerals associated with the organic matter but, more commonly, they are present within the organic matter itself (Krauskopf, 1979). Another group of trace elements exists which are the immobile elements which may be used to indicate the provenance of sediments.

Organophiles	Immobiles
As	Ce
Co	La
Cr	Nb
Cu	Y
Mo	Zr
Ni	
U	
V	

Table 9.4 Organophile and Immobile Elements of Shale

The major and trace elements of the shale from the boreholes of Oker Hill landslide were analysed by X-ray fluorescence (Harvey and Atkin, 1982). X-ray fluorescence spectrometry involves recording the emission of fluorescent X-rays produced by bombarding an atom with X-ray beams; each element emits fluorescent X-rays of characteristic energy and wavelength (Whalley, 1981). Appendix 4 contains the preparation methods of beads and pellets of the samples which were analysed to determine the percentages of the major elements in the form of oxides and the concentrations of the trace elements in parts per million respectively.

Figure 9.3

Distribution of Elements Through

Oker Hill Landslide: Borehole 1

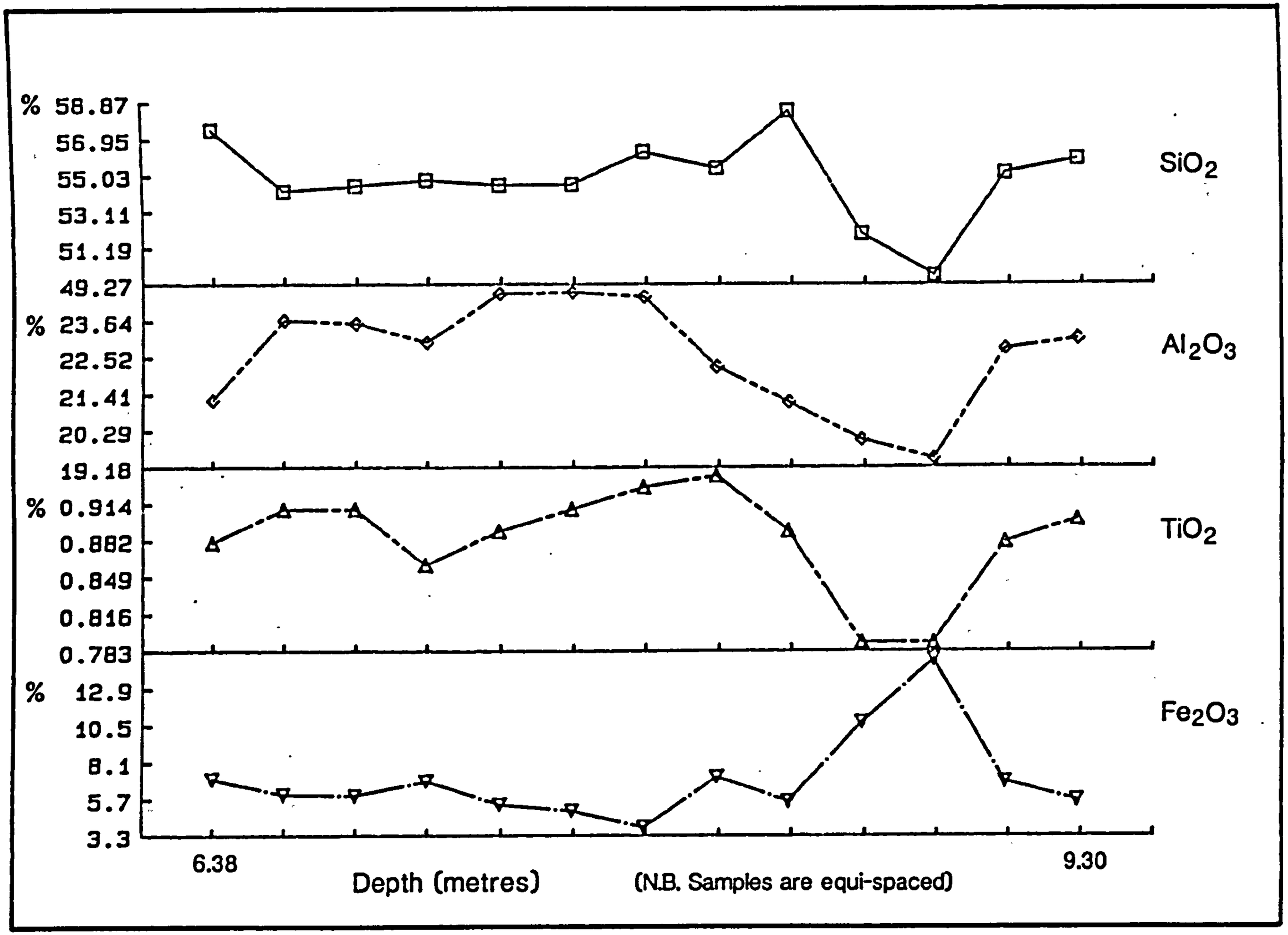
% 58.87
56.95
55.03
53.11
51.19
49.27
SiO2
% 23.64
22.52
21.41
20.29
19.18
Al2O3
% 0.914
0.882
0.849
0.816
0.783
TiO2
% 12.9
10.5
8.1
5.7
3.3
Fe2O3
6.38
9.30
Depth (metres)
(N.B. Samples are equi-spaced)

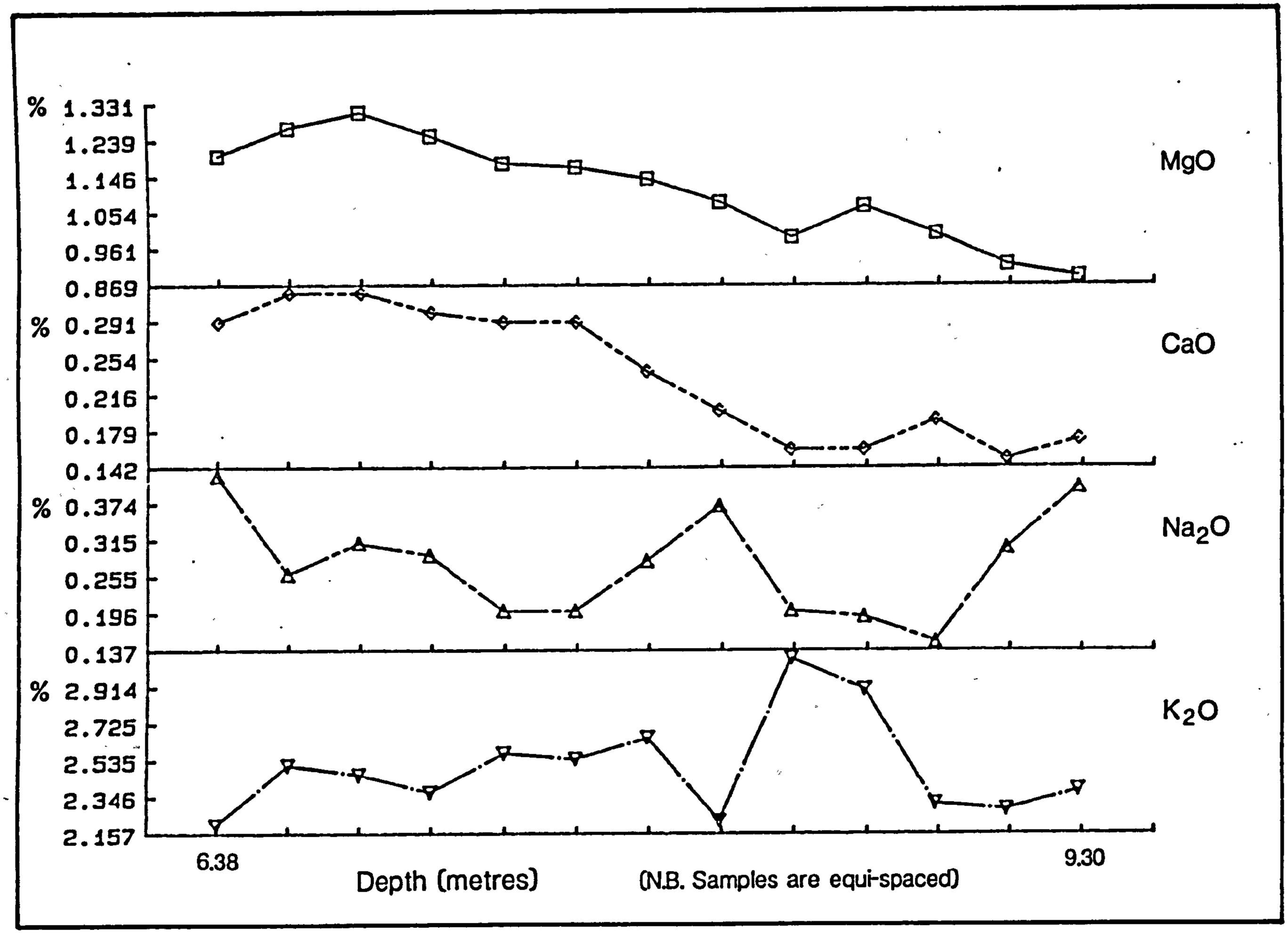
% 1.331
1.239
1.146
1.054
0.961
0.869
MgO
% 0.291
0.254
0.216
0.179
0.142
CaO
% 0.374
0.315
0.255
0.196
0.137
Na2O
% 2.914
2.725
2.535
2.346
2.157
K2O
6.38
9.30
Depth (metres)
(N.B. Samples are equi-spaced)

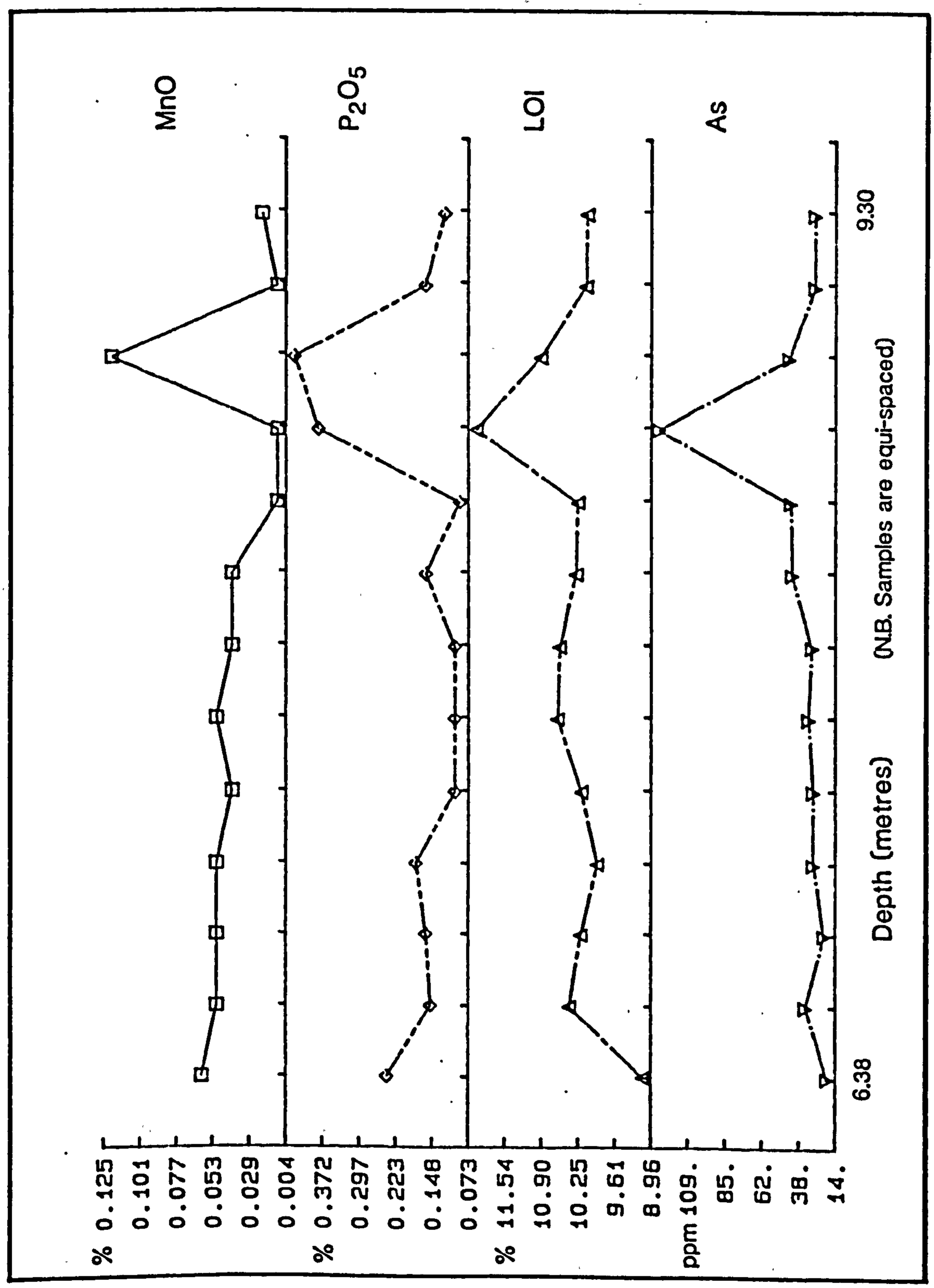
MnO
P_2O_5
LOI
As
% 0.125
0.101
0.077
0.053
0.029
0.004
% 0.372
0.297
0.223
0.148
0.073
% 11.54
10.90
10.25
9.61
8.96
ppm 109.
85.
62.
38.
14.
6.38
Depth (metres)
9.30
(N.B. Samples are equi-spaced)

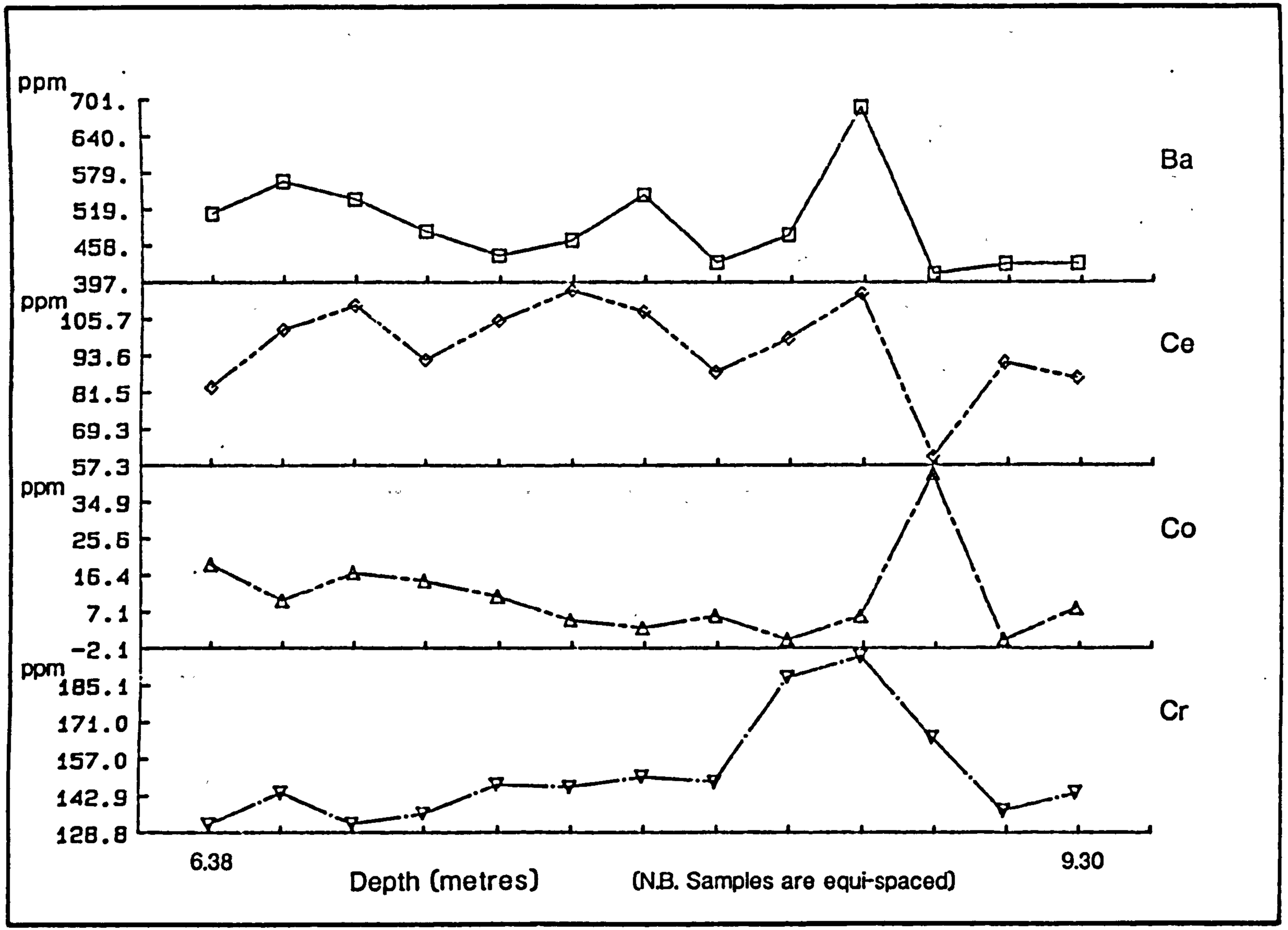
ppm
701.
640.
579.
519.
458.
397.
Ba
ppm
105.7
93.6
81.5
69.3
57.3
Ce
ppm
34.9
25.6
16.4
7.1
-2.1
Co
ppm
185.1
171.0
157.0
142.9
128.8
Cr
6.38
9.30
Depth (metres)
(N.B. Samples are equi-spaced)

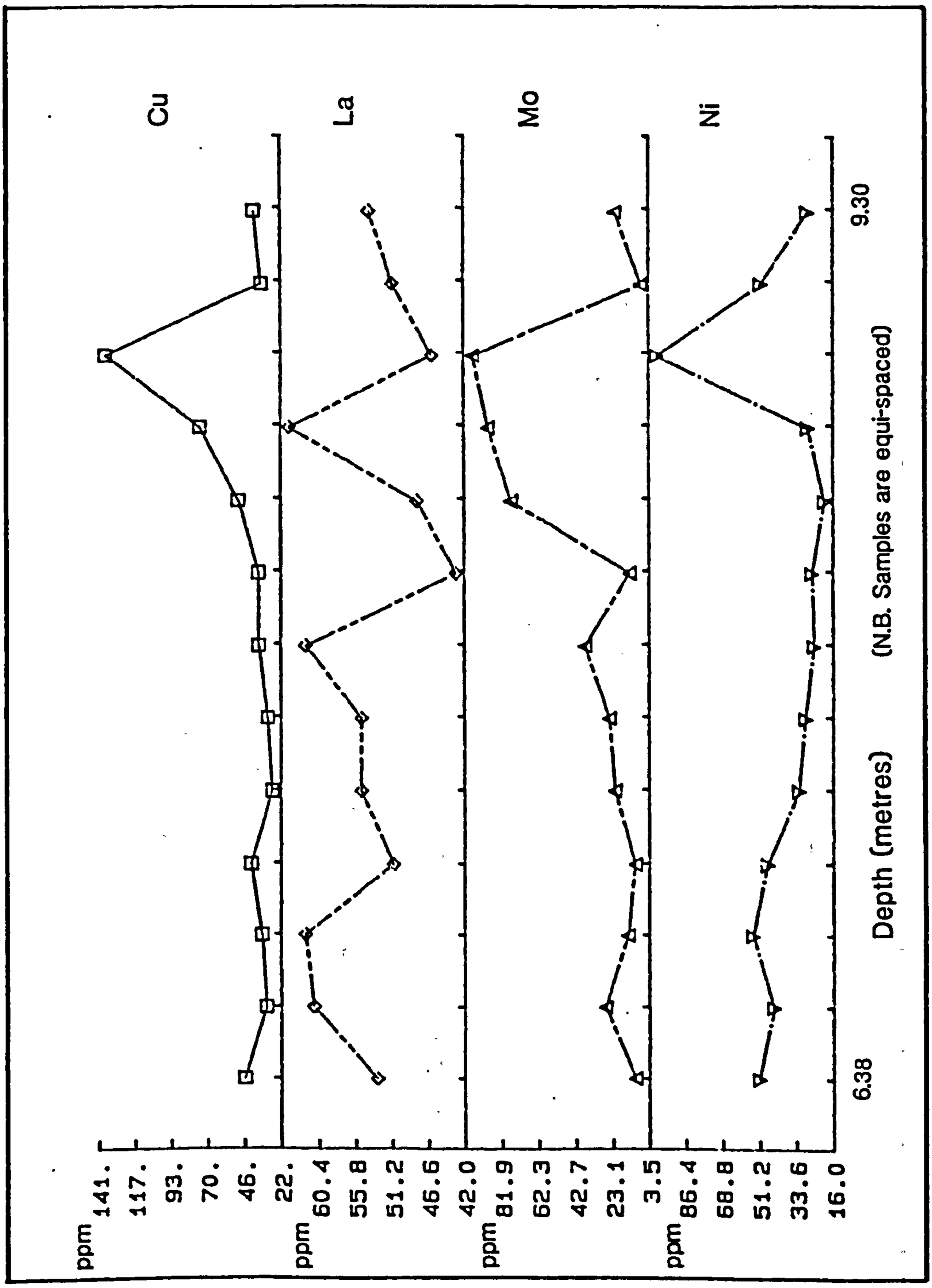
Cu
La
Mo
Ni
9.30
(N.B. Samples are equi-spaced)
Depth (metres)
6.38
ppm 141. 117. 93. 70. 46. 22.
ppm 60.4 55.8 51.2 46.6 42.0
ppm 81.9 62.3 42.7 23.1 3.5
ppm 86.4 68.8 51.2 33.6 16.0

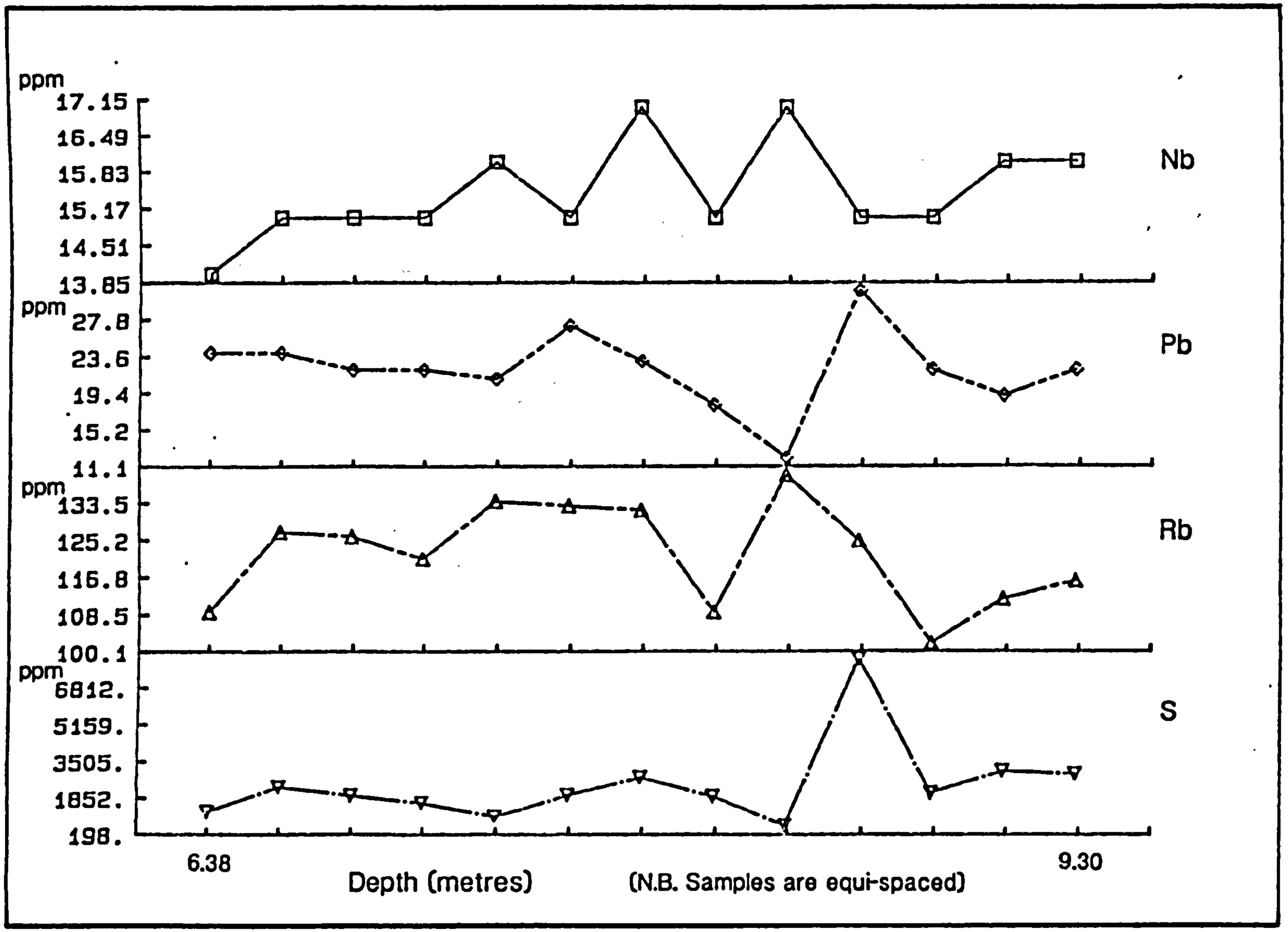
ppm
17.15
16.49
15.83
15.17
14.51
13.85
Nb
ppm
27.8
23.6
19.4
15.2
11.1
Pb
ppm
133.5
125.2
116.8
108.5
100.1
Rb
ppm
6812.
5159.
3505.
1852.
198.
S
6.38
9.30
Depth (metres)
(N.B. Samples are equi-spaced)

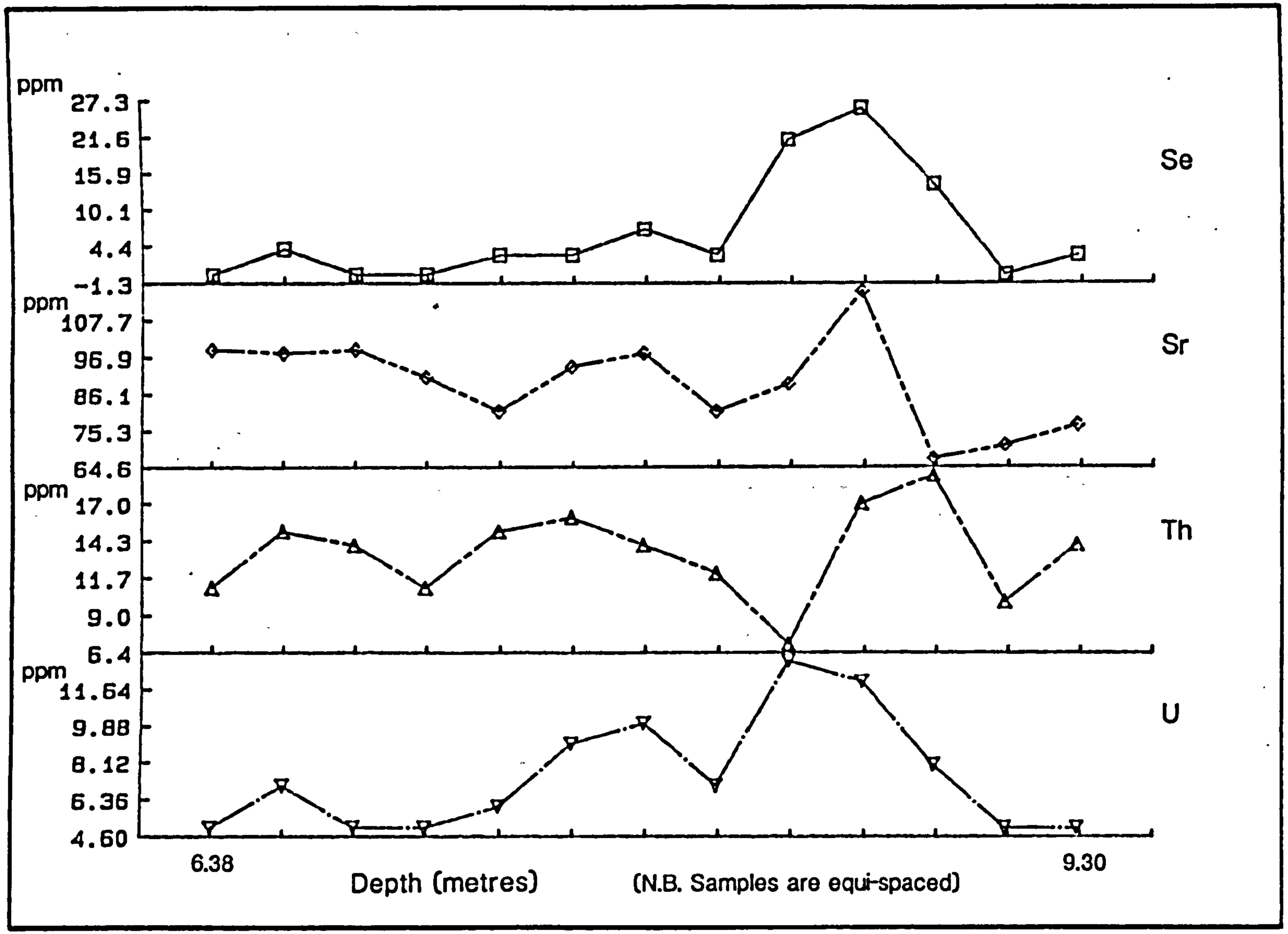
ppm
27.3
21.6
15.9
10.1
4.4
-1.3
Se
ppm
107.7
96.9
86.1
75.3
64.6
Sr
ppm
17.0
14.3
11.7
9.0
6.4
Th
ppm
11.64
9.88
8.12
6.36
4.60
U
6.38
9.30
Depth (metres)
(N.B. Samples are equi-spaced)

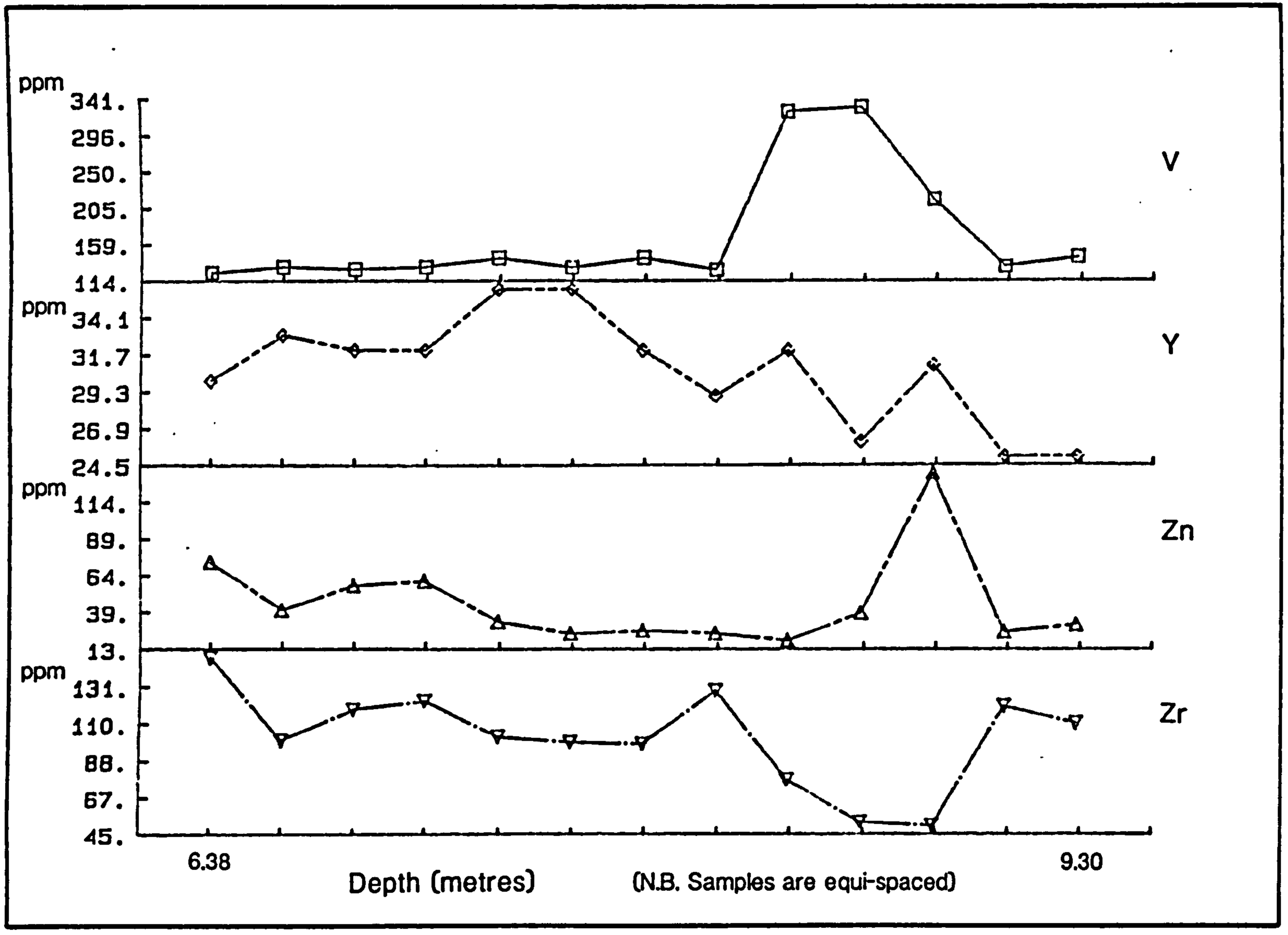
ppm
341.
296.
250.
205.
159.
114.
V
ppm
34.1
31.7
29.3
26.9
24.5
Y
ppm
114.
89.
64.
39.
13.
Zn
ppm
131.
110.
88.
67.
45.
Zr
6.38
9.30
Depth (metres)
(N.B. Samples are equi-spaced)

Figure 9.4

Distribution of Elements Through

Oker Hill Landslide: Borehole 2

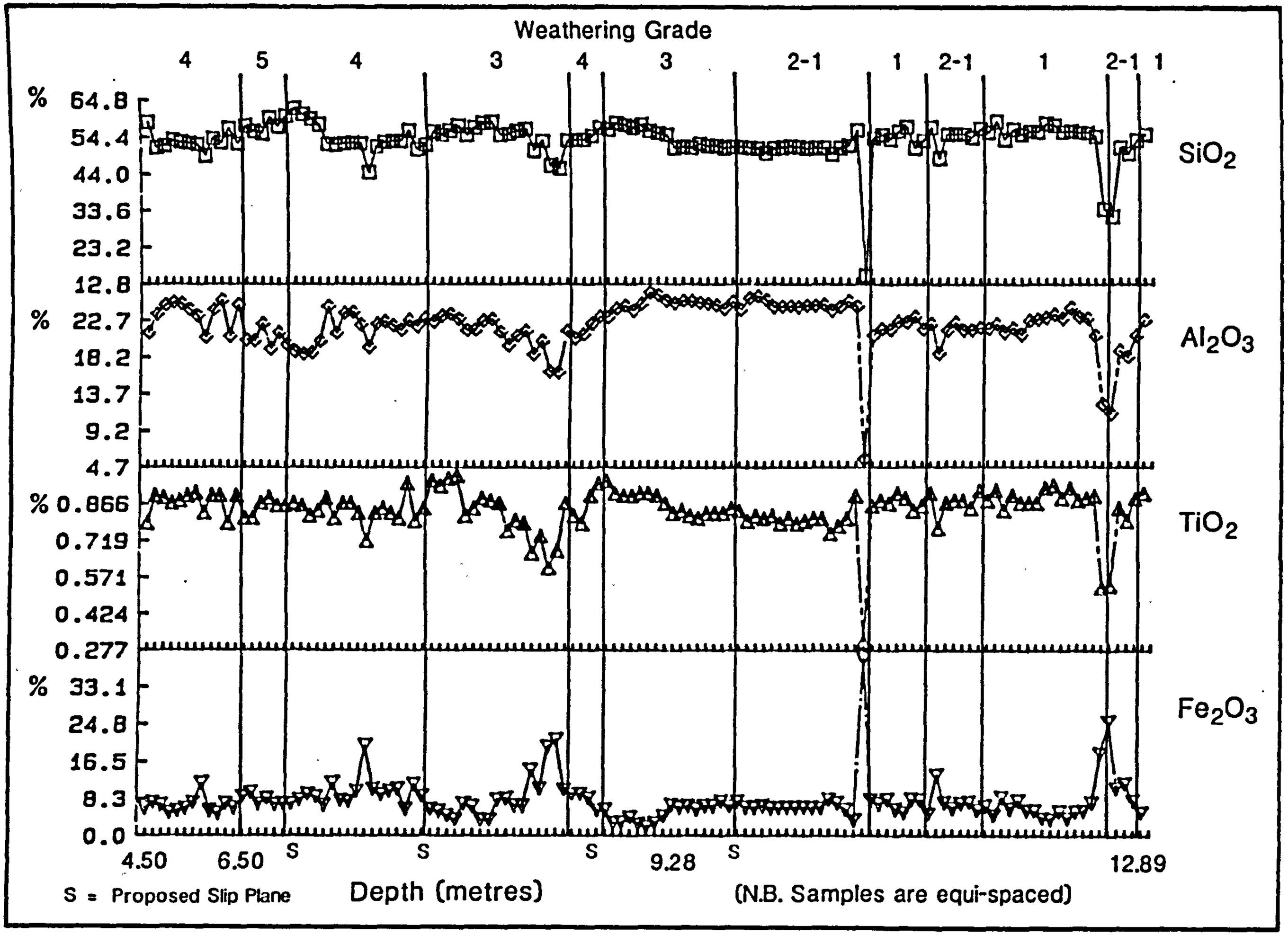
Weathering Grade
4
5
4
3
4
3
2-1
1
2-1
1
2-1
1
%
64.8
54.4
44.0
33.6
23.2
12.8
SiO2
%
22.7
18.2
13.7
9.2
4.7
Al2O3
%
0.866
0.719
0.571
0.424
0.277
TiO2
%
33.1
24.8
16.5
8.3
0.0
Fe2O3
4.50
6.50
S
S
S
9.28
S
12.89
S = Proposed Slip Plane
Depth (metres)
(N.B. Samples are equi-spaced)

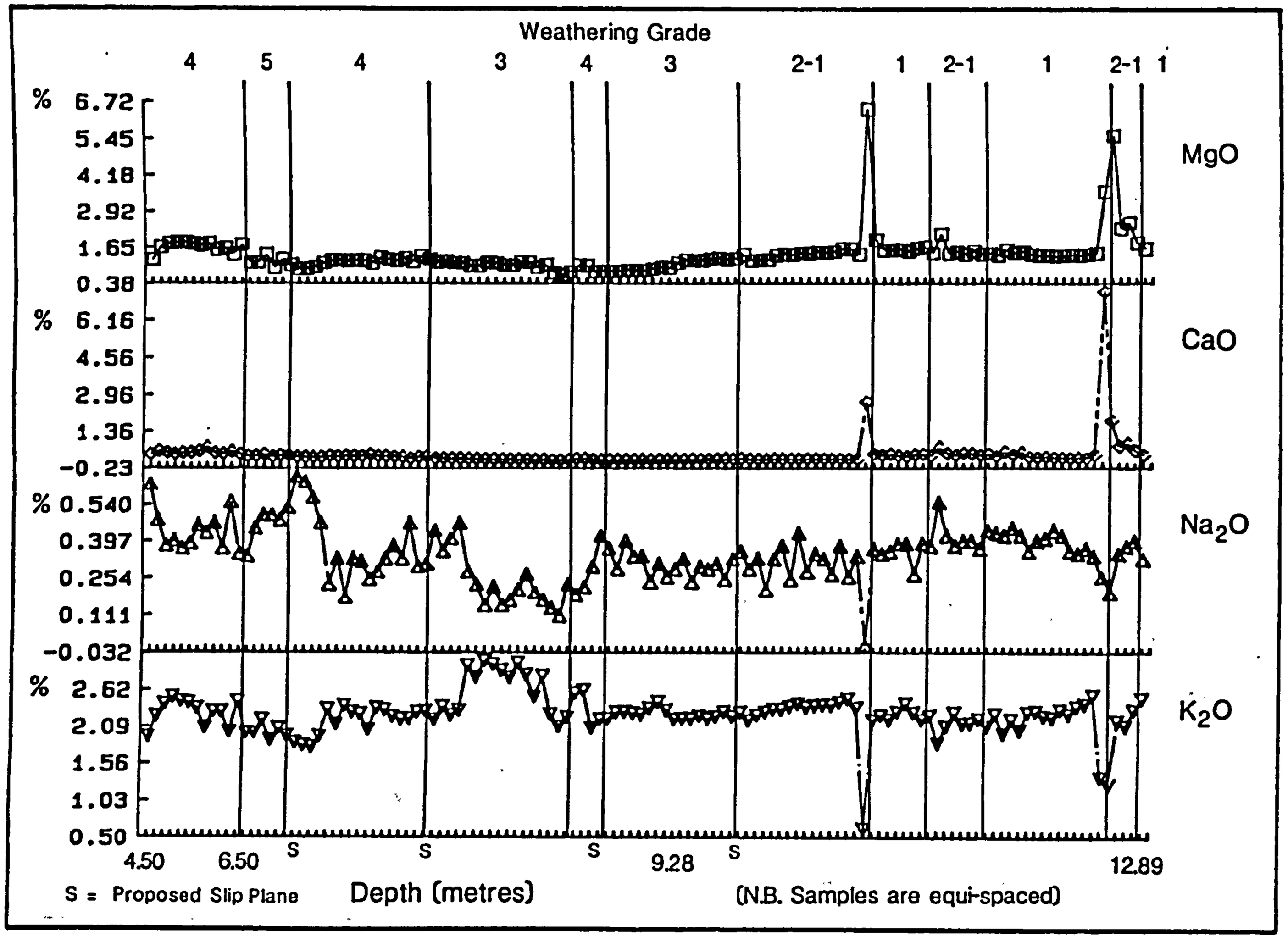
Weathering Grade
4 5 4 3 4 3 2-1 1 2-1 1 2-1 1
% 6.72
5.45
4.18
2.92
1.65
0.38
MgO
% 6.16
4.56
2.96
1.36
-0.23
CaO
% 0.540
0.397
0.254
0.111
-0.032
Na2O
% 2.62
2.09
1.56
1.03
0.50
K2O
4.50
6.50
S
S
S
9.28
S
12.89
S = Proposed Slip Plane
Depth (metres)
(N.B. Samples are equi-spaced)

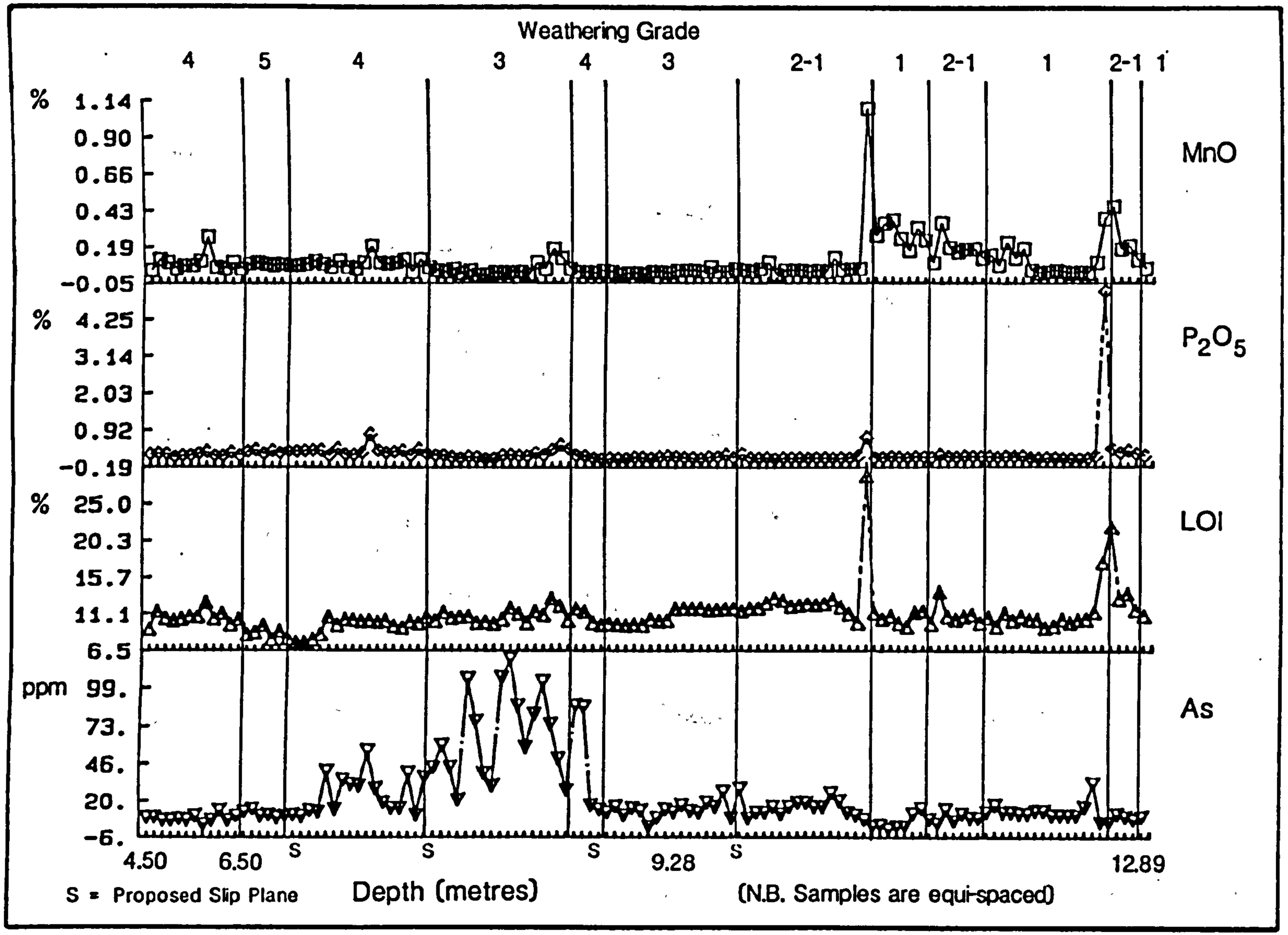
Weathering Grade
4
5
4
3
4
3
2-1
1
2-1
1
2-1
1
% 1.14
0.90
0.66
0.43
0.19
-0.05
MnO
% 4.25
3.14
2.03
0.92
-0.19
P_2O_5
% 25.0
20.3
15.7
11.1
6.5
LOI
ppm 99.
73.
46.
20.
-6.
As
4.50
6.50
S
S
S
9.28
S
12.89
S = Proposed Slip Plane
Depth (metres)
(N.B. Samples are equi-spaced)

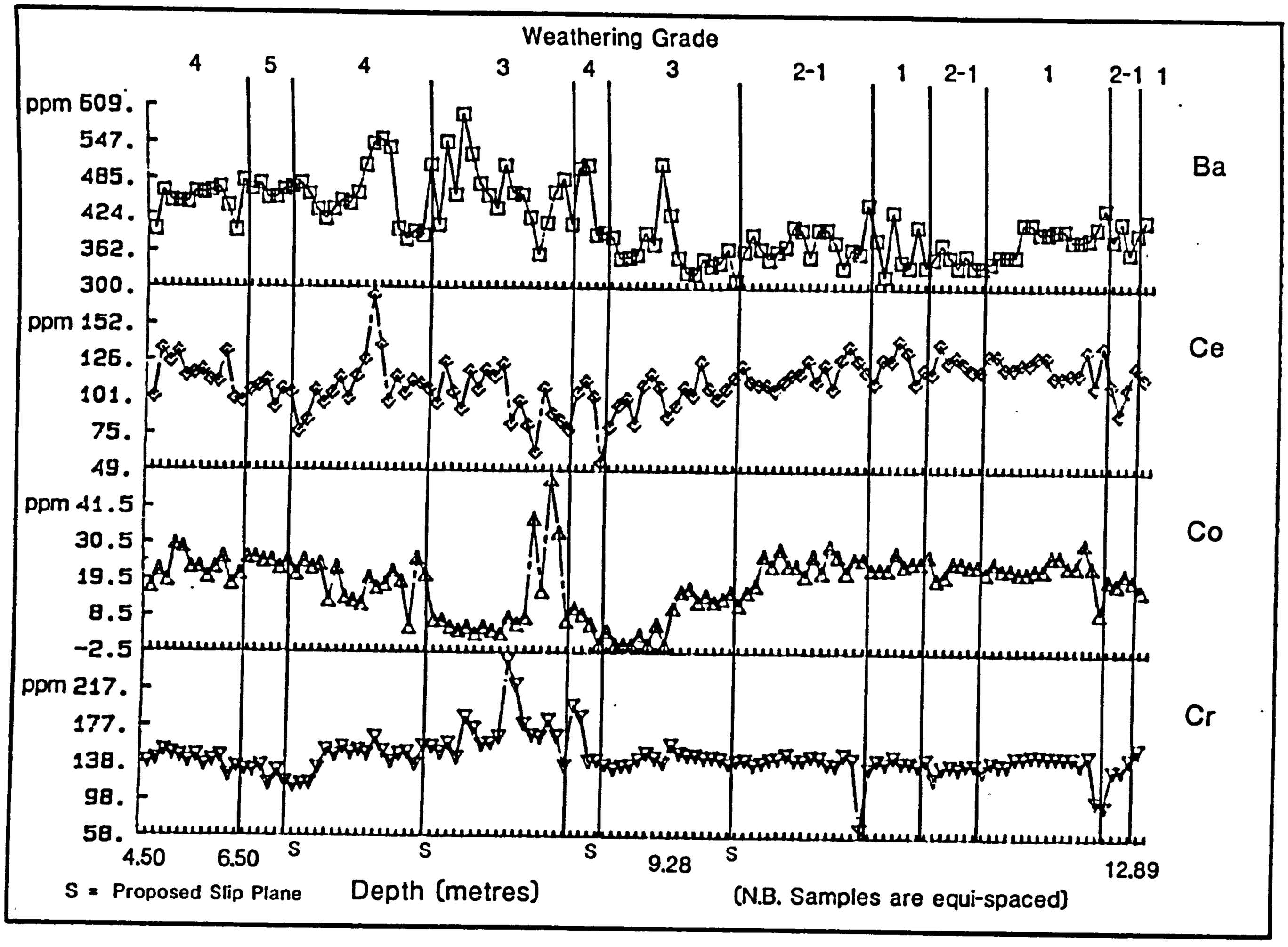
Weathering Grade
4
5
4
3
4
3
2-1
1
2-1
1
2-1
1
ppm 609.
547.
485.
424.
362.
300.
Ba
ppm 152.
126.
101.
75.
49.
Ce
ppm 41.5
30.5
19.5
8.5
-2.5
Co
ppm 217.
177.
138.
98.
58.
Cr
4.50
6.50
S
S
S
9.28
S
12.89
S = Proposed Slip Plane
Depth (metres)
(N.B. Samples are equi-spaced)

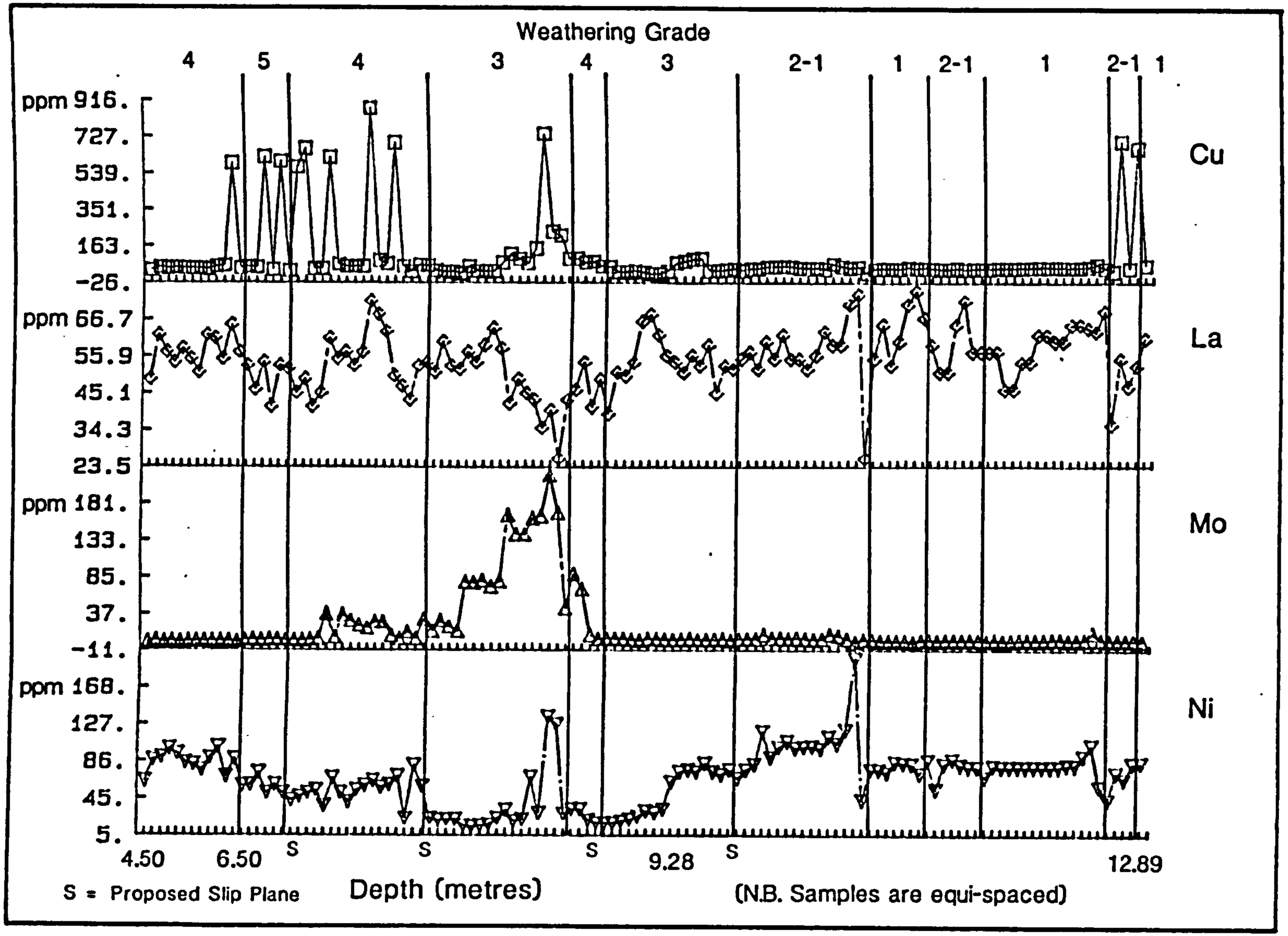
Weathering Grade
4
5
4
3
4
3
2-1
1
2-1
1
2-1
1
ppm 916.
727.
539.
351.
163.
-26.
Cu
ppm 66.7
55.9
45.1
34.3
23.5
La
ppm 181.
133.
85.
37.
-11.
Mo
ppm 168.
127.
86.
45.
5.
Ni
4.50
6.50
S
S
S
9.28
S
12.89
S = Proposed Slip Plane
Depth (metres)
(N.B. Samples are equi-spaced)

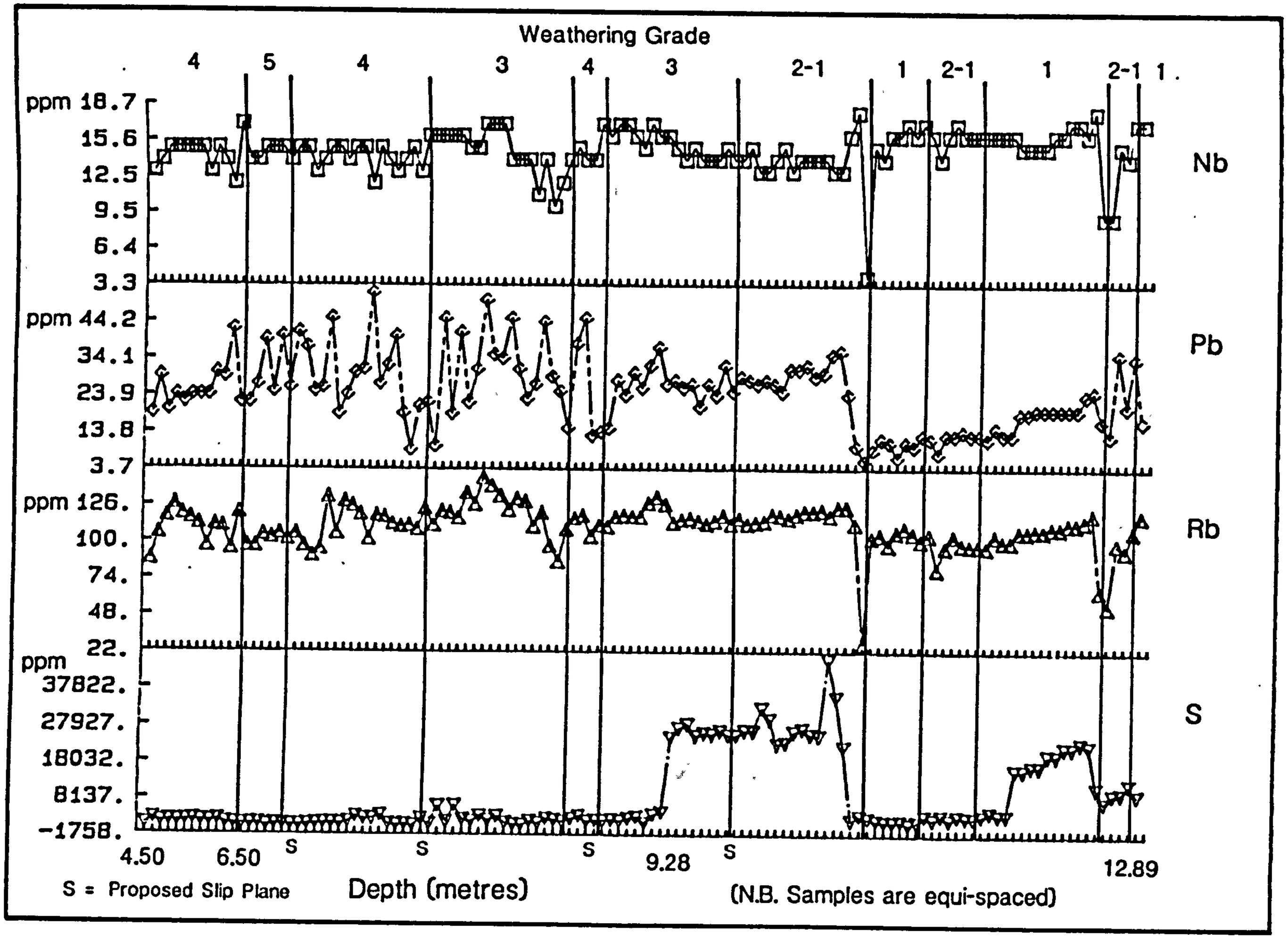
Weathering Grade
4
5
4
3
4
3
2-1
1
2-1
1
2-1
1
ppm 18.7
15.6
12.5
9.5
6.4
3.3
Nb
ppm 44.2
34.1
23.9
13.8
3.7
Pb
ppm 126.
100.
74.
48.
22.
Rb
ppm
37822.
27927.
18032.
8137.
-1758.
S
4.50
6.50
S
S
S
9.28
S
12.89
S = Proposed Slip Plane
Depth (metres)
(N.B. Samples are equi-spaced)

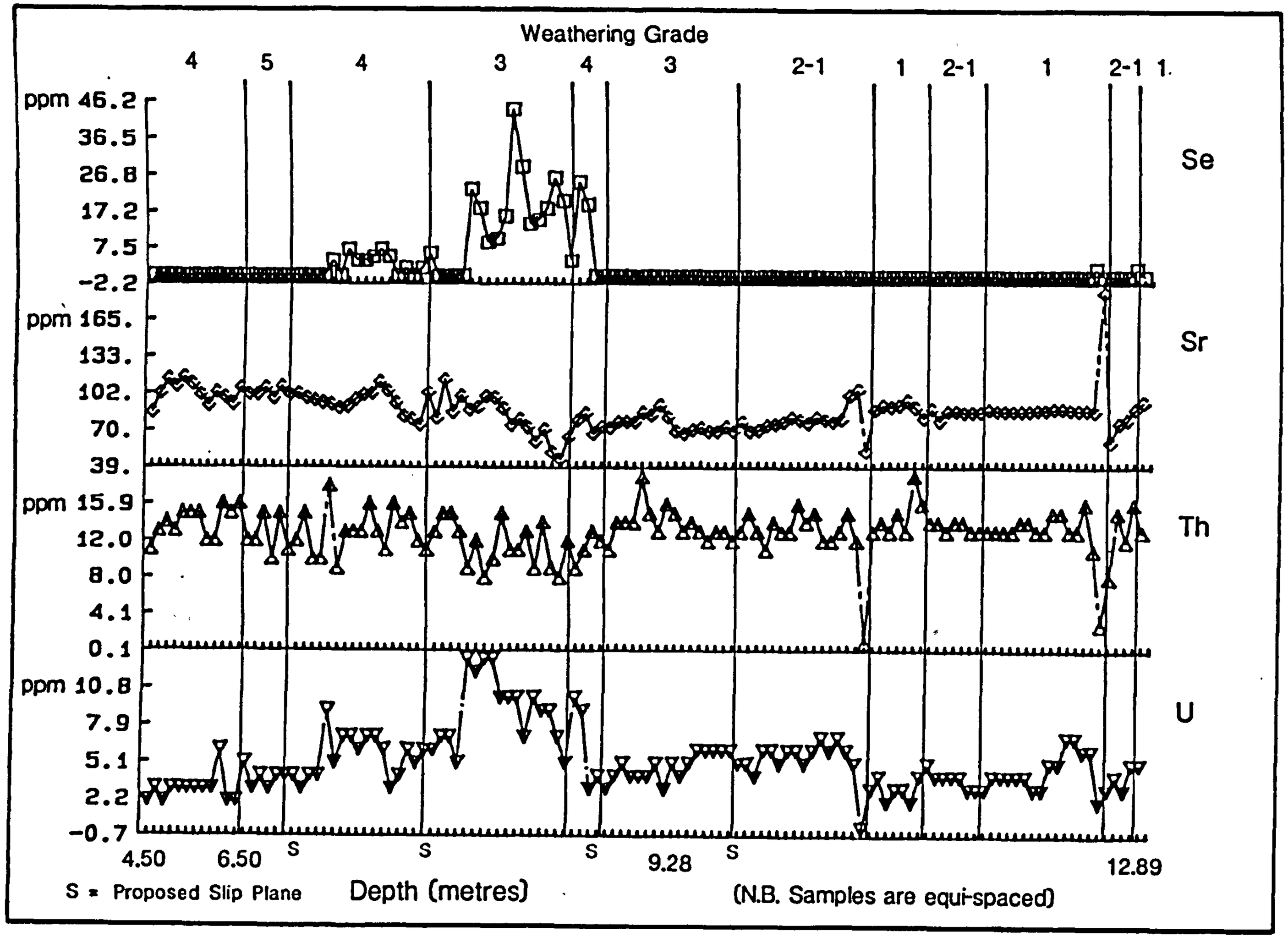
Weathering Grade
4
5
4
3
4
3
2-1
1
2-1
1
2-1
1
ppm 46.2
36.5
26.8
17.2
7.5
-2.2
Se
ppm 165.
133.
102.
70.
39.
Sr
ppm 15.9
12.0
8.0
4.1
0.1
Th
ppm 10.8
7.9
5.1
2.2
-0.7
U
4.50
6.50
S
S
S
9.28
S
12.89
S = Proposed Slip Plane
Depth (metres)
(N.B. Samples are equi-spaced)

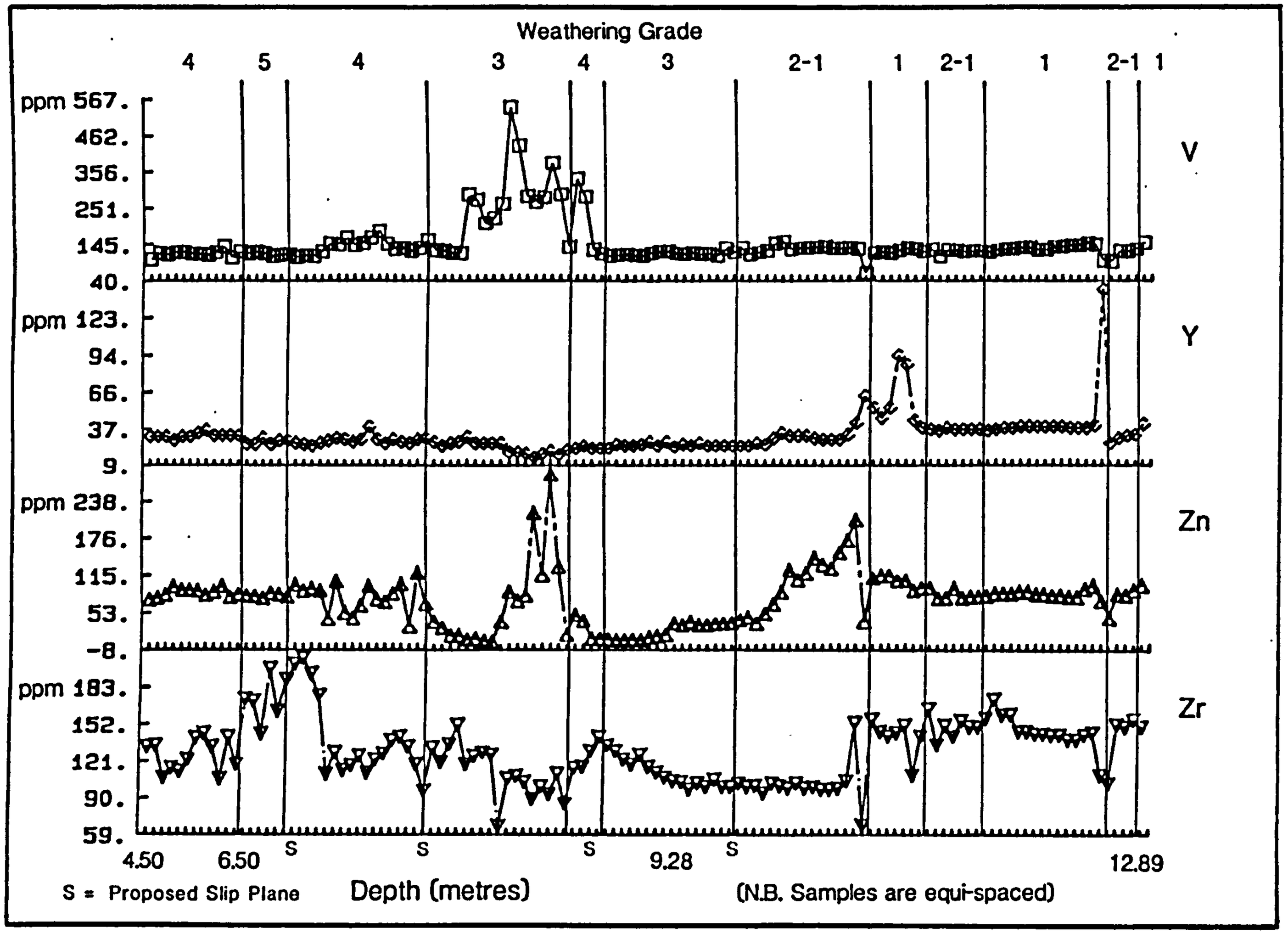
Weathering Grade
4
5
4
3
4
3
2-1
1
2-1
1
2-1
1
ppm 567.
462.
356.
251.
145.
40.
V
ppm 123.
94.
66.
37.
9.
Y
ppm 238.
176.
115.
53.
-8.
Zn
ppm 183.
152.
121.
90.
59.
Zr
4.50
6.50
S
S
S
9.28
S
12.89
S = Proposed Slip Plane
Depth (metres)
(N.B. Samples are equi-spaced)

TABLE 9.5a THE AVERAGE MAJOR ELEMENT COMPOSITION OF OKER HILL SHALE

Element	Minimum	Maximum	Mean
	%	%	%
SiO_2	44.61	62.48	54.00
Al_2O_3	16.29	26.14	22.63
TiO_2	0.61	0.98	0.85
Fe_2O_3	1.92	21.26	7.42
MgO	0.67	2.10	1.25
CaO	0.13	0.67	0.25
Na_2O	0.11	0.65	0.34
K_2O	1.79	3.03	2.30
MnO	0.00	0.36	0.07
P_2O_5	0.06	0.79	0.17
LOI	7.56	13.92	10.70

TABLE 9.5b THE AVERAGE TRACE ELEMENT COMPOSITION OF OKER HILL SHALE

Element	Minimum	Maximum	Mean
	ppm	ppm	ppm
As	0	119	25
Ba	314	595	419
Ce	55	172	110
Co	0	50	17
Cr	112	248	147
Cu	17	873	112
La	26	75	55
Mo	0	218	23
Ni	14	199	64
Nb	10	18	15
Pb	7	52	26
Rb	81	146	114
S	491	45468	7637
Se	0	44	3
Sr	46	115	87
Th	8	19	13
U	2	13	5
V	103	543	154
Y	15	94	30
Zn	6	285	74
Zr	66	207	124

9.3.1 Major Element Geochemistry

The distributions of the major elements have been plotted against depth for both Boreholes 1 and 2, and are shown in Figures 9.3 and 9.4 respectively. Both boreholes show the same general trends and concentrations of elements. The minimum, maximum and mean of major elements from Borehole 2 are given in Table 9.5a.

(i) SiO_2

Of the minerals listed in Table 9.3 as commonly occurring in shales SiO_2 is dominantly found in quartz and clay minerals, and it also occurs in feldspars and accessory minerals (i.e. zircon). However, in considering the distribution of SiO_2 in the core material from Oker Hill the contributions from the latter sources are likely to be negligible in comparison to the quartz and combined silica in the clays. The quartz content of the average shale is between twenty and thirty percent (Table 9.3), therefore, of the average value of approximately fifty-four percent SiO_2 for the Oker Hill shale between twenty-four and thirty-four percent may be attributable to clays.

(ii) Al_2O_3

The clay minerals are the main source of Al_2O_3 and the high proportion of this oxide in these samples reflects the domination of clays in fine-grained sediments. XRD analysis also revealed small amounts of the plagioclase feldspar albite in some samples, however, the contribution to the total value of Al_2O_3 is minor in comparison to the clays.

(iii) TiO_2

TiO_2 may occur in the form of either rutile or anatase, both of which are accessory minerals and have not been identified in the XRD analysis. However, this does not rule out the presence of a mineral as small amounts (less than approximately five percent) are not picked up by XRD techniques. In shale from the British Carboniferous Coal Measures Collins (1976) noted that TiO_2 is dominantly found in the clays with small quantities also occurring as anatase. In the Tansley borehole Amin (1979) found that TiO_2 was relatively concentrated in the non-marine shales along with P_2O_5 and siderite.

(iv) Fe_2O_3

Fe_2O_3 is contained mainly in pyrite, siderite, haematite and possibly chlorite. It is interesting to note that the weathered shale shows no indication of a loss of Fe_2O_3 although there is a decrease in concentration around 9.15 metres. This trough is immediately above the shale which contains the first appearance of pyrite in the weathering profile. In the detailed log of the core material (Appendix 3), the shale in this area was noted to be less iron-stained and harder than the shale above with the laminations becoming thicker; this band of shale did not exhibit the characteristics of a slip plane. The iron oxides in the weathered shale have most likely been derived from either pyrite or siderite; by considering the other minerals and elements associated with marine and non-marine shales it may be possible to assign this weathered shale to either of the two environments of deposition.

(v) MgO

The commonly occurring minerals in shale containing Mg are dolomite and ankerite. Neither of these minerals were recorded on the XRD traces, however, as already mentioned above, the technique is not sensitive to trace amounts and, therefore, the presence of dolomite and ankerite cannot be ruled out. Smectite and chlorite account for some MgO although by a comparison of their distributions down the borehole it is apparent that the major features of the MgO distribution - the peaks at 10.70 and 12.70 metres - are not related to these clays. In fact, MgO follows the trend of Fe_2O_3 from 10.70 metres downward which suggests that Mg is substituting for Fe in the mineral siderite.

(vi) CaO

Apart from peaks at 10.70 and 12.70 metres only background levels of CaO are present within the Oker Hill shale. These peaks are not associated with the calcium-bearing minerals calcite, dolomite, ankerite or gypsum as they were not identified on the corresponding XRD traces. These minerals may, however, be present in trace amounts and would, therefore, provide the low background values for CaO. The siderite concretionary band at 10.70 metres appears to show some substitution of Fe by Ca. The peak in CaO concentration at 12.70 metres, however, cannot be explained in the same manner as although siderite is present in this shale it is less abundant than in the concretionary band. Consequently, another mineral must account for

this increase in CaO. As this peak appears to be associated with an increase in P_2O_5 (Figure 9.4), CaO may be attributable to the presence of apatite.

(vii) Na_2O

From Table 9.3 it can be seen that the main mineral containing Na_2O is smectite, although Na may also substitute for K in illites and for SiO_2 in quartz. Therefore, in general Na_2O can be attributed to the clays. Nicholls and Loring (1960) suggest that variations in the ratio of Na^+/K^+ are due to variations of this ratio in illite. Pearson (1979) also notes this association with the micas.

(viii) K_2O

The dominant source of K_2O in these shales is illite with mixed-layer illite-smectites also contributing to the total concentration. It can be seen that Al_2O_3 and K_2O follow similar trends in distribution down the borehole, although K_2O peaks between 7.7 and 8.3 metres whereas Al_2O_3 decreases slightly. This may indicate that illite is the most dominant clay mineral at this depth. From the calculation of the quantity of each clay mineral as a percentage of total clay content (Figure 9.2) the increase in illite between 7.7 and 8.3 metres is confirmed. The ratio of K_2O/Al_2O_3 also provides an indication of clay mineralogy, the higher the ratio the greater the proportion of illite to kaolinite. Figure 9.5 shows the variation of this ratio down the borehole; it can be seen that illite is dominant between 7.7 and 8.8 metres. According to Amin (1979) the marine shale in the Tansley borehole has a higher illite content than the

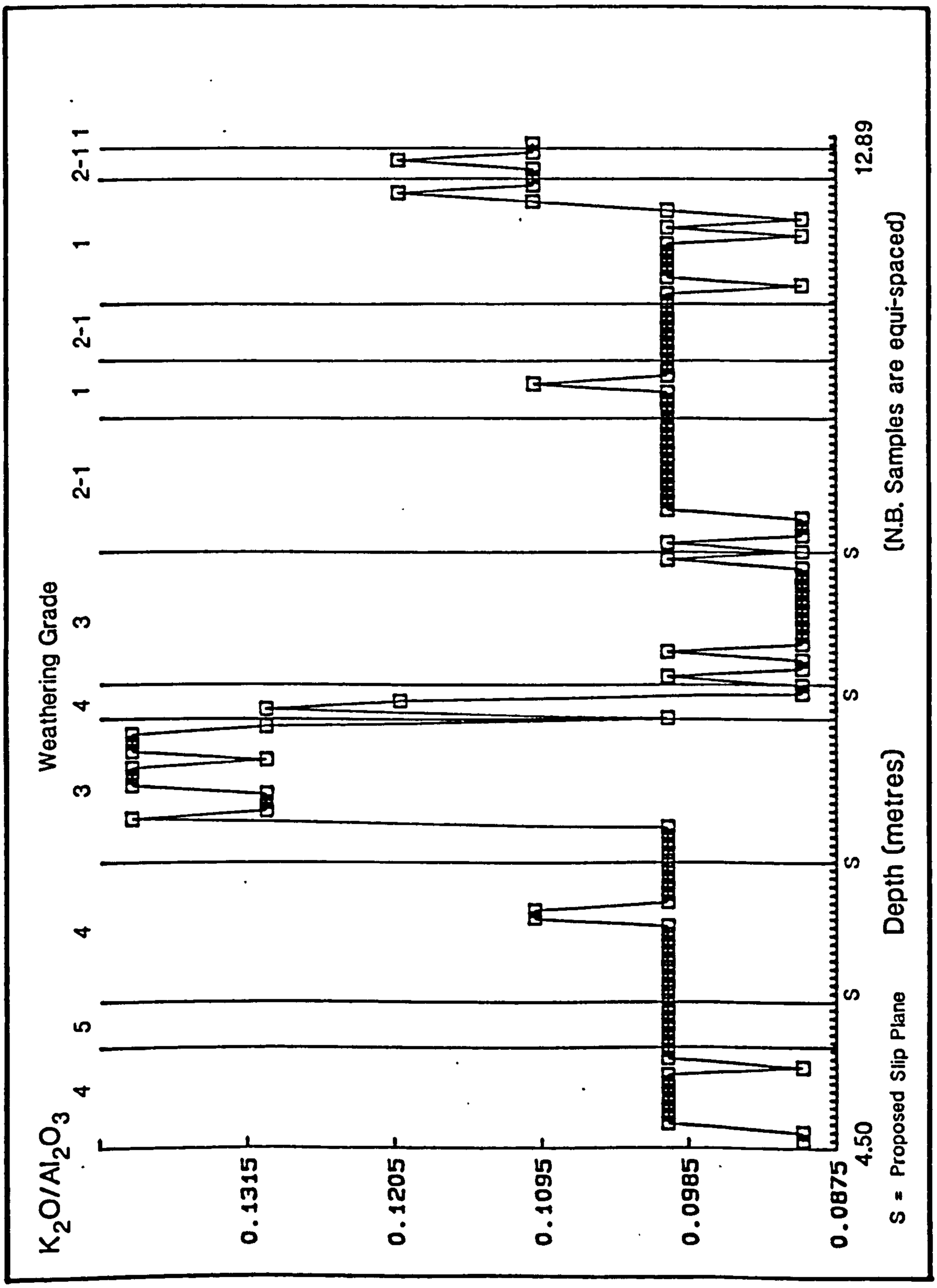

Figure 9.5 Variation of K_2O/Al_2O_3 Through Oker Hill Landslide: Borehole 2

non-marine shale which is reflected in a higher K_2O/Al_2O_3 ratio.

(ix) MnO

From the similarity in distributions down the borehole MnO would appear to occur in association with Fe_2O_3. From Table 9.3 it can be seen that Mn can substitute for Fe in pyrite, pyrrhotite and siderite and in the iron-bearing clays.

(x) P_2O_5

The dominant feature in the distribution of P_2O_5 is the peak at 12.7 metres. This has already been explained in conjunction with CaO as indicating the presence of apatite. P_2O_5 is also slightly enriched in the concretionary band of siderite at 10.70 metres, and small peaks also occur at approximately 6.5 and 8 metres. The significance of the small peaks is uncertain.

(xi) Loss On Ignition

The loss on ignition component (LOI) is made up of organic matter, water held in clays, CO_2 from carbonate minerals and the change in the oxidation state of iron. In general the shale at Oker Hill has a LOI value of around eleven percent which is likely to be derived from the organic matter and clays. The deviations from this percentage occur in shale which is known to contain siderite, i.e. at 10.70 and 12.70 metres depth, and apatite may also be present in the latter sample. Both siderite and apatite will contribute to the LOI component as siderite is a carbonate and apatite contains (OH, F, Cl) which will be transformed to the gaseous phase on heating to 1,000°C.

The most striking features of these plots of the major elements against depth (Figure 9.4) are the sharp increases in Fe_2O_3, MgO, CaO, MnO and LOI, and the corresponding decreases in SiO_2, Al_2O_3, TiO_2, Na_2O and K_2O at 10.70 metres. A similar feature is also found at around 12.70 metres. The first peak/trough is related to the concretionary band of siderite. Siderite is an iron carbonate and therefore, on analysis by XRF, the iron is represented as Fe_2O_3 and the carbonate forms part of the LOI value. The remaining peaks correspond to the ionic substitutions for Fe by Mn, Mg and Ca into the siderite lattice (Table 9.3). The second peak/trough differs from the first with respect to the peaks of CaO and P_2O_5 which show increases in abundance as opposed to the decreases shown by Fe_2O_3, MnO, LOI and, to a lesser extent, MgO. This may indicate that apatite, a calcium phosphate, is enriched at 12.70 metres. In an attempt to confirm the presence of apatite this sample was analysed by XRD, but unfortunately, the main peaks for this mineral coincide with those of siderite, quartz and kaolinite. Consequently, apatite cannot be positively identified but the XRF data points strongly to its presence. Further support for its identification as apatite is the peak in Sr (Figure 9.4) which is known to substitute for Ca.

The weathering grades have been drawn onto the graphs of the distribution of the major elements down Borehole 2 (Figure 9.4). Weathering grade appears to have very little effect; at most, the shale in Groups III, IV and V may show a slightly greater fluctuation in concentrations of SiO_2, Al_2O_3, TiO_2, Fe_2O_3, Na_2O and K_2O.

9.3.2 Trace Element Geochemistry

The variations in concentrations of the trace elements, in parts per million, down the cores taken through Oker Hill landslide are shown in Figures 9.3 and 9.4. The minimum, maximum and mean of the trace elements for Borehole 2 are given in Table 9.5b.

(i) As

The enrichment of As around eight metres depth indicates either a zone of high illite or organic matter content. As may also substitute for Fe in pyrite.

(ii) Ba

Ba also appears to be enriched in the shale between about 7.5 and 8.5 metres although this trend is not as distinct as that of As. In the shale from the Tansley borehole Amin (1979) found that Ba was mainly related to illite and feldspar. If this is also the case for the Oker Hill shale this may explain the relationship between the distributions of Ba and As: the similarity arising from their common association with illite, and the difference resulting from As being an organophile and Ba occurring in albite. Table 9.3 shows that Ba may also substitute for Ca in calcite, but as calcite was not detected by XRD the influence of this mineral on the distribution of Ba cannot be ascertained.

(iii) Ce

Ce is an immobile element and as such its distribution is unaffected

by organic matter. Of the minerals listed in Table 9.3 Ce is only found in apatite, however, the sample at 12.70 metres containing apatite is not enriched in this element with respect to the surrounding shale and, therefore, this substitution would appear to be limited and to have little or no influence on the distribution of Ce. The main features of this distribution are the peak at 7.2 metres and the troughs at 6.8 and 8.85 metres. The increase in concentration corresponds to increases in Fe_2O_3, MnO, P_2O_5, As, Ba, Cu, La, Pb, Th and Y, the significance of which is uncertain.

(iv) Co

The concentration of Co within these shales is highest around 8.35 metres. This peak coincides with those of As, Ba, Cr, Cu, Mo, Ni, Se, U, V, and Zn and is, therefore, indicative of the illite/organic rich zone. In addition to this, Co is also concentrated in carbonates and pyrite in the Tansley shale (Amin, 1979).

(v) Cr

Cr shows slight enrichment around eight metres and in the Tansley borehole it is known to be mainly related to illite and feldspar. Table 9.3 shows that Cr may also occur in chlorite.

(vi) Cu

The distribution of Cu is interesting in that it either has low background values of approximately 100ppm or it has high values of over 540ppm with little inbetween. Cu is associated dominantly with organic matter and pyrite (Amin, 1979; Krauskopf, 1979) and the

organic rich zone in the Oker Hill borehole does contain a narrow band of shale enriched in Cu, although the pyritic shale only has background levels. It may be that the high levels represent a copper-bearing mineral that has not been identified by XRD analysis.

(vii) La

On the basis of the minerals known to be present within this shale the distribution of La cannot be explained, although the sudden decrease in concentration at 10.70 metres does indicate that this element is not associated with siderite. Like Ce it does peak at about 7.2 metres depth along with Fe_2O_3 and its associated elements, therefore, in this particular horizon La may be related to an iron-bearing mineral.

(viii) Mo

Mo is an organophile and, as would therefore be expected, the shale is most enriched in this element between seven and eight metres depth. Either side of this band Mo is only present at very low background values.

(ix) Ni

From Table 9.3 it can be seen that Ni substitutes mainly for Fe in pyrite, pyrrhotite, chlorite and smectite. In addition to this, Ni is also an organophile which would account for the high concentration between 8.35 to 8.4 metres. Either side of this horizon are very low values similar to the pattern shown by Co. In fact, these two elements have very similar distributions through the core material

(Figure 9.4), and it is interesting to note that they both show an increase at the point where pyrite is first found within the core. Consequently this suggests that both Ni and Co may be related to pyrite.

(x) Nb

Nb may be enriched in aluminium hydroxides and in phosphates (Degens, 1965), however, in the Oker Hill shale Nb does not appear to be related to P_2O_5. The distribution of Nb is relatively constant down the borehole with sharp decreases at 10.70 and 12.70 metres which indicate that this element is not associated with siderite or apatite. There is also a slight decrease in concentration around eight metres which may indicate that it is not related to organic matter, illite or an iron-bearing mineral. The distribution of Nb most closely follows those of SiO_2, Al_2O_3 and TiO_2, therefore, this indicates that Nb is found in the detrital component of the sediment.

(xi) Pb

The distribution of Pb down the borehole is likely to be influenced by the presence of organic matter and pyrite, as was found by Amin (1979) for the Tansley shale. Above 7.5 metres Pb and Cu show the same pattern of variation in concentration and this is repeated below 12.70 metres; it was suggested above for Cu that these high levels may be attributable to a mineral that has not been identified by XRD. Around eight metres, the enrichment of Pb may be due to a high organic matter content as this element is an organophile. From 9.4 to 10.4 metres the relatively constant level of Pb is likely to be

related to the presence of pyrite.

(xii) Rb

In the Tansley shale Amin (1979) found that Rb was mainly related to illite and feldspar. This observation is supported by the Oker Hill shale as Rb has a similar distribution to SiO_2 and to Al_2O_3 in particular. Therefore, SiO_2, Al_2O_3, TiO_2, Nb and Rb all appear to be forming the detrital component of the shale.

(xiii) S

S is only present in significant quantities in the unweathered shale from depths of 9.4 to 10.45 metres and 12.2 to 12.35 metres. These are the bands of shale within which pyrite has been identified and as the only other sulphur-bearing minerals occurring in shale are both weathering products (gypsum and jarosite) it is reasonable to attribute the high levels of S to pyrite alone.

(xiv) Se

Se follows a similar distribution to Mo and to Va in particular, being concentrated between 7.0 and 8.75 metres depth. Although Se is not usually associated with organic matter or illite, in this case it would appear to be related by its association with Mo and Va. Apart from two samples near the base of the core and this zone of enrichment, Se is absent from the shale.

(xv) Sr

The main feature of the distribution of Sr is the sharp peak in

concentration at 12.70 metres (Figure 9.4). This peak corresponds with those of CaO and P_2O_5 which have been interpreted as indicating the presence of apatite, therefore it would appear that Sr is substituting for Ca (Table 9.3). Apart from the influence of apatite at 12.70 metres Sr has a similar distribution to SiO_2, Al_2O_3, TiO_2, Nb and Rb indicating a detrital origin. It is also known to occur in the smectite clays (Table 9.3) and it may substitute for Ca in calcite (Amin, 1979).

(xvi) Th

According to Degens (1965) Th may be enriched in aluminium hydroxides. In the Oker Hill shale Th does follow approximately the distribution of the detrital components SiO_2 and Al_2O_3.

(xvii) U

U is an organophile and its enrichment around a depth of eight metres further signifies a zone of organic-rich shale.

(xviii) V

The distribution of V is very similar to that of Se being enriched between 7.0 and 8.75 metres. In the Tansley borehole Amin (1979) noted that Va was related to organic matter and illite, and there is much evidence in this study that this relationship also holds for the nearby shale ot Oker Hill.

(xix) Y

In the Tansley shale Y could not be assigned to either a particular

element group or to a mineral. In the Oker Hill shale Y appears to be associated with apatite as the peak at 12.70 metres corresponds with those of CaO, P_2O_5 and Sr. Y is also slightly enriched in the siderite concretionary band at 10.70 metres. The enrichment at 10.90 metres cannot be explained.

(xx) Zn

Amin (1979) found that Zn was concentrated in illite, pyrite, carbonates and organic matter in the shale from the Tansley borehole. The distribution of Zn encountered in this analysis shows that it is concentrated in the illite/organic-rich zone around eight metres, and also in the pyritic shale around ten metres. These observations would appear to be consistent with those of the Tansley shale.

(xxi) Zr

Above 7.0 metres the distribution of Zr most closely follows those of Na_2O and kaolinite; the reasons for this are unclear, although according to Degens (1965) Zr may be enriched in aluminium hydroxides. Amin (1979) noted that the non-marine shales of the Tansley borehole were richer in Zr than the marine shales and that Zr was mainly present in the form of zircon. The sideritic shale analysed for this work also had higher concentrations of Zr compared to the pyritic shale.

The most striking feature of these distributions of elements is the peak around eight metres depth shown by As, Ba, Co, Cr, Cu, Mo, Ni, Se, U, V and Zn. All but Ba, Cr, Se and Zn are listed in Table 9.4

as organophiles, therefore, this is an indication of a potentially organic-rich shale in this zone. There is further support for this interpretation as LOI shows a slight increase around eight metres also. However, Fe_2O_3 and K_2O contents also show an increase (Figures 9.3 and 9.4), and Figure 9.2 shows that illite peaks at this depth and is the dominant clay mineral. The source of K_2O will be dominantly illite and although Fe_2O_3 is contained in the iron oxides and hydroxides, pyrite and siderite, Amin (1979) found that Fe in the Tansley shale is also related to illite. Unfortunately, the actual percentage total clay content of the core material was not measured, therefore, it cannot be determined whether the increase in LOI is related specifically to an increase in clay content or organic content. Of the trace elements that are enriched in this zone As, Ba, Cr, Cu, Mo, U, V and Zn are known to be enriched in the aluminium hydroxides (clays). In the geochemical analysis of the Tansley borehole shale Amin (1979) noted that Ba, Cr, Rb, V and Zn were, in part, related to illite. He also noted that the K_2O/Al_2O_3 ratio was higher in marine shales as a result of the higher illite content of this group of shales (see Chapter 8.1).

Therefore, from the XRD analysis of clay mineralogy it is known that illite is the dominant clay mineral at a depth of around eight metres in the two boreholes through Oker Hill landslide, and on the basis of the distribution of elements down the boreholes it can be concluded that the presence of illite causes an increase in certain trace elements. However, these elements may also indicate an increase in organic matter within this zone.

It is interesting to note that in a regional geochemical reconnaissance survey of Derbyshire Nichol et al. (1970) found that waters draining from parts of the Namurian-Visean shale outcrops showed markedly high concentrations of As and Mo, with lesser enrichment in Co, Cr, Cu, Fe, Ni, Ti, V and Zn. They also noted that there were great geochemical variations within the same lithology evident in the considerable differences in metal content and metal ratios in these shale facies. This variation is apparent in the Oker Hill shale.

Curtis (1969) divided some British Carboniferous sediments into marine and non-marine shales on the basis of fossil content; Table 9.2b shows their trace element composition. He noted that geochemical interpretation is aided considerably by this grouping and he recognised three distinct trends:

(i) Ba, Co, Cu, Ni and Pb are concentrated in the basal marine sediments together with pyrite and organic matter.

(ii) Mn is negatively correlated with clay content and positively correlated with total diagenetic Fe.

(iii) B, Cr, Ga, Sr and V reflect the clay content.

It is known from XRD analysis of the whole rock samples that the boreholes at Oker Hill pass through both marine and non-marine shales as indicated by the presence and absence of pyrite and siderite. The

presence of pyrite is clearly depicted by the distribution of S which shows sudden increases in concentration from depths of 9.4 to 10.45 and 12.2 to 12.35, and as stated in the previous section siderite is indicated at 10.70 metres by the sudden increases in Fe_2O_3, LOI, MnO, MgO and CaO. In addition to this, Amin (1979) found that these two groups of shale were also recognisable by variations in their trace element geochemistry. Table 9.3 shows that As, Co, Cu, Mn, Ni, Pb and Zn may be associated with pyrite, while Mn, Mg and Ca may substitute for Fe in siderite. Amin (1979) went on to calculate that the trace elements having the greatest percentage increase from non-marine to marine shales in the Tansley sediments are, in descending order: Pb, Cu, V, Ni, Sr and Zn. He also found that Cu, Sr and Pb were the most effective discriminators between the two groups of shale.

Figure 9.6 shows the range of concentrations of each major and trace element for the pyritic (marine) and sideritic (non-marine) samples of shale that were analysed by XRD. Sample 10.70 was excluded as it represents a concretionary band of siderite rather than shale itself and would, therefore, give extreme values which might be misleading. It can be seen that the elements with no overlap in concentrations are Al_2O_3, Fe_2O_3, CaO, MnO, As, Pb, Rb and S; Al_2O_3, As, Pb, Rb and S contents being higher in the pyritic shale, and Fe_2O_3, CaO and MnO being more abundant in the sideritic shale. From Figure 9.6 it can be seen that Cu and Sr contents cannot be used to discriminate between pyrite-rich and siderite-rich shale and that for the Oker Hill shale greatest separation between the shales appears to be given by MnO, Pb

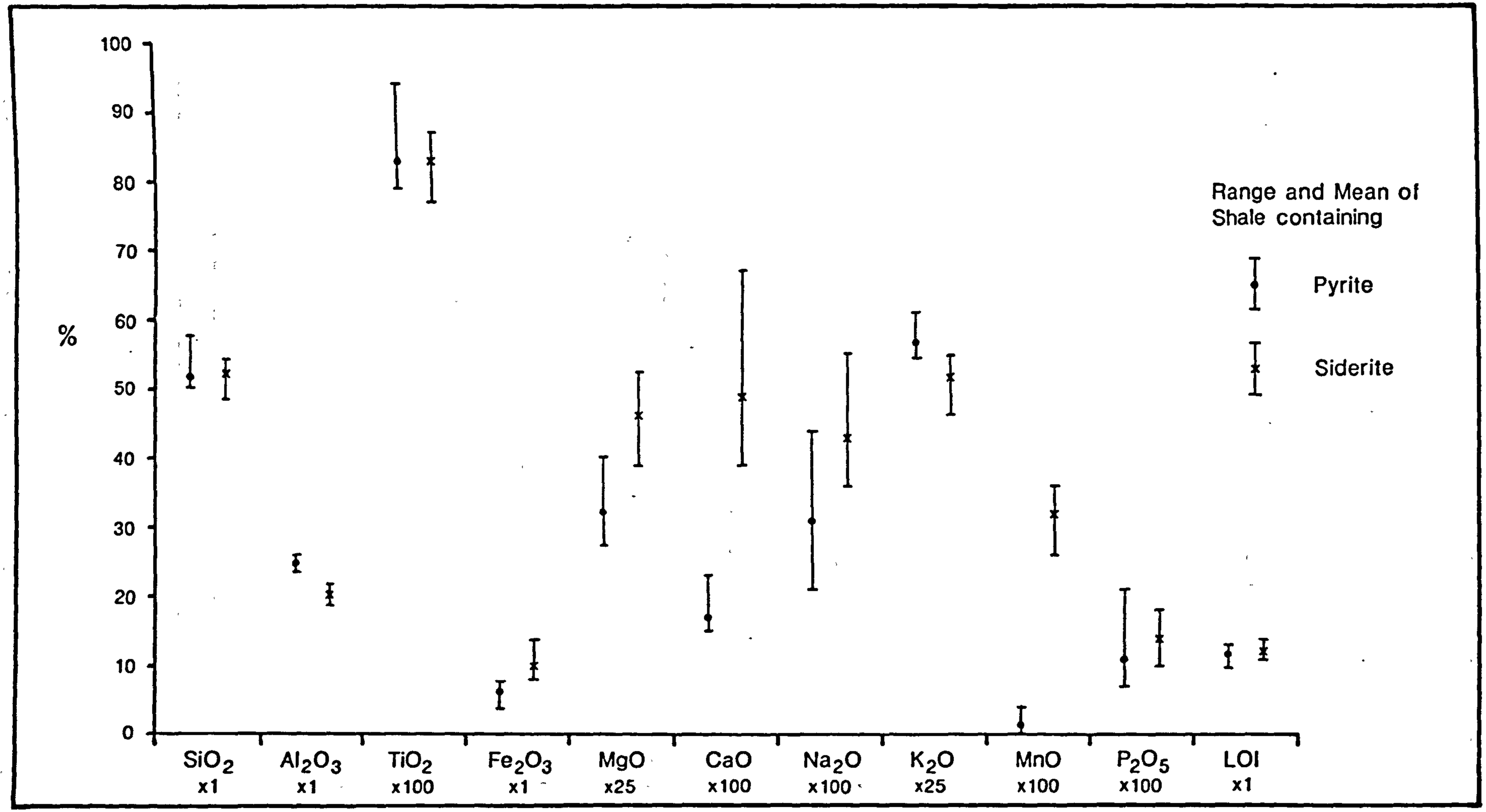

Figure 9.6 Geochemistry of Pyritic and Sideritic Shale, Oker Hill

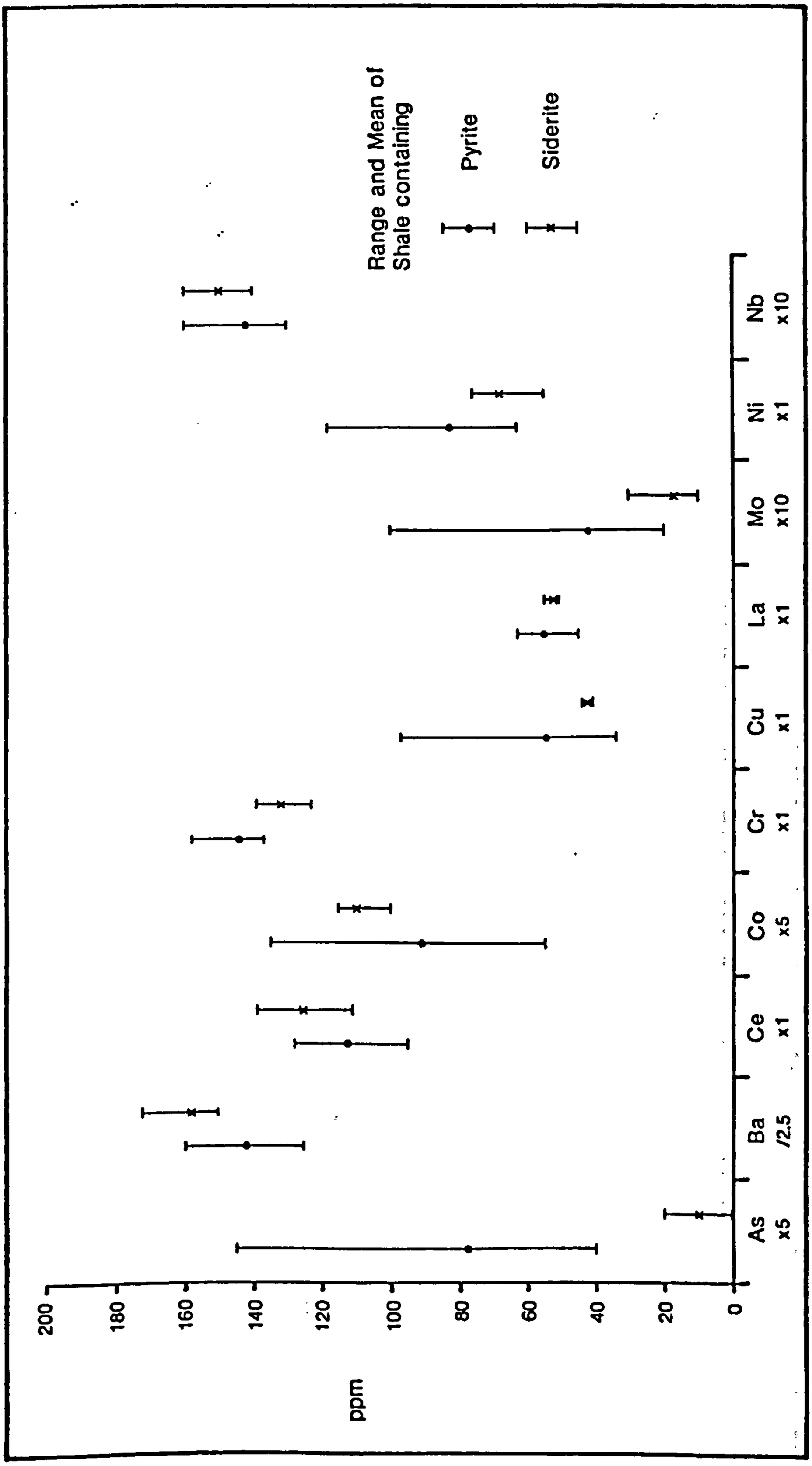

Figure 9.6 (continued)

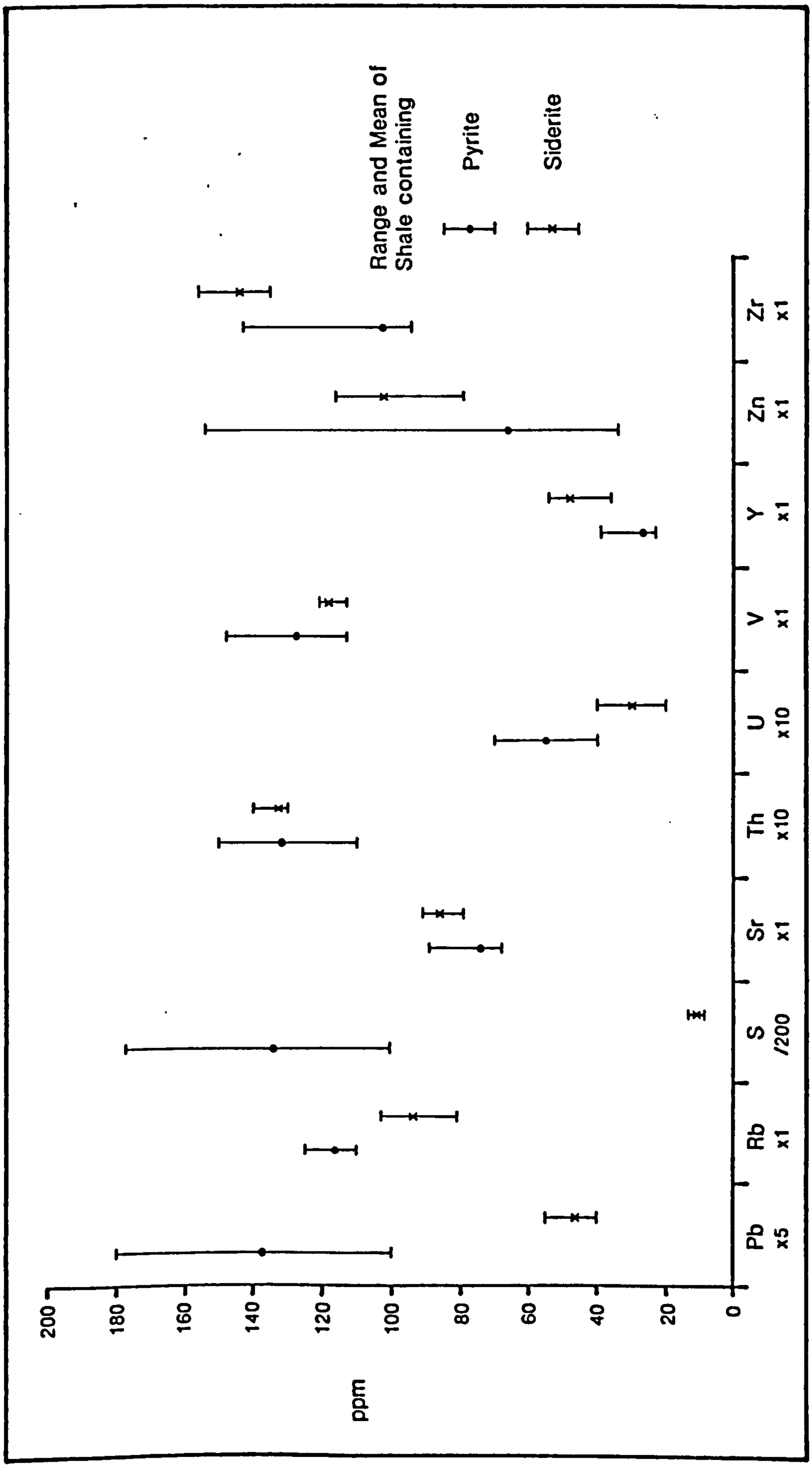

Figure 9.6 (continued)

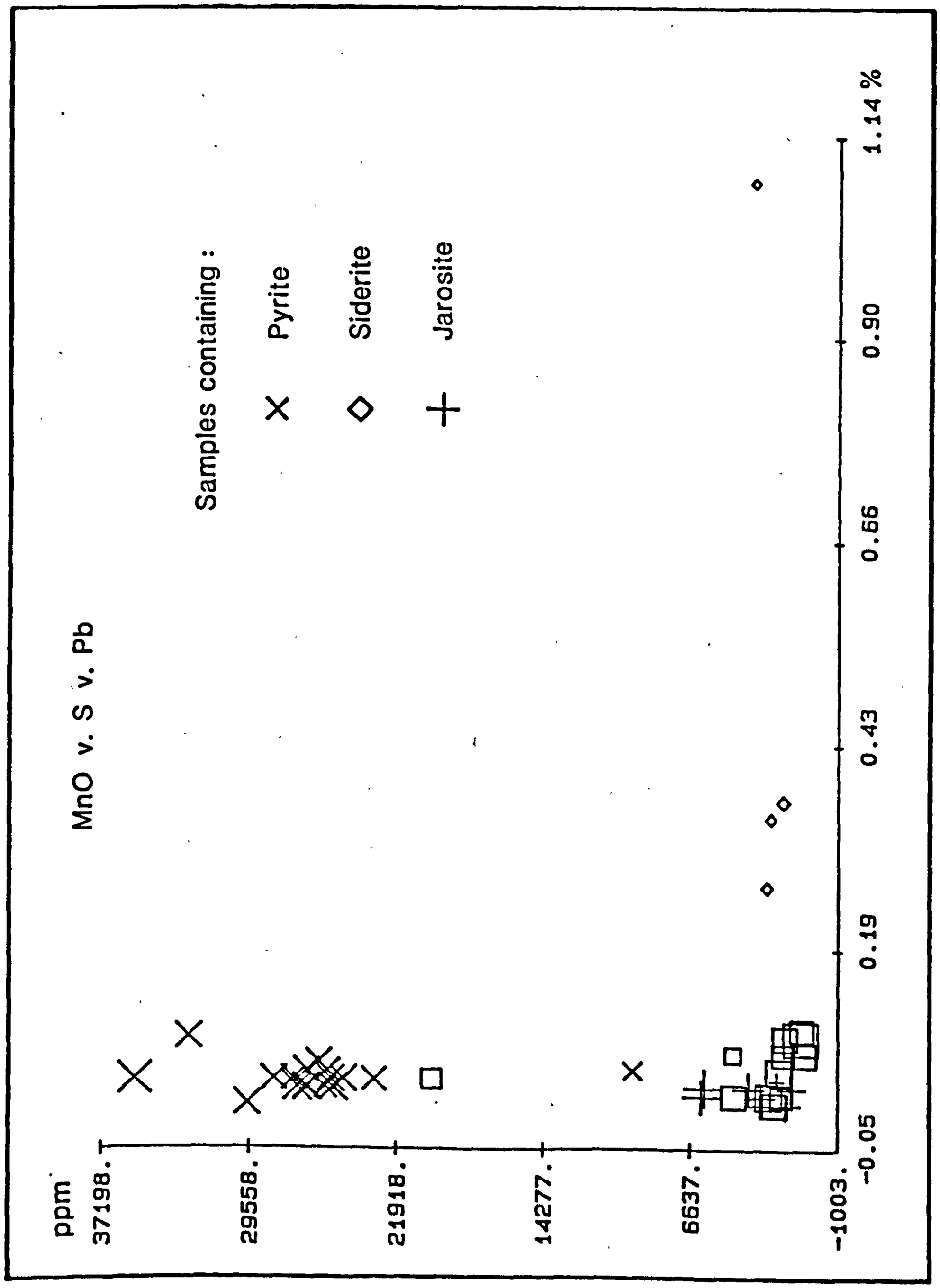

Figure 9.7 Dis

and S. All the samples analysed by whole rock XRD are plotted on the graph of MnO v. S v. Pb in Figure 9.7; pyritic and sideritic samples are labelled. The discrimination between marine and non-marine shale is quite good. However, another group can be identified that has lower concentrations of S and MnO, that of weathered shale.

As the basal slip plane is believed to occur at or near the base of the weathered zone and this work is particularly concerned with the shale which has slipped, it would be interesting to determine whether this shale is marine or non-marine. However, as the samples of weathered shale cluster separately from those of the unweathered pyritic and sideritic shale on the graph of MnO v. S v. Pb another method of discrimination must be employed. Also, as there are a limited number of samples in the data sets (sixteen pyritic samples and six sideritic samples) the significance of the above findings cannot be stated with confidence. Further research is necessary to assess the relationships between geochemistry and pyritic (marine) or sideritic (non-marine) shales, this could involve palaeo-interpretation of the weathered shale to identify the environments of deposition.

CHAPTER 10 THE MINERALOGY AND GEOCHEMISTRY OF OKER HILL SHALE IN RELATION TO SLOPE INSTABILITY

10.1 Introduction to Weathering and Slope Instability at Oker Hill

As explained in Chapter 7 the weathering of a shale slope affects its stability either by resulting in a decrease in strength of the material or through general deterioration of the rock quality. At Mam Tor Vear and Curtis (1981) propose that the periodic large scale instability of the existing landslide is attributable to pyrite oxidation of the shale causing a net volume loss of 0.66 millilitres per litre of water, with internal stresses set up in the rock through precipitation of weathering products away from the site of origin along bedding planes and fissures which are inherent planes of weakness.

Oker Hill has been studied to assess the influence of pyrite oxidation on slope stability in the Matlock region. The occurrence of pyrite oxidation has been implied from the presence of an ochreous spring at this site. Several hypotheses to be tested by this investigation were set out in Chapter 8.2 and are as follows:

(i) There is a change of mineralogy and/or geochemistry at the slip plane.

(ii) Any difference in mineralogy and/or geochemistry at the slip plane is pre-slope failure.

(iii) Any difference in mineralogy and/or geochemistry at the slip plane is post-slope failure.

(iv) The slip plane is located in the pyritic shale due to weakness caused by pyrite oxidation.

(v) There is active pyrite oxidation going on within the landslide at present, and therefore there is potential for further slip movement.

(vi) The slip plane is located in the zone with most potential, when unweathered, for weathering.

This chapter assesses the influence of mineralogy and geochemistry on slope stability at Oker Hill with the aid of these hypotheses.

10.2 Summary and Comparison of Oker Hill and Tansley Shale

In Chapter 9 the distributions of some of the major and trace elements were explained in terms of the minerals identified by XRD. This section draws together this information to define the relationships between mineralogy and geochemistry which may then be used to assess their influence on slope instability at Oker Hill.

From XRD analysis quartz, kaolinite, illite, expandable clays, chlorite, pyrite, siderite, haematite and albite were positively identified in samples taken from two cores through the landslide at Oker Hill. These mineral assemblages are borne out by XRF analysis by the levels of SiO_2, Al_2O_3 and Fe_2O_3. From the analysis of the

distribution of major and trace elements down the boreholes it is possible to make the following summary of the relationships between the mineralogy and geochemistry of the Oker Hill shale:

(i) The elements associated with illite at a depth of around eight metres are K_2O, As, Ba, Co, Cr, V, Zn, and possibly Se.

(ii) As, Co, Mo, Ni, Pb, Se, U, V and Zn are enriched in the organic-rich zone around eight metres depth.

(iii) Increases in Co, Ni, Pb and, to a lesser extent, Zn are related to the presence of pyrite.

(iv) Siderite exhibits substitution of Fe by Mg, Mn and Ca.

(v) High concentrations of CaO, P_2O_5, Sr and Y suggest that apatite is present within the core material at a depth of 12.70 metres.

The band of shale between 7.7 and 8.8 metres appears to be enriched in both illite and organic matter, therefore, it is not possible to assign the elements that show increased concentration in this zone specifically to one or the other component.

As the Oker Hill and Tansley boreholes are only six kilometers apart (Figure 8.1) and they are all in the shale deposited in the same basin in the Millstone Grit Series they should show the same relationships between mineralogy and geochemistry. The relationships identified in the Tansley shale (Amin, 1979; Spears and Amin, 1981a) have been stated in Chapter 8.1; the analysis of the Oker Hill shale

will be compared directly with these observations.

10.2.1 Major Element Geochemistry

(i)

Tansley: In the marine group, increases in concentrations of Fe_2O_3, SO_3 and CaO are associated with pyrite and calcite. Fe_2O_3 is related to iron hydroxides, illite and pyrite, (although the iron in pyrite is FeO it is determined as Fe_2O_3).

Oker Hill: Taking those samples containing pyrite as being marine shale increases in Fe_2O_3 and S are associated with an increase in pyrite. Fe_2O_3 is also related to iron hydroxides (haematite) and illite. As calcite was not identified no conclusion can be made about CaO, although CaO does seem to be more concentrated in the shale containing siderite and has been attributed to taking part in ionic substitution in this mineral.

(ii)

Tansley: The K_2O/Al_2O_3 ratio is higher in marine shales as a result of the higher content of illite in this group.

Oker Hill: The band of shale enriched in illite and organic matter around eight metres depth does have an increased K_2O/Al_2O_3 ratio in comparison with the rest of the shale. However, as this is in the weathering zone and neither pyrite or siderite are present, this

shale cannot be identified as being of marine origin. The pyritic and sideritic shale samples have similar amounts of illite and similar K_2O/Al_2O_3 ratios.

(iii)

Tansley: Siderite is only found in the non-marine shales in which phosphate and TiO_2 are relatively concentrated.

Oker Hill: Accepting that siderite is only found in non-marine shales, TiO_2 occurs in slightly greater quantities in the sideritic shale than in the pyritic samples. Levels of P_2O_5 are about the same in both shales but the siderite concretionary band at 10.70 metres does exhibit a marked increase in this element.

(iv)

Tansley: In the non-marine group, an increase in FeO concentration is related to siderite.

Oker Hill: FeO was not measured but is incorporated in Fe_2O_3 which is related to siderite in the non-marine shale.

(v)

Tansley: FeO is also related to chlorite.

Oker Hill: As for siderite above, the FeO related to chlorite is measured as Fe_2O_3.

10.2.2 Trace Element Geochemistry

(i)

Tansley: The elements having the greatest percentage increase from non-marine to marine shales are, in descending order: Pb, Cu, V, Ni, Sr and Zn. The concentrations of Cu, Sr and Pb were found to be the most effective discriminators between the two groups of shale.

Oker Hill: From Figure 9.6 it was determined that the elements (major and trace) giving discrimination between the sideritic and pyritic shales are, in descending order of degree of separation: S, MnO, Pb, CaO, As, Al_2O_3, Rb and Fe_2O_3. Of these the concentrations of S, Pb, As, Al_2O_3 and Rb are highest in the pyritic samples, the first three elements being associated with pyrite and the last two probably indicating a higher clay content. Fe_2O_3, CaO and MnO contents are higher in the sideritic samples, Ca and Mn being cations which commonly substitute for Fe in siderite. Figure 9.7 shows that the most effective discriminators of unweathered pyritic and sideritic shales are MnO, S and Pb.

(ii)

Tansley: Pb and Cu show a strong positive correlation with Fe_2O_3 (pyrite). Ni, Cu and Pb are believed to be concentrated in pyrite and organic matter.

Oker Hill: In the pyritic samples Pb is positively correlated with

Fe_2O_3 but Cu is not correlated. Pb, Ni and Co are believed to be related to both pyrite and organic matter. P_2O_5 also appears to be correlated with Fe_2O_3 in the pyritic samples but the reason for this is not known.

(iii)

Tansley: V is concentrated in organic matter and in illite.

Oker Hill: The concentration of V peaks around eight metres depth in the band of shale identified as being enriched in both illite and organic matter.

(iv)

Tansley: Sr is concentrated in calcite.

Oker Hill: Calcite was not identified in this shale and the peak in Sr content at 12.70 metres in conjunction with CaO and P_2O_5 is interpreted as indicating the presence of apatite.

(v)

Tansley: The increase in Zn appears to be related to the increase in illite and, therefore, it is thought that Zn is dominantly of detrital origin. Together with Co and Mn, Zn is also concentrated in carbonates, pyrite and organic matter.

Oker Hill: Zn appears to be related to illite, organic matter and pyrite.

(vi)

Tansley: The non-marine shales were higher in Mn due to its association with siderite, and in Zr which is mainly present as elemental zircon.

Oker Hill: MnO was found to be associated with siderite through ionic substitution. Zr contents of the sideritic shale are higher than those of the pyritic samples.

(vii)

Tansley: Cr, Rb and Ba are mainly related to illite and feldspars.

Oker Hill: Cr, Ba and, to a lesser extent, Rb are all enriched in the illite/organic rich shale around eight metres depth. Although albite was identified it is not possible to assess the significance of these elements with repect to the feldspar.

(viii)

Tansley: Y could not be assigned to either a particular element group or mineral.

Oker Hill: Y appears to be related to apatite.

It can be seen that there is some agreement between the relationships of mineralogy and geochemistry of the Tansley and Oker Hill shales

and, therefore, greater confidence can be placed on these results. Where discrepancies occur they may be due to the different scales at which the investigations were carried out and the nature of the core material. For example, the Tansley core appears to have been sampled at irregular intervals through the shale between the overlying Ashover Grit and the underlying limestone (see Figure 8.2), whereas the Oker Hill core was sampled at five centimetre intervals between depths of 4.5 to 13 metres. The observations made of the Oker Hill shale may, therefore, be specific to a restricted shale sequence, whilst the results from the Tansley borehole represent more general relationships between mineralogy and geochemistry. It is also important to bear in mind that only the lower 3.5 metres of the Oker Hill core is considered to be in situ shale with the material above being weathered and disturbed by slope movement. The effect of weathering and slope stability on mineralogy and geochemistry will be discussed below.

The similarity between the Tansley and Oker Hill shale suggests that the effects of mineralogy and geochemistry on slope instability at the Oker Hill landslide may be applicable to other shale slopes in the area.

10.3 The Effect of Weathering on Mineralogy and Geochemistry of Oker Hill Shale

The Oker Hill shale is known from XRD analysis to be composed

dominantly of quartz and clay minerals, with the plagioclase feldspar albite also present in many samples. Iron oxide minerals (haematite and goethite) are present mainly in the weathered shale; below the weathered zone iron is contained in pyrite and siderite. The calcium-bearing mineral apatite was only identified in one sample, and other calcium and magnesium minerals such as calcite and dolomite, if present, do not exist in sufficient concentrations to be detected by XRD analysis.

Quartz, clay minerals and feldspars are all of detrital origin, therefore, they are relatively stable under atmospheric conditions. On the other hand, accessory minerals such as pyrite and siderite form during or immediately after the deposition of the sediment, therefore, they are stable under the conditions of their formation, i.e. pyrite in a reducing anaerobic marine environment and siderite in a brackish/fresh water environment. On exposure to atmospheric conditions both pyrite and siderite are brought out of equilibrium with the environment as oxidising conditions prevail. In addition, infiltrating rainwater may be acidic and organic matter also provides carbonic acid (H_2CO_3) as water infiltrates the soil and shale, these acids aid in weathering.

Therefore, of the minerals composing the Oker Hill shale pyrite and siderite will be most affected by weathering being oxidised to form haematite and goethite. Pyrite oxidation was discussed in detail in Chapter 7.5, and the subsequent reactions in which the weathering products take part are set out in Figure 7.1 (Vear, 1981). The

weathering of siderite leads to the production of carbonic acid (H_2CO_3) which will also take part in subsequent reactions, however, not to the same extent as the sulphuric acid produced by pyrite oxidation due to its lower strength. The H^+ ions produced by the oxidation of these iron-bearing minerals will be consumed, then, in further reactions with fresh pyrite and siderite as well as with clay minerals and any calcite or dolomite that may be present, as represented in Figure 7.1. The iron released by oxidation will form the iron oxides and hydroxides of haematite and goethite and may be transported out of the system by percolating solutions. On emergence at the surface these solutions precipitate the iron compounds as indicated by ochreous springs.

In Appendix 3 the weathering grades of the core from Borehole 2 were given. It is necessary to assess the effect of weathering on the mineralogy and geochemistry of this shale in order to attempt to separate original differences from differences arising from weathering.

The weathering grades are included on the plots of the distribution of the elements down Borehole 2 (Figure 9.4) in order to determine whether changes in the concentration of each element are related to weathering. The main features that were noted are the absence of high levels of S in the weathered shale indicating pyrite oxidation or the initial absence of pyrite in this zone, and the localised increases in Co, Ni and illite immediately below the junction of weathering grades III and II-I at 9.65 metres marked by the absence

of iron-staining below this depth. In fact, very few elements show any correspondence of their distribution to weathering grade and where any correspondence does occur it cannot be confidently ascribed to weathering as it may be due to original variations in shale composition down the core.

To assess the influence of weathering on the mineralogy and geochemistry of shale accurately it is really necessary to analyse samples of shale from the same horizon at different stages of weathering. Unfortunately, this was not possible in this study. Apted (1977) studied the effects of weathering on the chemistry of London Clay using samples of varying degree of weathering from the same horizon. He suggests that weathering results in the oxidation of pyrite and marcasite with the associated conversion of calcite to selenite, and although the proportion of ferric iron (Fe^{3+}) to ferrous iron (Fe^{2+}) increased as oxidation occurred, the overall iron content is not necessarily affected. He also noted that there was a slight increase in the montmorillonite/illite ratio. The proportion of metallic elements and silica of London Clay does not appear to be affected by weathering.

It can, however, be concluded that pyrite oxidation is occurring within the shale of Oker Hill at the base of the weathering zone. This is shown by the presence of pyrite in the iron-stained shale immediately above 9.65 metres. As the zone containing both visible iron oxide and pyrite is at the centre of a U100 sample which was noted at the time of coring to contain the change from iron-stained

to fresh shale, it can be certain that this is the present zone of active weathering. The subsequent reactions in which the weathering products of pyrite oxidation take part will be confined to the shale at and below this depth as this is the zone in which ground water will become charged with the H^+ ions from H_2SO_4. The shale above 9.4 metres will experience less weathering as most, if not all, of the pyrite has been destroyed and, therefore, the only source of H^+ ions is from rainwater and organic matter. Not all of the iron released from pyrite oxidation is precipitated within the shale as iron oxides or hydroxides, some iron is carried by the ground waters to the surface where it is precipitated, however such ochreous springs are not common. It would have been interesting to have analysed the composition of the ground waters at Oker Hill landslide, however time would not allow.

10.4 The Mineralogy and Geochemistry of the Slip Planes

Several observations of the geochemistry of slip planes within shale of the Upper Coal Measures of the Carboniferous have been recorded by Early and Skempton (1972) in their study of the landslide at Walton's Wood, Staffordshire. Firstly, they noted a decrease of the K_2O/Al_2O_3 ratio. This ratio is a measure of the proportion of illite to kaolinite and Early and Skempton (1972) interpret the decrease in the ratio as indicative of the leaching of potassium ions from illite and mixed-layer clays to produce kaolinite. In Figure 7.1 Vear (1981) shows that the illite to kaolinite transformation in the shale at Mam

Tor landslide is a consequence of the production of H^+ ions by pyrite oxidation. Prior and Graham (1974) noted that the maximum value of Na^+ ions coincided with the slip plane of a landslide in Carboniferous shale in Northern Ireland, however, they do not suggest a cause for this distribution.

Early and Skempton (1972) also noticed a decrease in the Fe_2O_3 content of the shale in the shear zone which they explain by proposing that chemical reduction by percolating waters has taken place subsequent to failure resulting in a decrease in Fe_2O_3 content and a colour change from the adjacent yellow/brown clay to light grey. Contrary to this observation and interpretation Amin (1979) and Steward (1984) identified haematite (Fe_2O_3) in the region of the slip plane of the Mam Tor landslide. They interpret this as indicating the percolation of oxygenated waters along this plane of increased permeability. It may be more probable that iron is actually being lost and transported away from the slip plane of Walton's Wood landslide rather than being reduced, as by considering both the FeO and Fe_2O_3 contents of the shear zone compared to the ambient clay (Table 10.1) it can be seen that there is an overall decrease in total iron content. However, as suggested by Early and Skempton, the agent involved is percolating water which flows preferentially along the more permeable slip plane carrying with it the ferric ions (Fe^{3+}). Such colour changes at the slip plane were also noted by Prior and Graham (1974).

Table 10.1 Iron Content of the Shale of Walton's Wood Landslide

(Early and Skempton, 1972)

	Ambient Clay	Shear Zone
FeO	0.4%	0.4%
Fe_2O_3	11.9%	2.5%

Both of the above observations of the geochemistry of slip planes in Carboniferous shale may be associated with pyrite oxidation, and are subsequent to slope failure as they require the percolation of water along the more permeable zone provided by the presence of the slip plane. Other mineralogical changes occur as a result of the production of H^+ ions by pyrite oxidation, as shown in Figure 7.1 (Vear, 1981). Therefore, other mineralogical and geochemical characteristics may also be found. For example, dissolution of calcite and dolomite, clay dissolution, and precipitation of weathering products (i.e. gypsum, jarosite, iron oxides and hydroxides). However, these alterations will also occur throughout the weathered shale , therefore, if the slip plane is within the weathered shale it will not differ greatly in mineralogy or geochemistry to the surrounding shale unless it is a zone of significantly greater permeability. Also, any loss of calcite or dolomite and corresponding gain in gypsum in the Oker Hill shale will probably not be noticed in the geochemistry as, if these minerals are

present, they only occur in trace amounts. Furthermore, as stated in Chapter 9.2, gypsum will not form if the calcium content of the shale is less than 0.5 percent by weight (Nixon, 1978); the average CaO content of the Oker Hill shale is 0.25 percent and therefore there is insufficient Ca present to form gypsum.

During detailed logging of the core from Borehole 2 (Appendix 3) several planes of discontinuity were noted which may be slip planes (see Chapter 8.5). The first of these at 6.80 metres is suggested by the apparent displacement of shale along a diagonal line marking the junction between structureless clay and faintly laminated shale. The contact at 6.70 metres between soft grey clay above and slightly stiffer brown/grey clay below may also be associated with this possible shear zone. At 7.45 to 7.50 metres, although the shale is a disturbed sample, there does appear to be a junction between faintly-laminated and well-laminated shale: the junction between weathering grades IV and III, respectively. Unfortunately, the nature of the contact is not known, however, the possibility of this sample being a slip plane cannot be ruled out. Between 8.55 and 8.85 metres depth there are several features that may be related to a shear zone. At 8.55 to 8.75 metres there is an increase in weathering grade of the shale with depth from Grade III to IV; the nature of this change is not known as it is a disturbed sample. The shale between 8.75 to 8.85 metres is intensely iron-stained with laminations only just visible. Below 8.85 metres the shale is again well-laminated and of weathering grade III. Therefore, the shale between 8.55 and 8.85 metres appears to be more weathered than the shale above and below,

which may represent a zone of increased permeability as may be expected of a slip plane. The deepest discontinuity that may be a slip plane is at 9.65 metres indicated by the diagonal contact between iron-stained and fresh shale coinciding with a change in angle of inclination of the bedding planes (Plate 8.1). Evidence of shearing movement is also found between 10.10 and 10.45 metres in the form of polished bedding planes.

Analysis of the shale from Borehole 2 by XRD showed no distinct mineralogical differences between the slip planes and the surrounding shale. However, the analysis of the whole rock samples was not quantitative and therefore, any differences in mineralogy are noted as the presence or absence of a mineral rather than relative quantities of each mineral. The first occurrence of pyrite at 9.40 metres may, however, be associated with the discontinuity at 9.65 metres as the band of shale between 9.40 and 9.65 metres appears to be the present zone of active weathering as discussed above in Chapter 10.3.

The dominant geochemical characteristics of the slip planes of the Oker Hill landslide are shown in Table 10.2. Analysis of the clay mineralogy showed that the proportion of the expandable clays drops for the shale around 9.65 metres while chlorite increases. Kaolinite and illite show no change, but the ratio of K_2O/Al_2O_3 is at its lowest in the shale between 9.4 and 9.7 metres indicating that kaolinite is dominant over illite. For the proposed basal slip plane at 9.65 metres depth As and Ba concentrations are slightly lower than

TABLE 10.2 GEOCHEMICAL AND MINERALOGICAL CHARACTERISTICS OF THE PROPOSED SLIP PLANES OF OKER HILL LANDSLIDE

Slip Plane (depth in metres)	Elements and Minerals showing an increase in concentration	Elements and Minerals showing a decrease in concentration
6.80	SiO_2, Na_2O, Cu, Pb, Zr, kaolinite	Al_2O_3, K_2O, LOI, Ce, illite, chlorite
7.45-7.50	SiO_2, TiO_2, S - below 7.50m	Fe_2O_3, MnO, Co, Ni, Zn - below 7.50m
8.75-8.85	SiO_2, Al_2O_3, TiO_2, Na_2O, La, Nb, Rb, Sr, Th, Zr, kaolinite - below 8.85m	K_2O/Al_2O_3
9.65	S, chlorite	As, Ba, K_2O/Al_2O_3, expanding clays

those of the adjacent shale, Ba being at its lowest concentration encountered in the core. These two elements are probably associated with illite.

The low K_2O/Al_2O_3 ratio has already been mentioned with respect to leaching of K^+ from illite to produce kaolinite (Early and Skempton, 1972; Vear, 1981). If this ratio is indicating clay transformation rather than an original feature of the shale mineralogy then it may indicate a zone of high permeability enabling percolating waters charged with H^+ from pyrite oxidation to attack clay minerals. However, there is no decrease in iron content in this shale while such a decrease was noted along the slip plane of Walton's Wood landslide by Early and Skempton (1972). (Caution must be exercised in comparing the findings at Walton's Wood landslide with the measurements of Fe_2O_3 on the proposed slip planes of Oker Hill landslide as in the latter case all the iron has been determined as Fe_2O_3 whereas Early and Skempton separate the iron compounds into ferrous (FeO) and ferric (Fe_2O_3) oxides.) In fact, the shale at and immediately around this possible slip plane has very high S content which is known to be due to the presence of pyrite. This may be contrary to the concept of a slip plane being a plane of greater permeability as the percolation of oxygenated water should result in the destruction of the pyrite. Although the iron oxide staining on the faces of joints and fissures in the shale above 9.65 metres shows that the pyrite is being oxidised, the persistence of pyrite suggests that this is the present zone of active weathering. If the junction between the iron-stained and fresh shale is a slip plane with

increased permeability, pyrite would not be expected to be present, particularly as the landslide is likely to be several thousand years old.

Therefore, the evidence suggests that the plane at 9.65 metres marks the abrupt base of the weathering zone, and that the shale between 9.4 and 9.65 metres is the present zone of active pyrite oxidation. Although the location of a slip plane is commonly at the base of the weathering zone, at the time of failure this zone is likely to have been at a shallower depth than at present. However, the apparent change in the dip of the bedding planes, as noted in the detailed logs of Borehole 2 (Appendix 3), does support the concept that this is a slip plane along which rotational movement has taken place, although it is possible that weathering along bedding planes and fissures in the shale above and disturbance during drilling may have produced this effect.

The band of increased weathering grade between 8.75 and 8.85 metres also shows no apparent decrease in iron content, but the ratio of K_2O/Al_2O_3 does show a sharp decrease over this zone to one of the lowest values found in this core. The sharp decrease in this ratio is partly due to the presence of the illite-rich shale identified around eight metres depth being immediately above. SiO_2, Al_2O_3, TiO_2, Na_2O, La, Nb, Rb, Sr, Th, Zr and kaolinite appear to increase slightly below 8.85 metres before decreasing at 9.4 metres as a result of the increases in Fe_2O_3 content related to pyrite. Many of these elements are associated with the detrital components of the

shale and may, therefore, be indicating a decrease in the elements associated with minerals such as pyrite which are more susceptible to weathering.

The location of this band of shale between 8.75 to 8.85 metres in relation to the zone of enriched illite and organic matter may be significant. This zone would be the main source of carbonic acid within the shale derived from water percolating through the organic matter which would then attack the shale in and immediately below this horizon. In the Tansley borehole Amin (1979) found that marine shale was high in illite, pyrite and organic matter, therefore, this band of enriched illite and organic matter may also have contained pyrite at a time when the depth of weathering was above approximately eight metres, and consequently, it is possible that sulphuric acid from pyrite oxidation may also have contributed to the weathering of the shale below. It follows that this shale at 8.75 to 8.85 metres may have been preferentially weathered producing a weaker zone along which failure may occur.

The sample at 7.45 to 7.50 metres marks the junction between faintly-laminated shale above and well-laminated shale below; this is also the junction between weathering grades IV and III. Unfortunately, the nature of the contact is not known as this is a disturbed sample. The noticeable changes in geochemistry at this depth are increases in SiO_2, TiO_2 and S below this horizon, and decreases in Fe_2O_3, MnO, Co, Ni and Zn. Two samples in this zone have very low Ba and Pb contents whilst the other samples have high concentrations. The reasons for

these distributions are not known. The change in element distribution is restricted in extent as 0.2 metres below this zone is the band of shale enriched in illite and organic matter which is known to affect trace element concentrations. There is no change in the K_2O/Al_2O_3 ratio to indicate clay transformation by leaching, and the decrease in Fe_2O_3 occurs in the better laminated shale which would be below the slip plane and, therefore, not in the zone of increased permeability. Consequently, geochemical evidence would appear not to support the interpretation of this band as a slip plane.

The contact between structureless clay and faintly laminated shale (weathering grades V and IV, respectively) occurs at 6.80 metres. This horizon has the highest SiO_2 content recorded for the core and levels of Na_2O, Cu, Zr and Pb are also high. Kaolinite constitutes a high proportion of the clay minerals with the proportions of illite and chlorite being low in this shale; this may be associated with the lower levels of Al_2O_3 and K_2O. The clay mineralogy of the proposed slip plane at 6.80 metres would, therefore, appear to differ from that of the adjacent shale, whether this is due to the presence of the slip plane or an original mineralogical feature is not known. The constant K_2O/Al_2O_3 ratio across the slip plane does not indicate loss of potassium ions in an illite to kaolinite transformation, but kaolinite is known to be the dominant clay mineral. The drop in Al_2O_3 percentage probably indicates a decrease in clay content which may be caused by clay dissolution resulting from attack of acidic solutions from pyrite oxidation (Vear, 1981). Of course, a lower

clay content could also be related to the environment of deposition where factors such as distance from the shoreline and the rate of sedimentation are important controls on grain size of the sediment.

10.5 Conclusions on Slope Instability and the Composition of Oker Hill Shale

From the observations of the mineralogical and geochemical compositions of the proposed slip planes the hypothesis that there is a change in mineralogy and/or geochemistry at the slip plane can be accepted on the assumption that these planes are slip planes. Most confidence can be placed in the interpretation of the discontinuities at 6.80 metres and at 8.75 to 8.85 metres being slip planes on the basis of the physical appearance of the core material and geochemical characteristics described above. The contact between iron-stained and fresh shale at 9.65 metres is best interpreted as the present base of the weathering zone, however, visual examination of the contact did reveal an apparent change in the angle of inclination of the bedding planes which could have been produced by slope failure. Also, the presence of polished faces in the shale between 10.10 and 10.45 metres suggests that this shale has taken up some movement although displacement appears to be minimal. This zone may, therefore, have accommodated some of the strain involved in slope failure along the plane at 9.65 metres. For pyrite still to be present the slip plane would have to be a zone of insignificantly increased permeability or one in which conditions were non-oxidising.

There is little evidence to support the location of a slip plane at 7.45 to 7.50 metres beyond the transition with depth to shale with its original structure preserved.

Whether any compositional difference is pre- or post-slope failure is difficult to judge, although, as a slip plane is a plane of increased permeability, percolating waters will alter this zone either by the destruction of minerals by weathering or by the precipitation of weathering products.

It should be remembered that the nature of this landslide suggests that there may be more than one slip plane within the core as it is a multiple failure. Due to the method of coring and sample extraction it is very probable that not all the slip planes were identified. This problem could have been overcome by using a continuous sampling method, unfortunately, equipment for this was not available. It would also have been an advantage to have drilled two adjacent boreholes and to have taken two cores with the U100 samples staggered so that the disturbed shale in the cutting shoe of one core would have been sampled in the U100 tube of the other core down the length of the borehole avoiding gaps in sampling (Hutchinson, 1982). Unfortunately, in this study the first borehole was not sampled with U100 tubes and time would not allow a third hole to be drilled. Also, although visual examination of the core material showed apparently <u>in situ</u> shale towards the base of Borehole 2, the deeper slip plane predicted from slope profiling in Figure 6.11 cannot be totally discounted. Therefore, it has to be acknowledged that this is

a major limitation to this work as the core material obtained may not include the slip plane.

Pyrite oxidation is evident within the shale at Oker Hill towards the base of the weathering zone and Vear (1981) and Steward (1984) demonstrate that this process results in the deterioration of the rock quality at Mam Tor landslide in north Derbyshire. It is therefore proposed that the recognition of pyrite-rich marine shales within landslide material and in slopes liable to failure is important as these shales would appear to contribute to continued slope instability.

CHAPTER 11 SUMMARY AND CONCLUSIONS

11.1 Aims of the Project

This work has aimed to provide a greater understanding of slope instability in the Matlock region of Derbyshire using reconnaissance and site investigation techniques. It was also the intention to assess these techniques of remote sensing, ground and subsurface investigation with respect to their usefulness and the quantity and quality of information yielded both individually and in conjunction with each other.

This chapter draws together the information from this multidisciplinary investigation of slope instability in Derbyshire.

11.2 Slope Instability in the Matlock Region

The distribution of landslides in Derbyshire was demonstrated in Figure 1.1 to follow closely the outcrop of the sandstone and shale of the Millstone Grit Series, with the isolated slope failures in the limestone being dominantly associated with interbedded weathered basalts. Furthermore, the locations of those landslides with areas greater than 0.25km^2 show additional factors influencing their distributions. The first of these locations is in the highest part of the county in the north where steep slopes of great relative

relief are conducive to large-scale failure (e.g. Mam Tor, Alport Castles and Kinderscout). The other site for large landslides is on the steep shale slopes adjacent to, and undercut by, the biggest river in the county, the River Derwent (e.g. Oker Hill, Starkholmes and Belper).

In the past, research has tended to concentrate on the northern landslides. However, as the Matlock region is an area where residential and industrial development is concentrated, this area has greater potential for slope instability affecting man's activities. The geomorphological sketch map constructed from aerial photographs (Figure 5.1) shows clearly the sites of major landslips at the points along the valley where the river undercuts steep shale slopes. In the past two decades there have been several cases where landsliding has affected houses and roads in this region (e.g. Matlock Bath, Starkholmes and Oker Hill).

This study has concentrated on Oker Hill and assumes that this landslide is representative of the large-scale slope failures around Matlock. There is evidence of instability on both sides of the hill, although movement on the northern side has been deep-seated while the southern side is characterised by shallower failures. However, it is the southern and eastern sides of Oker Hill that cause most problems as these are the sites of the villages and are crossed by roads. Indeed, at the present time only the eastern end of Oker Hill is being undercut by the Derwent and it was confirmed that there are current problems with slope movement on Sitch Road on this eastern

side (Leadbeater, pers. comm.) (Figure 6.2). Housing has also been affected on Oker Hill by modification of slopes for gardens and excavations for foundations. In one case the foundations were of inadequate design for a house on such ground which lead to dismantling and rebuilding.

It is likely that after the Devensian the river undercut Oker Hill on the northern side for longer periods of time, either by the river channel being adjacent to the foot of the slope through normal meander migration or by increased discharge following snowmelt and after heavy prolonged rainfall. At times of flood the narrow limestone gorge would have restricted the free flow of water down the valley thus causing a bottleneck and flood water would be held up in Darley Dale. Consequently, the possibility of landsliding by undercutting and by high pore-water pressures acting within the slopes would be increased. It is postulated that such conditions were the trigger mechanism for landsliding on the north-facing slope of Oker Hill.

From field mapping the morphology of the deep-seated landslide on the north face of Oker Hill was defined (Figures 6.5 and 6.7). As the upper part of the landslide is narrower than the area of rotated slump blocks in the middle region of the hillslope, it would appear that these multiple rotations have been regressive, working back upslope. This was probably the result of decreasing support at the foot of the hillslope, due to undercutting by the River Derwent, reducing the shearing resistance of the shale mass. The backscar of

the landslide is vegetated with small trees, bushes and grass indicating that the main period of movement has long since ceased. However, there are several indications of recent slope instability that were noted whilst mapping: (i) tree stumps and gateposts leaning at an angle, (ii) small scars in the steep shale slopes, and (iii) tracks blocked by earth slumps (now cleared). Tension cracks are present at the crown of the landslide and they often appear to have been widened by the burrowing activity of animals. These burrows may even increase the potential for further slippage as they allow easier access of water into the hillside.

The deep-seated rotational movement gives way to flow in the lower slopes indicating high moisture content at the time of failure. Other flow features were noted elsewhere on Oker Hill. For example, in the upper part of the landslide there is a narrow track of a mudflow originating in a steep slope which was probably the backscar of a previous slump (Figure 6.7). Although the main slip movement is likely to have taken place several thousand years ago, recent flow type movement is found on the southern side of Oker Hill at Reilly's Bog; this mudflow has been dated at fifty to sixty years old, a time when the climatic conditions and geomorphic processes were the same as those of today. This suggests that high moisture content within the hillslopes is still an important consideration in slope instability in this area, as it was after the end of the Devensian.

Denness (1972) explains the importance of ground water held within permeable strata overlying impermeable strata in slope instability in

terms of the "reservoir principle". Ground water is held within the permeable layer (the reservoir) and is gradually discharged at the spring line at the top of the lower impermeable layer. This surface zone of the impermeable layer becomes softer due to the high water content and deforms under stresses caused by gravity and the weight of the overlying rock. When slope failure occurs the disturbed material takes up more water and the final movement may be a more or less viscous flow of debris. Considering the fact that the rainfall catchment area of Oker Hill is so small, the amount of water present is remarkable and, consequently, the water-holding capacity of the hill would appear to be high. It would appear that landsliding has increased the porosity and permeability of the shale through fracturing, thus allowing storage and continuous discharge of ground water throughout the year.

It is suggested that conditions at Oker Hill are suitable for the reservoir principle of mass movement to be operative, and it is also proposed that it may have been a factor in slope instability at this site during the period of major instability. However, Denness (1972) states that the installation of simple drainage of the water-bearing stratum is sufficient to stabilise landslides caused by this process and the slide mapped in detail at Oker Hill (Figure 6.7) has several agricultural drains channelling water from seepage points to water troughs for cattle. Therefore, these simple drains may be contributing to the stabilisation of the landslide. It should also be remembered that springs and seeps act as a release to the build up of water pressure within the shale and thus contribute to slope

stability.

Two springs which precipitate ochre (an iron oxide crust) on emergence (Plate 6.1) were found on Oker Hill. A similar ochreous spring occurs on the Mam Tor landslide. Research into this by Vear (1981) has demonstrated that the ochre is a product of pyrite weathering of the shale. This chemical breakdown of the pyrite leads to a net volume loss of the shale resulting in an overall deterioration of the rock. It is believed that this process may be responsible for the periodic major movements experienced on the Mam Tor landslide. It follows that the presence of similar ochreous springs on Oker Hill is also indicative of pyrite weathering of the shale and may thus be evidence of continued weakening of the rock mass. Ochreous springs are common on the Namurian shale slopes of Derbyshire (Farey, 1811; Naylor, 1983; Watson, 1811) and may indicate areas within the shale where pyrite oxidation is particularly active. Consequently, if other conditions are favourable for landsliding (i.e. steep slopes, slope undercutting) these slopes may have greater potential for failure. Farey (1811) provides a list of the locations of many ochreous, chalybeate and sulphurous springs.

A core of shale through this landslide was analysed to assess the influence of pyrite oxidation on slope stability in the Matlock region. Detailed logging of core material through the Oker Hill landslide revealed several planes of discontinuity which may be slip planes and, together with mineralogical and geochemical analyses, confirmed the presence of pyrite oxidation within the shale. Pyrite

oxidation leads to other chemical reactions as represented in Figure 7.1 (Vear, 1981) which may also lead to volume changes, for example, the dissolution of calcite and dolomite, clay dissolution, and precipitation of weathering products (i.e. gypsum, jarosite, iron oxides and hydroxides). Samples of shale throughout the core material were analysed to determine if the slip planes identified were characterised by such mineralogical and geochemical changes.

Pyrite oxidation is occurring within the shale of Oker Hill at the base of the weathering zone. This is shown by the presence of pyrite in the iron-stained shale immediately above 9.65 metres (Appendix 3). The subsequent reactions in which the weathering products of pyrite oxidation take part will be confined to the shale at and below this depth as this is the zone in which ground water will become charged with the H^+ ions from H_2SO_4. The shale above 9.4 metres will experience less weathering as most, if not all, of the pyrite has been destroyed and therefore, the only sources of H^+ ions are from rainwater and organic matter. Not all of the iron released from pyrite oxidation is precipitated within the shale as iron oxides or hydroxides, some iron is carried by the ground waters to the surface where it is precipitated, however such ochreous springs are not common. It would have been interesting to have analysed the composition of the ground waters at Oker Hill landslide, however time would not allow.

Analysis of the shale from Borehole 2 by XRD showed no distinct mineralogical differences between the slip planes and the surrounding

shale. However, if the slip plane is within the weathered shale it will not differ greatly in mineralogy or geochemistry to the surrounding shale unless it is a zone of significantly greater permeability. Also, calcite is not present in sufficient quantity (Schultz, 1964) to enable gypsum formation on reaction with sulphate from pyrite oxidation. In addition, the analysis of the whole rock samples was not quantitative and therefore, any differences in mineralogy are noted as the presence or absence of a mineral rather than relative quantities of each mineral. The first occurrence of pyrite at 9.40 metres may, however, be associated with the discontinuity at 9.65 metres as the band of shale between 9.40 and 9.65 metres appears to be the present zone of active weathering as discussed above. The proposed slip planes were found to have different geochemical characteristics to the adjacent shale, these are summarised in Table 10.2.

From the observations of the mineralogical and geochemical composition of the proposed slip planes the hypothesis that there is a change in mineralogy and/or geochemistry at the slip plane can be accepted on the assumption that these planes are slip planes. Most confidence can be placed in the interpretation of the discontinuities at 6.80 and 8.75 to 8.85 metres being slip planes on the basis of the physical appearance of the core material and geochemical characteristics described above. The contact between iron-stained and fresh shale at 9.65 metres is best interpreted as the present base of the weathering zone, however visual examination of the contact did reveal an apparent change in the angle of inclination of

the bedding planes which could have been produced by slope failure. Also, the presence of polished faces in the shale between 10.10 and 10.45 metres suggests that this shale has taken up some movement although displacement appears to be minimal. This zone may, therefore, have accommodated some of the strain involved in slope failure along the plane at 9.65 metres. For pyrite to still be present this slip plane would have to be a zone of insignificantly increased permeability or one in which conditions were non-oxidising.

Whether any compositional difference is pre- or post-slope failure it is difficult to judge, although, as a slip plane is a plane of increased permeability, percolating waters can be expected to alter this zone either by the destruction of minerals by weathering or by the precipitation of weathering products.

It should be remembered that the nature of this landslide suggests that there may be more than one slip plane within the core as it is a multiple failure. Due to the method of coring and sample extraction it is very probable that not all the slip planes were sampled. It has to be acknowledged that this is a major limitation to this work as the core material obtained may not include the slip plane.

Further research should compare the differences in mineralogy and geochemistry between failed and <u>in situ</u> slopes in the same horizon of shale which would arise through slope failure and weathering. This should also involve the measurement of the engineering properties of the shale to assess the influence of shale composition on its

strength (this was not possible in this study due to the method of sampling).

11.3 Assessment of the Techniques Used in Slope Instability Studies of Matlock

Table 11.1 contains assessments of the techniques of remote sensing, ground and subsurface investigations used in this study of slope instability in the Matlock region. As little previous work had been carried out on the role of satellite imagery in slope stability studies the assessment of Landsat imagery will be discussed in greatest detail.

Landslides cannot be expected to have a characteristic spectral signature as they are inhomogeneous features with variations in material, vegetation, moisture content, and slope angle. Consequently, their detection from all types of remotely-sensed imagery must be concerned with pattern recognition involving the identification of areas of anomalous character with respect to the surrounding conditions. The features which may thus be detected are morphology, drainage, and vegetation (Crozier, 1984). Procedures were developed for both the direct detection of slope instability and for the recognition of factors contributing to instability on Landsat Thematic Mapper imagery of the Edale region of north Derbyshire. The latter approach led to the production of a landslide potential hazard zonation map. Direct detection of landslides was poor for the

TABLE 11.1 ASSESSMENT OF TECHNIQUES EMPLOYED IN THE STUDY OF LANDSLIDING IN DERBYSHIRE (see text for discussion)

	ELEMENTS OF SLOPE STABILITY STUDIES (see below) (subjective "value" assessment made on an ascending scale from 1 to 10 (best))							
TECHNIQUE	I	II	III	IV	V	VI	VII	VIII
(a) Landsat TM imagery	2	2	-	-	-	-	1	b,c,e
(b) Panchromatic aerial photography	8	9	9	-	1	-	8	c,d,e
(c) Infrared colour photography (hand-held/aerial)	-/9	6/9	7/9	-	6/6	-	-/8	b,d,e
(d) Morphological mapping	7	9	10	-	-	-	7	b,e,f
(e) Geomorphological mapping	10	10	10	5	4	4	7	b,c,d, f,g,h
(f) Surveying	7	7	10	-	-	-	10	e
(g) Slope profiling	5	6	6	8	-	-	8	b,e,h, i
(h) Borehole logging	2	5	-	9	7	10	-	b,c,e, g,i
(i) Mineralogical and geochemical analyses	2	-	-	5	-	10	-	e,g,h

I Identification of potentially unstable slopes
II Identification of landslides
III Identification of surface form of landslide
IV Locating slip plane
V Information on water conditions within landslide or slope
VI Information on material of slipped mass
VII Monitoring of slip movement
VIII Combinations of techniques yielding most information

following reasons:

(i) area of failed ground too small to occupy a sufficient number of pixels on the image for recognition.

(ii) landslide has weak morphological expression due to either degrading, or shallow nature of failure.

(iii) for those landslides with strong morphological expression aspect will influence their detection: those landslides in valleys trending northwest to southeast will be suppressed.

(iv) tree cover, whether partial or complete, will obscure the landslide.

It is concluded that the classification of an area of ground as a landslide from Landsat imagery can be done with greatest confidence if the outline of the landslide is expressed as a result of the difference in nature of the failed ground from the stable ground, whether the difference is due to morphology, and therefore shadow and highlight, or vegetation, or drainage. Within this area, tonal mottling or spectral reflectances contrasting with the surrounding land increase the confidence of classification as a landslide. However, some causes of mottling on an image, such as glacial deposits and varying vegetation conditions, may have nothing to do with slope instability, consequently, mottling should not be considered in isolation.

Therefore, landslide recognition from Landsat imagery, as recommended

above, uses the same principles as aerial photo-interpretation, although aerial photographs have the main advantages of greater spatial resolution and stereoscopic viewing. The stereoscopic capability of SPOT will greatly improve landslide detection on the basis of form from satellites, but it is probable that, due to the cost and poor spatial resolution, it will be unable to compete with aerial photography. Stereoscopic Landsat imagery may be created by introducing parallax into a Landsat image, either by using digital terrain elevation data or using information already present in the image (Batson et al., 1976; Eliason et al., 1981; Siegal and Gillespie, 1980). In its monoscopic form Landsat appears to be of little use in detecting landslides in the Edale region.

With respect to the recognition of factors contributing to instability (e.g. slope angle, lithology, drainage), it was concluded that it is possible to produce a very basic landslide hazard assessment for Edale. The hazard map thus produced indicates areas which should be investigated in more detail and is, consequently, most useful at the reconnaissance level of a slope instability survey. However, the information extracted from the images would have been more accurately obtained from aerial photographs and existing maps and in greater detail.

With this in mind it must be said that for adequately mapped and accessible areas Landsat imagery is of very little use in landslide hazard assessment. Although, if the significance of lineaments can be determined and shown to influence slope instability by

representing weak zones within the rock and lines of high pore-water pressure, then Landsat imagery would provide information not readily available from any ground-based source.

Landsat imagery of Matlock provided very little information on slope instability due to the complexity of the images resulting from high frequency spatially-variable ground cover influencing the visual interpretation of relief, drainage and slope stability by distracting from, and masking of, the features of interest.

The main conclusions drawn from assessing the use of Landsat imagery in studying landslides in the Edale region were that only landslides with certain characteristics of morphology, vegetation cover and aspect are likely to be detected, and that any hazard assessment of slope instability can only be very basic. Consequently, Landsat imagery will be of greatest use at the reconnaissance stage of landslide investigations in areas with poor map coverage and/or poor accessibility. This imagery should be used in conjunction with ground information from aerial photography and field mapping.

Other types of remote sensing may be of potential use in landslide and lineament recognition and for the regional measurement of soil moisture. These are discussed in Chapters 2 and 4, and it is recommended that any further work on the use of remote sensing in landslide studies should focus on radar and thermal infrared imagery.

Aerial photo-interpretation is an invaluable technique in both

specific slope instability studies and general geomorphological surveys (Table 11.1). It provides a regional view of an area, as does Landsat, but the much greater spatial resolution and stereoscopic capability allow a more detailed and accurate analysis. This synoptic viewing enables landforms to be studied easily in the context of situation, i.e. in relation to the surrounding environment. Although the types of photography used in this study are very limited it is still possible to draw some conclusions. Stereoscopic aerial photographs can be used to produce morphological and geomorphological maps, the former involving the mapping of surface form and the latter providing the interpretation of the morphology; interpretation should be verified in the field. The photographs can be studied at several scales by the enlargement of the standard prints.

A variety of films may be employed in aerial surveys: panchromatic, colour, black and white infrared and colour infrared. Colour and colour infrared photography provide more information on vegetation type and land cover in general. Although the ground-based colour infrared photography proved to be of little advantage over normal colour photography at such a close range, it was evident that it provided greater contrast between vegetation types. Therefore, it is understandable that this type of film is so useful in aerial surveys involving vegetation. It should also be noted that the time of the year will affect infrared photography as vegetation growth is dependent on season. This variation in vegetation throughout the year will influence the use of infrared imagery in detecting such

factors as soil moisture conditions. The effect of season on the study of slope instability by photography is, therefore, of great importance.

Aerial photography in general is of great use in studying landsliding as it provides much information about the geomorphology of the area of interest and enables an understanding of the interaction of the various processes in operation which may affect slope stability.

Field mapping was essential for the recognition of rotated slump blocks and signs of present instability. It also provided much information on ground water conditions and indications of pyrite oxidation within the shale (Table 11.1). In addition to morphological and geomorphological field mapping the more accurate technique of surveying using an Autoset level was employed. The main advantage of levelling is that the edges of the slump blocks and hence the morphology can be mapped accurately both in position and height. This is of particular importance for monitoring movement of landslides by repeated surveying (Table 11.1), and for instances where an accurate detailed map is necessary. However, as levelling is very time-consuming and requires two people, morphological field mapping is ideal for quick surveys which do not require extreme accuracy.

The main advantage of mapping from field work as opposed to aerial photography is that more detailed information can be obtained (Table 11.1). For example, surface water features and their influence on the

vegetation can be seen in more detail, and evidence of recent instability may be present which is not visible on the aerial photographs. Slope gradients are much more easily measured in the field either by slope profiling as in Figure 6.11 or by measuring the angle of slope units as in the morphological map of Figure 6.5. Where aerial photography has the advantage of providing a regional setting for a feature of interest, field work provides the detailed site information.

Finally, slope profiling, as well as providing information on slope form and helping in the recognition of the component parts of the landslide, enables an estimation of the position of the slip plane to be drawn. However, in this study there was a discrepancy between the predicted depth and the depth to the proposed 9.65 metre basal slip plane. Used in conjunction with data from several boreholes, slope profiling can provide a picture of subsurface conditions (i.e. water table, slip plane) down the slope (e.g. Figure 8.3).

All these field techniques aid in the recognition and assessment of slope instability and provide information which is of use in further studies such as subsurface investigations. In addition, landform recognition from field mapping and aerial photo-interpretation enables the optimum sites for a subsurface investigation to be located such that most information can be gained from this more costly and time-consuming technique.

On site borehole logging provided information on ground water levels

and perched water tables as well as lithology. However, the possible locations of slip planes could only be identified by detailed logging of the somewhat disturbed core material. The problems caused by the relatively poor quality of this core material obtained by the shell and auger rig shows the need for continuous or staggered sampling as described in Chapter 10.5. Trial pits are recommended for identifying shallow slip planes and for detailed logging and sampling of the strata with the minimum of disturbance.

Mineralogical and geochemical analyses enable horizons of shale to be defined which may contribute to slope instability. For example, the high concentrations of organophile elements indicate zones of high organic matter content which may provide carbonic acid to the percolating waters to attack minerals in the shale below. Likewise, pyrite-rich shale is a source of sulphuric acid and the destruction of pyrite by oxidation leads to the deterioration in quality of the rock. Slip planes in shale may exhibit certain geochemical characteristics such as decreases in the Fe_2O_3 content and the K_2O/Al_2O_3 ratio (Early and Skempton, 1972) associated with the destruction of iron minerals (particularly pyrite) and the leaching of elements from clays by ground water flowing along these zones of increased permeability. Therefore, geochemical composition can provide an indication of the location of slip planes although these need to be verified by visual evidence of failure. It is also possible to study the weathering profile through the landslide from the core. With the knowledge of the location of the slip planes, the weathering grades and mineralogical and geochemical data on the

shale, the processes which lead to the deterioration of the rock quality and thus increase potential slope instability may be identified.

Considering the equipment and time involved in each of these techniques it has been found in this study that stereoscopic aerial photo-interpretation combined with field mapping of morphology and geomorphology are the techniques which provide most information on slope instability in the Matlock region. Field mapping has been shown to provide information not only on ground conditions but also on subsurface conditions by the inference of pyrite oxidation within the shale by the presence of ochreous springs. Together, geomorphological aerial photo-interpretation and field mapping enable the study of a specific landform in relation to its surrounding environment.

REFERENCES

Al-Dabbagh, T.H. 1985 A study of residual shear strength of Namurian Shale in respect of slopes in North Derbyshire. Unpublished PhD Thesis, University of Sheffield.

Alfoldi, T.T. 1974 Landslide analysis and susceptibility mapping, Ontario. Proc. Symp. Remote Sens. and Photo-Interpretation, 1, 379-387.

Allen, J.R.L. 1960 The Mam Tor sandstones: a turbidite facies of the Namurian deltas of Derbyshire. J. Sed. Petrol., 30, 193-208.

Amin, M.A. 1979 Geochemistry and mineralogy of Namurian sediments in the Pennine Basin, England. Unpublished PhD Thesis, University of Sheffield.

Anderton, R., Bridges, P.H., Leeder, M.R. and Sellwood, B.W. 1979 A Dynamic Stratigraphy of the British Isles: A Study in Crustal Evolution. George Allen and Unwin, London, 301pp.

Apted, J.P. 1977 Effects of weathering on some geotechnical properties of London Clay. Unpublished PhD Thesis, Univ. of London.

Arman, A. and McManis, K.L. 1976 Effects of storage and extrusion on sample properties. Soil Specimen Preparation for Laboratory Testing, Am. Soc. Testing and Materials, Spec. Tech. Publ. 599, 66-87.

Astaras, T. and Silleas, N. 1984 Land classification of part of central Macedonia (Greece) by the use of remote-sensing techniques. Int. J. Remote Sens., 5(2), 289-302.

Bastiansen, R., Moum, J., and Rosenqvist, I.Th. 1957 Some investigations of alum slate in construction. Norw. Geotech. Inst. Publ. 22, 69pp.

Bateman, T. 184 Vestiges of the Antiquities of Derbyshire. John Russell Smith, London, 246pp.

Batson, R.M., Edwards, K. and Eliason, E.M. 1976 Synthetic stereo and Landsat pictures. Photogramm. Eng. Remote Sens., 42(10), 1279-1284.

Berner, R.A. 1984 Sedimentary pyrite formation: an update. Geochim. Cosmochim. Acta, 48, 605-615.

Berner, R.A. and Raiswell, R. 1984 C/S method for distinguishing freshwater from marine sedimentary rocks. Geology, 12, 365-368.

Bjerrum, L. 1967 Progressive failure in slopes of over-consolidated plastic clay and clay shales. J. Soil Mech. Found. Div., Proc. Am. Soc. Civ. Eng., 93, No. SM5, 3-49.

Bonnard, C. 1983 Determination of slow landslide activity by multidisciplinary measurement techniques. in: Kovari, K., ed. Field Measurements in Geomechanics. Proc. Int. Symp., Zurich, September 5-8, A.A. Balkema, Rottedam, 619-638.

Brown, G., ed. 1961 The X-Ray Identification and Crystal Structure of Clay Minerals. Mineralogical Society (Clay Minerals Group), London, 544pp.

Brown, J.B. 1971 Jarosite - goethite stabilities at 25°C, 1 atm. Mineral. Deposita, 6, 245-252.

Brunsden, D. 1979 Mass movements. in: Embleton, C. & Thornes, J., eds., Process in Geomorphology. Edward Arnold Ltd., 130-186.

Brunsden, D. and Jones, D.K.C. 1972 The morphology of degraded landslide slopes in South West Dorset. Q. J. Eng. Geol., 5, 205-222.

Burnett, A.D. and Fookes, P.G. 1974 A regional engineering geological study of the London Clay in the London and Hampshire Basins. Q. J. Eng. Geol., 7, 257-295.

Burns, K.L. & Brown, G.H. 1978 Human perception of lineaments. Remote Sens. Environ., 7(2), 163-178.

Burns, K.L., Shepherd, J. & Berman, M. 1976 Reproducibility of geological lineaments and other discrete features interpreted from imagery: measurement by a coefficient of association. Remote Sens. Environ., 5, 267-301.

Cancelli, A. 1977 Residual shear strength and stability analysis of a landslide in fissured over-consolidated clays. Bull. Int. Assoc. Eng. Geol., No.16, (Thematic Issue on Landslides and Other Mass Movements), 193-197.

Carrara, A., Catalono, E., Sorriso Valvo, M., Realli, C. and Ossi, I. 1978 Digital terrain analysis for land evaluation. Geol. Appl. Idrogeol., 13, 69-127.

Chandler, R.J. 1969 The effect of weathering on the shear strength properties of Keuper Marl. Geotechniq., 19, 321-334.

1972 Lias Clay: Weathering processes and their effect on shear strength. Geotechniq., 22, 403-431.

Chandler, R.J. and Apted, J.P. 1988 The effect of weathering on the strength of London Clay. Q. J. Eng. Geol., 21, 59-68.

Chao, G.Y. 1969 2θ (Cu) Table for Common Minerals. Geol. Paper

69-2, Carleton University, Ottawa, Canada.

Clayton, K.M. 1968 Structure-surface relationships in the middle part of the Derwent Basin. East Midl. Geogr., 4(6), 321-328.

Collins, R.J. 1976 A method for measuring the mineralogical variation of spoils from British colleries. Clay Miner., 11, 31-50.

Cooke, R.U., Brunsden, D., Doornkamp, J.C., and Jones, D.K.C. 1982 Urban Geomorphology in Drylands. Oxford University Press, Oxford, 324pp.

Cooke, R.U. & Doornkamp, J.C. 1974 Geomorphology in Environmental Management. Oxford University Press, Oxford, 413pp.

Cosgrove, M.E. and Hodson, F. 1963 Jarosite from Meal Bank Quarry, Ingleton, Yorkshire. Proc. Yorks. Geol. Soc., 34, 81-90.

Cripps, J.C. and Taylor, R.K. 1981 The engineering properties of mudrocks. Q. J. Eng. Geol., 14, 325-346.

Cross, M. 1987 An engineering geomorphological investigation of slope instability in the Peak District of Derbyshire. Unpublished PhD Thesis, University of Nottingham.

Crozier, M.J. 1984 Field assessment of slope instability. in:

Brunsden, D. and Prior, D., eds. Slope Instability. John Wiley and Son, Chichester, 103-142.

Cubbitt, J.M. 1975 A regression technique for the analysis of shales by X-ray diffraction. J. Sed. Petrol., 45, 546-553.

Curran, P.J. 1981 The estimation of the surface moisture of a vegetated soil using aerial infrared photography. Int. J. Remote Sens., 2, 369-378.

1985 Principles of Remote Sensing. Longman, London, 282pp.

Curtis, C.D. 1967 Diagenetic iron minerals in some British Carboniferous sediments. Geochim. Cosmochim. Acta, 31, 2109-2123.

1969 Trace element distribution in some British Carboniferous sediments. Geochim. Cosmochim. Acta, 33, 519-523.

Curtis, L.F. 1973 The application of photography to soil mapping from the air. in: Cruise, J. and Newman, A., eds. Photographic Techniques in Scientific Research I. Academic Press, London, 57-110.

Dalrymple, J.B., Blong, R.J. and Conacher,A.J. 1968 A hypothetical nine unit land surface model. Zeitschr. Geomorphologie, 12, 60-76.

Deer, W.A., Howie, R.A. and Zussman, J. 1966 An Introduction to the Rock Forming Minerals. Longman, England, 528pp.

Degens, E.T. 1965 Geochemistry of Sediments: A Brief Survey. Prentice-Hall, Inc., New Jersey. 342pp.

Demek, J., ed. 1972 Manual of Detailed Geomorphological Mapping. Academia, Prague, 368pp.

Denness, B. 1972 The Reservoir Principle of Mass Movement. Inst. Geol. Sci., Rep. No. 72/7, 13pp.

Donker, N.H.W. and Meijerink, A.M.J. 1977 Digital processing Landsat imagery to produce a mazimum impression .of terrain ruggedness. ITC J., 1977-4, 683-704.

Doornkamp, J.C. 1971 The Derwent gorge below Matlock. East Midl. Geogr., 5(3), 142-143.

Dougherty, M.T. and Barsotti, N.J. 1972 Structural damage and potentially expansive sulphide minerals. Bull. Assoc. Eng. Geol., 9, 105-125.

Drury, S.A. 1986 Remote sensing of geological structure in temperate agricultural terrains. Geol. Mag., 123(2), 113-121.

Dumbleton, M.J. and West, G. 1966 Some factors affecting the relation between the clay minerals in soils and their plasticity. Clay Miner., 6, 179-193.

Early, K.R. and Skempton, A.W. 1972 Investigations of the landslide at Walton's Wood, Staffordshire. Q. J. Eng. Geol., 5, 19-41.

Edwards, M. and Trotter, F.M. 1954 The Pennines and Adjacent Areas. 3rd Edn. (British Regional Geology). Inst. Geol. Sci., HMSO, London, 86pp.

Eliason, P.T., Soderblom, L.A. and Chavez, P.S. 1981 Extraction of topographic and spectral albedo information from multispectral images. Photogramm. Eng. Remote Sens., 48(11), 1571-1579.

Elkington, M.D. and Hogg, J. 1981 The characterisation of soil moisture content and actual evapotranspiration from crop canopies using thermal infrared remote sensing. in: Allan, J.A. and Bradshaw, M., eds. Remote Sensing in Geological and Terrain Studies. Remote Sensing Society, Reading, 69-90.

Farey, J. 1811 General View of the Agriculture and Minerals of Derbyshire. Vol. 1. The Board of Agriculture, London, 532pp.

Fellows, P.M. and Spears, D.A. 1978 The determination of feldspars in mudrocks using an X-ray powder diffraction method. Clays

Clay Miner., 26, 231-236.

Fookes, P.G., Dearman, W.R. and Franklin, J.A. 1971 Some engineering aspects of rock weathering with field examples from Dartmoor and elsewhere. Q. J. Eng. Geol., 4, 139-185.

Fookes, P.G. and Horswill, P. 1969 Discussion on engineering grading zones. in: Proc. Conf. In Situ Testing Soils and Rock, Inst. Civ. Engrs, London, 53-57.

Franks, J.W. and Johnson, R.H. 1964 Pollen analytical dating of a Derbyshire landslide. New Phytol., 63, 209-216.

Gagnon, H. 1975 Remote sensing of landslide hazards on quick clays of Eastern Canada. Proc. 10th Int. Symp. Remote Sens. Environ., Environ. Res. Inst. Michigan, Ann Arbor, 803-810.

Gallois, R.W. and Horton, A. 1981 Field investigation of British Mesozoic and Tertiary mudstones. Q. J. Eng. Geol., 14, 311-323.

Garrels, R.M. and Thompson, M.E. 1960 Oxidation of pyrite by iron sulfate solutions. Am. J. Sci., 258A, 57-67.

Geological Society Engineering Group Working Party 1970 The logging of rock cores for engineering purposes. Q. J. Eng. Geol., 3, 1-24.

1972 The preparation of maps and plans in terms of engineering geology. Q. J. Eng. Geol., 5, 293-381.

Goetz, A.F.H. & Rowan, L.C. 1981 Geologic remote sensing. Science, 211, 781-791.

Goetz, A.F.H., Rock, B.N. and Rowan, L.C. 1983 Remote sensing for exploration: an overview. Econ. Geol., 78, 573-590.

Gold, D.P. & Krohn, D.M. 1976 Stop 12 - Bald Eagle Road cut. in: Gold, D.P. & Parizek, R.R., eds. Field Guide to Lineaments and Fractures in Central Pennsylvania. 2nd Int. Conf. New Basement Tectonics, The Pennsylvania State University, 70-72.

Grainger, P. 1983 Aspects of the engineering geology of mudrocks, with reference to the Crackington Formation of South-West England. Unpublished PhD Thesis, University of Exeter.

1984 The classification of mudrocks for engineering purposes. Q. J. Eng. Geol., 17, 381-387.

Grainger, P. and Harris, J. 1986 Weathering and slope stability on Upper Carboniferous mudrocks in south-west England. Q. J. Eng. Geol., 19, 155-173.

GSL 1987 Landsliding in Britain. Report for the Department of the Environment prepared under contract by Geomorphological Services Ltd.

Gurney, R.J. 1979 The estimation of soil moisture content and actual evapotranspiration using thermal infrared remote sensing. in: Allan, J.A. and Bradshaw, M., eds. Remote Sensing and National Mapping. Remote Sensing Society, Reading, 101-109.

Hansen, A. 1984 Landslide hazard analysis. in: Brunsden, D. and Prior, D.B., eds. Slope Instability. John Wiley and Sons Ltd., Chichester, 523-595.

Harvey, P.K. and Atkin, B.P. 1982 Automated X-ray fluorescence analysis. in: Sampling and Analysis for the Mineral Industry. Inst. Min. Metal. Spec. Publ.

Harvey, P.K., Taylor, D.M., Hendry, R.D. and Bancroft, F. 1973 An accurate fusion method for the analysis of rocks and chemically related materials by X-ray fluorescence spectrometry. X-Ray Spectrom., 2, 33-44.

Henkel, D.J. and Skempton, A.W. 1954 A landslide at Jackfield. Proc. Europ. Conf. Stability of Earth Slopes, 1, Stockholm, 90-101.

Hicks, B.G. and Smith, R.D. 1981 Management of steeplands impacts by landslide hazard zonation and risk evaluation. J. Hydrol N.Z., 20, 63-70.

Higginbottom, I.E. and Fookes, P.G. 1970 Engineering aspects of periglacial features in Britain. Q. J. Eng. Geol., 3, 85-117.

Hirst, D.M. and Kaye, M.J. 1971 Factors controlling the mineralogy and chemistry of an Upper Visean sedimentary sequence from Rockhope, County Durham. Chem. Geol., 8, 37-59.

Howard, J. and Mitchell, C. 1980 Phytogeomorphic classification of the landscape. Geoforum, 11, 85-106.

Hunt, G.R. and Salisbury, J.W. 1971 Visible and near-infrared spectra of minerals and rocks: ii. carbonates. Mod. Geol., 2, 23-30.

1976 Visible and near-infrared spectra of minerals and rocks: xi. sedimentary rocks. Mod. Geol., 5, 211-217.

Huntington, J.F. & Raiche, A.P. 1978 A multi-attribute method for comparing geological lineament interpretation. Remote Sens. Environ., 7, 145-161.

Hutchinson, J.N. 1982 Methods of locating slip surfaces in landslides. British Geomorph. Res. Grp., Techn. Bull. No. 30,

30pp.

Idso, S.B., Jackson, R.D. and Reginato, R.J. 1975 Detection of soil moisture by remote surveillance. Am. Sci., 63, 549-557.

Johnson, R.H. 1965 A study of the Charlesworth landslides near Glossop, North Derbyshire. Inst. Br. Geogr. Trans. and Papers No. 37, 111-126.

Johnson, R.H. 1980 Hillslope stability and landslide hazard - a case study from Longdendale, north Derbyshire, England. Proc. Geol. Assoc., 91, 315-325.

Johnson, R.H. 1981 Four maps for Longdendale - a geomorphological contribution to environmental management in an upland Pennine valley. Manchester Geogr., 2(2), 6-34.

Johnson, R.H. and Vaughan, R.D. 1983 The Alport Castles, Derbyshire: a south Pennine slope and its geomorphic history. East Midl. Geogr., 8, 79-88.

Johnson, R.H. and Walthall, S. 1979 The Longdendale landslides. Geol. J., 14(2), 135-158.

Kapur, A. 1974 The Perception of Flood Hazard in the Derwent Valley, Derbyshire. Unpublished BA Thesis, Geog. Dept., University of Nottingham.

Kennard, M.F., Knill, J.L. and Vaughan, P.R. 1967 The geotechnical properties and behaviour of Carboniferous shale at Balderhead dam. Q. J. Eng. Geol., 1, 3-24.

Kertesz, A. 1979 The representation of the morphology of slopes on engineering geomorphological maps with special reference to slope morphometry. Q. J. Eng. Geol., 12, 235-241.

Kienholz, H. 1978 Maps of geomorphology and natural hazards of Grindelwald, Switzerland, scale 1:10000. Arct. Alp. Res., 10, 169-184.

King, C.A.M. 1966 Geomorphology. in: Edwards, K.C., ed. Nottingham and Its Region. British Association for the Advancement of Science, Nottingham, 41-59.

Kondratyev, K.Y., Vassilyev, O.B., Grigoryev, A.A. and Ivanian, G.A. 1973 An analysis of the Earth's Resources Satellite (ERTS-1) data. Remote Sens. Environ., 2, 273-283.

Krauskopf, K.B. 1979 Introduction to Geochemistry. 2nd Edn. McGraw-Hill, New York. 617pp.

Kritikos, H.N. and Shuie, J. 1979 Microwave sensing from orbit. IEEE Spectr., 16(8), 34-41.

Kuznetsov, S.I., Ivanov, M.V. and Lyalikova, N.N. 1963 Introduction to Geological Microbiology. McGraw-Hill, New York, 252pp.

Lake, S.D., Munday, T.J. & Dewey, J.F. 1984 Lineament mapping and analysis in the Wessex basin of southern England: a comparison between MSS and TM data. in: Satellite Remote Sensing - Review and Preview. Proc. 10th Anniv. Int. Conf., Remote Sensing Society, Reading, 361-374.

Leadbeater, A.D. 1985 A57 Snake Pass, remedial work to slip near Alport Bridge. in: Failures in Earthworks. Inst. Civ. Eng. Symp., Thomas Telford Ltd., London, 29-38.

Leussink, H. and Muller-Kirchenbauer, H. 1967 Determination of the shear strength behaviour of sliding planes caused by geologic features. Proc. Geotech. Conf. Oslo, 1, 131-137.

Levinson, A.A. 1974 Introduction to Exploration Geochemistry. Photopress Incorporated, Illinois, 614pp.

Loffler, E. 1977 Landform interpretation with modern remote sensors - examples from Papua New Guinea. Die Erde, 108, 202-216.

Lillesand, T.M. and Kiefer, R.W. 1979 Remote Sensing and Image Interpretation. John Wiley and Sons, New York, 612pp.

Linton, D.L. 1956 Geomorphology. in: Linton, D.L., ed. Sheffield

and Its Region. British Association for the Advancement of Science, Sheffield, 24-43.

Mahr, T. and Malgot, J. 1978 Zoning maps for regional and urban development based on slope stability. in: Proc. 3rd Int. Congress Int. Assoc. Eng. Geol., 1, 124-137.

Marsland, A. 1971 Shear strength of stiff fissured clays. Build. Res. Stn Curr. Pap., 21/71.

Moore, D.M. 1978 A sample of the Purington Shale prepared as a geochemical standard. J. Sed. Petrol., 48, 995-998.

Morgenstern, N.R. 1968 Shear strength of stiff clay. Proc. Geotechnical Conf. Oslo, 2, 59-71.

Morgenstern, N.R. 1970 Discussion: Black shale heaving at Ottawa, Canada, by R.M. Quigley and R.W. Vogan 1970. Can. Geotech. J., 7, 114-115.

Morgenstern, N.R. and Eigenbrod, K.D. 1974 Classification of argillaceous soils and rocks. J. Geol. Div., Proc. Am. Soc. Civ. Eng., 100, 1137-1156.

Morgenstern, N.R. and Tchalenko, J.S. 1967 Microstructural observations on shear zones from slips in natural clays. Proc. Geotech. Conf. Oslo, 1, 147-152.

Naylor, P.J. 1983 Ancient Wells and Springs of Derbyshire. Scarthin Books, Cromford, 80pp.

Ni, Xiang Shao and He, Min Zhen 1984 Digital Landsat image enhancement for geomorphological mapping of the southern Huariron County of Beijing, China. in: Satellite Remote Sensing - Review and Preview. Proc. 10th Anniv. Int. Conf., Remote Sensing Society, Reading, 421-429.

Nichol, J., Thornton, I., Webb, J.S., Fletcher, W.K., Horsnail, R.F., Khaleelee, J. and Taylor, D. 1970 Regional geochemical reconnaissance of the Derbyshire area. Inst. Geol. Sci. Rep. 70/2, 37pp.

Nicholls, G.D. and Loring, D.H. 1960 Some chemical data on British Carboniferous sediments and their relationship to the clay mineralogy of these rocks. Clay Miner. Bull., 4, 196-207.

Norman, J.W., Leibowitz, T.H. and Fookes, P.G. 1975 Factors affecting the detection of slope instability with air photographs in an area near Sevenoaks, Kent. Q. J. Eng. Geol., 8, 159-176.

Nixon, P.J. 1978 Floor heave in buildings due to the use of pyritic shales as fill material. Chem. Ind., 4, 160-164.

Norrish, K. 1972 Factors in the weathering of mica to vermiculite. Proc. Int. Clay Conf., Madrid, 417-432.

O'Leary, D.W., Freidman, J.D. & Pohn, H.A. 1976 Lineaments, linear, lineation - some proposed new standards for old terms. Geol. Soc. Am. Bull., 87, 1463-69.

Pain, C.F. 1985 Mapping of landforms from Landsat imagery: an example from Eastern New South Wales, Australia. Remote Sens. Environ., 17(1), 55-65.

Parry, D.E. 1978 Some examples of the use of satellite imagery (Landsat) for natural resource mapping in Western Sudan. in: Collins, W.G. and van Genderen, J.L., eds. Remote Sensing Applications in Developing Countries. Remote Sensing Society, Reading, 1-12.

Parry, R.H.G. 1972 Some properties of heavily over-consolidated Lower Oxford Clay at a site near Bedford. Geotechniq., 22, 485-507.

Patton, F.D. and Deere, D.U. 1970 Significant geological factors in rock slope stability. in: van Rensburg, P.W. J., ed. Planning Open Pit Mines (S. Afr. Inst. Min. Metal.), 143-151.

Pearson, M. 1979 Geochemistry of the Hepworth Carboniferous sediment sequence and origin of the diagenetic iron minerals

and concretions. Geochim. Cosmochim. Acta, 43, 927-941.

Penn, S. 1984 Colour enhanced infra-red photography of landslips. Q. J. Eng. Geol., 17, ii-v.

Penner, E., Eden, W.J. and Gillott, J.E. 1973 Floor heave due to biochemical weathering of shale. Proc. 8th Int. Conf. Soil Mech. Found. Eng., 2, Moscow, 151-158.

Penner, E., Eden, W.J. and Grattan-Bellew, P.E. 1972 Expansion of pyritic shales. Can. Build. Dig., Div. Build. Res., National Research Council of Canada, 152.1-152.4.

Petley, D.J. 1984 Ground investigation, sampling, testing for studies of slope instability. in: Brunsden, D. and Prior, D.B., eds. Slope Instability. John Wiley and Sons, Chichester, 67-101.

Pettijohn, F.J. 1975 Sedimentary Rocks. 3rd Edn. Harper and Row, New York, 628pp.

Piteau, D.R. 1970 Geological factors significant to the stability of slopes cut in rock. in: van Rensburg, P.W. J., ed. Planning Open Pit Mines (S. Afr. Inst. Min. Metal.), 33-53.

Pitty, A.F. 1968 A simple device for the field measurement of hillslopes. J. Geol., 76, 717-720.

Prior, D.B. and Graham, J. 1974 Landslides in the Magho district of Fermanagh, Northern Ireland. Eng. Geol., 8, 341-359.

Pulinowa, M.Z., Pawlak, W. and Woropajew, E. 1977 A contribution to the problem of morphogenetical principles of landslide mapping. Bull. Int. Assoc. Eng. Geol., 16, 56-62.

Quigley, R.M. and Vogan, R.W. 1970 Black shale heaving at Ottawa, Canada. Can. Geotech. J., 7, 106-115.

Ramsbottom, W.H.C., Rhys, G.H. and Smith, E.G. 1962 Boreholes in the Carboniferous rocks of the Ashover district, Derbyshire. Bull. Geol. Surv. G.B., 19, 75-168.

Ramsbottom, W.H.C., Sabine, P.A., Dangerfield, J. and Sabine, P.W. 1981 Mudrocks in the Carboniferous of Britain. Q. J. Eng. Geol., 14, 257-262.

Ray, R.G. 1960 Aerial photographs in geologic interpretation and mapping. Geol. Soc. Am. Prof. Paper 373, 230pp.

Redda, A., Hansom, J.D. and Brown, R.D. 1985 Edale End Landslide. in: Briggs, D.J., Gilbertson, D.D. and Jenkinson, R.D.S., eds. Peak District and Northern Dukeries: Field Guide. Quaternary Research Association, Cambridge, 94-100.

Rib, H.T. 1966 An Optimum Multisensor Approach for Detailed Engineering Soils Mapping. Vol. 1 and 2, Jnt Highway Res. Project 22, Purdue University, 406pp.

Rib, H.T. and Laing, T. 1978 Recognition and identification. in: Schuster, R.L. and Krizek, R.J., eds. Landslides - Analysis and Control. Trans. Res. Board Spec. Rep. 176, Nat. Acad. Sci., Washington D.C., 34-80.

Richey, J.E. 1964 Elements of Engineering Geology. Sir Isaac Pitman and Sons Ltd., London, 157pp.

Robertson, A.M. 1970 The interpretation of geological factors for use in slope theory. in: van Rensburg, P.W. J., ed. Planning Open Pit Mines (S. Afr. Inst. Min. Metal.), 55-71.

Russell, D.J. and Parker, A. 1979 Geotechnical, mineralogical and chemical inter-relationships in weathering profiles of an over-consolidated clay. Q. J. Eng. Geol., 12, 107-116.

Sabins, F.F. 1987 Remote Sensing: Principles and Interpretation. 2nd Edn., W.H. Freeman, New York, 449pp.

Said, M. 1969 The Pleistocene Geomorphology of the Burbage Basin. Unpublished PhD Thesis, University of Sheffield.

Saroso, B.S., Dowling, J.W.F. and Beaven, P.J. 1984 Low cost remote

sensing of landslides endangering roads in West Java. Proc. 18th Int. Symp. Remote Sens. Environ., 1, Environ. Res. Inst. Michigan, Ann Arbor, 563.

Sauchyn, D.J. and Trench, N.R. 1978 Landsat applied to landslide mapping. Photogramm. Eng. Remote Sens., 44(6), 735-741.

Schultz, L.G. 1964 Quantitative interpretation of mineralogical composition form X-ray and chemical data for the Pierre Shale. U.S. Geol. Surv. Prof. Paper 391-C, C1-C31.

Shaw, D.B. and Weaver, C.E. 1965 The mineralogical composition of shales. J. Sed. Petrol., 35, 213-222.

Shaw, H.F. 1981 Mineralogy and petrology of the argillaceous sedimentary rocks of the U.K. Q. J. Eng. Geol., 14, 277-290.

Sherrell, F.W. 1971 The Nag's Head landslips, Cullompton By-Pass, Devon. Q. J. Eng. Geol., 4, 37-73.

Shimwell, D.W. 1981 Disappearing Peak. Geog. Mag., 53, 684.

Siegal, B.S. and Gillespie, A.R., eds. 1980 Remote Sensing in Geology. John Wiley and Sons, New York, 702pp.

Siegal, B.S. and Goetz, A.F.H. 1977 Effect of vegetation on rock and soil type discrimination. Photogramm. Eng. Remote Sens.,

43, 191-196.

Singer, P.C. and Stumm, W. 1970 Acidic mine drainage: The rate determining step. Geochim. Cosmochim. Acta, 40, 441-447.

Skempton, A.W. 1964 Long-term stability of clay slopes. Geotechniq., 14, 77-101.

Skempton, A.W. and Petley, D.J. 1967 The strength along structural discontinuities in stiff clays. Proc. Geotech. Conf. Oslo, 2, 29-46.

Smith, E.G., Rhys, G.H. and Eden, R.A. 1967 Geology of the county around Chesterfield, Matlock and Mansfield. Mem. Geol. Surv. G.B., London, 403pp.

Smith, G.N. 1982 Elements of Soil Mechanics. 5th Edn., Granada, London, 493pp.

Sowers, G.F. and Royster, D.L. 1978 Field investigation. in: Schuster, R.L. and Krizek, R.J., eds. Landslides - Analysis and Control. Trans. Res. Board Spec. Rep. 176, Nat. Acad. Sci., Washington D.C., 81-111.

Spears, D.A. 1964 The major element geochemistry of the Mansfield Marine Band in the Westphalian of Yorkshire. Geochim. Cosmochim. Acta, 28, 1679-1696.

Spears, D.A. and Amin, M.A. 1981a Geochemistry and mineralogy of marine and non-marine Namurian black shales from the Tansley Borehole, Derbyshire. Sedimentology, 28, 407-417.

1981b A mineralogical and geochemical study of turbidite sandstones and interbedded shales, Mam Tor, Derbyshire, U.K. Clay Miner., 16, 333-345.

Spears, D.A. and Taylor, R.K. 1972 The influence of weathering on the composition and engineering properties of in situ Coal Measures rock. Int. J. Rock Mech. Min. Sci., 9, 729-756.

Stefouli, M. & Osmaston, H.A. 1984 The remote sensing of geological linear features using Landsat: matching analytical approaches to practical applications. in: Satellite Remote Sensing - Review and Preview. Proc. 10th Anniv. Int. Conf., Remote Sensing Society, Reading, 227-236.

Steward, H.E. 1984 Links between geochemical and engineering properties in weathered pyritic shales. Unpublished PhD Thesis, University of Sheffield.

Steward, H.E. and Cripps, J.C. 1983 Some engineering implications of chemical weathering of pyritic shale. Q. J. Eng. Geol., 16, 281-289.

Tallis, J.H. and Johnson, R.H. 1980 The dating of landslides in Longdendale, north Derbyshire, using pollen-analytical techniques. in: Cullingford, R.A., Davidson, D.A. and Lewin, J., eds. Timescales in Geomorphology. John Wiley and Sons, Chichester, 189-205.

Tanguay, M.G. and Chagnon, J.Y. 1972 Thermal infrared imagery at the St. Jean-Vianney landslide. Proc., 1st Can. Symp. Remote Sens., Can. Center Remote Sens. and Can. Inst. Surv., Ottawa, 387-402.

Taylor, F.M. 1966 A landslide at Matlock, Derbyshire, 1966. Mercian Geol., 1(4), 351-355.

Taylor, R.K. 1974 Letter to the Editor: Investigations of the landslide at Walton's Wood, Staffordshire, by Early, K.R. and Skempton, A.W. 1972 Q. J. Eng. Geol., 5, 19-41, Q. J. Eng. Geol., 7, 101.

1988 Coal Measures mudrocks: composition, classification and weathering processes. Q. J. Eng. Geol., 21, 85-99.

Taylor, R.K. and Spears, D.A. 1970 The breakdown of British Coal Measure rocks. Int. J. Rock Mech. Min. Sci., 7, 481-501.

Taylor, R.K. and Spears, D.A. 1981 Laboratory investigation of mudrocks. Q. J. Eng. Geol., 14, 291-309.

Terzaghi, K. 1950 Mechanism of landslides. Geol. Soc. Am. Bull., Berkey Volume, 83-122.

1962 Stability of steep slopes on hard unweathered rock. Geotechniq., 12, 251-270.

Terzaghi, R.D. 1965 Sources of error in joint surveys. Geotechniq., 15, 287-304.

Townshend, J.R.G., ed. 1981 Terrain Analysis and Remote Sensing. George Allen and Unwin Ltd., London, 16-37 and 59-108.

Trent River Authority 1971 Water Resources - A First Development: A Report on the Alternative Sites for a Reservoir Development in the River Dove and River Derwent Catchments. 76pp.

Trevett, J.W. 1986 Imaging Radar for Resource Surveys. Chapman and Hall, London, 313pp.

Varnes, D.J. 1983 Landslide Hazard Zonation: A Review of Principles and Practice. Commission on Landslides and Other Mass Movements on Slopes, Int. Assoc. Eng. Geol.

Vear, A. 1981 The geochemistry of pyritic shale weathering within an active landslide. Unpublished PhD Thesis, University of Sheffield.

Vear, A. and Curtis, C.D. 1981 A quantitative evaluation of pyrite weathering. Earth Surf. Processes Landf., 6, 191-198.

Voight, B. 1973 Correlation between Atterberg plasticity limits and residual shear strength of natural soils. Geotechniq., 23, 265-267.

Waters, R.S. and Johnson, R.H. 1958 The terraces of the Derbyshire Derwent. East Midl. Geogr., 1(9), 3-15.

Watson, W. 1811 The Strata of Derbyshire. Moorland Reprints, 1973. Moorland Publishing Company, Hartington, 77pp.

Wedepohl, K.H. 1971 Geochemistry. Holt, Rinehart and Winston, Inc., New York, 231pp.

Weir, A.H., Ormerod, E.C. and El Mansey, I.M.I. 1975 Clay mineralogy of sediments of the western Nile Delta. Clay Miner., 10, 369-387.

Whalley, W.B. 1981 Chemical Properties. in: Goudie, A., ed. Geomorphological Techniques. George Allen and Unwin, London, 104-120.

Whalley, W.B. 1984 Rockfalls. in: Brunsden, D. and Prior, D.B., eds. Slope Instability. John Wiley & Sons, Chichester, 217-

Wildey, R.L. 1984 Topography from single Radar images. Science, 224, 153-156.

Wise, D.U. 1977 Geologic lineaments: remotely sensed bonanzas and extravaganzas. Proc. 11th Int. Symp. Remote Sens. Environ., Environ. Res. Inst. Michigan, Ann Arbor, 179.

1982 Linesmanship and the practice of linear geo-art. Geol. Soc. Am. Bull., 93, 886-888.

Yaalon, D.H. 1962 Mineral composition of average shale. Clay Miner. Bull., 5, 31-36.

Appendix 1

Descriptions of the Edale Lineaments

APPENDIX 1 DESCRIPTIONS OF THE EDALE LINEAMENTS

A1.1 The Appearance of Lineaments on Landsat TM Imagery of the Edale Region (Figure 3.1 and O.S. 1:25,000 Outdoor Leisure Sheet 1)

Lineament 1 (Alport Moor): The river draining part of Alport Moor shows an abrupt change of direction which forms two lineaments orthogonal to each other. This configuration of lineaments may be indicative of orthogonal jointing in the sandstone, or faulting creating a line of weakness within the rock, which the river can exploit by preferential erosion.

Lineament 2 (Swint Clough to Ouzelden Clough): This lineament is defined by the alignment of two tributary valleys separated by Alport Castles landslide. On the false-colour composite image of Bands 5, 4 and 1 there is a dark line through the landslide which may be a zone of higher moisture content, however in the field it appears to be a topographical feature which would produce a shadow on Landsat imagery. It is unlikely that a geological feature such as a fault or a zone of closely-spaced jointing would be manifest through a deep-seated landslide such as Alport Castles and, therefore, the significance of the dark line through the landslide is questionable.

Lineaments 3 and 4 (Howden Deen to Ladybower Reservoir): These two lineaments are two aligned small valleys which appear to be connected by a distinct circular feature which is defined by the upper reaches

of streams draining the moor.

Lineament 5 (Kinder Reservoir to Fair Brook): This lineament cuts across Kinder Scout and passes through Kinder Downfall. On either side of the plateau the lineament is delineated by aligning valleys.

Lineament 6 (Wood Moor to Oyster Clough): Two aligned tributary streams to the River Ashop form this lineament. On the northern side of the river the lineament defines the western edge of the Cowms Moor landslide.

Lineament 7 (Crookstone Knoll to Rowlee Pasture): As for Lineament 2, part of this lineament is within a landslide (below Rowlee Pasture) and appears to be created by the topography of the landslide itself. However, this feature is in line with a stream on the opposite side of the valley.

Lineament 8 (Kinderlow End to Blackley Clough): This lineament crosses the Kinder plateau and is defined, in part, by the heads of valleys on the southern edge where the Kinderscout Grit outcrops as the backscars of landslides at Upper Tor and Nether Tor in Grindsbrook. Further to the east the lineament follows Jaggers Clough and Blackley Clough.

Lineament 9 (Two Thorns Field to Derwent Edge): Three aligned small valleys compose this lineament.

Lineament 10 (Kinder Reservoir to Barber Booth): For the main part, this lineament follows the upper reaches of the River Noe from Jacob's Ladder to Barber Booth. The lineament is interrupted at Jacob's Ladder by a spur but continues northwestward across Kinder Low and along a stream to the reservoir. At Jacob's Ladder there are two linear tributary streams offset by 200 metres at the lineament which may represent faulting.

Lineament 11 (Chapel-en-le-Frith to The Wicken, Snake Pass): This is a complex feature composed of several lineaments at its southwestern end. From Chapel-en-le-Frith the lineament follows a series of linear segments of a small valley joined at an angle of approximately 120°; this angular configuration may reflect the jointing pattern of the sandstone. The northeastern section of the lineament is composed of aligning valleys on both sides of the Kinder plateau.

Lineament 12 (Upper Booth to Grindsbrook): This lineament crosses the slopes on the southern side of Kinder at an oblique angle. The lineament follows aligned tributary valleys and may be related to Lineament 14 although this lineament has a slightly different orientation.

Lineament 13 (Slackhall to Nether Tor): This composite lineament is defined by aligning valleys and also follows the break of slope around Broadlee Tor near Edale.

Lineament 14 (Oller Brook to Nether Moor): Oller Brook and a

tributary of Lady Booth Brook form this lineament which may be an extension of Lineament 12.

Lineament 15 (Clough Farm to Fullwood Holmes): At Clough Farm this lineament follows a stream into the River Noe. On the false-colour composite image of Bands 5, 4 and 1 the lineament can be seen extending as a dark intermittent line crossing the middle slopes of Lose Hill. In the field these darker lines across Lose Hill were identified as probably being a wall which separates improved pasture on the lower slopes from rough grassland on the upper slopes.

Lineament 16 (Lord's Seat to Odin Mine): The Rushup Edge ridge, the backscar of the Rushup Edge landslide and the sidescar of the Mam Tor landslide form this lineament, and on the false-colour composite image of Bands 3, 2 and 1 a dark line can be seen to connect the two landslides along this path. This lineament may represent a fault which has been mapped in this area.

Lineaments 17 and 18 (Kinder Low End to Connies Dale): These two parallel lineaments can be seen on the false-colour composite image of Bands 6, 5 and 3. They appear as a band approximately 500 metres wide of different tone to the surrounding land. The northwest section of the band is red against blue whereas the southeastern section is dark green against green. This change in colour along the lineaments appears to occur at the junction of the sandstone/shale and the limestone.

A1.2 The Appearance of Lineaments on Aerial Photographs

The lineaments identified on the Landsat TM images of Edale were located on aerial photographs to determine their appearance more precisely. The majority of the lineaments were believed to follow aligned river courses on the satellite images and this is confirmed on the aerial photographs. Lineament 16 is of interest as it appears to be associated with the Rushup Edge and Mam Tor landslides; it may also coincide with a known fault. Lineaments 17 and 18 are also interesting cases as these are the only tonal lineaments identified consistently by several observers. These three lineaments are considered below in terms of their appearance on aerial photographs.

Lineament 16: From stereoscopic viewing of aerial photographs Lineament 16 can be defined by the backscar of Rushup Edge landslide and the sidescar of Mam Tor landslide. On the false-colour composite image of Bands 3, 2 and 1 a dark line connects the landslides; on the aerial photographs this line was located at a concave break of slope marked by a wall and lusher grassland on the downslope side. A fault is known to exist along Rushup Edge and on the southern edge of Mam Tor. However, by locating the lineament on the aerial photographs, it is apparent that it does not follow the same path as the fault, assuming that the fault has been mapped accurately. This lineament is defined by the landslides; if these slopes had not failed, would a lineament be present?

Individual observers have identified additional lineaments around Mam Tor, for example a line passing from the summit of Mam Tor and along the backscar of Cold Side landslide. This backscar does have a distinct right-angled corner which is clearly visible from both the satellite imagery and the aerial photographs, suggesting that the shape of the backscar has been determined by weaknesses in the rock (i.e. orthogonal jointing).

The location of these lineaments in the field proved to be difficult. Firstly, access to backscars is hazardous and was, therefore, greatly restricted. Secondly, a detailed joint survey would be necessary to pick up any variations in joint spacing related to the lineament as there was no obvious increase (or decrease) of fracture spacing visible.

Lineaments 17 and 18: These lineaments define a band approximately 500 metres in width which appears on the Landsat images as contrasting in tone to the surrounding land. On the aerial photographs the vegetation within the band in the northwest on sandstone and shale is of darker tone and rougher texture, being bracken and grass, compared to the adjacent grassland. This suggests that the lineaments can be detected on Landsat TM images as a result of a change in vegetation. However, whether this difference in vegetation represents a change of geological conditions remains to be tested. As these lineaments coincide with only one landslide their geological significance is of no importance to this study and, therefore, detailed field work was not carried out. The southeastern

section of the band crosses the limestone and it is less visible on the aerial photographs. However, the lineaments may follow the line of a shallow dry valley with cultivated land on the west and rougher pasture land on the east.

Appendix 2a

On Site Log of Borehole 1

Sheet 1 of 2

Location: Oker Hill Landslide

Grid Reference: SK 27256150

Formation: Carboniferous Millstone Grit Series

Borehole No.: 1

Date of Collection: 22 - 23/4/87

Depth (metres)	Lithology	Core Recovery	Comments
0	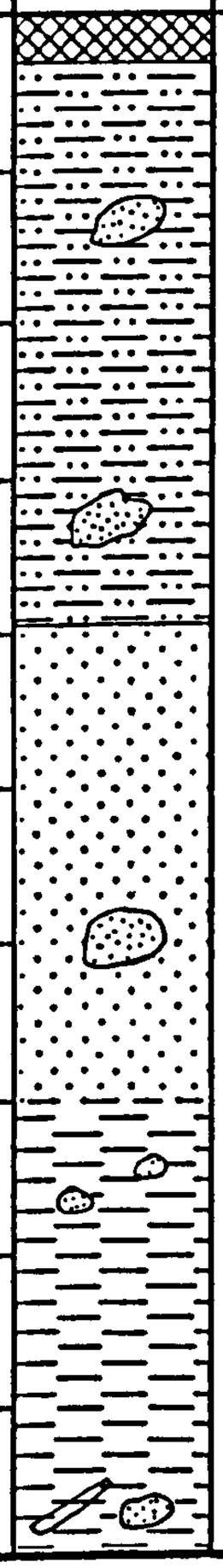		Brown Soil
0.5			SILTY CLAY - orange/brown with numerous small sandstone clasts (~30mm length) Large sandstone fragment (~80mm length)
1.0			
1.5			Large sandstone clast (~150 mm length).
2.0			
2.5			SAND - orange/brown with large sandstone fragments
3.0			
3.5			Gradual transition from sand to silty clay to clay.
4.0			GREY CLAY with grey fine-grained sandstone / siltstone fragments + shale lithorelicts with orange/brown iron-staining on surfaces.
4.5			
5.0			

Notes:

No samples taken.

Core recovery

U U100 sample

S mass sample

Sheet 2 of 2

Location: Oker Hill Landslide

Grid Reference: SK 27256150

Formation: Carboniferous Millstone Grit Series

Borehole No.: 1

Date of Collection: 22 - 23/4/87

Depth (metres)	Lithology	Core Recovery	Comments
5.0			GREY CLAY with shale lithorelicts + iron-staining
5.5			- Groundwater encountered
6.0			
6.5		S	
7.0		S	Weathered shale - iron-oxide staining - clayey
7.5		S	
8.0		S	
8.5		S	
9.0		S	
9.5		S	

Notes:

Core recovery

U U100 sample

S mass sample

Appendix 2b

On Site Log of Borehole 2

Location: Oker Hill Landslide

Sheet 1 of 6

Grid Reference: SK 27266151

Formation: Carboniferous Millstone Grit Series

Borehole No.: 2

Date of Collection: 2/6/87 - 3/7/87

Depth (metres)	Lithology	Core Recovery	Comments
0.0			Brown Soil
0.25			SND + SILT + CLAY orange/brown
0.5			
0.75			
1.0			
1.25			SAND + SILT with sandstone boulders. orange
1.5			
1.75			
2.0			
2.25			
2.5			

Notes:

Core recovery — No samples taken

U U100 sample

S mass sample

Location: Oker Hill Landslide

Grid Reference: SK 27266151

Formation: Carboniferous Millstone Grit Series

Borehole No.: 2

Date of Collection: 2/6/87 - 3/7/87

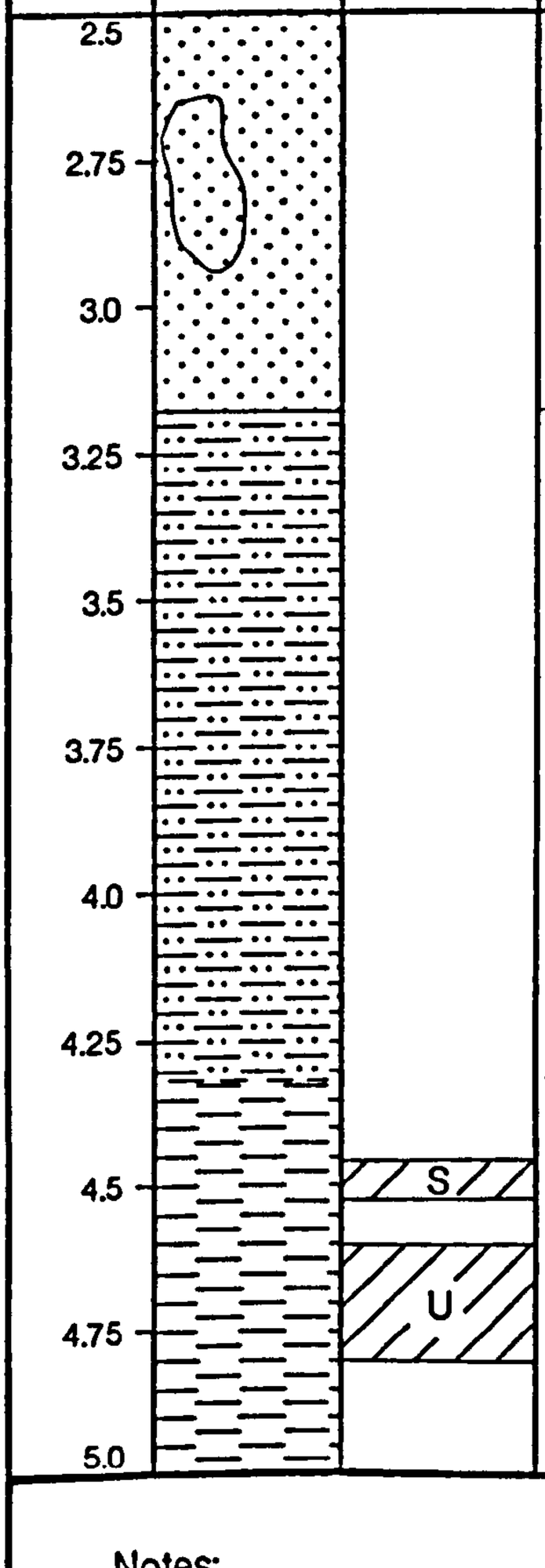

Comments

SAND + SILT
- orange
- sandstone boulders

— 3·3 m Groundwater level
Groundwater encountered when casing between 3·1 m and 4·3 m.

CLAY (grey) + SILT (cream/orange)
no fabric to shale.

Gradual change from silty clay to shale

Sample 1 4·48 - 4·52 m
SHALE - iron-oxide staining
Sample 2 4·6 - 4·8 m

Notes:

Core recovery

U U100 sample

S mass sample

Location: Oker Hill Landslide

Sheet 3 of 6

Grid Reference: SK 27266151

Formation: Carboniferous Millstone Grit Series

Borehole No. : 2

Date of Collection: 2/6/87 - 3/7/87

Depth (metres)	Lithology	Core Recovery	Comments
5.0			
5.25		U	Sample 3 5·25 – 5·65 m
5.5			
5.75		S	Sample 4 5·65 – 5·8 m
6.0			— Casing } End of Day 1
6.25			— Borehole } End of Day 1
6.5			GREY CLAY
6.75		U	Sample 5 6·5 – 6·95 m
7.0		S	Sample 6 6·95 – 7·1 m
7.25		U	Sample 7 7·0 – 7·45 m
7.5		S	Sample 8 7·45 – 7·5 m

Notes:

Core recovery

U U100 sample

S mass sample

Location: Oker Hill Landslide

Grid Reference: SK 27266151

Formation: Carboniferous Millstone Grit Series

Borehole No.: 2

Date of Collection: 2/6/87 - 3/7/87

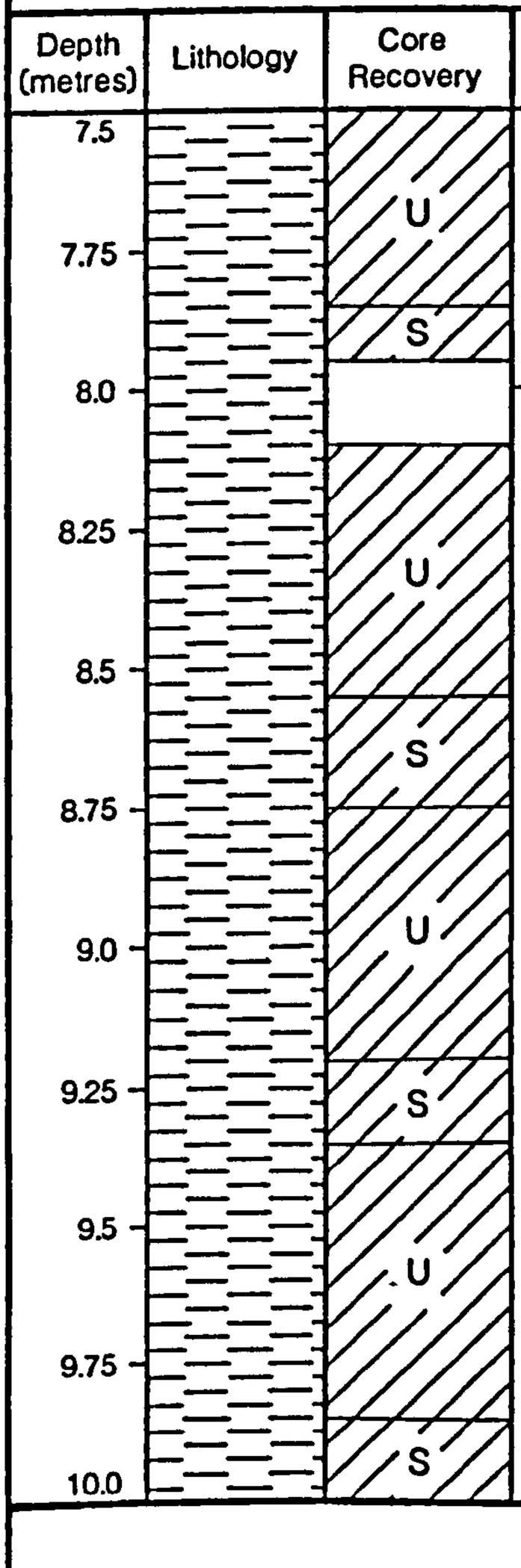

Comments

— Casing 7.6m at end of Day 2
Sample 9 7.45-7.85 SHALE with orange iron-oxide staining

Sample 10 7.85-7.95

— Borehole at 8.0m at end of Day 2

Sample 11 8.10-8.55 Laminated shale.

Sample 12 8.55-8.75
green/yellow mineral - jarosite?

Sample 13 8.70-9.2

— Casing at 9.2m at end of Day 3
Sample 14 9.2-9.35

Weathered shale
iron-oxide staining

Sample 15
9.35-9.85

SLIP PLANE?

Unweathered shale
-no iron-oxide

Sample 16 9.85-10.0 Laminated Shale

Notes:

Core recovery

U U100 sample

S mass sample

Location: Oker Hill Landslide

Sheet 5 of 6

Grid Reference: SK 27266151

Formation: Carboniferous Millstone Grit Series

Borehole No.: 2

Date of Collection: 2/6/87 - 3/7/87

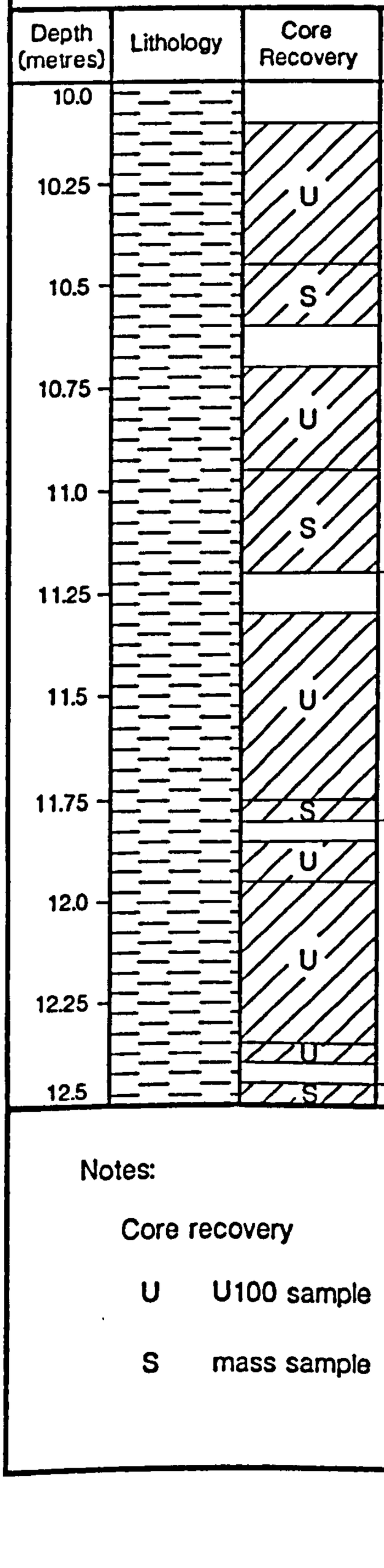

Comments

Borehole at 10.0m at end of Day 3

Sample 17 10.1 - 10.45
no iron-staining visible
no visible sign of weathering

Casing at 10.5m at end of Day 4

Sample 18 10.45 - 10.6
Hard unweathered SHALE

Sample 19 10.7 - 10.95

Casing at 11.0m at end of Day 5.

Sample 20 10.95 - 11.2

Samples lost down the borehole for 4 days

Borehole at 11.2m at end of Day 4

Drilling interrupted for 21 days during which groundwater entered the hole from between 10.5 and 11.2m

Sample 21 11.3 - 11.75

Large volume of water added to borehole to free the sampler. Recovered the next day

Sample 22 11.75 - 11.8

Borehole at 11.8m at end of Day 5.

Sample 23 11.85 - 11.95

Sample 24 11.95 - 12.35

Casing at end of Day 5

Sample 25 12.0 - 12.4 (overlap with Sample 24 - hole not cleared out)

Borehole at end of Day 6

Sample 26 12.45 - 12.6

Notes:

Core recovery

U U100 sample

S mass sample

Location: Oker Hill Landslide

Sheet 6 of 6

Grid Reference: SK 27266151

Formation: Carboniferous Millstone Grit Series

Borehole No.: 2

Date of Collection: 2/6/87 - 3/7/87

Depth (metres)	Lithology	Core Recovery	Comments
12.5		S	Sample 26 12·45 - 12·6m — Hard, unweathered shale.
		S	Sample 27 12·6 - 12·7m
12.75		U	Sample 28 12·7 - 12·88m — Slow drilling progress
		S	Sample 29 12·88 - 12·90m
13.0			End of Day 7. Casing 12·2m, Borehole 12·90m

Notes:

Core recovery

U U100 sample

S mass sample

Appendix 3

Detailed Log of Core Material

from Borehole 2

Location: Oker Hill Landslide

Sheet 1 of 15

Grid Reference: SK 27266151

Formation: Carboniferous Millstone Grit Series

Borehole No.: 2

U100 Sample No.: 2

Date of Collection: 2/6/87

Depth (metres)	Lithology	Structure	Comments
4.60		IV	Fragments of grey, micaceous Sandstone Sandstone – poorly cemented. Iron-oxide coating on faces of fragments.
4.65		III	Large fragment of Sandstone: 105mm x 100mm Sandstone – grey, micaceous, poorly cemented, massive. Iron-oxide coating on surface. Irregular contact with shale.
4.70			Shale – weathered, original structure lost. Dark grey + few patches of orange iron-oxide. Occasional small fragments of unweathered shale ~3mm diam. – lithorelicts.
S 4.75		IV	Shale – weathered, clayey matrix with lithorelicts of shale up to 10mm diam. in plate form.
4.80			

Notes:

S — Sample for XRD and XRF analysis

I – V — Weathering Grade

▭ Lithorelict of shale.

Location: Oker Hill Landslide

Grid Reference: SK 27266151

Formation: Carboniferous Millstone Grit Series

Borehole No.: 2 U100 Sample No.: 3

Date of Collection: 2/6/87

Depth (metres)	Lithology	Structure	Comments
S 5.25	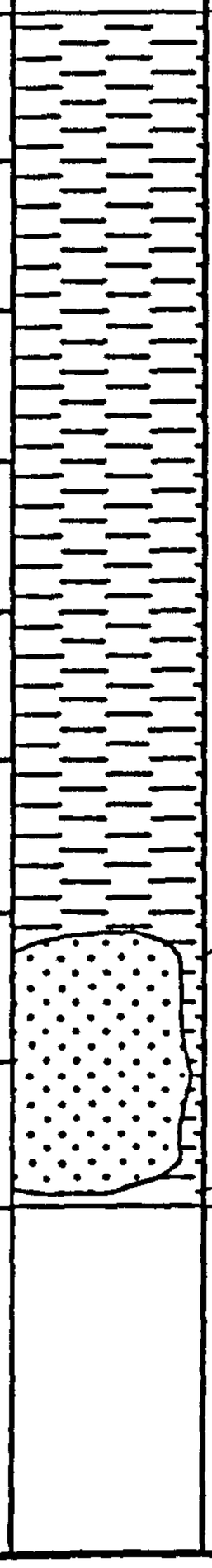	IV	Shale – weathered; original structure lost; lithorelicts dominate over clayey matrix. Lithorelicts of shale - subangular, unweathered, but coated by orange iron-oxide. Up to 45mm diam. laminated – easily split along laminations. Orange iron-oxide also occurs in patches throughout the weathered material.
S 5.30			
S 5.35			
S 5.40			
S 5.45			
S 5.50			
S 5.55		III	Large Sandstone fragment 900mm x 700mm. - micaceous - poorly cemented - weathered
S 5.60			
S 5.65			Shale below Sandstone more clayey + softer than shale above + fewer lithorelicts.

Notes:

S Sample for XRD and XRF analysis

I - V Weathering Grade

Location: Oker Hill Landslide

Grid Reference: SK 27266151

Formation: Carboniferous Millstone Grit Series

Borehole No.: 2 U100 Sample No.: 5

Date of Collection: 3/6/87

Depth (metres)	Lithology	Structure	Comments
			Core quite wet - probably result of groundwater entering hole overnight.
S 6.50			Very clayey - soft, mouldable, grey clay.
S 6.55			Occasional fragments of Sandstone upto 5mm diameter, subangular, easily broken, poorly cemented.
S 6.60			
S 6.65		V	
S 6.70			Contact obscured by splitting sample.
			Sandstone fragments 18mm diam. with iron oxide coating.
S 6.75			Brown/grey clay - slightly stiffer than clay above + below this band.
			Slip Plane? Contact obscured by splitting sample
S 6.80			Faintly laminated aligned shale lithorelicts within clayey matrix
S 6.85			with small sandstone fragments
		IV	
S 6.90			? iron nodule - oxidised. 15mm diam.
			Small sandstone fragments ~5mm diam.
S 6.95			

Notes:

S Sample for XRD and XRF analysis

I - V Weathering Grade

o Round clasts ~3 to 4 mm diam. Sandy, orange/yellow (iron-oxide) with flakes of mica. - possibly poorly cemented sandstone clasts nearly disintegrated.

Sheet 4 of 15

Location: Oker Hill Landslide

Grid Reference: SK 27266151

Formation: Carboniferous Millstone Grit Series

Borehole No.: 2 U100 Sample No.: 7

Date of Collection: 3/6/87

Depth (metres)	Lithology	Structure	Comments
S 7.00			Overlap with Sample No. 6
S 7.05			Shale throughout section : - faintly laminated - highly oxidised - dark grey - orange patches of iron-oxide - soft with shale lithorelicts upto 6mm diam.
S 7.10			
S 7.15			
S 7.20		IV	Shale lithorelicts - faces coated with red & orange oxides of iron.
S 7.25			
S 7.30			
S 7.35			7.33 m Green/yellow coating on clay - jarosite ?
S 7.40			
S 7.45			

Notes:

S Sample for XRD and XRF analysis

I - V Weathering Grade

Almost disintegrated Sandstone clast

Sandstone fragments

Shale lithorelict

Location: Oker Hill Landslide

Grid Reference: SK 27266151

Formation: Carboniferous Millstone Grit Series

Borehole No.: 2 U100 Sample No.: 9

Date of Collection: 3/6/87

Depth (metres)	Lithology	Structure	Comments
			Junction between faintly laminated and laminated shale — slip plane?
S 7.45			} Overlap with Sample No.8
S 7.50			Shale — dark grey — laminated - closely spaced 1-2 mm. — soft, friable — laminations emphasised by orange iron-oxide
S 7.55			
S 7.60			— orange band of iron-oxide
S 7.65		III	} less iron-oxide
S 7.70			—
S 7.75			More iron-oxide More friable
S 7.80			
S 7.85			

Notes:

S Sample for XRD and XRF analysis

I - V Weathering Grade

Laminations curve downwards at edges — due to deformation during either sampling or extraction from U100 tubes

Location: Oker Hill Landslide

Grid Reference: SK 27266151

Formation: Carboniferous Millstone Grit Series

Borehole No. : 2 U100 Sample No. : 11

Date of Collection: 4/6/87

Depth (metres)	Lithology	Structure	Comments
S 8.10			} May be debris not cleared out of hole
S 8.15			Shale throughout section:
S 8.20			- dark grey
		III	- laminations : 1-2mm spacing
S 8.25			- orange iron-oxide along laminations
S 8.30			- soft, friable
S 8.35			
			- more iron-oxide
S 8.40			
8.45			Shale lost during extraction from U100 tube
8.50			
8.55			

Notes:

S Sample for XRD and XRF analysis

I - V Weathering Grade

Laminations curve downward at edges - due to deformation during sampling or extraction from U100 tube.

Sheet 7 of 15

Location: Oker Hill Landslide

Grid Reference: SK 27266151

Formation: Carboniferous Millstone Grit Series

Borehole No. : 2 U100 Sample No. : 13

Date of Collection: 4/6/87

Depth (metres)	Lithology	Structure	Comments
S 8.70		IV	Shale : soft, clayey, structureless with patches of iron-oxide - may be debris from Samples 11 & 12
S 8.75			Irregular contact
S 8.80		IV	Shale : friable ; faintly laminated with intense orange iron-oxide
S 8.85			- 8.84 m yellowish coating on shale - jarosite? 8.75 - 8.87 - Failure zone?
S 8.90		III	Shale : friable but relatively hard. Laminations distinct + closely spaced - 1-2 mm. Intense iron-oxide staining - green/yellow coating - jarosite?
S 8.95			
S 9.00			
S 9.05		III	Shale : harder, less weathered, occasional iron-staining Laminations more distinct with wider spacing 5-8 mm. -less curved at edges due to greater hardness of shale.
S 9.10			
S 9.15			
S 9.20			

Notes:

S Sample for XRD and XRF analysis

I - V Weathering Grade

Laminations curve downward at edges due to deformation during sampling or extraction from U100 tube.

Sheet 8 of 15

Location: Oker Hill Landslide

Grid Reference: SK 27266151

Formation: Carboniferous Millstone Grit Series

Borehole No.: 2 U100 Sample No.: 15

Date of Collection: 4/6/87

Depth (metres)	Lithology	Structure	Comments
S 9.40		III	Shale – dark grey, fissile, laminated – spacing 2-8mm – dipping at ~20°
S 9.45			Fractures coated with orange iron-oxide
S 9.50			} Band of shale without iron-oxide
S 9.55			
S			
S 9.60			9.60m yellow coating – jarosite?
S			Straight contact along plane of laminations in underlying shale. Angle of 40-50°
S			Shale dark grey, laminated, shale in fragments smaller than those in shale above or below
S 9.65			
S 9.70		II-I	Shale – dark grey, fissile laminated – dipping at 40-50°
S 9.75			Tiny cubic crystals – pyrite?
S 9.80			No visible sign of weathering or sampling – Band of harder shale at base

Notes:

S Sample for XRD and XRF analysis

I-V Weathering Grade

Angle of dip cannot be measured accurately as angle of inclination of borehole is not known.

Location: Oker Hill Landslide

Sheet 9 of 15

Grid Reference: SK 27266151

Formation: Carboniferous Millstone Grit Series

Borehole No.: 2 U100 Sample No.: 17

Date of Collection: 5/6/87

Depth (metres)	Lithology	Structure	Comments
S 10.10		II-I	} May be debris not cleared out of hole
S 10.15			Shale – dark grey friable laminated
S 10.20			Laminations dip at ~40-50° with spacing of 2-5mm
S 10.25			
S 10.30			Faces of laminations - polished – + covered with white flecks (gypsum ?) throughout section
S 10.35			
S 10.40			
S 10.45			– orange iron-oxide on base of section (result of storage?)

Notes:

S Sample for XRD and XRF analysis

I - V Weathering Grade

Location: Oker Hill Landslide

Grid Reference: SK 27266151

Formation: Carboniferous Millstone Grit Series

Borehole No.: 2 U100 Sample No.: 19

Date of Collection: 5 - 9/6/87

Depth (metres)	Lithology	Structure	Comments
S 10.70		II	Angular concretions, possibly of siderite, upto 20mm diam. All surfaces covered with orange iron-oxide
S 10.75			Contact dips at ~50°
S 10.80		I	Shale - dark grey unweathered laminated - spacing ~6mm dipping at ~20-30°
S 10.85			-10.86m - white mineral coating shale, slightly powdery - gypsum?
S 10.90			- Shale less friable than shale above
S 10.95			

Notes:

S Sample for XRD and XRF analysis

I - V Weathering Grade

Location: Oker Hill Landslide

Grid Reference: SK 27266151

Formation: Carboniferous Millstone Grit Series

Borehole No.: 2 U100 Sample No.: 21

Date of Collection: 1/7/87

Depth (metres)	Lithology	Structure	Comments
11.30			
11.35			Sample extremely wet & fragmented Broke up on extraction from sampling tube. Discarded.
11.40			Drilling interrupted for 21 days during which time groundwater collected in the hole.
11.45			Also, large amount of water had been added to the borehole during drilling as the sampler became stuck.
11.50		I	When sampler retrieved :
11.55			Shale - dark grey, hard, unweathered.
11.60			During storage shale became highly oxidised due to the artificially high water content.
11.65			
11.70			
11.75			

Notes:

S Sample for XRD and XRF analysis

I -V Weathering Grade

No samples taken for analysis.

Sheet 12 of 15

Location: Oker Hill Landslide

Grid Reference: SK 27266151

Formation: Carboniferous Millstone Grit Series

Borehole No.: 2 U100 Sample No.: 23

Date of Collection: 2/7/87

Depth (metres)	Lithology	Structure	Comments
11.85			
S		II-I	Core broke up on extraction from sampling tube Shale ± v. crumbly matrix with shale fragments
11.90			
S			- Shale more intact & harder. Slight weathering during storage
11.95			

Notes:

S Sample for XRD and XRF analysis

I-V Weathering Grade

Drilling progress becoming slower as shale becomes harder

Location: Oker Hill Landslide

Grid Reference: SK 27266151

Formation: Carboniferous Millstone Grit Series

Borehole No.: 2 U100 Sample No.: 24

Date of Collection: 2/7/87

Depth (metres)	Lithology	Structure	Comments
S 11.95			
S 12.00			Shale - dark grey unweathered hard laminated - spacing 5-10mm
S 12.05		II-I	
S 12.10			Shale above 12.20m was disturbed during sample extraction + splitting, therefore angle of dip not known
S 12.15			
S 12.20			
S 12.25		I	Shale more intact, with thinner laminations (~3-5mm) Angle of dip not known
S 12.30			
S 12.35			

Notes:

S Sample for XRD and XRF analysis

I - V Weathering Grade

Location: Oker Hill Landslide

Grid Reference: SK 27266151

Formation: Carboniferous Millstone Grit Series

Borehole No.: 2 U100 Sample No.: 25

Date of Collection: 2/7/87

Depth (metres)	Lithology	Structure	Comments
S 12.00			
S 12.05			Shale - dark grey unweathered structureless
S 12.10			Loss of structure results from drilling - this is material from Sample No. 24 which has not been removed from the borehole before sampling
S 12.15			
S 12.20			- Large shale fragment
S 12.25			
S 12.30			
S 12.35		I	Undisturbed shale - dark grey, unweathered, hard, laminated - spacing 2-7mm. Angle of dip not known.
S 12.40			

Notes:

S Sample for XRD and XRF analysis

I - V Weathering Grade

This Sample overlaps with Sample No. 24.

Sheet 15 of 15

Location: Oker Hill Landslide

Grid Reference: SK 27266151

Formation: Carboniferous Millstone Grit Series

Borehole No.: 2 U100 Sample No.: 28

Date of Collection: 3/7/87

Depth (metres)	Lithology	Structure	Comments
12.70			
S			Shale - hard, well-laminated
12.75			
S			- less intact than shale above
12.80		II-I	Core is very wet due to water added to borehole to aid drilling. This increased water content has resulted in the shale starting to oxidise
S			
12.85			
S			
12.90			

Notes:

S Sample for XRD and XRF analysis

I-V Weathering Grade

Core broke up on extraction from U100 tube, therefore angle of dip is not known.

Appendix 4

Analytical Techniques

APPENDIX 4 ANALYTICAL TECHNIQUES

A4.1 X-Ray Diffractometry

The mineralogy of Oker Hill shale was determined using a Philips X-ray diffractometer equipped with Cu target at the Department of Geology, University of Nottingham.

A4.1.1 Whole Rock Analysis

Pellets of unorientated powdered shale (see XRF preparation for trace element analysis) were scanned from 5° to 70° 2θ at 40V, 20A with 1° slits. A total of thirteen samples from Borehole 1 and forty-two samples from Borehole 2 were analysed. The resulting paper traces were interpreted using tables of 2θ values for common minerals by Chao (1969).

A4.1.2 Clay Mineral Analysis

The clay fraction of all the shale samples from both boreholes was separated by sedimentation and coated onto ceramic tiles. They were then analysed by X-ray diffraction from 2° to 14° 2θ at 40V, 20A with $\frac{1}{4}$° slits with the following treatments:

(a) air-dried

(b) glycolated

(c) heated to 375°C for $\frac{1}{2}$ hour

(d) heated to 550°C for ½ hour

(e) treated with 2NHCl (17 samples only)

Percentages of kaolinite, illite, expanding clays and chlorite were calculated using the method described by Weir et al. (1975) and also using two slight modifications of this method:

(i) The method of Weir et al. (1975) is based on the assumptions that kaolinite gives 2.5 times the reflection intensity of illite, expanding clays collapsed to 10 Å give the same intensity as illite, and chlorite gives twice the intensity of illite. Therefore,

$$\% \text{ kaolinite (K2)} = (P_K/2.5)/P_T$$

$$\% \text{ illite (I2)} = P_I/P_T$$

$$\% \text{ expanding clays (E2)} = (P_{I+E}-P_I)/P_T$$

$$\% \text{ chlorite (Ch2)} = (P_{Ch}/2)/P_T$$

where

P_K = 7.1 Å peak intensity of kaolinite, treatments (a), (b) and (c)

P_I = 10 Å peak intensity of illite, treatments (a) and (b)

P_{I+E} = 10 Å peak intensity of illite + expanding clays, treatment (d)

P_{Ch} = 14 Å peak intensity of chlorite, treatment (c)

P_T = total peak intensity of clays $(P_K/2.5+P_I+P_E+P_{Ch}/2)$

(ii) The chlorite appears to have been destroyed in many cases on heating to 375°C possibly indicating poor crystallinity, therefore it was felt that a more accurate measure of chlorite percentage would be

based on the 14 Å peak intensity of chlorite on the air-dried sample. Re-calculations on the same assumptions as the method of Weir et al. (1975) produced percentages for K1, I1, E1 and Ch1 as given in Appendix 5.

(iii) As the 7.1 Å reflectance peak is made up of chlorite as well as kaolinite calculations were repeated to give percentages of K3, I3 and E3 where K3 = kaolinite + chlorite.

Comparison of the above three methods of calculating clay percentages showed that they did in fact follow the same trends, therefore only the values of K1, I1, E1 and Ch1 were used in the discussion of mineralogy and geochemistry.

A4.2 X-Ray Fluorescence Spectrometry

In total thirteen samples from Borehole 1 and 122 samples from Borehole 2 were analysed for ten major and twenty-one trace elements at the Department of Geology, University of Nottingham using a Philips PW1400 spectrometer equipped with a rhodium X-ray tube.

Two methods of sample preparation were used:

A4.2.1 Major Elements

For major element analysis fusion beads were prepared following the

method of Harvey et al. (1973). The flux used was Johnson-Matthey Spectroflux 105 which consists of lithium tetraborate 47.0%, lithium carbonate 36.7% and lanthanum oxide 16.3% and has a melting point of 715°C.

A4.2.2 Trace Elements

A pressed powder pellet method was used for the trace elements. Homogenised rock powder (250 mesh) was pressed between polished WC plattens to ten tons. For a pellet of 31.5 millimetres in diameter approximately ten grams of sample were used to ensure that the pellet was of "infinite thickness".

The element concentrations were calculated using the methods of Harvey and Atkin (1982) and as a check of the precision and accuracy a set of international standards and internal monitors were also analysed. Results are presented in Appendix 5.

Appendix 5a

XRF Data for Borehole 1

Var.\ID:	NSD-1	NSD-2	NSD-3	NSD-4	NSD-5	NSD-6	NSD-7	NSD-8	NSD-9	NSD-10	NSD-11	NSD-12
SiO2	57.46	54.23	54.51	54.81	54.54	54.57	56.30	55.43	58.43	51.92	49.71	55.16
Al2O3	21.23	23.66	23.56	22.98	24.46	24.50	24.36	22.21	21.15	20.01	19.43	22.77
TiO2	0.88	0.91	0.91	0.86	0.89	0.91	0.93	0.94	0.89	0.79	0.79	0.88
Fe2O3	7.01	5.96	5.68	6.85	5.29	4.89	3.80	7.11	5.51	10.69	14.76	6.82
MgO	1.20	1.27	1.31	1.25	1.18	1.17	1.14	1.08	0.99	1.07	1.00	0.92
CaO	0.29	0.32	0.32	0.30	0.29	0.29	0.24	0.20	0.16	0.16	0.19	0.15
Na2O	0.42	0.26	0.31	0.29	0.20	0.20	0.28	0.37	0.20	0.19	0.15	0.30
K2O	2.20	2.51	2.46	2.37	2.57	2.54	2.65	2.22	3.06	2.90	2.31	2.29
MnO	0.06	0.05	0.05	0.05	0.04	0.05	0.04	0.04	0.01	0.01	0.12	0.01
P2O5	0.24	0.15	0.16	0.18	0.10	0.10	0.10	0.16	0.09	0.38	0.43	0.16
LOI	9.11	10.41	10.21	9.97	10.20	10.62	10.58	10.29	10.26	12.04	10.91	10.11
Total	100.10	99.73	99.68	99.86	99.76	99.84	100.42	100.05	100.75	100.16	99.80	99.56
As	19	33	21	28	28	31	29	42	43	128	44	27
Ba	511	565	535	481	441	466	542	429	475	687	411	427
Ce	83	102	110	92	105	115	108	88	99	114	60	93
Co	19	10	17	15	11	5	3	6	0	6	42	0
Cr	132	144	132	136	147	146	150	148	188	196	165	137
Cu	45	31	34	41	27	30	36	36	49	74	136	34
La	53	61	62	51	55	55	62	43	48	64	46	51
Mo	11	27	15	11	22	25	38	14	77	85	97	8
Ni	51	44	54	47	32	29	25	26	20	28	100	50
Nb	14	15	15	15	16	15	17	15	17	15	15	16
Pb	24	24	22	22	21	27	23	18	12	31	22	19
Rb	109	127	126	121	134	133	132	109	140	125	102	112
S	1216	2336	1938	1604	987	1955	2760	1900	574	8090	2056	3046
Se	0	4	0	0	3	3	7	3	21	26	14	0
Sr	99	98	99	91	81	94	98	81	89	116	67	71
Th	11	15	14	11	15	16	14	12	7	17	19	10
U	5	7	5	5	6	9	10	7	13	12	8	5
V	124	131	128	131	142	130	142	127	325	331	215	131
Y	30	32	32	32	36	36	32	29	32	26	31	25
Zn	73	40	57	60	32	24	26	24	19	38	134	25
Zr	148	100	118	123	102	99	98	129	77	52	50	120
DEPTH	6.38	6.78	7.11	7.20	7.30	7.40	7.55	7.75	7.97	8.30	8.65	8.95
K1	27.5	29.2	36.4	27.4	30.2	30.6	25.1	29.8	30.2	22.3	27.2	41.3
I1	29.6	28.8	26.7	28.3	28.2	32.2	31.4	16.0	34.3	31.6	28.8	25.1
E1	23.4	24.3	21.8	27.2	25.6	22.1	24.2	35.5	20.6	26.7	19.4	19.6
CH1	19.5	17.7	15.2	17.1	16.0	15.1	19.3	18.7	14.9	19.4	14.6	14.0
K2	31.4	32.0	39.0	31.1	34.4	34.8	29.0	33.7	31.3	26.1	29.3	45.1
I2	33.9	31.6	28.6	32.1	32.1	36.6	36.2	18.1	35.5	36.9	41.9	27.4
E2	26.7	26.7	23.4	30.8	29.2	25.2	27.9	40.2	21.3	31.3	20.9	21.3
CH2	8.0	9.7	9.1	6.0	4.4	3.4	7.0	8.0	11.8	5.7	7.9	6.1
K3	34.1	35.5	42.9	33.0	36.0	36.0	31.1	36.7	35.5	27.7	31.8	48.1
I3	36.8	34.9	31.4	34.2	33.5	37.9	38.9	19.7	40.3	39.2	45.5	29.2
E3	29.1	29.6	25.7	32.8	30.5	26.1	29.9	43.7	24.2	33.1	22.7	22.7

Var.\ID:	NSD-13
SiO2	55.91
Al2O3	23.07
TiO2	0.90
Fe2O3	5.60
MgO	0.89
CaO	0.17
Na2O	0.40
K2O	2.38
MnO	0.02
P2O5	0.12
LOI	10.09
Total	99.55
As	27
Ba	428
Ce	86
Co	9
Cr	144
Cu	39
La	54
Mo	22
Ni	28
Nb	16
Pb	22
Rb	116
S	2917
Se	3
Sr	77
Th	14
U	5
V	143
Y	25
Zn	30
Zr	110
DEPTH	9.30
K1	27.8
I1	28.4
E1	23.2
CH1	20.6
K2	32.2
I2	32.8
E2	26.8
CH2	8.2
K3	35.1
I3	35.7
E3	29.2

Appendix 5b

XRF Data for Borehole 2

Var.\ID:	SD1-4.5	SD2-4.75	SD3-5.25	SD3-5.3	SD3-5.35	SD3-5.4	SD3-5.45	SD5.5	SD5.55	SD5.6	SD5.65	SD4-5.73
SiO2	58.61	51.50	52.03	53.59	53.05	52.78	52.36	49.23	53.99	52.88	56.74	52.56
Al2O3	21.15	23.49	24.62	24.96	24.77	24.05	23.24	20.60	24.01	25.18	20.75	24.66
TiO2	0.79	0.90	0.89	0.87	0.89	0.90	0.91	0.83	0.90	0.90	0.79	0.90
Fe2O3	6.16	7.43	6.84	5.12	5.54	6.09	7.35	11.68	5.47	4.91	7.12	6.19
MgO	1.22	1.66	1.79	1.82	1.83	1.78	1.72	1.78	1.58	1.62	1.41	1.74
CaO	0.35	0.49	0.42	0.36	0.41	0.42	0.49	0.66	0.40	0.37	0.46	0.36
Na2O	0.62	0.48	0.38	0.40	0.37	0.39	0.46	0.43	0.47	0.37	0.55	0.39
K2O	1.94	2.23	2.41	2.51	2.45	2.47	2.35	2.07	2.30	2.30	2.01	2.45
MnO	0.03	0.10	0.08	0.04	0.04	0.06	0.09	0.25	0.05	0.04	0.08	0.04
P2O5	0.19	0.21	0.20	0.11	0.15	0.16	0.22	0.27	0.15	0.14	0.25	0.16
LOI	9.20	11.45	10.53	10.23	10.47	10.81	10.77	12.58	10.52	11.19	9.78	10.45
Total	100.26	99.94	100.19	100.01	99.98	99.87	99.96	100.38	99.84	99.90	99.94	99.84
As	8	8	6	6	7	6	9	3	6	13	6	9
Ba	397	463	446	445	464	462	460	464	470	438	396	492
Ce	100	134	125	132	115	117	119	112	111	132	99	97
Co	17	22	19	20	29	23	23	20	23	26	18	21
Cr	128	141	150	147	144	139	145	135	140	144	124	133
Cu	37	51	45	50	47	46	45	41	55	61	591	47
La	49	62	57	54	58	55	51	62	61	55	65	57
Mo	0	2	0	1	0	1	1	1	1	1	1	0
Ni	64	87	90	99	94	84	82	76	89	101	69	89
Nb	13	14	15	15	15	15	15	12	15	14	12	17
Pb	19	29	20	24	22	24	24	24	30	29	42	22
Rb	97	106	118	127	120	117	113	97	112	111	95	121
S	806	2296	1354	1749	1614	1807	2056	1718	1404	2041	1187	1377
Se	0	0	0	0	0	0	0	0	0	0	0	0
Sr	85	101	113	107	115	109	100	91	102	98	92	106
Th	11	13	14	13	15	15	15	12	12	16	15	14
U	2	3	2	3	2	2	3	3	3	6	2	2
V	103	120	116	123	124	119	118	115	122	139	108	125
Y	31	31	31	29	31	31	34	36	32	32	32	32
Zn	75	79	83	97	91	91	90	83	88	98	80	84
Zr	133	124	107	115	112	122	140	144	133	106	141	118
DEPTH	4.50	4.75	5.25	5.30	5.35	5.40	5.45	5.50	5.55	5.60	5.65	5.73
K1	31.2	32.8	33.0	27.9	30.4	22.5	29.7	30.7	34.8	26.0	28.8	28.0
I1	22.9	25.2	29.0	32.6	33.8	35.2	31.3	27.4	29.0	28.9	30.4	21.4
E1	22.9	21.0	17.9	18.6	16.9	21.1	19.5	23.7	14.5	21.7	19.0	18.5
CH1	22.9	21.0	20.1	20.9	19.0	21.1	19.5	18.2	21.7	23.5	21.8	22.1
K2	32.7	35.8	34.6	30.0	32.4	29.5	32.2	33.7	37.5	28.6	31.5	31.5
I2	24.0	27.5	31.8	35.0	36.0	35.2	32.9	30.1	31.3	31.7	33.2	35.3
E2	24.0	22.9	19.6	20.0	18.0	21.1	21.2	26.1	15.6	23.8	20.7	20.7
CH2	19.2	13.8	12.3	15.0	13.5	21.1	12.7	10.0	15.6	15.9	14.5	12.4
K3	40.5	41.5	41.3	35.3	37.5	28.6	36.9	37.5	44.4	34.0	36.9	36.0
I3	29.8	31.9	36.3	41.2	41.7	44.6	38.8	33.5	37.0	37.7	38.8	40.3
E3	29.8	26.6	22.3	23.5	20.8	26.8	24.3	29.0	18.5	28.3	24.3	23.7
K/A	0.09	0.09	0.10	0.10	0.10	0.10	0.10	0.10	0.10	0.09	0.10	0.10
C/A	0.02	0.02	0.02	0.01	0.02	0.02	0.02	0.03	0.02	0.01	0.02	0.01

Var.\ID:	SD6.5	SD6.55	SD6.6	SD6.65	SD6.7	SD6.75	SD6.8S	SD6.85	SD6.9	SD6.95	SD7.0	SD6-7.03
SiO2	57.53	56.08	55.51	59.63	57.49	60.34	62.48	60.85	59.60	57.97	52.55	52.19
Al2O3	20.24	20.13	22.22	19.17	21.14	19.69	18.80	18.52	18.69	20.10	24.43	21.11
TiO2	0.81	0.81	0.87	0.89	0.86	0.86	0.87	0.86	0.82	0.84	0.89	0.81
Fe2O3	8.73	9.60	7.08	8.29	6.97	7.22	7.15	8.03	9.24	8.67	6.87	11.70
MgO	1.12	1.13	1.39	0.94	1.23	1.04	0.90	0.90	0.97	1.10	1.19	1.20
CaO	0.29	0.29	0.35	0.25	0.32	0.30	0.25	0.24	0.23	0.25	0.30	0.27
Na2O	0.34	0.45	0.50	0.30	0.48	0.53	0.65	0.63	0.57	0.47	0.23	0.33
K2O	1.99	1.99	2.18	1.89	2.06	1.95	1.85	1.81	1.79	1.94	2.33	2.12
MnO	0.07	0.08	0.07	0.06	0.07	0.04	0.06	0.07	0.09	0.07	0.05	0.09
P2O5	0.28	0.33	0.21	0.30	0.24	0.29	0.28	0.30	0.32	0.31	0.15	0.37
LOI	8.57	8.81	9.69	7.94	8.97	8.06	7.56	7.57	7.91	8.59	10.75	9.73
Total	99.97	99.70	100.07	100.05	99.83	100.34	100.85	99.78	100.23	100.31	99.74	99.92
As	12	14	9	10	8	9	10	9	13	12	41	14
Ba	467	476	452	453	464	471	477	459	432	416	433	447
Ce	105	108	112	93	106	103	76	84	105	96	103	114
Co	26	26	25	25	23	25	21	25	22	24	13	23
Cr	130	129	134	134	129	114	112	114	115	132	151	146
Cu	55	51	622	40	400	35	571	644	44	45	620	68
La	53	46	54	41	53	52	45	49	41	45	61	56
Mo	3	3	2	3	3	2	2	2	3	4	37	6
Ni	59	60	73	51	60	51	43	47	51	54	37	67
Nb	14	14	15	15	15	14	15	15	13	14	15	15
Pb	22	27	39	25	40	26	41	37	25	26	45	19
Rb	97	97	105	103	106	102	106	97	90	95	132	106
S	961	963	1093	491	933	933	622	612	853	1030	1122	1272
Se	0	0	0	0	0	0	0	0	0	0	4	0
Sr	100	100	106	97	107	100	101	97	95	93	92	89
Th	12	12	15	10	15	11	12	15	10	10	18	9
U	5	7	4	3	4	4	4	3	4	4	9	5
V	119	125	120	112	116	117	109	114	112	125	147	146
Y	25	25	30	25	29	28	26	25	24	26	28	30
Zn	82	81	78	86	84	81	100	90	84	90	44	104
Zr	173	171	144	198	163	199	202	207	194	176	110	129
DEPTH	6.50	6.55	6.60	6.65	6.70	6.75	6.80	6.85	6.90	6.95	7.00	7.03
K1	31.9	30.8	40.6	39.3	39.7	41.7	44.8	44.8	36.7	36.2	31.0	34.0
I1	29.4	31.5	28.5	26.1	28.4	27.9	25.1	28.9	31.2	27.7	28.1	34.0
E1	23.1	21.0	17.4	20.0	15.4	17.0	18.4	13.6	17.3	23.4	26.9	18.0
CH1	15.7	16.6	13.6	14.6	13.5	13.3	11.7	12.7	14.7	12.8	14.0	13.2
K2	34.0	32.8	43.5	42.2	42.4	43.9	47.6	46.9	39.1	37.8	33.8	35.6
I2	31.3	33.6	30.5	28.1	30.3	29.3	26.6	30.1	33.2	28.9	30.6	30.6
E2	24.6	22.4	18.6	21.5	19.7	17.9	19.5	14.2	18.5	24.4	29.4	19.8
CH2	10.1	11.2	7.4	8.3	7.6	8.9	6.2	8.9	9.2	8.9	6.1	8.9
K3	37.8	37.0	46.9	46.0	45.9	48.2	50.8	51.4	43.1	41.5	34.0	39.1
I3	34.8	37.8	33.0	30.6	32.8	32.2	28.4	33.1	36.6	31.7	37.6	39.1
E3	27.4	25.2	20.1	22.4	21.3	19.6	20.8	15.6	20.3	26.8	31.3	21.7
K/A	0.10	0.10	0.10	0.10	0.10	0.10	0.10	0.10	0.10	0.10	0.10	0.10
C/A	0.01	0.01	0.02	0.01	0.02	0.02	0.01	0.01	0.01	0.01	0.01	0.01

Var.\ID:	SD7.05	SD7.1	SD7.15	SD7.2	SD7.25	SD7.3	SD7.35	SD7.4	SD9-7.45	SD7.45	SD8-7.47S	SD7.5
SiO2	52.54	52.77	52.56	44.61	51.79	52.99	53.27	53.31	56.28	51.05	52.26	55.98
Al2O3	23.56	23.68	22.14	19.39	22.26	22.51	22.04	21.50	22.69	21.98	22.99	22.50
TiO2	0.87	0.87	0.83	0.72	0.83	0.85	0.83	0.81	0.95	0.80	0.85	0.96
Fe2O3	7.85	7.62	9.94	19.91	10.43	9.15	9.92	10.46	5.90	11.48	8.84	5.84
MgO	1.17	1.19	1.18	1.09	1.28	1.23	1.18	1.27	1.15	1.24	1.24	1.13
CaO	0.30	0.29	0.39	0.36	0.29	0.29	0.27	0.27	0.20	0.27	0.30	0.21
Na2O	0.18	0.23	0.32	0.25	0.29	0.33	0.38	0.33	0.47	0.30	0.31	0.24
K2O	2.38	2.29	2.26	2.04	2.35	2.32	2.23	2.19	2.20	2.29	2.31	2.19
MnO	0.05	0.04	0.08	0.19	0.08	0.07	0.08	0.10	0.02	0.10	0.05	0.03
P2O5	0.18	0.18	0.24	0.79	0.31	0.24	0.27	0.31	0.16	0.36	0.21	0.17
LOI	10.46	10.39	10.20	10.29	10.13	10.24	9.60	9.42	10.19	9.99	10.78	10.37
Total	99.54	99.65	100.04	99.64	100.03	100.22	100.07	99.97	100.21	99.95	100.14	99.72
As	35	32	31	55	29	19	15	15	40	10	37	44
Ba	442	461	508	545	552	536	399	382	395	389	509	404
Ce	99	115	127	172	137	97	115	103	112	110	106	96
Co	14	13	12	20	17	18	22	19	5	26	21	7
Cr	154	148	151	147	165	150	139	147	149	136	156	155
Cu	56	54	57	873	87	70	694	57	31	63	60	36
La	57	53	57	72	68	63	50	47	43	53	54	51
Mo	36	28	22	18	27	26	8	4	13	4	30	14
Ni	51	41	54	59	64	57	60	69	23	81	58	23
Nb	14	15	15	12	15	14	13	14	15	13	16	14
Pb	24	30	31	52	27	32	40	19	9	21	22	10
Rb	129	126	120	102	119	118	113	111	112	109	124	112
S	991	1503	2944	2361	2763	3272	907	610	933	523	2354	1002
Se	7	4	4	5	7	5	0	2	0	2	6	0
Sr	90	96	100	101	111	103	93	82	80	75	102	81
Th	13	13	13	16	13	11	16	14	15	12	11	13
U	7	7	6	7	7	6	3	4	6	5	6	6
V	164	144	150	165	184	148	133	135	127	136	157	129
Y	29	27	29	39	29	26	29	27	26	29	30	27
Zn	54	45	66	98	76	72	86	101	31	120	69	39
Zr	113	117	125	111	122	127	138	141	133	118	96	132
DEPTH	7.05	7.10	7.15	7.20	7.25	7.30	7.35	7.40	7.45	7.45	7.47	7.50
K1	25.3	28.0	23.4	28.1	24.7	27.3	30.5	30.6	29.5	29.1	30.8	28.4
I1	31.6	28.0	32.3	31.0	27.2	28.6	27.5	32.8	28.5	31.6	30.0	28.2
E1	25.9	26.0	24.2	22.9	25.9	24.2	24.4	24.0	25.2	23.9	24.5	25.0
CH1	17.2	18.0	20.2	18.0	22.2	19.8	17.6	12.6	16.8	15.3	14.9	18.4
K2	28.6	29.8	26.3	30.6	27.8	30.3	33.3	31.8	33.5	30.9	33.5	30.9
I2	35.7	29.8	36.3	33.8	30.6	31.8	30.0	34.1	32.3	33.5	32.3	30.7
E2	29.2	27.7	27.2	24.9	29.2	26.9	26.7	25.0	28.5	25.4	26.6	27.2
CH2	6.5	12.8	10.2	10.7	12.5	11.0	10.0	9.1	5.7	10.2	7.6	11.1
K3	30.6	34.1	29.3	34.3	31.7	34.1	37.0	35.0	35.5	34.4	36.2	34.8
I3	38.2	34.1	40.4	37.8	34.9	35.7	33.3	37.5	34.3	37.3	35.0	34.6
E3	31.3	31.7	30.3	27.9	33.3	30.2	29.6	27.5	30.2	28.3	28.8	30.7
K/A	0.10	0.10	0.10	0.11	0.11	0.10	0.10	0.10	0.10	0.10	0.10	0.10
C/A	0.01	0.01	0.01	0.02	0.01	0.01	0.01	0.01	0.01	0.01	0.01	0.01

Var.\ID:	SD7.55	SD7.6	SD7.65	SD7.7	SD7.75	SD7.8	SD7.85	SD10-7.9	SD8.1	SD8.15	SD8.2	SD8.25
SiO2	55.11	56.28	57.59	55.14	57.18	58.38	58.68	55.10	55.30	56.17	56.67	50.67
Al2O3	23.24	23.46	22.87	21.45	21.52	22.64	22.80	21.26	19.63	20.77	21.37	18.52
TiO2	0.94	0.97	0.98	0.82	0.85	0.89	0.88	0.87	0.76	0.80	0.79	0.67
Fe2O3	5.39	4.44	3.56	7.14	6.43	3.47	3.50	8.04	8.29	6.61	6.53	14.57
MgO	1.17	1.12	1.11	1.00	1.00	1.12	1.10	1.03	1.01	1.14	1.12	0.94
CaO	0.21	0.20	0.20	0.19	0.17	0.17	0.17	0.16	0.16	0.16	0.16	0.15
Na2O	0.36	0.41	0.47	0.26	0.23	0.15	0.22	0.15	0.17	0.21	0.27	0.20
K2O	2.37	2.25	2.32	2.97	2.80	3.03	2.98	2.89	2.79	3.00	2.83	2.52
MnO	0.02	0.04	0.01	0.03	0.00	0.00	0.02	0.01	0.02	0.02	0.00	0.08
P2O5	0.17	0.11	0.09	0.13	0.11	0.06	0.07	0.17	0.18	0.15	0.14	0.25
LOI	11.36	10.65	10.79	10.82	10.07	10.09	9.90	10.46	11.92	11.14	10.03	11.46
Total	100.34	99.93	99.98	99.97	100.32	100.00	100.32	100.14	100.23	100.17	99.91	100.03
As	59	44	21	105	74	40	31	106	119	87	58	81
Ba	548	458	595	528	477	457	435	508	442	458	419	357
Ce	125	104	92	119	106	120	115	124	82	98	81	62
Co	7	5	4	5	3	5	4	3	8	6	8	38
Cr	149	159	144	187	175	158	159	166	248	222	180	168
Cu	27	29	19	55	33	30	31	75	120	95	73	148
La	60	53	52	57	54	59	64	58	42	49	45	43
Mo	28	20	14	79	78	81	73	80	166	141	141	162
Ni	21	22	22	15	14	15	16	23	32	20	22	68
Nb	16	16	16	15	15	17	17	17	14	14	14	11
Pb	45	19	41	22	31	50	35	34	45	31	23	27
Rb	122	121	117	135	127	146	140	133	122	131	129	111
S	5918	1628	6066	2217	1695	3128	1960	3017	1293	820	746	1726
Se	0	0	0	23	15	9	10	16	44	29	14	15
Sr	113	86	99	88	90	99	98	89	75	80	72	61
Th	15	15	13	9	12	8	10	15	11	11	13	9
U	7	7	5	13	12	13	13	10	10	10	7	10
V	127	121	121	290	275	208	222	264	543	432	286	270
Y	24	26	27	31	26	26	26	26	19	19	19	15
Zn	29	16	16	10	11	7	6	39	89	74	83	230
Zr	120	135	151	118	125	128	126	66	106	109	103	89
DEPTH	7.55	7.60	7.65	7.70	7.75	7.80	7.85	7.90	8.10	8.15	8.20	8.25
K1	33.8	31.2	30.6	36.1	27.2	25.6	26.9	24.7	21.3	18.5	25.6	20.6
I1	39.3	39.3	36.9	36.1	46.2	38.3	38.2	33.1	48.9	43.7	40.4	46.0
E1	21.4	23.8	28.6	23.9	17.4	23.3	21.3	29.1	17.0	25.2	24.9	25.3
CH1	14.5	14.6	13.9	13.9	9.2	12.8	13.6	13.1	12.8	12.6	9.1	8.1
K2	37.1	34.4	33.9	40.6	29.0	27.6	29.4	26.6	22.0	19.7	26.2	20.9
I2	33.2	33.4	30.0	29.4	49.3	41.4	41.6	35.8	50.5	46.7	41.4	46.7
E2	23.5	26.2	31.7	26.9	18.6	25.2	23.2	31.4	17.6	27.0	25.5	25.6
CH2	6.2	6.0	4.7	3.1	3.0	5.7	5.8	6.2	9.9	6.6	6.9	6.9
K3	29.5	36.5	35.5	41.9	29.9	29.3	31.2	28.4	24.4	21.1	28.1	22.4
I3	35.4	35.5	31.3	30.3	50.9	43.0	44.2	38.1	56.1	50.0	44.4	50.1
E3	25.1	27.9	33.2	27.8	19.2	26.8	24.6	33.5	19.5	28.9	27.4	27.5
K/A	0.10	0.10	0.10	0.14	0.13	0.13	0.13	0.14	0.14	0.14	0.13	0.14
C/A	0.01	0.01	0.01	0.01	0.01	0.01	0.01	0.01	0.01	0.01	0.01	0.01

Var.\ID:	SD8.3	SD8.35	SD8.4	SD12-8.45	SD8.7	SD8.75	SD8.8	SD8.85S	SD8.9	SD8.95	SD9.0	SD9.05
SiO2	53.38	46.58	45.69	53.41	53.61	53.72	54.84	57.05	56.71	58.41	57.91	57.15
Al2O3	20.10	16.42	16.29	21.39	20.45	21.00	22.29	23.14	23.11	24.18	24.52	23.91
TiO2	0.74	0.61	0.68	0.87	0.82	0.79	0.90	0.95	0.96	0.91	0.90	0.90
Fe2O3	10.56	19.76	21.26	10.23	9.33	9.31	8.44	5.66	5.71	2.86	2.98	4.06
MgO	1.03	0.75	0.67	0.79	1.02	0.99	0.79	0.81	0.80	0.81	0.84	0.82
CaO	0.15	0.13	0.13	0.15	0.19	0.19	0.15	0.14	0.14	0.14	0.14	0.14
Na2O	0.17	0.14	0.11	0.23	0.19	0.22	0.30	0.42	0.37	0.29	0.40	0.34
K2O	2.81	2.26	2.09	2.22	2.57	2.61	2.07	2.19	2.20	2.29	2.30	2.28
MnO	0.04	0.17	0.11	0.04	0.02	0.02	0.01	0.03	0.02	0.00	0.01	0.01
P2O5	0.17	0.34	0.48	0.36	0.16	0.15	0.08	0.06	0.08	0.07	0.07	0.11
LOI	11.00	13.13	12.17	10.32	11.82	11.43	10.06	9.78	9.90	9.85	9.71	9.81
Total	100.15	100.29	99.48	100.01	100.18	100.43	99.93	100.23	100.00	99.81	99.78	99.52
As	103	74	50	28	87	86	17	14	12	16	10	15
Ba	410	463	485	408	504	509	390	294	386	350	352	357
Ce	107	89	84	78	104	112	101	55	80	95	100	82
Co	16	50	34	7	11	9	6	0	4	0	0	0
Cr	166	184	167	135	200	156	140	141	134	132	135	136
Cu	741	236	215	96	96	76	80	57	54	38	26	33
La	35	40	26	42	46	54	41	49	39	51	50	54
Mo	165	218	169	45	89	70	9	4	5	4	4	7
Ni	29	124	126	29	33	32	21	18	18	19	20	22
Nb	14	10	12	14	15	14	14	17	16	17	17	16
Pb	44	29	25	15	29	45	13	14	15	28	24	30
Rb	121	97	86	109	117	119	104	112	111	118	119	115
S	1191	2474	2157	1723	2475	3227	1754	3145	2060	2254	1919	2590
Se	18	26	20	4	25	19	0	0	0	0	0	0
Sr	71	52	46	65	79	85	68	74	73	78	79	78
Th	14	9	8	12	9	11	13	12	11	14	14	14
U	9	9	7	5	10	9	3	4	3	4	5	4
V	283	381	291	139	335	284	131	119	112	115	117	114
Y	18	20	17	21	22	24	22	22	22	25	24	24
Zn	117	285	130	18	51	41	12	11	10	9	9	10
Zr	99	93	110	85	115	116	129	141	134	129	122	118
DEPTH	8.30	8.35	8.40	8.45	8.70	8.75	8.80	8.85	8.90	8.95	9.00	9.05
K1	20.4	22.9	27.8	32.4	19.7	28.7	39.3	41.4	42.8	33.5	30.5	36.8
I1	31.0	35.8	41.7	36.6	36.7	40.2	31.7	31.8	28.3	29.0	30.0	41.2
E1	17.0	27.5	19.4	22.5	30.5	18.9	22.2	17.2	21.5	27.0	30.6	16.5
CH1	11.7	13.7	11.1	8.6	13.2	12.3	6.9	9.6	7.4	10.5	9.0	5.5
K2	20.4	22.9	27.8	33.5	20.7	30.6	39.3	42.6	44.6	34.7	30.5	36.8
I2	31.0	35.8	41.7	37.8	38.7	42.9	31.7	32.8	29.5	30.0	30.0	41.2
E2	17.0	27.5	19.4	23.2	32.1	20.1	22.2	17.8	22.4	28.0	30.6	16.5
CH2	11.7	13.7	11.1	5.4	9.4	6.4	6.9	6.8	3.5	7.3	9.0	5.5
K3	23.1	26.6	31.3	35.4	22.6	32.7	42.2	45.7	46.2	37.4	33.5	39.0
I3	37.7	41.6	46.9	40.0	42.3	45.8	34.0	35.2	30.5	32.4	32.9	43.6
E3	19.2	31.9	21.9	24.6	35.1	21.5	23.8	19.1	23.3	30.2	33.6	17.4
K/A	0.14	0.14	0.13	0.10	0.13	0.12	0.09	0.09	0.10	0.09	0.09	0.10
C/A	0.01	0.01	0.01	0.01	0.01	0.01	0.01	0.01	0.01	0.01	0.01	0.01

Ver.\ID:	SD9.1	SD9.15	SD9.2	SD14-9.2B	SD9.4	SD9.45	SD9.5	SD9.55	SD9.575	SD9.6W	SD9.625W	SD9.6S
SiO2	57.97	56.30	55.62	55.12	51.44	51.70	51.44	52.54	51.89	51.99	51.26	51.71
Al2O3	24.78	26.14	25.88	25.15	24.84	25.13	25.09	24.91	24.75	24.61	24.14	25.05
TiO2	0.91	0.91	0.90	0.87	0.83	0.84	0.82	0.81	0.83	0.83	0.83	0.85
Fe2O3	2.58	1.92	2.86	4.32	6.79	6.33	6.61	5.87	6.61	6.62	7.64	6.55
MgO	0.83	0.89	0.96	0.92	1.09	1.20	1.20	1.19	1.25	1.28	1.22	1.26
CaO	0.14	0.14	0.15	0.14	0.15	0.15	0.16	0.16	0.16	0.17	0.18	0.17
Na2O	0.34	0.24	0.31	0.26	0.29	0.33	0.24	0.30	0.29	0.31	0.25	0.33
K2O	2.26	2.35	2.44	2.32	2.19	2.20	2.20	2.24	2.20	2.23	2.30	2.23
MnO	0.00	0.02	0.02	0.01	0.03	0.03	0.03	0.02	0.05	0.02	0.02	0.04
P2O5	0.10	0.07	0.12	0.14	0.12	0.09	0.09	0.07	0.12	0.12	0.18	0.10
LOI	9.75	10.48	10.25	10.38	11.50	11.82	11.82	11.87	11.63	11.72	11.79	11.85
Total	99.66	99.46	99.51	99.62	99.61	99.82	99.70	99.98	99.78	99.90	99.81	100.14
As	13	2	8	14	12	17	13	12	19	16	27	8
Ba	393	375	511	425	352	327	324	349	339	344	367	314
Ce	109	117	108	87	95	108	102	126	107	100	107	115
Co	3	0	6	0	11	14	17	13	15	13	14	14
Cr	142	149	144	139	158	149	147	147	144	145	143	138
Cu	25	18	17	33	73	82	93	97	34	34	39	44
La	66	68	62	56	54	51	56	53	59	45	53	52
Mo	2	4	4	3	3	3	4	3	3	3	4	2
Ni	25	31	29	33	63	74	76	74	83	74	71	76
Nb	15	17	16	16	15	14	15	14	14	14	15	14
Pb	26	32	37	27	29	24	27	21	27	24	32	25
Rb	118	128	132	127	114	116	117	115	113	115	119	113
S	3006	1409	3630	4256	24429	27206	28230	25155	25910	25561	26480	25441
Se	0	0	0	0	0	0	0	0	0	0	0	0
Sr	86	84	92	82	70	68	71	73	70	70	74	70
Th	19	15	13	16	15	13	14	13	12	12	13	12
U	4	4	5	3	5	4	5	6	6	6	6	6
V	112	120	125	126	119	118	122	117	119	112	134	123
Y	25	27	24	27	23	25	24	26	24	24	24	24
Zn	9	14	16	18	37	34	39	34	34	36	37	38
Zr	126	116	111	107	104	103	97	102	99	105	99	99
DEPTH	9.10	9.15	9.20	9.28	9.40	9.45	9.50	9.55	9.57	9.60	9.63	9.65
K1	35.9	37.2	36.0	39.7	33.4	31.2	34.4	35.2	41.9	39.1	31.1	35.7
I1	27.6	28.1	32.0	29.4	31.6	32.3	30.7	33.0	34.4	31.6	36.1	35.7
E1	27.6	23.3	22.0	22.1	22.6	20.4	23.7	19.9	11.5	15.3	13.8	8.9
CH1	8.8	11.4	9.0	8.8	12.4	16.1	11.2	11.9	12.2	13.9	19.0	19.6
K2	37.2	40.6	37.1	41.9	35.4	32.3	36.0	35.9	43.6	39.9	33.3	37.7
I2	28.6	30.7	33.0	31.0	33.5	33.4	32.2	33.6	35.8	32.3	39.7	37.7
E2	28.6	25.4	23.7	23.3	23.9	21.1	24.9	20.3	11.9	15.6	14.8	9.4
CH2	5.5	3.2	6.2	3.9	7.2	13.2	6.9	10.2	8.7	12.2	13.2	15.1
K3	39.4	42.0	39.6	43.5	38.3	37.2	38.7	40.0	47.7	45.4	38.3	44.4
I3	30.3	31.7	35.2	32.3	36.1	38.5	34.6	37.4	39.2	36.7	44.6	44.4
E3	30.3	26.3	25.3	24.2	25.8	24.3	26.7	22.6	13.1	17.8	17.1	11.1
K/A	0.09	0.09	0.09	0.09	0.09	0.09	0.09	0.09	0.09	0.09	0.10	0.09
C/A	0.01	0.01	0.01	0.01	0.01	0.01	0.01	0.01	0.01	0.01	0.01	0.01

Var.\ID:	SD9.65W	SD9.65U	SD9.7	SD9.75	SD9.8	SD16-9.93	SD10.1	SD10.15	SD10.2	SD10.25	SD10.3	SD10.35
SiO2	51.62	51.45	51.24	50.01	51.21	51.43	51.60	51.61	51.22	51.46	51.35	49.73
Al2O3	24.04	25.48	25.74	25.30	24.35	24.41	24.46	24.37	24.58	24.54	24.67	23.94
TiO2	0.84	0.80	0.82	0.81	0.82	0.79	0.81	0.79	0.80	0.81	0.81	0.75
Fe2O3	7.59	6.35	6.29	6.68	6.12	6.21	6.25	6.28	6.35	6.29	6.24	6.10
MgO	1.29	1.19	1.20	1.21	1.27	1.41	1.39	1.44	1.43	1.49	1.46	1.50
CaO	0.19	0.17	0.16	0.16	0.18	0.17	0.18	0.17	0.18	0.18	0.18	0.18
Na2O	0.36	0.29	0.33	0.21	0.33	0.38	0.25	0.43	0.28	0.35	0.33	0.27
K2O	2.29	2.18	2.25	2.30	2.34	2.34	2.38	2.42	2.37	2.39	2.40	2.40
MnO	0.03	0.02	0.04	0.08	0.00	0.03	0.03	0.03	0.02	0.03	0.02	0.11
P2O5	0.21	0.09	0.08	0.10	0.07	0.09	0.09	0.09	0.08	0.09	0.09	0.08
LOI	11.52	11.84	11.91	12.54	13.14	12.84	12.13	12.26	12.44	12.32	12.47	12.98
Total	100.08	99.86	100.06	99.40	99.93	100.10	99.77	99.89	99.75	99.95	100.02	100.04
As	29	8	12	12	16	11	16	19	19	16	16	26
Ba	363	391	368	350	363	372	405	399	355	400	401	379
Ce	123	112	110	110	106	112	117	118	127	132	124	107
Co	12	16	18	27	24	29	24	24	21	27	22	30
Cr	141	142	137	139	143	144	148	142	142	146	145	138
Cu	35	44	45	54	55	57	55	49	47	48	43	69
La	55	57	52	60	55	62	55	55	52	56	63	59
Mo	4	4	4	10	5	5	4	5	4	3	4	10
Ni	67	76	82	118	59	101	107	100	101	102	99	112
Nb	14	15	13	13	14	15	13	14	14	14	14	13
Pb	29	28	27	28	27	25	31	31	32	29	30	35
Rb	117	113	114	115	120	119	117	120	122	122	123	119
S	25277	24568	24519	32449	29629	23037	23316	26232	27020	25535	25150	45468
Se	0	0	0	0	0	0	0	0	0	0	0	0
Sr	78	70	71	75	74	78	82	80	77	82	80	78
Th	13	15	13	11	14	13	13	16	14	15	12	12
U	5	5	4	6	6	5	6	6	5	6	7	6
V	135	117	123	128	148	153	122	126	126	128	140	135
Y	24	24	26	25	30	34	32	32	32	30	29	29
Zn	43	47	37	53	69	89	125	109	120	145	134	108
Zr	102	99	100	94	102	100	98	102	98	99	97	97
DEPTH	9.65	9.65	9.70	9.75	9.80	9.93	10.10	10.15	10.20	10.25	10.30	10.35
K1	33.2	38.8	40.1	35.3	34.9	34.8	42.3	34.2	35.4	39.0	32.6	37.7
I1	35.0	40.1	36.7	44.7	40.5	40.7	32.8	41.5	37.6	32.5	35.2	34.6
E1	15.5	11.1	11.2	5.6	12.3	6.9	14.6	3.5	13.3	17.3	14.5	16.8
CH1	16.3	10.0	12.0	14.4	12.3	15.6	10.2	20.7	13.8	11.1	17.6	11.0
K2	36.2	39.9	40.3	35.7	35.3	35.1	44.1	36.2	36.4	39.0	33.1	37.9
I2	38.1	41.2	34.9	45.1	41.0	38.9	34.2	43.8	38.6	32.5	35.7	34.7
E2	16.8	11.5	11.4	5.4	12.4	6.6	15.2	3.7	13.6	17.3	14.7	16.8
CH2	8.9	7.4	11.4	13.6	11.2	19.4	6.4	16.3	11.4	11.1	16.5	10.5
K3	39.7	43.1	45.5	41.7	39.8	43.6	47.2	43.2	41.0	43.9	39.6	42.4
I3	41.8	44.6	41.7	52.2	46.2	48.2	36.6	52.3	43.6	36.6	42.8	38.8
E3	18.5	12.4	12.8	6.5	14.0	8.2	16.3	4.5	15.4	19.5	17.6	18.8
K/A	0.10	0.09	0.09	0.09	0.10	0.10	0.10	0.10	0.10	0.10	0.10	0.10
C/A	0.01	0.01	0.01	0.01	0.01	0.01	0.01	0.01	0.01	0.01	0.01	0.01

Var.\ID:	SD10.4	SD10.45	SD10.53	SD10.7	SD10.75	SD10.8	SD10.85	SD10.9	SD10.95	SD11.07	SD11.78	SD11.85
SiO2	51.38	52.16	56.32	15.21	54.11	55.03	53.79	56.02	57.23	51.38	53.40	57.16
Al2O3	24.42	25.15	24.41	5.72	20.82	21.63	21.55	22.56	22.47	23.15	21.61	22.31
TiO2	0.78	0.81	0.90	0.31	0.86	0.88	0.87	0.91	0.89	0.84	0.86	0.91
Fe2O3	7.27	5.92	3.50	39.43	7.91	7.08	8.03	5.87	5.10	8.08	7.97	4.86
MgO	1.61	1.59	1.41	6.47	1.90	1.55	1.56	1.57	1.51	1.62	1.67	1.45
CaO	0.18	0.18	0.18	2.65	0.40	0.35	0.39	0.32	0.28	0.37	0.39	0.31
Na2O	0.38	0.26	0.34	0.00	0.37	0.35	0.36	0.39	0.39	0.27	0.39	0.38
K2O	2.44	2.49	2.36	0.62	2.18	2.25	2.19	2.30	2.42	2.29	2.19	2.25
MnO	0.03	0.04	0.04	1.09	0.26	0.24	0.36	0.24	0.16	0.31	0.23	0.08
P2O5	0.09	0.09	0.15	0.71	0.10	0.11	0.13	0.11	0.10	0.13	0.12	0.11
LOI	12.03	11.17	10.08	28.52	11.29	10.53	10.90	10.02	9.59	11.39	11.54	9.96
Total	100.61	99.86	99.69	100.69	100.20	100.10	100.13	100.21	100.14	99.83	100.77	99.78
As	20	12	10	7	2	3	0	2	2	11	15	7
Ba	336	367	361	444	384	322	431	347	338	404	338	352
Ce	126	137	127	119	111	128	127	141	133	111	121	119
Co	27	22	26	26	23	23	23	28	24	25	25	27
Cr	137	148	143	67	133	142	139	146	140	140	137	143
Cu	57	48	53	24	43	46	44	43	51	44	49	46
La	59	71	74	26	55	65	53	60	71	75	67	59
Mo	8	4	0	3	3	1	1	1	1	0	2	3
Ni	105	120	199	43	76	76	73	84	83	82	72	86
Nb	13	16	18	4	15	14	16	16	17	16	17	16
Pb	36	24	10	6	9	12	11	7	11	10	13	12
Rb	125	125	113	28	102	105	98	107	110	106	101	105
S	35462	22171	2193	3424	2707	2110	1833	1732	1990	1153	1840	3371
Se	0	0	0	0	0	0	0	0	0	0	0	0
Sr	80	100	105	53	88	92	91	92	96	90	81	89
Th	13	15	12	1	13	14	13	15	13	19	16	14
U	7	6	5	0	3	4	2	3	3	2	4	5
V	135	137	132	64	121	125	121	129	136	133	125	132
Y	29	33	42	63	54	46	54	94	87	44	38	37
Zn	154	175	208	40	112	116	116	108	108	92	96	96
Zr	98	104	153	67	156	146	142	145	151	109	142	165
DEPTH	10.40	10.45	10.53	10.70	10.75	10.80	10.85	10.90	10.95	11.07	11.78	11.88
K1	40.8	36.5	39.0	51.0	34.7	35.4	34.6	27.0	28.2	34.5	30.8	38.0
I1	33.6	35.1	38.6	49.0	35.4	33.4	32.9	41.5	37.5	32.2	37.0	36.6
E1	15.2	19.1	12.2	0.0	19.4	19.7	22.3	17.8	23.5	21.9	24.7	14.0
CH1	10.4	9.2	10.2	0.0	10.4	11.4	10.2	13.7	10.9	11.3	17.5	11.2
K2	42.0	36.4	38.1	51.0	36.0	36.6	35.2	27.8	28.9	36.5	21.3	39.1
I2	34.6	35.0	37.7	49.0	36.7	34.6	33.5	42.8	38.6	34.1	37.9	37.7
E2	15.6	19.1	11.9	0.0	20.1	20.4	22.7	18.3	24.1	23.2	25.2	14.4
CH2	7.8	9.5	12.4	0.0	7.2	8.4	8.6	11.1	8.4	6.2	15.6	8.8
K3	45.5	40.2	43.3	51.0	38.8	40.0	38.5	31.3	31.6	38.9	25.2	42.9
I3	37.5	38.7	43.0	49.0	39.5	37.7	36.7	48.1	42.1	36.7	44.9	41.3
E3	17.0	21.1	13.6	0.0	21.7	22.3	24.8	20.6	26.3	24.8	29.9	15.8
K/A	0.10	0.10	0.10	0.11	0.10	0.10	0.10	0.10	0.11	0.10	0.10	0.10
C/A	0.01	0.01	0.01	0.46	0.02	0.02	0.02	0.01	0.01	0.02	0.02	0.01

Var.\ID:	SD11.9	SD11.95	SD25-12.0	SD12.0	SD25-12.05	SD12.05	SD25-12.1	SD12.10	SD12.15	SD25-12.15	SD12.2	SD25-12.2
SiO2	48.55	55.09	55.23	55.23	54.39	54.82	55.69	58.72	53.69	56.55	55.09	55.99
Al2O3	18.66	21.42	22.39	21.47	21.52	21.81	21.66	22.24	21.17	21.71	20.94	22.65
TiO2	0.77	0.87	0.88	0.88	0.85	0.92	0.88	0.92	0.84	0.90	0.87	0.87
Fe2O3	13.57	7.34	6.14	7.20	7.49	5.72	6.62	4.53	8.51	6.05	7.81	5.61
MgO	2.10	1.44	1.50	1.41	1.53	1.41	1.45	1.37	1.56	1.45	1.50	1.41
CaO	0.67	0.41	0.34	0.42	0.40	0.34	0.39	0.29	0.48	0.35	0.44	0.25
Na2O	0.55	0.42	0.38	0.40	0.40	0.37	0.44	0.43	0.42	0.45	0.42	0.36
K2O	1.85	2.09	2.29	2.13	2.14	2.20	2.09	2.27	1.99	2.19	2.04	2.29
MnO	0.34	0.18	0.15	0.17	0.17	0.11	0.13	0.06	0.21	0.11	0.17	0.03
P2O5	0.18	0.13	0.11	0.14	0.13	0.13	0.13	0.10	0.13	0.12	0.14	0.08
LOI	12.92	10.89	10.49	10.86	11.10	10.11	10.74	9.59	11.28	10.37	10.90	10.50
Total	101.16	100.28	99.90	100.31	100.05	99.94	100.22	100.52	100.28	100.25	100.32	100.04
As	4	14	6	11	8	8	12	17	12	12	11	11
Ba	376	355	338	358	338	338	346	357	357	357	411	411
Ce	139	126	130	125	120	120	131	131	122	122	125	125
Co	20	21	25	25	24	24	22	25	23	23	22	22
Cr	123	135	137	134	138	138	132	141	138	138	146	146
Cu	41	42	48	40	44	44	44	48	47	47	49	49
La	51	51	65	72	57	57	57	57	46	46	54	54
Mo	1	2	2	2	2	2	1	2	1	1	2	2
Ni	55	82	87	81	79	79	68	80	79	79	79	79
Nb	14	16	17	16	16	16	16	16	16	16	15	15
Pb	8	13	13	14	13	13	12	15	13	13	19	19
Rb	81	96	104	98	97	97	96	104	100	100	107	107
S	2493	3457	2405	3324	2940	2940	3513	4444	3677	3677	16063	16063
Se	0	0	0	0	0	0	0	0	0	0	0	0
Sr	79	87	87	84	86	86	88	87	87	87	87	87
Th	14	13	14	14	13	13	13	13	13	13	14	14
U	4	4	4	4	3	3	3	4	4	4	4	4
V	113	130	130	126	128	128	124	131	134	134	138	138
Y	36	38	37	37	37	37	36	37	38	39	39	39
Zn	79	80	95	80	82	82	82	87	87	97	90	90
Zr	135	151	142	155	150	150	157	173	160	160	146	146
DEPTH	11.93	11.95	12.00	12.00	12.05	12.05	12.10	12.10	12.15	12.15	12.20	12.20
K1	24.7	36.4	31.1	25.4	30.6	25.5	34.0	36.5	28.8	30.3	31.4	29.5
I1	29.4	48.1	30.5	41.2	30.1	35.3	31.2	34.4	44.1	32.5	35.8	31.9
E1	33.2	15.5	31.1	16.7	28.5	26.3	24.6	18.5	11.7	27.8	20.1	29.6
CH1	12.8	0.0	7.2	16.7	10.8	12.9	10.2	10.6	15.3	9.4	12.7	9.0
K2	24.8	36.4	30.3	25.8	32.2	25.8	35.5	38.0	29.4	31.1	32.9	29.5
I2	29.6	48.1	29.7	41.9	31.7	35.7	32.5	35.8	45.0	33.4	37.4	31.9
E2	33.5	15.5	30.3	17.0	30.0	26.6	25.6	19.3	11.9	28.6	21.9	29.6
CH2	12.1	0.0	9.8	15.3	6.0	11.9	6.4	6.9	13.8	6.9	8.7	9.0
K3	28.3	36.4	32.5	30.5	34.3	29.3	37.9	40.8	34.0	33.4	36.0	32.4
I3	33.7	48.1	32.9	49.5	33.8	40.5	34.7	38.5	52.1	35.9	41.0	35.0
E3	38.1	15.5	33.5	20.1	31.9	30.2	27.4	20.7	13.8	30.7	23.0	32.6
K/A	0.10	0.10	0.10	0.10	0.10	0.10	0.10	0.10	0.09	0.10	0.10	0.10
C/A	0.04	0.02	0.02	0.02	0.02	0.02	0.02	0.01	0.02	0.02	0.02	0.01

Ver.\ID:	SD25-12.25	SD12.25	SD12.3	SD25-12.3	SD12.35	SD25-12.35	SD25-12.4	SD12.53	SD12.65	SD12.7	SD12.75	SD12.8
SiO2	55.85	58.27	57.69	55.89	56.17	55.66	55.62	54.57	34.08	32.04	51.40	49.83
Al2O3	22.81	23.04	23.42	22.97	24.25	23.14	22.94	20.81	12.41	11.34	18.99	18.24
TiO2	0.87	0.93	0.94	0.89	0.93	0.88	0.89	0.90	0.53	0.54	0.85	0.80
Fe2O3	5.52	3.84	3.65	5.39	3.92	5.36	5.58	7.44	18.52	25.50	10.80	11.75
MgO	1.26	1.37	1.74	1.35	1.79	1.76	1.41	1.44	3.59	5.53	2.31	2.50
CaO	0.23	0.26	0.23	0.22	0.21	0.22	0.22	0.37	7.39	1.65	0.74	0.86
Na2O	0.40	0.41	0.44	0.42	0.36	0.35	0.37	0.34	0.26	0.20	0.35	0.38
K2O	2.31	2.24	2.22	2.33	2.27	2.38	2.42	2.54	1.34	1.25	2.17	2.10
MnO	0.01	0.02	0.03	0.02	0.01	0.02	0.01	0.08	0.37	0.45	0.17	0.19
P2O5	0.07	0.09	0.08	0.07	0.07	0.07	0.07	0.15	5.11	0.37	0.25	0.21
LOI	10.44	9.45	9.67	10.54	10.11	10.48	10.56	11.48	17.64	22.09	12.10	13.75
Total	99.87	99.92	99.71	100.09	99.69	99.92	100.09	100.12	101.26	101.16	101.13	100.71
As	13	13	10	10	10	10	16	33	5	5	11	9
Ba	396	396	401	401	383	383	387	405	437	755	414	367
Ce	120	120	116	116	118	118	134	109	137	110	90	108
Co	23	23	27	27	24	24	31	24	10	20	19	22
Cr	148	148	147	147	146	146	140	148	99	94	132	133
Cu	52	52	51	51	50	50	54	68	47	32	704	48
La	62	62	60	60	65	65	64	63	69	36	55	47
Mo	2	2	3	3	2	2	3	12	3	2	2	2
Ni	79	79	79	79	81	81	91	103	59	43	73	66
Nb	15	15	16	16	17	17	16	16	9	9	15	14
Pb	20	20	20	20	20	20	24	25	17	13	35	21
Rb	108	108	110	110	112	113	115	120	66	55	99	94
S	17104	17104	20068	20068	22126	22126	23441	22605	11385	7565	9712	10047
Se	0	0	0	0	0	0	0	2	0	0	0	0
Sr	88	88	89	89	88	86	88	87	189	61	77	80
Th	13	13	15	15	13	13	16	11	3	8	15	12
U	3	3	5	5	7	7	6	6	2	3	4	3
V	131	131	140	140	144	144	151	145	100	97	127	126
Y	39	39	39	39	38	38	38	40	145	26	30	32
Zn	86	86	84	84	82	82	95	100	75	47	84	85
Zr	144	144	143	143	139	139	143	145	109	102	152	150
DEPTH	12.25	12.25	12.30	12.30	12.35	12.35	12.40	12.53	12.65	12.73	12.77	12.82
K1	32.9	27.5	20.4	34.0	34.4	30.1	28.5	22.1	29.9	24.2	25.1	29.8
I1	30.5	31.7	37.2	31.5	31.8	32.2	29.6	38.6	49.0	40.4	44.4	34.6
E1	28.4	24.9	17.2	24.9	21.5	24.6	33.0	31.7	21.0	35.4	22.2	26.1
CH1	8.2	15.9	15.2	9.6	12.3	13.1	8.9	7.6	0.0	0.0	8.2	9.4
K2	32.9	26.3	31.4	33.4	36.7	31.5	28.5	22.1	29.9	24.2	25.1	29.8
I2	30.5	32.6	38.4	32.8	34.0	33.6	29.6	38.6	49.0	40.4	44.4	34.6
E2	28.4	25.5	17.8	24.0	22.9	25.6	33.0	31.7	21.0	35.4	22.2	26.1
CH2	8.2	13.6	12.4	5.9	6.4	9.3	8.9	7.6	0.0	0.0	8.2	9.4
K3	35.9	32.7	35.8	37.6	39.2	34.7	31.2	22.9	29.9	24.2	27.4	32.9
I3	33.2	37.7	41.8	34.8	36.6	37.0	32.5	41.8	49.0	40.4	48.4	38.2
E3	30.9	29.6	20.4	27.6	24.5	28.3	36.2	34.3	21.0	35.4	24.2	28.9
K/A	0.10	0.10	0.09	0.10	0.09	0.10	0.11	0.12	0.11	0.11	0.11	0.12
C/A	0.01	0.01	0.01	0.01	0.01	0.01	0.01	0.02	0.60	0.16	0.04	0.05

Var.\ID:	SD12.95	SD12.89
SiO2	53.49	55.14
Al2O3	20.83	22.78
TiO2	0.89	0.91
Fe2O3	7.87	5.23
MgO	1.81	1.60
CaO	0.54	0.35
Na2O	0.40	0.23
K2O	2.33	2.50
MnO	0.10	0.04
P2O5	0.22	0.16
LOI	11.70	11.01
Total	100.18	100.05
As	7	9
Ba	395	417
Ce	123	115
Co	20	17
Cr	145	156
Cu	669	63
La	53	61
Mo	2	1
Ni	83	84
Nb	17	17
Pb	34	17
Rb	109	119
S	12424	9596
Se	2	0
Sr	89	95
Th	16	13
U	5	5
V	133	151
Y	33	41
Zn	93	101
Zr	154	150
DEPTH	12.86	12.89
K1	18.7	20.9
I1	30.5	38.2
E1	40.7	27.3
CH1	10.2	13.6
K2	18.7	20.9
I2	30.5	38.2
E2	40.7	27.3
CH2	10.2	13.6
K3	20.8	24.2
I3	33.9	44.2
E3	45.2	31.6
K/A	0.11	0.11
C/A	0.03	0.02

S = Proposed Slip Plane

K/A = K_2O/Al_2O_3

C/A = CaO/Al_2O_3